UNIVERSIDAD DE GRANADA

Pathological and therapeutic mechanisms in CoQ deficiency: the role of the proteins involved in the Q-Junction

Research Group **CTS-101**
Biomedical Research Center (CIBM)
Physiology Department
Faculty of **Medicine**
University of Granada

Pilar González García

PhD Program in **Biomedicine 2023**

Supervisors: Germaine Escames Rosa
Luis Carlos López García

Editor: Universidad de Granada. Tesis Doctorales
Autor: Pilar González García
ISBN: 978-84-1117-796-2
URI: https://hdl.handle.net/10481/81257

Predoctoral Contracts

FPU Contract, Ministry of Science, Innovations and Universities, Spain (FPU17/05961).
Full time 31/10/2018 – 24/03/2023
Organism: University of Granada
Center: Biomedical Research Center (CIBM), Faculty of Medicine
Department: Physiology

Participation in Research Projects

Descifrando los mecanismos patológicos y terapéuticos en la deficiencia primaria en Coenzima Q
Reference: PID2021-126788OB-I00
Principal Investigator: Luis Carlos López García
Agency: Ministerio de Ciencia e Innovación e Universidades, Proyectos Generales de Conocimiento 2021, Gobierno de España
Date: 01/01/2022 – 31/08/2026
Funds: 211.750,00 €

Evaluación de tratamientos farmacológicos con alto potencial traslacional en nuevos modelos de enfermedades mitocondriales (MitoFarma)
Reference: PEER-0083-2020
Principal Investigator: Mª. Elena Díaz Casado y Luis Carlos López García
Agency: Junta de Andalucía, Proyectos en Salud
Date: 28/10/2021 – 31/12/2023

Funds: 123,750.00 €

Descifrando los mecanismos de acción de los derivados del ácido hidroxibenzoico en la mitocondria: implicaciones para el tratamiento de enfermedades raras y comunes.
Reference: P20_00134
Principal Investigator: Luis Carlos López García
Agency: Junta de Andalucía, Proyectos de Excelencia 2020
Date: 01/01/2021 – 30/06/2023
Funds: 177,334.00 €

New therapeutic molecules for the treatment of mitochondrial diseases.
Reference: MDA-602322
Principal Investigator: Luis Carlos López García
Agency: Muscular Dystrophy Association (MDA, USA)
Date: 01/02/2019 – 31/01/2023
Funds: 289.865,00 $

Treatment of CoQ Deficiencies: therapeutic potential of the biosynthetic precursors and the importance of the endocrine interactions.
Reference: RTI2018-093503-B-I00
Principal Investigator: Luis Carlos López García
Agency: Ministerio de Ciencia, Innovación e Universidades, Proyectos I-D-i 2018, Gobierno de España (MCIU)
Date: 01/01/2019 – 30/06/2022
Funds: 193.600,00 €

Modulación simultánea del metabolismo de 1 carbono y la síntesis endógena de Coenzima Q con fines terapéuticos.
Reference: PPJIB2020.04
Principal Investigator: Pilar González García
Agency: Universidad de Granada, Proyectos de Investigación Precompetitivos para Jóvenes Investigadores del Plan Propio 2020
Date: 01/01/2021 – 31/12/2021
Funds: 1.700,00 €

Funding and Awards

Research initiation grant. Ministry of Education, Culture and Sport, Spain.
Period: 01/11/2017 – 30/06/2018
Organism: University of Granada
Center: Biomedical Research Center (CIBM), Faculty of Medicine
Funds: 3.000,00 €

European Consortium grant, EPIC-XS funded by the Horizon 2020 programme of the European Union (EPIC-XS-0000040).
Period: 13/01/2020 – 24/01/2020
Organism: University of Utrecht
Center: Bijvoet Center for Biomolecular Research
Funds: 1.500,00 €

FPU short-term stay. Ministry of Science, Innovations and Universities, Spain (EST19/00804).

Period: 01/04/2021 – 30/06/2021

Organism: University of Utrecht

Center: Bijvoet Center for Biomolecular Research

Funds: 4.290,00 €

Publications

Main publications supporting this doctoral thesis:

González-García P, Díaz-Casado ME, Hidalgo-Gutiérrez A, Jiménez-Sánchez L, Bakkali M, Barriocanal-Casado E, Escames G, Zenezini Chiozzi R, Völlmy F, Zaal EA, Berkers CR, Heck AJC, López LC (2022). The Q-junction and the inflammatory response are critical pathological and therapeutic factors in CoQ deficiency. *Redox Biology*. DOI: 1016/j.redox.2022.102403
IF: 10.787; D1 (27/297), Biochemistry & Molecular Biology

González-García P, Hidalgo-Gutiérrez A, Mascaraque C, Barriocanal-Casado E, Bakkali M, Ziosi M, Botagoz Abdihankyzy U, Sánchez-Hernández S, Escames G, Prokisch H, Martín F, Quinzii CM, López LC (2020). Coenzyme Q_{10} modulates sulfide metabolism and links the mitochondrial respiratory chain to pathways associated to one carbon metabolism. *Human Molecular Genetics.* DOI: 10.1093/hmg/ddaa214
IF: 6.150; Q1 (63/295), Biochemistry & Molecular Biology

Other publications:

González-García P, Barriocanal-Casado E, Díaz-Casado ME, López-Herrador S, Hidalgo-Gutiérrez A, López LC (2021). Animal Models of Coenzyme Q Deficiency: Mechanistic and Translational Learnings. *Antioxidants*. DOI: 10.3390/antiox10111687
IF: 7.675; D1 (4/63), Chemistry, Medicinal

Hidalgo-Gutiérrez A, Barriocanal-Casado E, Díaz-Casado ME, **González-García P**, Zenezini Chiozzi R, Acuña-Castroviejo D, López LC (2021). b-RA targets mitochondrial metabolism and adipogenesis, leading to therapeutic benefits against CoQ deficiency and age-related overweight. *Biomedicines.* DOI: 10.3390/biomedicines9101457
IF: 4.757; Q2 (121/297), Biochemistry & Molecular Biology

Hidalgo-Gutiérrez A, **González-García P**, Díaz-Casado ME, Barriocanal-Casado E, López-Herrador S, Quinzii CM, López LC (2021). Metabolic Targets of Coenzyme Q_{10} in Mitochondria. *Antioxidants*. DOI: 10.3390/antiox10040520
IF: 7.675; D1 (4/63), Chemistry, Medicinal

Díaz-Casado ME, Quiles JL, Barriocanal-Casado E, **González-García P**, Battino M, López LC, Varela-López A (2019). The Paradox of Coenzyme Q_{10} in Aging. *Nutrients*. DOI: 10.3390/nu11092221
IF: 4.546; Q1 (17/89), Nutrition & Dietetics

Barriocanal-Casado E, Hidalgo-Gutiérrez A, Raimundo N, **González-García P**, Acuña-Castroviejo D, Escames G, López LC (2019). Rapamycin administration is not a valid therapeutic strategy for every case of mitochondrial disease. *EBioMedicine.* DOI: 10.1016/j.ebiom.2019.03.025
IF: 5.736; Q1 (18/139), Medicine, Research & Experimental

Conference Attendance

Oral communications related with this doctoral thesis:

González-García P, Mascaraque C, Hidalgo-Gutiérrez A, Barriocanal-Casado E, Ziosi M, Guerra-Librero A, Sánchez- Hernández S, Prokisch H, Schuelke M, Martín F, Quinzii CM, López LC. *Connection between coenzyme Q_{10} and sulfide metabolism through SQOR levels.*
I Congreso de Investigadores del PTS. National Conference. Granada, Spain, 2019.

González-García P, Hidalgo-Gutiérrez A, Mascaraque C, Barriocanal-Casado E, Bakkali M, Ziosi M, Botagoz Abdihankyzy U, Sánchez-Hernández S, Escames G, Prokisch H, Martín F, Quinzii CM, López LC. *Coenzyme Q_{10} regulates sulfide metabolism and pathways connected to one carbon metabolism involved in mitochondrial dysfunction.*
IV Congreso Nacional de Jóvenes Investigadores en Biomedicina. National Conference. Granada, Spain, 2020.

Poster communications related with this doctoral thesis:

González-García P, Mascaraque C, Hidalgo-Guitiérrez A, Barriocanal-Casado E, López LC. *H_2S metabolism in mitochondrial Complex I deficiency. Influence of Coenzyme Q_{10} supplementation.*
1st Global Congress of Pharmacy Faculties. Innovation in Pharmacy: Advances and Perspectives (IPAP18). International Conference. Salamanca, Spain, 2018.

González-García P, Hidalgo-Gutiérrez A, Mascaraque C, Barriocanal-Casado E, Bakkali M, Ziosi M, Botagoz Abdihankyzy U, Sánchez-Hernández S, Escames G, Prokisch H, Martín F, Quinzii CM, López LC. *Regulation of sulfide metabolism by Coenzyme Q_{10} and the connection with one carbon metabolism.*
Mitochondrial Medicine Congress. International Conference. Virtual event, 2020.

González-García P, Cerván-Martín M, Carmona FD, López LC. *Simultaneous Modulation of 1-Carbon Metabolism and the Endogenous Biosynthesis of Coenzyme Q with therapeutic purposes.*
Mitochondrial Medicine Congress. International Conference. Virtual event, 2021.

González-García P, Díaz-Casado ME, Hidalgo-Gutiérrez A, Jiménez-Sánchez L, Barriocanal-Casado E, López LC. *Coenzyme Q deficiency therapy regulates the Q-junction and the inflammatory response.*
Cell Symposia: Metabolites in Signaling and Disease. International Conference. Lisboa, Portugal, 2022.

González-García P, Díaz-Casado ME, Hidalgo-Gutiérrez A, Jiménez-Sánchez L, Barriocanal-Casado E, López LC. *The Q-Junction and the Inflammatory Response Determine the Pathological Features and the Therapeutic Success in a Model of Fatal Mitochondrial Encephalopathy.*
FENS Forum 2022. International Conference. Paris, France, 2022.

González-García P, Díaz-Casado ME, Hidalgo-Gutiérrez A, Jiménez-Sánchez L, Barriocanal-Casado E, López LC. *The Neuroinflammatory Response and the Q-Junction Determine the Pathological Features and the Therapeutic Success in a Model of Fatal Mitochondrial Encephalopathy.*

MitoNice 2022. International Conference. Nice, France, 2022.

To my family

Table of contents

Abbreviations

2,4-diHB	2,4-Dihydroxybenzoic acid
3,4-diHB	3,4-Hydroxybenzoic acid
3-MST	3-Mercaptopyruvate sulfurotransferase
4-HB	4-Hydroxybenzoic acid
4-HBz	4-Hydroxybenzaldehyde
4-HMA	4-Hydroxymandelate
4-HPP	4-Hydroxyphenylpyruvate
AADAT	Mitochondrial alpha-aminoadipate aminotransferase
BN-PAGE	Blue native polyacrylamide gel electrophoresis
CBS	Cystathionine β-synthase
CHDH	Choline dehydrogenase
CoQ	Coenzyme Q or ubiquinone
CoQH•	Ubisemiquinone
$CoQH_2$	Ubiquinol
CSE	Cystathionine γ-lyase
Cyt c	Cytochrome c
DHODH	Dihydroorotate dehydrogenase
DMQ	Demethoxyubiquinone
ETC	Electron transport chain
ETF	Electron transfer flavoprotein
ETFDH	Electron transfer flavoprotein-dehydrogenase
ETHE1	Ethylmalonic encephalopathy dioxygenase
G3PDH	Mitochondrial glycerol-3-phosphate dehydrogenase
GPD2	Mitochondrial glycerol-3-phosphate dehydrogenase
GPX4	Glutathione peroxidase 4
GSSH	Glutathione disulfide

GSH	Glutathione
H_2S	Hydrogen sulfide
HPDL	Hydroxyphenylpyruvate dioxygenase-like protein
IMM	Inner mitochondrial membrane
LC-MS	Liquid chromatography – mass spectrometry
MEFs	Mouse embryonic fibroblasts
mPTP	Mitochondrial permeability transition pore
mtDNA	Mitochondrial DNA
NAC	N-acetylcysteine
nDNA	Nuclear DNA
OXPHOS	Oxidative phosphorylation
pABA	p-Aminobenzoate
PRODH	Proline dehydrogenase
RET	Reverse electron transport
ROS	Reactive oxygen species
SAAR	Restriction in sulfur aminoacids
SCs	Respiratory chain supercomplexes
SDO	Sulfide dioxygenase
SO	Sulfite oxidase
SQOR	Sulfide:quinone oxidoreductase
Tyr	Tyrosine
TAT	Tyrosine aminotransferase
TCA	Tricarboxylic acid cycle
TR	Thiosulfate reductase
TST	Thiosulfate sulfurotransferase or rhodanese
UCPs	Uncoupling proteins
VA	Vanillic acid
β-RA	β-Resorcylic acid

Abstract

Mitochondria are present in most cell types. Structurally, mitochondria have two phospholipid membranes that define four biochemically distinct compartments: the outer membrane, the intermembrane space, the inner membrane and the mitochondrial matrix. Mitochondria perform a very wide range of functions and are vital in the integration of several cellular metabolic processes, most of them converging in energy production through the oxidative phosphorylation (OXPHOS). In the OXPHOS system, coenzyme Q (CoQ) is a unique electron carrier that transfer electrons from complex I and complex II to complex III, as well as from other mitochondrial enzymes, such as the electron transfer flavoprotein (ETF), the dihydroorotate dehydrogenase (DHODH), the mitochondrial glycerol-3-phosphate dehydrogenase (G3PDH or GPD2), the choline dehydrogenase (CHDH), the proline dehydrogenase (PRODH) and the sulfide:quinone oxidoreductase (SQOR).

Any mitochondrial dysfunction can trigger a wide variety of pathologies, including primary mitochondrial diseases. These disorders are clinically diverse and can manifest in the neonatal phase, childhood or adulthood. This clinical heterogeneity suggests that multiple pathogenic and adaptive mechanisms are involved in the clinical manifestations of mitochondrial diseases. Recently, the remodeling of folate cycle, and its link to H_2S and nucleotides metabolism, have been proposed as novel mechanisms contributing to the pathophysiological features of mitochondrial diseases. Currently, there is no available treatment for most of the mitochondrial disorders, so the therapeutic

option is usually limited to palliative cares. In general, CoQ_{10} supplementation is recommended for patients with mitochondrial disorders or other diseases with secondary mitochondrial dysfunction, and clinical improvements have been reported in some cases, but others do not show any positive response.

CoQ levels can be severely reduced in a group of mitochondrial disorders known as CoQ deficiencies. The identification of the genetic defect in CoQ deficiency is essential to differentiate primary forms, due to mutations in *COQ* genes, from secondary forms, due to mutations in genes not directly involved in the biosynthesis of CoQ or to not-genetic factors. The identification of common pathogenic pathways for all patients is complex due to the heterogeneity in clinical presentation, age of onset and severity of the disease. The conventional treatment for CoQ deficiency is the exogenous supplementation of high doses of CoQ_{10}. However, this treatment has limited efficiency, especially in patients with neurological symptoms. The failure of CoQ_{10} therapy could be explained by the low absorption and bioavailability of exogenous CoQ_{10}, limiting the dose that access to the affected tissues. Moreover, CoQ_{10} supplementation does not reduce the accumulation of intermediate metabolites or improve the endogenous biosynthesis of CoQ, although it can partially rescue the levels of SQOR in *in vivo* models. To overcome the disadvantages of classical therapy, new therapeutic strategies based on the use of structural analogs of the CoQ precursor 4-hydroxybenzoic acid (4-HB) has been developed. 4-HB analogs seem to modulate CoQ biosynthesis but they have limitations in rescuing SQOR levels.

In the *Coq9*^{R239X} mouse model with fatal mitochondrial encephalopathy due to CoQ deficiency, we have tested the therapeutic potential of the 4-HB analog, vanillic acid (VA). VA rescued the phenotypic, morphological and histopathological signs of the encephalopathy, leading to a significant increase in the survival. VA and other 4-HB analog, the β-resorcylic acid (β-RA), partially decrease the DMQ/CoQ ratio in peripheral tissues and normalize the mitochondrial proteome and metabolism related with the CoQ-linked proteins in the Q-junction in *Coq9*^{R239X} mice. Specifically, the levels of PRODH, ETFDH, DHODH and CHDH are increased in the context of CoQ deficiency and normalized by the treatment with 4-HB analogs. Moreover, β-RA and VA also normalize the serum levels of acylcarnitines and some other metabolites and proteins that have the potential to be used as biomarkers to follow the progression of the disease and the response to treatments in CoQ deficiency.

Additionally, here we showed that the supplementation with CoQ_{10} in CoQ or Complex I deficiency, induces the overexpression of SQOR, one component of the Q-junction and the first enzyme of the mitochondrial H_2S oxidation pathway, leading to a downregulation of CBS and CSE, enzymes from the transsulfuration pathway. These changes are independent of sulfur aminoacids availability. The modulation of sulfide metabolism induced by CoQ_{10} causes the adaptation of metabolic pathways closely connected to the transsulfuration pathway and unbalanced in a variety of models of mitochondrial diseases, such as the serine biosynthesis, the folate cycle and the nucleotides metabolism. Finally, the co-administration of CoQ_{10} and VA *in vitro* leads to synergic effects in CoQ deficiency.

Collectively, this work contributes to advance in the knowledge about the cellular functions of CoQ, the metabolic consequences of CoQ deficiency and the therapeutic potential of 4-HB analogs.

Resumen

Las mitocondrias están presentes en la mayoría de los diferentes tipos de células. Estructuralmente, las mitocondrias tienen dos membranas de fosfolípidos que definen cuatro compartimentos bioquímicamente distintos: la membrana externa, el espacio intermembrana, la membrana interna y la matriz mitocondrial. Las mitocondrias modernas realizan una amplia gama de funciones y son vitales en la integración de varios procesos metabólicos celulares. Convergiendo muchos de ellos en la producción de energía a través de la fosforilación oxidativa (OXPHOS). En el sistema OXPHOS, la coenzima Q (CoQ) es un transportador de electrones único que transfiere electrones desde el complejo I y el complejo II al complejo III, así como desde otras enzimas mitocondriales como la flavoproteína de transferencia de electrones (ETF), la dihidroorotato deshidrogenasa (DHODH), la glicerol-3-fosfato deshidrogenasa mitocondrial (G3PDH o GPD2), la colina deshidrogenasa (CHDH), la prolina deshidrogenasa (PRODH) y la sulfuro:quinona oxidorreductasa (SQOR).

Cualquier disfunción mitocondrial puede desencadenar una gran variedad de patologías, incluyendo las enfermedades mitocondriales primarias. Estos trastornos son clínicamente diversos y pueden manifestarse en la fase neonatal, en la infancia o en la edad adulta. Esta heterogeneidad clínica sugiere que múltiples mecanismos patogénicos y adaptativos están involucrados en las manifestaciones clínicas de las enfermedades mitocondriales. Recientemente, la remodelación del ciclo del folato y su vínculo con el H_2S y el metabolismo de los nucleótidos se han propuesto como nuevos mecanismos que contribuyen a las

características fisiopatológicas de las enfermedades mitocondriales. Actualmente, no existe un tratamiento disponible para la mayoría de los trastornos mitocondriales, por lo que el tratamiento suele limitarse a los cuidados paliativos. En general, la suplementación con CoQ_{10} se recomienda para pacientes con trastornos mitocondriales u otras enfermedades con disfunción mitocondrial secundaria, y se han registrado mejoras clínicas en algunos casos, aunque otros no muestran ninguna respuesta positiva.

Los niveles de CoQ pueden reducirse severamente en un grupo de trastornos mitocondriales conocidos como deficiencias en CoQ. La identificación del defecto genético en la deficiencia en CoQ es fundamental para diferenciar las formas primarias, debidas a mutaciones en los genes *COQ*, de las formas secundarias, debidas a mutaciones en genes no implicados directamente en la biosíntesis de la CoQ o a factores no genéticos. La identificación de vías patogénicas comunes para todos los pacientes es compleja debido a la heterogeneidad en la presentación clínica, edad de inicio y gravedad de la enfermedad. El tratamiento convencional para la deficiencia en CoQ es la suplementación exógena de altas dosis de CoQ_{10}. Sin embargo, este tratamiento tiene una eficacia limitada, especialmente en pacientes con síntomas neurológicos. El fracaso de la terapia con CoQ_{10} podría explicarse por la baja absorción y biodisponibilidad de la CoQ_{10} exógena, limitando la dosis que accede a los tejidos afectados. Además, la suplementación con CoQ_{10} no reduce la acumulación de metabolitos intermedios ni mejora la biosíntesis endógena de CoQ, aunque puede rescatar parcialmente los niveles de SQOR en modelos *in vivo*. Para superar las desventajas de la terapia clásica, se han desarrollado nuevas estrategias terapéuticas basadas en el

uso de análogos estructurales del precursor de la CoQ, el ácido 4-hidroxibenzoico (4-HB). Los análogos del 4-HB parecen modular la biosíntesis de CoQ pero tienen limitaciones para rescatar los niveles de SQOR.

En el modelo de ratón *Coq9*^{R239X} con encefalopatía mitocondrial por deficiencia en CoQ, hemos probado el potencial terapéutico del análogo de 4-HB, el ácido vanílico (VA). El VA eliminó los signos fenotípicos, morfológicos e histopatológicos de la encefalopatía, lo que condujo a un aumento significativo de la supervivencia. El VA y otro análogo de 4-HB, el ácido β-resorcílico (β-RA), disminuyeron parcialmente el cociente DMQ/CoQ en tejidos periféricos y normalizaron el proteoma mitocondrial y el metabolismo relacionado con las proteínas ligadas a CoQ en la confluencia Q en ratones *Coq9*^{R239X}. Específicamente, los niveles de PRODH, ETFDH, DHODH y CHDH aumentan en el contexto de la deficiencia en CoQ y se normalizan mediante el tratamiento con análogos del 4-HB. Además, β-RA y VA también normalizaron los niveles séricos de acilcarnitinas y algunos otros metabolitos y proteínas que tienen potencial para emplearse como biomarcadores para seguir la progresión de la enfermedad y la respuesta a los tratamientos en la deficiencia en CoQ.

Además, aquí mostramos que el suplemento con CoQ_{10} en la deficiencia en CoQ o Complejo I induce la sobreexpresión de SQOR, componente de la confluencia Q y la primera enzima de la ruta de oxidación del H_2S mitocondrial, lo que conduce a una regulación a la baja de CBS y CSE, enzimas de la ruta de transulfuración. Estos cambios son independientes de la disponibilidad de aminoácidos azufrados. La

modulación del metabolismo del sulfuro de hidrógeno inducida por la CoQ_{10} provoca la adaptación de rutas metabólicas estrechamente conectadas a la ruta de transulfuración y alteradas en modelos de enfermedades mitocondriales, como la biosíntesis de serina, el ciclo del folato y el metabolismo de nucleótidos. Finalmente, la administración conjunta de CoQ_{10} y VA *in vitro* produce efectos sinérgicos en la deficiencia en CoQ.

En conjunto, este trabajo contribuye a avanzar en el conocimiento sobre las funciones celulares de la CoQ, las consecuencias metabólicas de la deficiencia en CoQ y el potencial terapéutico de los análogos de 4-HB.

1. Introduction

1.1. Mitochondria in Health

Life is a complex phenomenon. Life on the planet has evolved since very simple prokaryotic organisms, to more advanced and complicated life forms (1). Eukaryotic cell emerged with the acquisition of nucleus, endomembrane system and membrane-bound organelles, increasing in great complexity with respect to prokaryotes (2). In this context, mitochondria stands out as an organelle that is found in most eukaryotic cells (3). In humans, mitochondria consume approximately 98% of the oxygen breathe and directly relate it to energy production. In fact, without the supply of energy provided by mitochondria, the evolution of higher organisms would not have been possible. Therefore, mitochondria lies at the heart of life and cell death (4).

1.1.1. The Mitochondria

The term mitochondrion was coined in 1898 and came from the Greek word mitos (thread) and chondros (granule). Nevertheless, mitochondria were described long before, in 1857. The Swiss anatomist Rudolf von Koelliker was the first one to identify them in human muscle and denominated them as ‘sarcosomes’ (5).

In mammals, mitochondria are present in most cell types. Red blood cells are the only ones that do not have mitochondria in humans. The number of mitochondria in the cell depends on its energy and

metabolic requirements, being able to reach values of more 10^4. In extreme cases, for example in hummingbird flight muscle, mitochondria can constitute 35% of the cell volume. Mitochondria shape and size are very heterogeneous, although it used to be rod-shaped with a diameter of approximately 1 μm. Moreover, mitochondria can appear as a contiguous reticulated network or to move along microfilaments in a constant state of fission and fusion. The biological meaning of such morphological differences and dynamic behavior is still poorly understood (3).

Mitochondrial function is diverse. Mitochondria participates in a wide variety of interconnected functions: it is involved in the production of ATP and many biosynthetic intermediate, in the regulation of intracellular calcium levels, in the generation of reactive oxygen species (ROS), in the cellular defense against oxidative stress and in the mechanisms to induce cell death. In parallel, mitochondria are intimately interconnected, not only with other cellular compartments, but also with other structures of the organism, regulating communication between cells and tissues. This dynamic behavior of mitochondria influences human physiology and assumes that any mitochondrial dysfunction can originate a great diversity of diseases, including neurodegenerative and metabolic disorders (6).

1.1.1.1 The Endosymbiotic Origin of Mitochondria

Eukaryotes evolved thanks to the acquisition of the nucleus, the endomembrane system and the mitochondria (2). Until now, the origin of eukaryotes has been tried to be explained in more than twenty different endosymbiotic theories (Fig. 1). Common to all of them, a bacterium is

engulfed by a proto-eukaryotic cell. In this mutually beneficial relationship, the bacterium supply energy in the form of ATP from oxidative phosphorylation while the newly formed cell provides a safer place to survive (7-9). All the different endosymbiotic theories agree in that endosymbiotic origin of mitochondria was important, perhaps even crucial in eukaryogenesis (10-12). However, there is a heavily debate about the nature of the host or the endosymbiont, and in the order of events that originated the last eukaryotic common ancestor (LECA) (13).

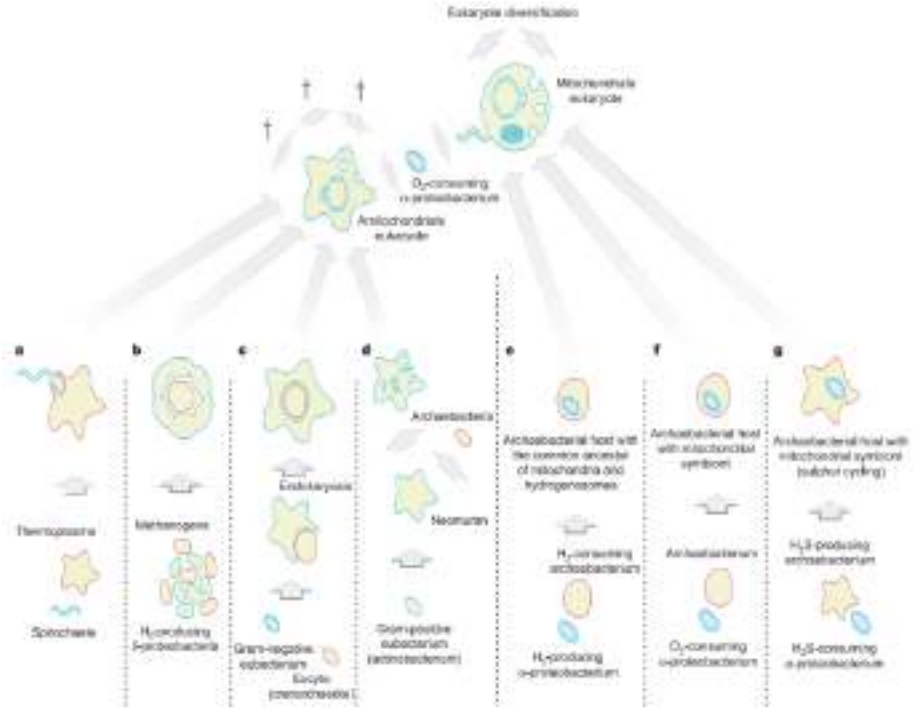

Figure 1. Models for endosymbiotic eukaryotic origin.

(A-D) Models that suggest the origin of a nucleus-bearing cell first followed by the acquisition of mitochondria in a eukaryotic host.

(E-G) Models that propose the origin of mitochondria in a prokaryotic host, followed by the acquisition of eukaryotic-specific features (14).

Additionally, there is no agreement if eukaryotes were evolved directly because of mitochondria or the mitochondria incorporation was the last step in the process because no fossil or genomic record of the intermediates between modern eukaryotes and prokaryotes has been found until now (10, 15-17).

In 1905, the endosymbiotic theory was first published. The author of the work was Konstantin Mereschkowsky, a Russian botanist. Firstly, the mitochondrion was not part of Mereschkowsky's theory but he hypothesized about the origin of chloroplasts suggesting a symbiont relation between the ancestors of plant chloroplasts and free-living cyanobacteria (18). Approximately a decade later, Paul Portier, based on Mereschkowsky's theory, proposed the symbiotic origin of mitochondria (19), a concept supported later on by Ivan Wallin (20). However, at that time, the endosymbiotic theories were strongly rejected by the scientific community and none of them were seriously considered (21). In 1967, Lynn Margulis published her famous *On the origin of mitosing cells* (22) where she set up the basis of her "Serial Endosymbiotic Theory" for the origin of the eukaryotic cell (23). In her manuscript, Margulis revived previous ideas proposing the endosymbiotic origin of mitochondria from purple bacteria (alphaproteobacteria). However, her theories were met with skepticism (24), until protein and DNA sequencing data revealed the bacterial origins of mitochondria (25). Following genomic analyses of mitochondrial genes and their genomic organization and distribution indicate that mitochondrial genomes are derived from an alpha-proteobacterium–like ancestor, probably due to a single ancient invasion of an Archea-type host that occurred more than 1.5 billion years ago (Ga) (Fig. 2) (26, 27). Oxygenic photosynthesis is thought to have started 3.5

Ga, with oxygen levels becoming substantial by about 2.2 Ga connecting the aerobic respiration with the origin of mitochondria (28, 29).

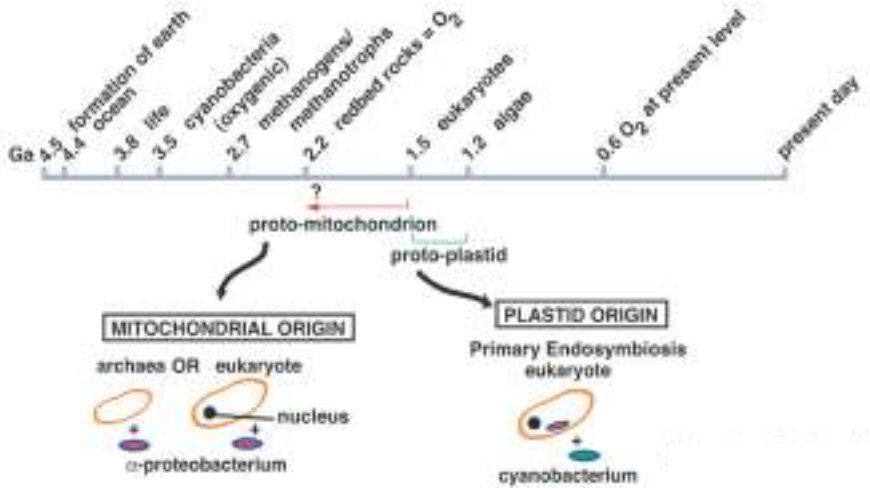

Figure 2. Time line for the origin of life and major invasions giving rise to mitochondria and plastids.

Mitochondria/α-proteobacteria are shown in red, plastids/cyanobacteria in green, and endomembranes around secondary plastids in yellow. Ga, billion years ago (26).

Classically, it has been considered that mitochondrion was phagocytosed by an anaerobic nucleus-bearing cell with eukaryote characteristics (Fig. 1a-d). This view considered that the mitochondrial endosymbiont was an obligate aerobe that provided the endosymbiont's ability to remove oxygen from the anaerobe host. It has been suggested that this mitochondrial endosymbiont was similar in physiology and lifestyle to modern *Rickettsia* species. However, this traditional view has some limitations because it does not explain the origin of anaerobic mitochondria or hydrogenosomes. Further studies should be made to explain the anaerobically functioning of mitochondria and its evolution from oxygen-dependent organisms (30-33).

On the other hand, alternative theories are based in the idea that was a prokaryotic host, an archeobacterium, the one that acquired the mitochondrion (Fig. 1e-g). In this case, the mitochondrial endosymbiont has been suggested to be a facultative anaerobe similar to modern Rhodobacteriales. The endosymbiont was able to live with or without oxygen, and could provide H_2 as a source of energy and electrons to a H_2 dependent host. In fact, this beneficial interaction is commonly observed in modern microbial communities as well as some prokaryotes living as endosymbionts within other prokaryotes. Similar arguments have been used to explain the sulfide metabolism in eukaryotes, i.e., in the hypothetical premitochondrial symbiosis, the proteobacterium oxidized H_2S to sulfur and the *Archeon* reduced it back to H_2S. Sulfur cycled repeatedly, in effect serving as an electron carrier between the two organisms. Nevertheless, the mechanism by which the mitochondrial endosymbiont came to reside within the prokaryotic host has not been described (34, 35).

The primary remaining evidence of the independent bacterial origin of mitochondria is the presence of mitochondrial DNA (mtDNA), similar to primitive bacteria DNA. Mitochondrial, as well as chloroplasts, are the only cellular organelles with their own DNA (36). Human mDNA is a simple doubled stranded structure of only 16.6kb. It encodes 13 proteins of the mitochondrial respiratory chain, two rRNAS and 22 tRNAs required for the synthesis of the 13 proteins. Thus, mDNA only have the information for the transcription of a fraction of mitochondrial proteins. The rest are encoded in the nuclear DNA (nDNA) and transported to the mitochondria (4).

It is important to highlight that some eukaryotic organisms have adapted to living in low-oxygen conditions in aquatic and terrestrial environments or in animal gastrointestinal tracts. In this condition, aerobic respiration is not a viable option to obtain energy. Therefore, these organisms have adapted and developed mitochondrion-related organelles (MROs) that can function anaerobically (37). The MROs have been classified into five types based on their energy metabolism: aerobic mitochondria, anaerobic mitochondria, hydrogen-producing mitochondria, hydrogenosomes, and mitosomes (Fig. 3) (38):

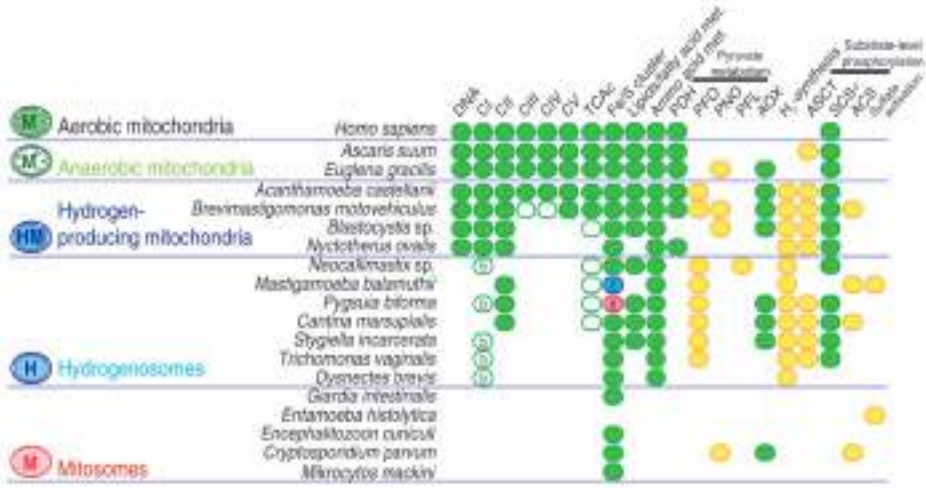

Figure 3. Mitochondrial bioenergetics in aerobic and anaerobic eukaryotes.
Presence or absence of aerobic and anaerobic enzymes in eukaryotes. Green cycle icon is for proteins typically found in aerobic mitochondria (but sometimes also in anaerobic mitochondria/MROs). White cycle icon represents proteins for aerobic pathways and yellow cycle icon indicates proteins for anaerobic metabolism. a: also involved in tricarboxylic acid cycle (TCAc), b: only NuoE and NuoF, c: NIF system (blue), d: SUF system (magenta). PDH: pyruvate dehydrogenase complex, PFO: pyruvate:ferredoxin oxidoreductase, PNO: pyruvate:NADPH oxidoreductase, PFL: pyruvate formate lyase, AOX: alternative oxidase, AcK: acetate kinase, SCS: succinyl-CoA synthase, and ASCT: acetate:succinyl-CoA transferase families 1b and 1c (37).

1.1.1.2 Mitochondria: Structural Characteristics

Mitochondrial structure has been clearly described thanks to advances in the development of the electron microscope and biochemical fractionation of submitochondrial membrane (5, 39). As a relic of their evolutionary endosymbiotic origin, mitochondria have two phospholipid membranes that define four biochemically distinct compartments. The outer mitochondrial membrane is in contact with the outside of the cell, while the inner boundary mitochondrial membrane is located inside the cell. Between the outer and inner membranes is the intermembrane space and surrounded by the inner membrane is the mitochondrial matrix (3, 21) (Fig. 4).

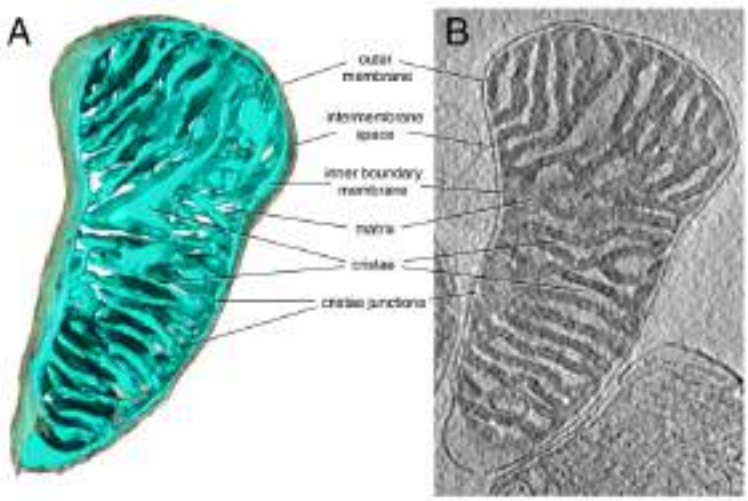

Figure 4. Representation of mouse heart mitochondria.

(A) Three-dimensional volume of a mouse heart mitochondria determined by cryo-ET.

(B) Tomographic slice through the map volume. The outer membrane is represented in grey color and the inner boundary membrane in blue. Inner membrane is highly invagenated into cristae. Mitochondrial matrix is represented in dark color in the electron microscope due to its high density in mitochondrial proteins (40).

The outer mitochondrial membrane is the boundary between the mitochondria and the cell cytoplasm, supporting the semi-autonomy of this cellular organelles (Fig. 4) (40). The structure of the outer membrane is similar to the one of the eukaryotic cell membranes. It is a semi permeable bilayer (< 5000–10,000 MW) composed of 50/50 protein-phospholipid (5, 21, 40, 41). The outer membrane is porous, so it is easily crossed by ions. Small molecules without charge can also traversed the outer membrane through pore-forming membrane proteins (porins), such as the voltage-dependent anion channel VDAC (42, 43). Any larger molecules, especially proteins, have to be imported by special translocases, like nuclear-encoded proteins through the translocase of the translocation outer membrane complex (TOM) (44). Because of its porosity, there is no membrane potential across the outer membrane. Moreover, the outer mitochondrial membrane can interact with other organelles like the nucleus, the ribosomes, the endoplasmic reticulum, and even other mitochondria (5, 41). Additionally, there are proteins located in the outer membrane such as the β-barrel protein-sorting and assembly machinery (SAM), the mitochondrial-shaping proteins (Mfn1,2, Fis1) and the proteins of apoptotic pathway (e.g., BAK) (45).

On the contrary, the inner mitochondrial membrane (IMM) is not easily traversed by ions or molecules. Specific membrane transport proteins are needed for each particular ion or molecule. This ion selectivity is the reason why all along the inner membrane, there is an electrochemical membrane potential of about 180 mV (40). The inner membrane is rich in proteins, highlighting the presence of the respiratory complexes required for electron transport and ATP production (21). It has also the particularity to have high content of the lipid cardiolipin,

which is essential for the optimal function of the mitochondrial respiratory chain. The inner mitochondrial membrane shows a complex ultrastructure. It is composed of two subdomains, the inner boundary membrane and the cristae (Fig. 4). The inner boundary membrane is connected to the outer membrane via direct physical contact sites. The inner boundary membrane contains the translocase of the inner membrane (TIM) (46), which shuttles proteins into the matrix , and proteins, such as Mia40 and Oxa1 (47), which are essential for the correct assembly and localization of intermembrane proteins (21). Cristae are membrane invaginations that protrude from the inner boundary membrane into the matrix space. Their frequency and morphology show substantial variations between different organisms and cell types as well as distinct metabolic and developmental states (48). Cristae also participate in the distribution of important molecules for ATP synthesis all along the inner membrane. Moreover, cristae are able to undergo conformational changes in order to regulate enzymatic reactions related to citric acid cycle and oxidative phosphorylation. They can also showed remodeling during apoptosis to facilitate the release of cytochrome c (21).

The third mitochondrial compartment is the intermembrane space. As previously mentioned, it is located between the two membranes and it has its own biochemical characteristics. It has a relatively low protein content, being cytochrome c an important component as well as other proteins involved in inner membrane remodeling (e.g. Opa1), apoptosis, and additional protein carrier (3, 5, 21). Classically, the intermembrane space has been considered as a small hydrophilic layer between the two mitochondrial membranes that,

because of the relatively large openings of the porin channels in the outer membrane, is very similar to the cytosol. Recently, it has been demonstrated the implication of the intermembrane space in the coordination of mitochondrial activities with other cellular processes. Among others, it is also involved in the transport of different cellular components between the matrix and the cytosol, in the regulation of the mitochondrial morphogenesis and apoptosis, in the detoxification of reactive oxygen species and in signaling pathways that regulate respiration and metabolic functions (49).

Finally, the mitochondrial matrix. It is characterized by high protein content of around 70% of the organelle's proteins. This is the reason why the mitochondrial matrix is the cellular space where hundreds of metabolic enzymes, including the citric acid cycle, fatty acid oxidation, heme synthesis and Fe–S biogenesis, take place. Especially important is to note that mtDNA is also located in the matrix, anchored to the inner membrane (21). Thus, mDNA replication, transcription, protein biosynthesis and numerous enzymatic reactions occur in the mitochondrial matrix (40).

1.1.1.3 Mitochondrial Function

Over 1,500 proteins are required for healthy mitochondrial function (50, 51). Thirteen proteins are encoded by mtDNA and the rest are encoded by nDNA, which are translated in the cytoplasm and the proteins are imported across the mitochondrial membrane through an intricate import machinery (52). Traditionally, research on mitochondria focused on bioenergetics, but from the last 15–20 years, studies have

revealed a greater than expected complexity and versatility of mitochondrial activities, integrating mitochondrial energetics (53).

Modern-day mitochondria perform a very wide range of functions and are vital in the integration of several cellular metabolic process, including oxidative phosphorylation, fatty acid oxidation, Krebs cycle, urea cycle, gluconeogenesis, ketogenesis and 1-carbon (1C) metabolism (52). Mitochondria are also actively involved in other important cellular processes, like (non-shivering) thermogenesis, amino acid and lipid metabolism, biosynthesis of hemo and iron–sulfur clusters, calcium homeostasis and apoptosis (3, 52, 54). Mitochondria coordinate cellular adaptation to stressors such as nutrient deprivation, oxidative stress, DNA damage and endoplasmic reticulum (ER) stress. In addition to ATP, mitochondria are continually producing the metabolic precursors necessary for cell structure. In parallel, mitochondria also generate metabolic waste products, such as reactive oxygen species (ROS) and ammonia, and is able to develop strategies to detoxify or inactivate them (55, 56).

Nevertheless, continued basic biological approaches are critical so we can understand on a molecular level and characterize new pathways that impact mitochondrial behavior and functions (56).

1.1.1.3.1 Mitochondrial Bioenergetics: The OXPHOS System

The main role of mitochondria is the energy production. Mitochondria extract energy from nutrients through a process named as

oxidative phosphorylation (OXPHOS). The final objective is to store energy as ATP or convert it into heat (57). In 1948, Eugene Kennedy and Albert Lehninger first described that mitochondria are the primary sites of energy production in eukaryotes cells and opened the door to the development of modern studies focused on biological energy transductions (58).

The OXPHOS system is located at the inner mitochondrial membrane and it is a unique assembly of protein complexes (complex I, II, II, IV and V) and mobile carriers that participate in the transport of electrons from reducing equivalents extracted from nutrients to molecular oxygen. This electron transference produces a proton-motive force accumulated in the intermembrane space that is used as energy source for cellular ATP synthesis (54). Different dehydrogenases are responsible for electron recruitment from catabolic pathways. At the end, all the electrons are supply in form of universal electron acceptors: nicotinamide nucleotides (NAD^+ or $NADP^+$) or flavin nucleotides (FMN or FAD) (58). Electrons are transported to the respiratory chain through redox shuttle moieties, $NADH+H^+$ for complex I and $FADH_2$ for complex II. In parallel with the electron flow, complexes I, II, III and IV translocate protons across the inner mitochondrial membrane from the matrix to the intermembrane space, generating an electrochemical gradient which is then exploited by complex V (or ATP synthase) to produce the condensation of ADP and P_i into ATP (57) (Fig. 5). Thus, the energy obtained in this process can be stored as ATP when the electron transfer is linked to oxidative phosphorylation or dissipates as heat, in case of non-association.

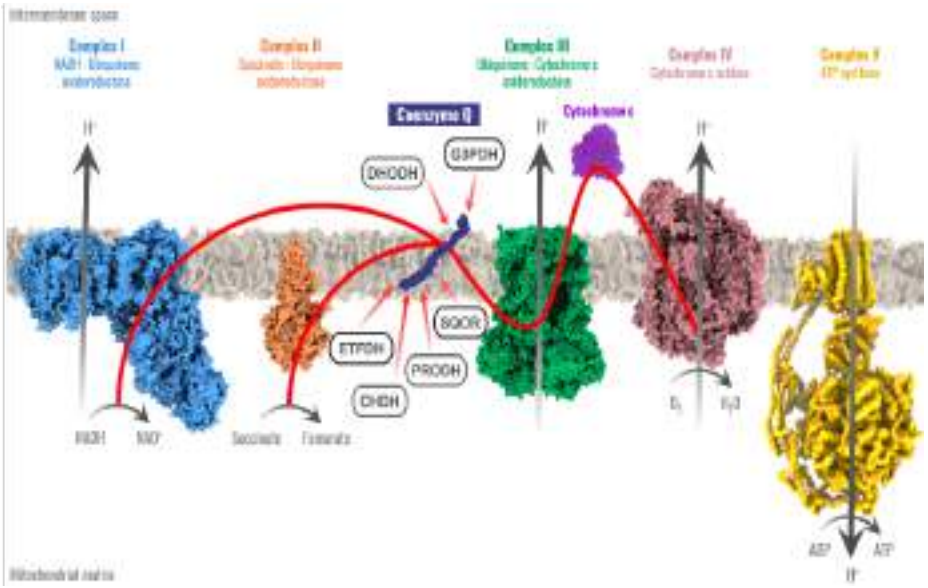

Figure 5. The OXPHOS system.

Red arrows represent electron flow. The electrons, obtained in the oxidation of NADH by Complex I or of succinate by Complex II, are transferred to Complex III through coenzyme Q and, then to Complex IV by the participation of cytochrome c. Coenzyme Q accepts electrons from complex I and complex II, sulfide:quinone oxidoreductase (SQOR), proline dehydrogenase and proline dehydrogenase 2 (PRODH), choline dehydrogenase (CHDH), mitochondrial glycerol-3-phosphate dehydrogenase (G3PDH), dihydroorotate dehydrogenase (DHOH), and electron transport flavoprotein dehydrogenase (ETFDH) (59).

Five multiheteromeric protein complexes (CI, CII, CIII, CIV and CV) and two electron mobile carriers, the coenzyme Q (CoQ) and the cytochrome c (cyt c), compose the OXPHOS system (Fig. 5).

Complex I is also known as NADH:ubiquinone oxidoreductase or NADH dehydrogenase. At high-resolution electron microscopy, complex I has a characteristic L-shape with one arm of the L in the membrane and the other extending into the matrix (Fig. 5). Complex I is

composed by 42 different polypeptide chains, including an FMN-containing flavoprotein and at least six iron-sulfur centers. Seven of these proteins are encoded by mtDNA genes. Complex I catalyzes two simultaneous and obligatory coupled processes: (a) the transfer of two electrons from NADH in the mitochondrial matrix to the CoQ, located in the lipid mass of the inner membrane, and (b) the transfer of protons from the matrix to the intermembrane space (58). The NADH electrons come from different reactions catalysed by various dehydrogenases in the mitochondrial matrix, including the isocitrate dehydrogenase, alpha-ketoglutarate dehydrogenase and malate dehydrogenase, three enzymes of the Krebs cycle, as well as hydroxyacyl coenzyme A dehydrogenase that acts in the mitochondrial oxidation of fatty acids.

Complex II, known as succinate dehydrogenase, is the most different complex compared to other ones. First, nDNA encodes for all proteins of complex II while, in general, some components of the other complexes are encoded in mtDNA. Secondly, complex II not only participates in the OXPHOS system, it is also an enzymatic component of the tricarboxylic acid cycle, and it is responsible for the oxidation of succinate to fumarate. In parallel, electrons from $FADH_2$ are transfer to the CoQ, the cofactor of the reaction. Finally, also making the difference with other complexes, complex II does not transport protons into the intermembrane space (3). Structurally, it contains five prosthetic groups of two types and four different protein subunits (58).

Complex III, also named cytochrome bc_1 complex or ubiquinone:cytochrome c oxidoreductase, participates in the transfer of electrons from CoQ to cytochrome c. At the same time, protons are

translocated across the membrane. The complex is a dimer of identical monomers, each with 11 different subunits, 1 of them mtDNA-encoded (58).

Complex IV is also named cytochrome oxidase. Complex IV catalyzes the last step in the mitochondrial respiratory chain: it transports the electron from reduced cytochrome c produced by complex III to molecular oxygen (O_2). Four electrons from cytochrome c as well as four protons coming from the matrix are required to reduce the oxygen molecule to water. Additionally, four protons are transported from the matrix to the intermembrane space (3). Mammalian mitochondrial cytochrome oxidase is a homodimer composed of 13 different subunits, 2 of them mtDNA-encoded (58).

Complex V or ATP synthase catalyzes the formation of ATP from ADP and P_i, accompanied by the flow of protons from the intermembrane space to the mitochondrial matrix. The ATP synthase is composed by two different compartments. One of them is a peripheral membrane protein, the F_1, and the other one, F_o is integrated in the membrane. The F_1 subunit is divided in nine subunits of five different types. The general composition of this F_1 is $\alpha_3\beta_3\gamma\delta\varepsilon$, being β subunits the ones with catalytic activity for ATP synthesis. F_o has a proton pore for protons transference. Through this F_o pore, protons return to the matrix and the electrochemical gradient created across the inner mitochondrial membrane (the proton-motive force) is the source of energy for the synthesis of ATP. Together, complex V is composed by 16 subunits, 2 of them mtDNA-encoded (58).

The classical view of the function of the electron mobile carriers is that CoQ transfer electrons from CI or CII to CIII, while cytochrome c transfer electrons between CIII and CIV. Nevertheless, in the case of CoQ, the electrons may come from other mitochondrial enzymes, such as the electron transfer flavoprotein (ETF) involved in fatty acids β-oxidation, the dihydroorotate dehydrogenase (DHODH) from *de novo* pyrimidine synthesis, the mitochondrial glycerol-3-phosphate dehydrogenase (G3PDH or GPD2) that connects fatty acids metabolism and glycolysis with OXPHOS system, the choline dehydrogenase (CHDH) related to the metabolism of glycine, the proline dehydrogenase (PRODH) of the proline and arginine metabolism and the sulfide:quinone oxidoreductase (SQOR) of H_2S metabolism (Fig. 5). This flux of electrons to the CoQ from different redox pathways is currently known as the Q-junction. This aspect will be deeply discussed further on.

1.1.1.3.1.1 The OXPHOS System and ROS generation

The mitochondrial respiratory chain leaks electrons in physiological and pathophysiological conditions, especially from complex I but also from complex III. Those electrons can reduce oxygen to superoxide anion, a ROS from which other types of ROS can be generated. Particularly, the formation of ROS in mitochondria is induced in two situations: (a) when there is a deficiency in ADP or O_2, so mitochondria is not producing ATP and, therefore, they have a large proton-motive force and a high CoQ reduced/oxidized ratio, and (b) when the $NADH/NAD^+$ ratio in the matrix is high. In this context, there is an accumulation of electrons because not all can enter to the

respiratory chain and the mitochondria is subjected to dangerous oxidative stress, since ROS can react with proteins, membrane lipids and nucleic acids. To deal with this problem, the cell defends itself thanks to what are known as antioxidant mechanisms. Antioxidants are enzymes or nonenzymatic agents with the ability of eliminate ROS or prevent the formation of them. The group of antioxidant enzymes is composed by the superoxide dismutase as well as various peroxidases like catalase and glutathione peroxidase. To prevent oxidative damage by superoxide radical ($^{\bullet}O_2^-$), cells have the enzyme superoxide dismutase, which catalyzes the transformation of $^{\bullet}O_2^-$ in hydrogen peroxide (H_2O_2). The hydrogen peroxide thus generated is neutralized by glutathione peroxidase. The oxidized glutathione is then recycled by the glutathione reductase in the presence of NADPH (Fig. 6) (58). Examples of nonenzymatic antioxidants are vitamins C and E, carotenoids, flavonoids, glutathione, hormones such as melatonin and synthetic compounds as N-acetylcysteine (NAC). Some of these antioxidants are water-soluble, located in the cytosol, while others are liposoluble and are found in cell membranes (60-63). Importantly, CoQ is an important nonenzymatic antioxidant in the cell, as it will be explained later.

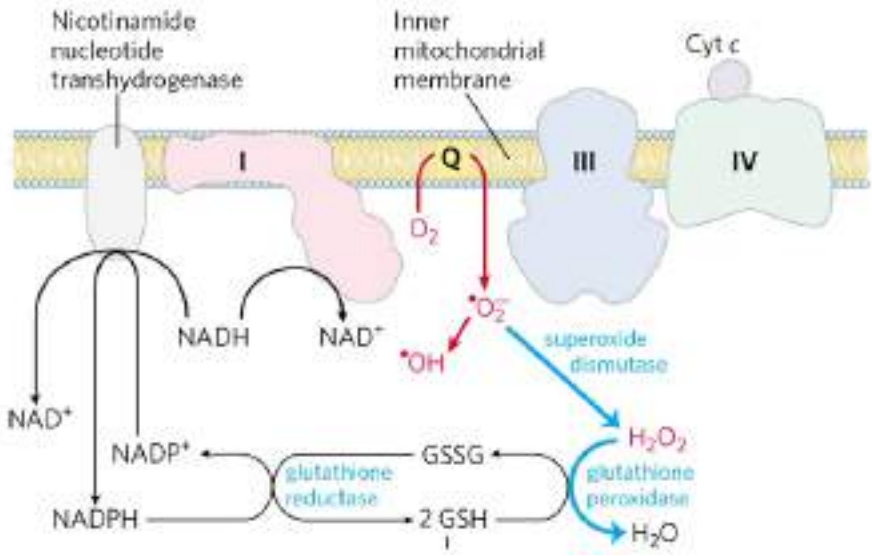

Figure 6. ROS formation in mitochondria and mitochondrial enzymatic antioxidant systems.

The superoxide free radical generated is highly reactive. Its formation also leads to the production of the even more reactive hydroxyl free radical (•OH). The reactions shown in blue defend the cell against the damaging effects of superoxide (58).

1.1.1.3.1.2 The OXPHOS System is structured in supercomplexes

For a long time, the structural organization of the electron transport chain complexes has been an interesting subject to contemplate. Since the discovery of these complexes, two main models, known as the "solid-state" and "fluid-state" models, were proposed to explain the structural organization of the complexes in the inner mitochondrial membrane (64).

The "solid-state" model was first introduced by Chance and Williams in 1955 (65). Their pioneer studies suggested the capability of

the electron transport chain (ETC) and OXPHOS proteins to form a functional unit termed "oxysome," which could facilitate electron transfer and ATP synthesis (66). This model could logically explain the structural proximity of the complexes to support their functional integrity. At the same time, elucidation of the physical and chemical properties of isolated complexes revealed that individual complexes could function separately and undergo oxidation-reduction (67).

The general vision gradually evolved into a "fluid-state" (or "random-collision") model, proposed by Hackenbrock and co-workers, in which all proteins and redox components of ETC and OXPHOS diffuse freely and randomly in the IMM (68). Since two decades ago, analysis of digitonin-solubilized mitochondrial proteins by blue native polyacrylamide gel electrophoresis (BN-PAGE) (69) enabled to separate high molecular mass multiprotein complexes with relatively preserved protein-protein interactions. By using this technique, ETC complexes were found to assemble into the multiprotein complexes or respiratory chain supercomplexes (SCs) in yeast and mammalian mitochondria (64). In eukaryotes, supercomplexes formed by complexes I, III and IV, together with CoQ and cyt c, the so-called respirasomes, have been observed at least in mitochondria of bovine heart (70, 71) and mouse liver (72). Associations of complexes III and IV have also been described in these organisms, as well as in *Saccharomyces cerevisiae*. Complex II, however, has not been proven to be in association with any other complex. There is clear consensus regarding the benefits it may bring to oxidative phosphorylation in the channeling of electrons, sequestration of ROS, induction of mitochondrial cristae shape and structural stabilization of individual complexes (73).

However, only certain fractions of individual complexes are assembled into the SCs. Based on this point, alternative studies by Ferguson- Miller and collaborators, and later by Schägger and Pfeiffer, formulate the "dynamic aggregate" or "plasticity" model (69, 72, 74, 75). In this model, there is a dynamic equilibrium between freely diffusing and associated-forms of the mitochondrial respiratory chain components. Therefore, the plasticity model reconciled the two classical models. The new representation of the respiratory chain defends the reversible association and the free lateral diffusion of all components simultaneously. Moreover, the transient formation of specific mitochondrial respiratory chain aggregates ensures more efficiency in the transfer of electrons as well as facilitates the regulation of the process (76).

Significant achievements in the understanding of the structural organization of SCs initiated new studies to understand the role of SCs in mitochondria in health and disease. A large number of studies using cell/animal models of human diseases, and biological samples from patients demonstrated disintegration of SCs during cardiovascular, and neurodegenerative disorders, Barth syndrome, diabetes, and aging, whereas exercise was found to stimulate SC assembly. In contrast, several studies were not able to find an associative link between diseases and SCs. Besides, the roles of SCs in substrate channeling and ROS prevention have been challenged (64).

1.1.2 The Coenzyme Q

CoQ is, as previously mention, a unique electron carrier in the mitochondrial respiratory chain (Fig. 5). Moreover, CoQ also receives electrons from other different mitochondrial enzymes that support different key aspects of the mitochondrial metabolism. Historically, the discovery of CoQ was the result of a long train of investigation into the mechanism of, and compounds involved in biological energy production (77). CoQ was first isolated in 1955 (78) but it was not until two years later that its presence and function in the respiratory chain were described (79). Following studies set light about CoQ cellular localization and chemical structure (80, 81). Finally, in 1978, Peter Dennis Mitchell was awarded the Nobel Prize in Chemistry "for his contribution to the understanding of biological energy transfer through the formulation of the chemiosmotic theory", where CoQ was included for its role in mitochondrial respiration.

1.1.2.1 Coenzyme Q: Structural and Physico-Chemical characteristics

CoQ or 2,3-dimethoxy-5-methyl-6-(polyprenyl)-1,4-benzoquinone is a lipophilic molecule composed by a benzoquinone ring hydroxylated in positions 1 and 4, linked to a lateral isoprenoid chain (Fig. 7A). The benzoquinone ring is responsible for the redox characteristics of the CoQ while the isoprenoid chain confers its hydrophobic character and solubility in polar solvents. It is assumed that the isoprenoid side chain stabilizes the molecule in the middle of the membrane bilayer while the quinone head moves from inside to the membrane surface depending on

its redox state, being the reduced form the one that predominantly moves to the surface because of its more polar character (82).

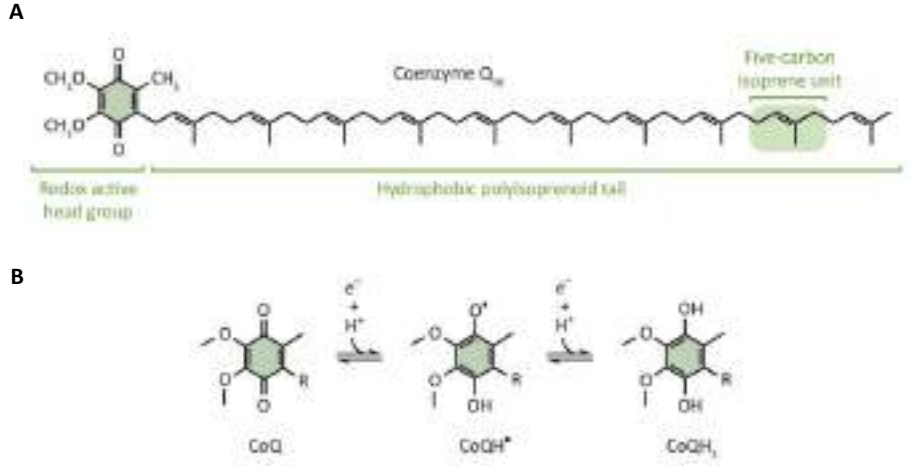

Figure 7. Coenzyme Q_{10} structure and redox cycle.

(A) Chemical structure of CoQ_{10}.

(B) Redox cycle of the CoQ head group. 'R' indicates the polyisoprenoid tail. CoQ or ubiquinone can accept one electron, becoming the ubisemiquinone radical (CoQH•), or two electrons, forming ubiquinol ($CoQH_2$) (83).

The benzoquinone ring of CoQ can be found in its completely oxidized form, named ubiquinone (CoQ); the semi-reduced form (ubisemiquinone, CoQH•) is originated after the addition of one proton and one electron; and the completely reduced form (ubiquinol, $CoQH_2$) is produced after receiving a second proton and electron (Fig. 7B) (59).

The lateral isoprenoid chain length is variable. Attending to this parameter, a major form of CoQ is found in each specie. In humans, the major CoQ form has 10 isoprene units (CoQ_{10}), as well as in zebrafish (*Danio rerio*) and *Schizosaccharomyces pombe*. CoQ with 9 isoprene units in its lateral chain (CoQ_9) is the major form in mice,

Caenorhabditis elegans and plants; with 8 units (CoQ_8) in *Escherichia coli*; and with 6 units (CoQ_6) in *Saccharomyces cerevisiae* (84). In some species, it is also possible to detect a minor form of CoQ, in addition to the dominant one, as CoQ_9 in humans or CoQ_{10} in mice. The reason of this variability is still unknown.

1.1.2.2 Biosynthesis of Coenzyme Q: the Complex Q

CoQ biosynthesis is located in the mitochondrial inner membrane. The biochemical pathway is not completely understood but it is proved that a group of nuclear-encoded COQ proteins participates (85) (Fig. 8). Nevertheless, some authors suggest that CoQ biosynthesis is not limited to mitochondria, and it is also located in other cellular compartments, specifically in the endoplasmic reticulum (ER)-Golgi system (86, 87). Moreover, it is important to highlight the communication between these two organelles in what is known as endoplasmic reticulum-mitochondria encounter structure (ERMES). In fact, a study in yeast showed that ERMES is involved in the coordination of CoQ biosynthesis in mitochondria (88).

The CoQ biosynthetic process in the mitochondria is similar in prokaryotes and eukaryotes. It starts with the condensation of a long polyisoprenoid lipid tail and a benzenoid precursor. Then, the benzenoid ring is modified in successive reactions to get the final CoQ structure (89, 90) (Fig. 8). Additionally, some of the proteins implicated in the biosynthetic process are assembled into a high molecular mass complex, named Complex Q (CoQ-synthome in yeast) (Fig. 8). The objective of

this association is to minimize the escape of intermediates and to improve the catalytic efficiency of the CoQ biosynthetic pathway (83).

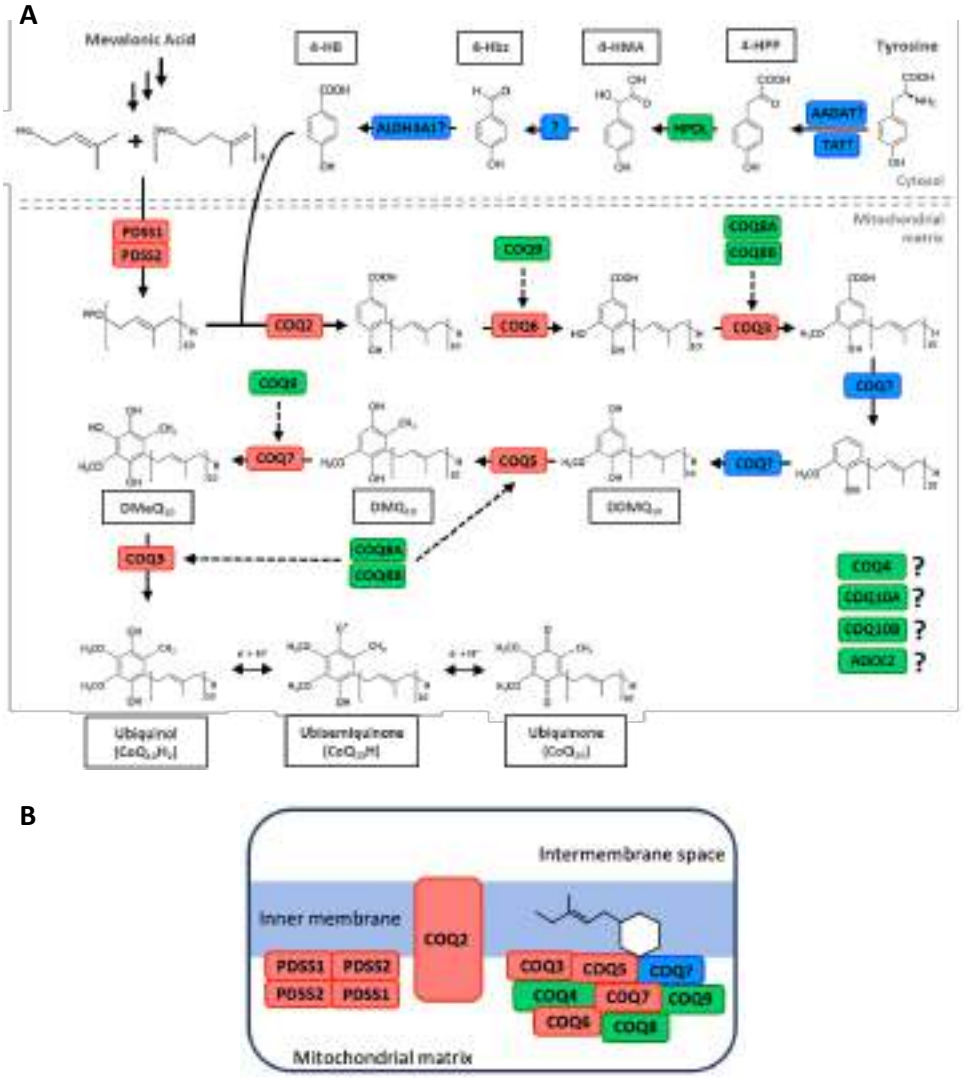

Figure 8. Coenzyme Q_{10} biosynthetic pathway.

(A) Proteins involved in the biosynthesis of CoQ_{10}. Red color indicates proteins with enzymatic activity. Green color indicates proteins with regulatory function. Blue color shows currently unidentified enzymes.

(B) Model of human CoQ_{10} biosynthetic complex, containing at least COQ3–COQ9 and lipids, such as CoQ itself.

4-HB = 4-hydroxybenzoic Acid; 4-Hbz = 4-Hydroxybenzaldehyde; 4-HMA = 4-Hydroxymandelate; 4-HPP = 4-Hydroxyphenylpiruvate; DDMQ = demethoxy-demethyl-ubiquinone; DMQ = demethoxyubiquinone; DMeQ = demethylubiquinone (59).

The precursors for CoQ biosynthesis are negatively charged small molecules that cannot passively cross the IMM. The mechanism involved in the transport of these polar CoQ precursors from their site of production outside of mitochondria into the mitochondrial matrix is unclear. Additionally, the COQ proteins also have to be transported into the mitochondrial matrix as they are encoded by nDNA. The specific mitochondrial import and processing pathways of COQ proteins remains not well defined. However, some transcriptional regulators (91) and post-transcriptional coordinators (92) of CoQ biosynthesis have been identified. Moreover, cycles of phosphorylation/dephosphorylation have been proposed as regulators of the process as well as a possible protease processing of COQ proteins (93, 94).

4-Hydroxybenzoic acid (4-HB) is the precursor of the benzoquinone ring of CoQ (95), although some other alternative ring precursors have being postulated (85). In mammals, 4-HB is derived from phenylalanine or tyrosine (Tyr) (96). However, bacteria and yeast can produce 4-HB *de novo* through the shikimate pathway (97-99) and yeast can also use p-aminobenzoate (pABA) as an alternative for the synthesis of the benzoquinone ring (100, 101). The sequence of reactions involved in the synthesis of 4-HB from Tyr is still unclear. It seems that tyrosine suffers a transamination to produce and intermediate called 4-hydroxyphenylpyruvate (4-HPP). The mammalian enzymes linked to the tyrosine transamination remain unidentified, but the mitochondrial

alpha-aminoadipate aminotransferase (AADAT) and the tyrosine aminotransferase (TAT) are possible candidates. Later, 4-HPP is used by the hydroxyphenylpyruvate dioxygenase-like protein (HPDL) to produce 4-hydroxymandelate (4-HMA). Afterwards, some not known reactions are needed to generate 4-hydroxybenzaldehyde (4-HBz). Finally, the ALDH3A1 has been proposed to catalyze the dehydrogenation of 4-HBz to generate the complete structure of 4-HB in mammals (83, 102).

In eukaryotes and some prokaryotes, CoQ side-chain comes from a polyisoprenoid lipid tail that is synthesizes in the mevalonate pathway (103). The precursors for the lipophilic polyprenyl tail are the dimethylallyl pyrophosphate (DMAPP) and the isopentenyl pyrophosphate (IPP). Both compounds are condensed by COQ1 in yeast and PDSS1/PDSS2 in humans and mice. Therefore, the responsible for the length of the polyprenyl tail is the heterotetramer PDSS1/PDSS2 (83, 103). PDSS1/PDSS2 are not associated with the Complex Q. It may be peripherally associated with the inner mitochondrial membrane (104).

Then, COQ2 or p-hydroxybenzoate:polyprenyl transferase, catalyzes in mammals the condensation of the polyisoprenoid tail to the ring precursor, generating the first membrane-bound CoQ intermediate (105). COQ2 is also not associated with the Complex Q. However, it acts as an integral membrane protein in the inner mitochondrial membrane.

From this step, the fully substituted benzoquinone ring of CoQ is produced after a total of seven reactions (one decarboxylation, three hydroxylation, and three methylation) (95). The hydroxylation in

position C5 is catalyzed by COQ6, the O-methylations by COQ3, the methylation in position C2 by COQ5 and the hydroxylation in C6 by COQ7. Unidentified proteins catalyze the hydroxylation and decarboxylation in position C1 (106-109). Additionally, there are some proteins without catalytic activity but necessary for CoQ synthesis. However, their exact functions are poorly understood. In humans and mice, these proteins are COQ4, COQ8A (also known as ADCK3), COQ8B (also known as ADCK4), COQ9, COQ10A, and COQ10B (110-115). The malfunction of any of these proteins induces a reduction in CoQ levels.

COQ4 is required for efficient CoQ biosynthesis because it has been suggested that it stabilizes Complex Q as scaffold protein that binds both proteins and lipids. However, the exact mechanism is unknown (83).

COQ8A and COQ8B enhance CoQ biosynthesis too. A physical and functional interaction between COQ8 and COQ5 may be particularly important (116). Initially, it was proposed a protein kinase activity for COQ8A and COQ8B (117). Furthermore, COQ8A was shown to bind lipid CoQ intermediates and have ATPase activity. Based on these findings, new models for COQ8A function were presented. One of them included the possibility that it acts primarily as an ATPase to facilitate the assembly of the Complex Q and the biosynthesis of CoQ. The other one supposed that its ATPase activity is indicative of small molecule or lipid kinase activity against an undiscovered substrate (104, 118).

COQ9 is required for CoQ biosynthesis as a member of the Complex Q and is peripherally associated with the inner mitochondrial membrane,

on the matrix side (119). COQ9 interacts physically and functionally with COQ7 to enhance the C6-hydroxylation reaction (120) being essential for COQ7 stability and activity (113). In fact, the presence of both human and mouse COQ9 and COQ7 are needed for the hydroxylation step catalyzed by COQ7 (120). In human cells and mice, a deficiency in COQ9 accumulate DMQ (demethoxyubiquinone), the same intermediate that accumulates in COQ7 deficient cells (113, 116, 121). An alternative/complementary model is that COQ9 is a lipid sensor that allosterically regulates Complex Q upon ligand binding, so it could provide DMQ to COQ7 (83).

COQ10A and COQ10B are not directly involved in CoQ biosynthesis. However, it seems to be required for efficient function and biosynthesis of CoQ because CoQ biosynthesis is less efficient in yeast with COQ10 mutations, and the CoQ produced is used less efficiently for OXPHOS (122). Thus, it is suggested that COQ10 might function as a lipid chaperone involving delivery of CoQ from site of synthesis to sites of function (83, 104).

1.1.2.3 Coenzyme Q Functions

Since its discovery, the major function attributed to CoQ is the transport of electrons between respiratory complexes in the inner mitochondrial membrane, being a key factor contributing to generate the membrane potential that is coupled to the oxidative phosphorylation. CoQ is also an important endogenous antioxidant. It is able to act as a radical scavenger but it can also support synergistically other cellular antioxidant components. In the last half of the 20th century, CoQ research

has been focused in the bioenergetics and antioxidant CoQ functions. Nevertheless, in the first decades of the new millennium, research has revealed novel functions of CoQ. More in-depth studies have focused on its role as cofactors of the uncoupling proteins (UCPs), in its regulation of the mitochondrial permeability transition pore (mPTP) and, more recently, in its key metabolic function linked to the Q-Junction (123, 124).

1.1.2.3.1 Coenzyme Q in the OXPHOS System

As it was previously mentioned, CoQ plays a central role in the mitochondrial electron transport chain, as it accepts electrons from complex I and/or from complex II and transfer them to complex III. Other electron mobile carrier, the cyt c transfers the electrons from complex III to complex IV. Moreover, CoQ is an essential component in the mitochondrial SCs, the supramolecular organization that joins the mitochondrial individual complexes in one single structure in order to improve the transfer of electrons in the mitochondrial respiratory chain. Classically, it was supposed that CoQ was free in the mitochondrial membranes in a homogeneous pool ready to be used by any enzyme that needed it (125). Nowadays, thanks to the supramolecular organization of complexes in SCs, it has been demonstrated that the CoQ molecules are divided in two different pools (126):

(a) the CoQ_{NADH} pool is linked to the SCs I+III and it is exclusively dedicated to the oxidation of NADH.

(b) the CoQ_{FADH} pool is a free pool available for CII or any other enzyme that uses CoQ as a cofactor.

Both pools are closely connected and adapt its composition to the system requirements. Importantly, it is demonstrated that the CoQ redox status acts as a metabolic sensor that modulate the configuration of the mitochondrial electron transport chain in order to adapt to the prevailing substrate profile (127). This modulation by the $CoQH_2$/CoQ ratio affects to the direction of the electrons flow and the formation of mitochondrial complexes/supercomplexes. If there is a decrease in the NADH/$FADH_2$ ratio, as a consequence of an energy shift from glucose to fatty acids, the CoQ_{FADH} pool can be over-reduced and the electron flux could be reversed in order to reduce NAD+ through the CoQ_{NADH} pool (126). This reverse electron transport (RET) from CoQ to NAD+ has two important implications for the cell. First, an increase in the scape of electrons and secondly, an enhancement in the production and accumulation of ROS (126, 128). This oxidative damage is specially localized at CI and it leads to the degradation of the complex. Immediately, there is the release of CIII and CoQ_{NADH} pool from the SCs. This CoQ_{NADH} pool free is then used to restore the oversaturated CoQ_{FADH} pool (124, 126, 127).

1.1.2.3.2 Coenzyme Q as Antioxidant

All along the electron transport chain, the leakage of electrons is the origin for the formation of ROS. These ROS induce oxidative damage in the cell due to the oxidation of lipids, proteins and DNA. Antioxidants can be enzymes or nonenzymatic agents with the ability of eliminate ROS or prevent the formation of them. Between the agents without

enzymatic activity, stand out glutathione, carotenoids, vitamins C and E, melatonin and the CoQ (80).

Coenzyme Q is an effective antioxidant of lipid peroxidation. Specifically, the reduced form of CoQ, ubiquinol or $CoQH_2$, inhibits the free radicals attack to lipids containing carbon-carbon double bond. The basis of this antioxidant role is complex. It has been described to be related to the interaction of CoQ during the peroxidation process (129). Lipid peroxidation is divided in three steps: initiation, propagation and termination. First, ROS remove a hydrogen from a polyunsaturated fatty acid, forming the carbon-centered lipid radical (L•). Secondly, a molecule of oxygen reacts with the lipid radical and lipid peroxy radical (LOO•) is formed. This LOO• radical will react and generate a new L• radical that continues the process (130). $CoQH_2$ is a potent inhibitor of lipid peroxidation because it is able to reduce the initiation and propagation steps. $CoQH_2$ interferes with the perferryl radical ($Fe^{3+}O_2$•) in the initial step, preventing the formation of the LOO• radical and the consequent propagation of the peroxidation. Moreover, LOO• radical can be directly removed by $CoQH_2$ in the termination step by the addition of a hydrogen atom to the radical. Other antioxidants, like vitamin E, can also participate in this final step and form nonradical products. Related to this, $CoQH_2$ has demonstrated its capacity to regenerate vitamin E, enhancing its effect as antioxidant not only due to its capability to directly reduce ROS but also to regenerate other antioxidants (Fig. 9) (80, 129, 131).

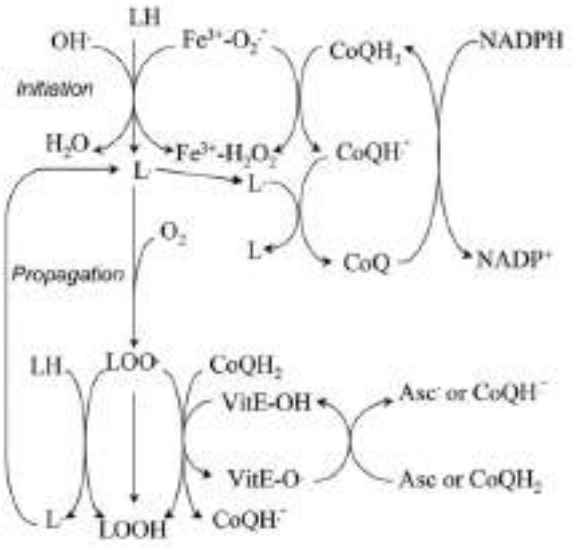

Figure 9. Coenzyme Q antioxidant role in lipid peroxidation.

LH, polyunsaturated fatty acid; $OH^{\bullet}$, hydroxyl radical; Fe^{3} $O_2^{\bullet -}$, perferryl radical; $CoQH_2$, reduced coenzyme Q; $CoQH^{\bullet -}$, ubisemiquinone; L•, carbon-centered radical; LOO•, lipid peroxyl radical; LOOH, lipid hydroperoxide; VitE-O•, vitamin E radical, asc•, ascorbyl radical (129).

The antioxidant effect of CoQ is not only limited to prevent lipid peroxidation. CoQ plays an important role in defending proteins from oxidation. Protein oxidation is linked with several mechanisms. It seems that the direct oxidation of amino acids residues is the most common of them. Nevertheless, the oxidation by lipid-derived free radicals can also occur. These compounds produce intra and intermolecular cross-linking in the protein structure due to covalent unions with basic amino acid residues. The surrounding mechanism for the protective effect of CoQ against protein oxidation has not been elucidated but it is related with the close distribution of CoQ and proteins in the membrane (129, 132). However, CoQ does not protect against all types of oxidative protein

oxidative damage (133). Additionally, it has been demonstrated that the effect of CoQ antioxidant also protects DNA from oxidation (134).

1.1.2.3.3 Coenzyme Q and Uncoupling Proteins (UCPs)

Uncoupling proteins (UCPs) are other mitochondrial components susceptible to be regulated by redox reactions. UCPs are localized in the inner mitochondrial membrane and they return the protons pumped by the respiratory chain in the intermembrane space to the mitochondrial matrix. Expressed differently, UCPs produce an uncoupling of the electron transport chain from the oxidative phosphorylation, dissipating stored energy as heat rather than producing ATP. That is the main mechanism involved in thermogenesis in the brown adipose tissue of mammals (135). Besides their role in thermogenesis, other potential roles of the UCP variants are thought to have an impact in obesity, diabetes, fatty acid metabolism, suppression of oxygen radicals, and, thus, aging and neurodegeneration (136). Five different UCPs forms have been described: UCP1, UCP2, UCP3, UCP4 and UCP5. UCP2 and UCP3 are present at much lower abundance than UCP1, and the uncoupling with which they are associated is not significantly thermogenic (137). UCP4 and UCP5 seem to be specific of the CNS and they may induce the uncoupling in response to excessive mitochondrial ROS production due to very high mitochondrial membrane potential.

Physiological uncoupling of oxidative phosphorylation must be strongly regulated to avoid deterioration of the energy supply and cell death, which is caused by toxic uncouplers. In this context, some experimental evidence has suggested that CoQ is a cofactor for UCPs,

connecting CoQ with the control of thermogenesis (136, 138). *In vitro* studies in bacteria found that CoQ is an obligatory cofactor for proton transport by UCP1 in liposomes. As CoQ is not a proton carrier, its role is supposed to be regulatory. Moreover, it suggests that the uncoupling activity of UCP1 depends on the redox state of CoQ thus the transport of protons was activated only by oxidized but not reduced CoQ. Additionally, the length of the CoQ chain seems to be also an important factor in UCPs function being short-chain forms of CoQ less effective (138). Further studies with UCP2 and UCP3 showed that the activity of both UCPs require CoQ (136).

Interestingly, the role of CoQ as a cofactor for UCPs is not only limited to the control of thermogenesis. It has been also related with an alternative mechanism for decreasing ROS inside mitochondria via UCPs-superoxide interaction. Superoxide increases mitochondrial proton transport through UCPs becoming a mechanism for decreasing the concentrations of ROS inside mitochondria. CoQ might mediate the activity of UCPs through the production of superoxide because the activation of UCPs by CoQ was abolished by superoxide dismutase. Additionally, if CoQ was replaced by xanthine plus xanthine oxidase (an exogenous system that generates superoxide) the proton transport increased, indicating that CoQ acted in mitochondria through the production of superoxide (137).

However, the role of CoQ in the regulation of the UCPs remains controversial, as other studies have rejected the connection between CoQ and UCPs (139, 140).

1.1.2.3.4 Coenzyme Q and the Mitochondrial Permeability Transition Pore (mPTP)

Mitochondrial membranes have intrinsically low permeability to ions and solutes. This fact is essential for the maintenance of the electrochemical gradient generated during electron transfer. In the inner mitochondrial membrane, there are located a series of channels and ionic transporters named as mitochondrial permeability transition pores (mPTP). mPTP are a Ca^{2+} sensitive channels that mediate cell death both in the context of necrosis and of apoptosis (141, 142). In a series of studies, several CoQ analogs have been tested to show that the mPTP is modulated by quinones, existing a quinone-binding site directly involved in mPTP regulation whose occupancy modulates its open-closed transitions, possibly through secondary changes of the Ca^{2+} binding affinity. Interestingly, quinones with very different structural features may have qualitatively similar effects on the mPTP while minor structural changes profoundly modify the effects of quinones (143, 144). CoQ seems also to prevent mPTP opening based on a study that demonstrated *in vitro* that CoQ provided effective protection against apoptosis of rabbit keratocytes. Experimentally, CoQ demonstrated its efficiency avoiding apoptosis by dramatically reducing apoptotic cell death as well as attenuating ATP decrease and hindered DNA fragmentation. Moreover, CoQ inhibits mitochondrial depolarization, cyt c release and caspase 9 activation. As all these events are related to mPTP opening, it was suggested that the antiapoptotic effect of CoQ could be related to its ability to prevent mPTP opening (145). Nevertheless, the regulation of mPTP by CoQ is not well stablished and more studies are required.

1.1.2.3.5 Coenzyme Q in Ferroptosis

Ferroptosis is a form of regulated cell death that is caused by the iron-dependent peroxidation of lipids. Classically, it has been considered that the enzyme glutathione peroxidase 4 (GPX4) controls ferroptosis. GPX4 modifies lipid hydroperoxides into non-toxic lipid alcohols and avoid lipids oxidation (146, 147). Recently, the ferroptosis suppressor protein 1 (FSP1) (previously known as apoptosis inducing factor mitochondrial 2 or AIFM2) has been described as a potent ferroptosis suppressor.

Figure 10. Anti-ferroptotic function of FSP1 mediated by Coenzyme Q.
Graphical abstract describing the anti-ferroptotic function of FSP1 as a glutathione-independent suppressor of phospholipid peroxidation by inhibition of lipid radical-mediated autoxidation, initiated by peroxyl radicals (PLOO•), of lipid bilayers. CoQ acts as a lipophilic radical-trapping antioxidant that stops the propagation of lipid peroxides (148).

Moreover, FSP1 has been identified as a key component of a nonmitochondrial CoQ antioxidant system that acts in parallel to the canonical glutathione-based GPX4 pathway. The data indicate that myristoylation recruits FSP1 to the plasma membrane, where it functions as an oxidoreductase that reduces CoQ. The reduced form of CoQ

removes lipid peroxyl radicals that mediate lipid peroxidation, whereas FSP1 catalyzes the regeneration of CoQ mediated by NADPH (148, 149) (Fig. 10). These findings indicate that the FSP1-CoQ-NADPH pathway exists as a stand-alone parallel system, which co-operates with GPX4 and glutathione to suppress phospholipid peroxidation and ferroptosis.

1.1.2.3.6 Coenzyme Q in the Q-Junction

The Q-junction is the functional structure located in the mitochondria that ensures the flow of electrons into the CoQ from complex I and complex II, and from other mitochondrial enzymes and pathways, and the further downstream of electrons to complex III and complex IV (Fig. 5) (124, 150).

In this context, CoQ receives electrons from:

- Electron transfer flavoprotein (ETF), together with the electron transfer flavoprotein-dehydrogenase (ETFDH). This protein forms a short electron transfer pathway that connect CoQ with the electrons produced in the fatty acid β-oxidation and amino acid catabolism from nine different mitochondrial flavin adenine dinucleotide (FAD)-containing acyl-CoA dehydrogenases (151).

- Dihydroorotate dehydrogenase (DHODH), which is directly involved in the reaction that obtain orotate from dihydroorotate within the pyrimidine *de novo* biosynthesis (152).

- Mitochondrial glycerol-3-phosphate dehydrogenase (G3PDH or GPD2), which is the enzyme responsible for the oxidation of glycerol-3-phosphate to dihydroxyacetone phosphate. The cytosolic form of glycerol-3-phosphate dehydrogenase (GPD1) reduced the dihydroxyacetone phosphate formed in the mitochondria back to glycerol 3-phosphate. This cycle allows the transport of the reducing equivalents of the cytosol (from NADH oxidation) to the mitochondria and its transfer via CoQ to the respiratory chain connecting the fatty acids metabolism and glycolysis with OXPHOS system (153).

- Choline dehydrogenase (CHDH), which is involved in the glycine metabolism and catalyzes the oxidation of choline to glycine betaine (154).

- Proline dehydrogenase and proline dehydrogenase 2 (PRODH and PRODH2), which participate in the first step in the oxidation of proline to glutamate. They are also related with glyoxylate and arginine metabolism (155).

- Sulfide:quinone oxidoreductase (SQOR), which is the first enzyme of the sulfide oxidation pathway, responsible for the detoxification of sulfide metabolism (H_2S). H_2S is oxidized by SQOR as two electrons are transferred to CoQ. The sulfur atom of H_2S is then transferred to an acceptor that can be a molecule of glutathione (GSH) or sulfite, leading to the production of glutathione disulfide (GSSH) or thiosulfate respectively (156).

Importantly, the implication of these CoQ-linked proteins in the Q-junction seem to be not the same in all cases, with tissues and cells specificities. Also, the CoQ deficiency seems to affect differently to the activities of the enzymes of the Q-junction, a fact that may be related with the compartmentalization of the CoQ pools. For instance, studies *in vitro*, in skin fibroblasts from patients with primary CoQ_{10} deficiency, and *in vivo*, in two different mouse models of primary CoQ deficiency, showed that CoQ deficiency produces a decrease in the protein levels and activity of SQOR, leading to a disruption in the sulfide metabolism (157, 158). Also, proteomics analysis in a mouse model of CoQ deficiency revealed that, at least in kidney, the levels of ETFDH, CHDH, DHODH, PRODH and PRODH2 are increased (120), most likely due to a compensatory mechanism. Nevertheless, it has not been yet evaluated the functional consequences of the changes of these CoQ-linked proteins in CoQ deficiency, as well as their response to therapies.

1.1.2.3.6.1 Coenzyme Q in the Q-Junction: sulfide metabolism

Sulfur is one of the first elements used as a nutrient by primitive life forms, together with other inorganic substances such as H_2, CO and N_2, in the production of energy and as structural molecule. The ability to oxidize sulfur and the connection of it with the energy production is conserved in higher eukaryotic organisms. In fact, for eukaryotes, sulfur is a source of energy to take into account since it facilitates reducing equivalents that are incorporated into the transport chain. Mammals assimilate dietary sulfur in the form of methionine and cysteine, amino

acids rich in this element and precursors of various sulfur-derived metabolites essential for cell homeostasis cell as H_2S and GSH (156).

In mammalian cells, H_2S metabolism involves the cytosolic transsulfuration pathway (biosynthetic) and the mitochondrial oxidation pathway (catabolic) (Fig. 11).

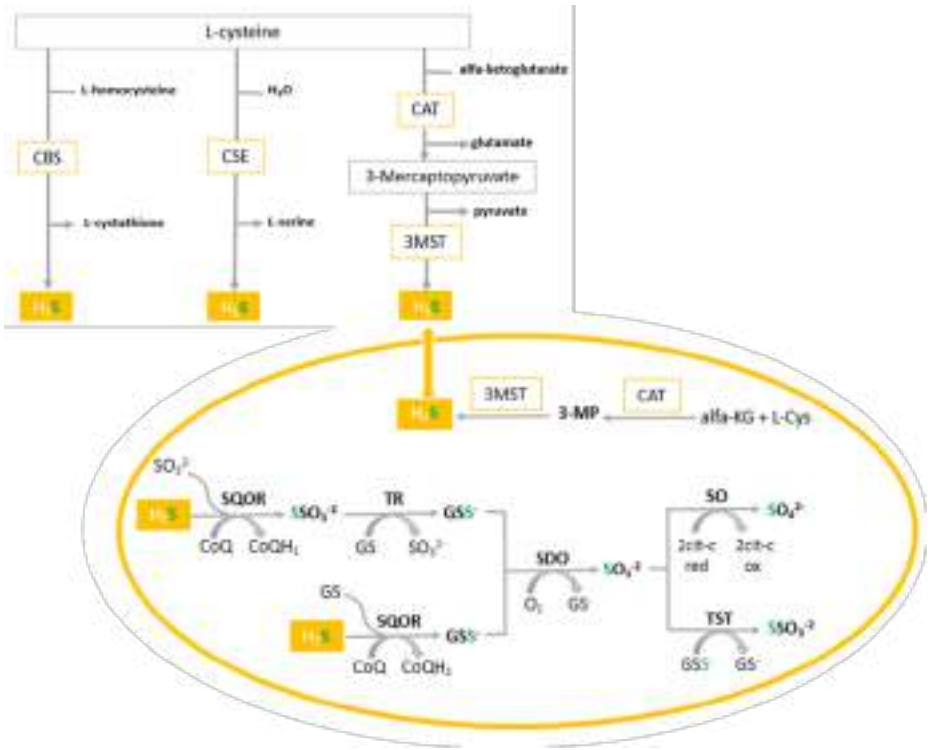

Figure 11. The biosynthetic (transsulfuration) and catabolic (oxidation) pathways of H_2S.

Transsulfuration pathway involves the enzymes cystathionine -synthase (CBS), cystathionine γ-lyase (CSE) and pyridoxal-50-phosphate (PLP)-independent 3-mercaptopyruvate sulfurtransferase (3MST). Mitochondrial H_2S oxidation pathway involves the enzymes sulfide:quinone oxidoreductase (SQOR), sulfur dioxygenase (SDO; also known as ETHE1 or persulfide dioxygenase), sulfite oxidase (SO), thiosulfate sulfurtransferase or rhodanese (TST) and thiosulfate reductase (TR).

H_2S is produced endogenously by two cytosolic enzymes, cystathionine β-synthase (CBS) and cystathionine γ-lyase (CSE), that participate in the desulfurization of cysteine or homocysteine. Similarly, H_2S is the product of the reaction catalyzed by the enzyme 3-mercaptopyruvate sulfurotransferase (3-MST), with both, cytosolic and mitochondrial localization, whose substrate is 3-mercaptopyruvate (156, 159, 160). The endogenous production of H_2S by each of these enzymes varies depending on the tissue, the concentration of the respective substrates and the expression level of each enzyme. CBS is active fundamentally in the nervous system, liver and kidney; CSE in liver, intestine, smooth muscle and pancreas; and 3-MST in the nervous system (especially in the cerebellum), in the kidney and in the vascular endothelium (157). Another important source of H_2S is the microbiota that colonizes the gastrointestinal tract of mammals. The genus *Desulfovibrio* is the main producer of H_2S in mammals since it is capable of carrying out sulfate reduction. Furthermore, some anaerobic bacteria such as *Echerichia coli*, *Salmonella enterica*, *Clostridia* and *Enterobacter aerogenes* generate H_2S from cysteine. Finally, H_2S is also the product of the action of sulfite reductase from *Rhodococcus, Salmonella, Enterobacter, Klebsiella, Bacillus, Staphylococcus* and *Corynebacterium* (161).

Furthermore, in mammals, at least four enzymes are involved in the catabolism of H_2S located in the mitochondria. The first of the enzymes involved in this pathway is, as previously mentioned, the sulfide:quinone oxidoreductase (SQOR), located in the inner mitochondrial membrane. H_2S is oxidized by SQOR and two electrons are transferred to CoQ. In parallel, the atom of sulfur transferred to a molecule of GSH or to a one

of sulfite, leading to the production of GSSH or thiosulfate, respectively. In the last case, the sulfur atoms of the thiosulfate can be transported by another sulfurotransferase called thiosulfate reductase (TR), with sulfate resulting excreted in the blood and eliminated in the urine, also obtaining GSSH. Next, a sulfide dioxygenase (SDO or ETHE1 - ethylmalonic encephalopathy dioxygenase) transforms GSSH, in sulfite, releasing GSH. Sulfite can be oxidized to sulfate by sulfite oxidase (SO) or to thiosulfate by the action of thiosulfate sulfurotransferase or rhodanase (TST) (162, 163).

Traditionally, H_2S has been considered exclusively as a toxic gas and an environmental hazard due to its inhibition of mitochondrial complex IV and the consequent blockade of the electron transport chain and the production of ATP. Nevertheless, in the last decades, H_2S has been attributed to multitude regulatory functions in the cell. H_2S is involved in numerous physiological functions related to cell proliferation, angiogenesis, cardiovascular protection, nerve development, prevention of oxidative stress and apoptosis, among others. (164). However, it is important to take into account the biphasic effect of this molecule depending on its local concentration. Generally, the effects observed at low concentrations are beneficial while those produced by high concentrations usually give rise to pathological phenomena or toxicity. That is the reason why the regulation of the oxidation and transsulfuration pathways have emerged as essential mechanism for control H_2S levels. This idea has been demonstrated in mice with Crohn diseases where there is a proliferation of microbial producers of H_2S as well as a reduction of H_2S oxidation pathway. The administration of H_2S scavengers significantly improved the phenotype and reduced the

progression of the disease (165). Additionally, as CoQ is a cofactor of SQOR, the first oxidation enzyme in the degradation of H_2S, it has been established that at concentrations between 1-10 μM, H_2S is used to maintain the electron transport chain and produce ATP in mammalian cells (160).

1.2. Mitochondria in Disease

Mitochondria plays a vital role in human health. Therefore, any dysfunction in this cellular organelle can trigger a wide variety of pathologies, especially in those tissues with high energy demand. In fact, primary mitochondrial dysfunction is associated with a wide variety of clinical manifestations that are included in what are known as mitochondrial diseases. Mitochondrial disorders are individually considered rare diseases (166, 167). In the European Union, a rare disease is, by definition, a disease that affects less than 1 in 2,000 people. In the United States, a rare disease is defined as the one that affects less than 200,000 people. Despite its low prevalence, it is considered that around 7% of the global population suffers from a rare disease, being between 27 and 36 million patients only in Europe. Nowadays, there have been described around 7,000 of different, life-threatening or chronic, rare diseases having the majority of them a genetic origin. As most of rare diseases have no available treatment, it has become a major public health concern due to their socioeconomic impact and the need to develop new sustainable health policies (168, 169). Mitochondrial diseases are one of the most common hereditary syndromes and it is an excellent example of the problems associated to the development of effective therapeutic options for rare diseases. Currently, there is no

available treatment for most of the mitochondrial disorders. The therapeutic option is usually limited to palliative cares and, given the relentlessly progressive nature of mitochondrial diseases, often worsening over time, it causes significant morbidity and mortality (166, 170).

1.2.1. Mitochondrial Diseases

Mitochondrial disease is the collective term for a heterogeneous group of genetic disorders characterized by defective oxidative phosphorylation. These disorders are clinically diverse and can manifest in the neonatal phase, childhood or adulthood. The prevalence of childhood-onset (<16 years) mitochondrial diseases has been estimated to range from 5 to 15 cases per 100,000 individuals. Moreover, mitochondrial diseases can involve any organ or tissue. Mostly, involve multiple systems, typically affecting organs that are highly dependent on aerobic metabolism. The heterogeneity in the clinical manifestation of mitochondrial diseases means that both diagnosis and management of these disorders are extremely difficult (52, 171).

The pathophysiology of mitochondrial diseases is complex because it is marked with a great genetic, clinical and biochemical heterogeneity. From a genetic point of view, mitochondrial diseases can be caused by mutations in the mtDNA or by mutations in the nDNA. nDNA mutations can be inherited autosomal or X-linked. On the other hand, mDNA mutations are always inherited from the mother. Some cases of *de novo* mutations have also been reported. Genetics heterogeneity is more complex in patients with mtDNA because mtDNA mutations are usually

heteroplasmic. It means that in the same cell there is a mix of mutated and wild-type mtDNA. Typically, heteroplasmy determines the cellular phenotype and high levels of mutated mtDNA (>50%) are required to result in cellular defects (52, 57, 172). Heteroplasmic point mutations have been associated to different clinical phenotypes, such as mitochondrial encephalomyopathy with lactic acidosis and stroke-like episodes (MELAS) (173), myoclonic epilepsy with ragged red fibers (MERRF) (174), neurogenic weakness, ataxia and retinitis pigmentosa (NARP) (175) and Leigh syndrome (LS). Leber's hereditary optic neuropathy (LHON) is one of the main disease associated with homoplasmic mtDNA mutations (176). Additionally, single deletions or duplications of mtDNA are implicated in sporadic progressive external ophthalmoplegia (PEO) , Kearns–Sayre syndrome (KSS) (177) and Pearson's syndrome (178). Mutations in the nDNA have affected to proteins involved in mtDNA maintenance and/or replication machinery, structural subunits of the respiratory chain complexes, assembly factors of the respiratory complexes, components of the translation apparatus and proteins of the execution pathways, such as fission/fusion and apoptosis (171, 179) (Fig. 12). This clinical heterogeneity suggests that multiple pathogenic and adaptive mechanisms are involved in the clinical manifestations of mitochondrial diseases. Recently, the remodeling of folate cycle, and its link to H_2S and nucleotides metabolism, have been proposed as novel mechanisms contributing to the pathophysiological features of mitochondrial diseases (157, 158, 180-183).

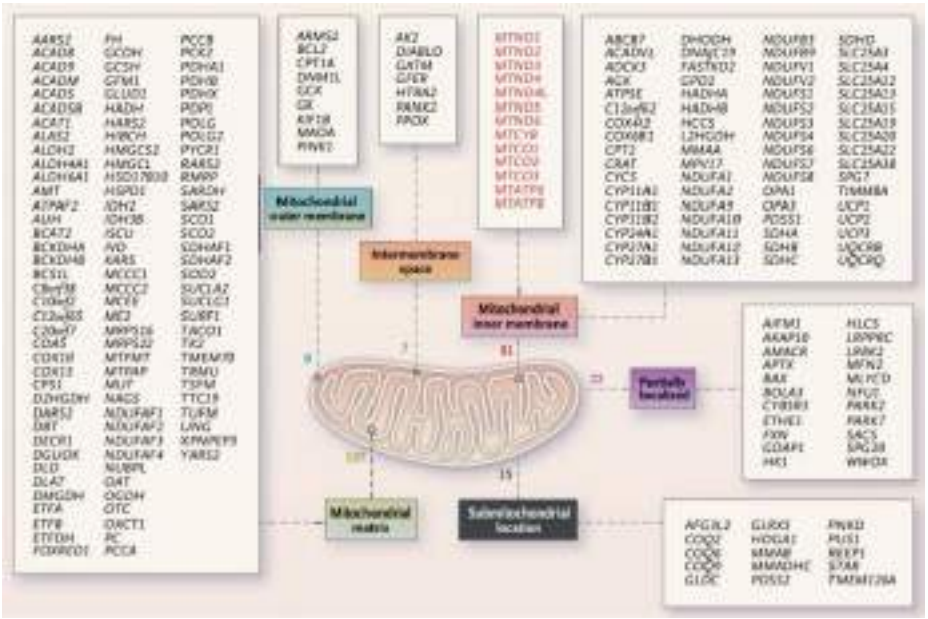

Figure 12. Mutations in genes that encode for mitochondrial proteins linked to human diseases.

Currently identified mtDNA-encoded (red) and nDNA-encoded (black) genes associated with mitochondrial diseases in humans when mutated. The genes are categorized according to the predicted localization of their corresponding proteins in the mitochondrial matrix (107 genes), the outer membrane (9 genes), the intermembrane space (7 genes), and the inner membrane (81 genes). Also included are gene products of unknown submitochondrial location (15 genes) and gene products that partially localize to mitochondria (22 genes) (179).

Therapeutic strategies in mitochondrial diseases can be classified in two groups: the "generalist" strategies that could be applied to a wide spectrum of different disease conditions, and "disease-tai-lored" strategies, specific for a single disease. The first group includes: (a) regulation/activation of mitochondrial biogenesis; (b) regulation/activation of mitochondrial autophagy; (c) inhibition of mitochondrial apoptosis; (d) scavenging of toxic compounds; (e) bypass of electron transfer chain defects; and (f) nuclear transfer. The second

group includes (a) scavenging of specific toxic compounds in specific diseases, (b) supplementation of nucleotides, and (c) gene- and cell-replacement therapies. Each of these strategies can be pursued by different approaches, such as pharmacological treatments, gene transfer to express the missing or a therapeutic protein, stem-cell/organ transplantation (57). In general, CoQ_{10} supplementation is recommended for patients with mitochondrial disorders or other diseases with secondary mitochondrial dysfunction, and clinical improvements have been reported in some cases, but others do not show any positive response. The therapeutic mechanisms of CoQ_{10} supplementation in the treatment of mitochondrial disorders can be explained by the development of secondary CoQ_{10} deficiency, which frequently occurs (184-187).

1.2.1.1. Mitochondrial Diseases: Coenzyme Q Deficiency

CoQ is a key molecule for cellular metabolism and homeostasis. Nevertheless, CoQ levels can be severely reduced in a group of mitochondrial disorders known as CoQ deficiencies. Low CoQ levels in the clinic was first reported in 1989 in two sisters that, since early childhood, suffered from a myopathic and encephalopathic syndrome characterized by muscle weakness, abnormal fatigability, myoglobinuria and generalized seizure disorder or cerebellar symptoms. Both patients showed, in muscle, an important disruption in the OXPHOS system originated by a CoQ content of only 4% compared to the control CoQ content (188). From that moment, CoQ deficiency has been associated with a large number of different multisystemic manifestations. Nowadays, in the global population, it is estimated that 1 in 50,000

people is affected by a form of CoQ deficiency but only less than 1 in 3,000,000 is due to known pathogenic variants. Importantly, this occurrence is probably underestimated because the techniques of next-generation sequencing used in the diagnosis are not implemented worldwide (189, 190).

The identification of the genetic defect in CoQ deficiency is essential to differentiate primary forms, due to mutations in *COQ* genes, from secondary forms, due to mutations in genes not directly involved in the biosynthesis of CoQ or to not-genetic factors, like other physiological processes or pharmacological treatments (Fig. 13).

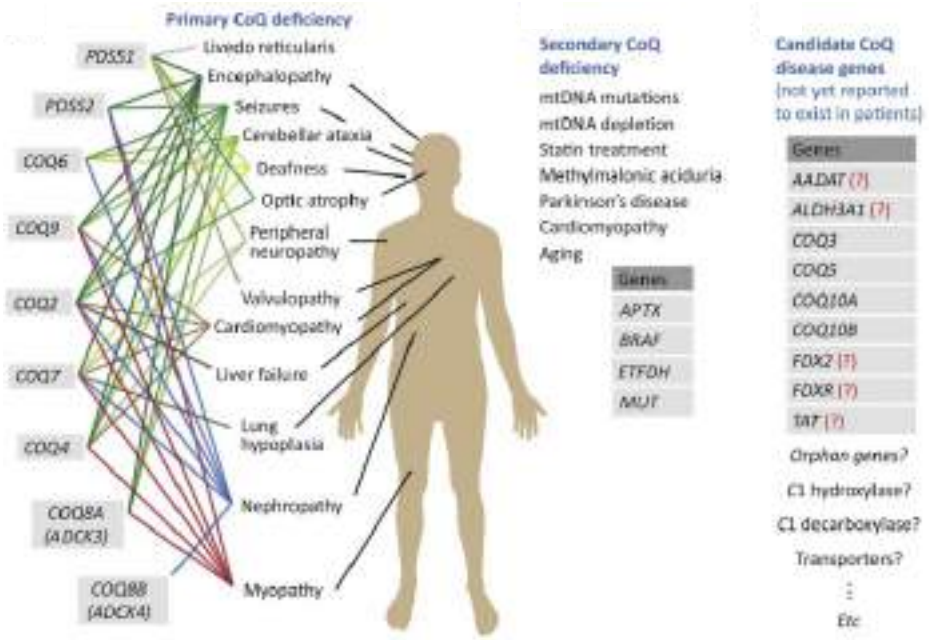

Figure 13. CoQ deficiency in humans.

Phenotypes and genes associated with primary CoQ deficiency; diseases, conditions, drugs, and genes linked to secondary CoQ deficiency; and candidate disease genes for potential primary CoQ deficiencies that have not yet been reported to be mutated in patients. '(?)' indicates an unproven ortholog relationship to a yeast gene that has been linked to CoQ (83).

1.2.1.1.1. Primary Coenzyme Q Deficiency

Primary CoQ deficiencies are clinically and genetically heterogeneous disorders with autosomal recessive heritance. Classically, it has been associated with five major phenotypes (191-194):

(a) Encephalomyopathy with recurrent myoglobinuria, encephalopathy, and mitochondrial myopathy.
(b) Cerebellar ataxia with cerebellar atrophy associated with other neurologic manifestations and, occasionally, endocrine dysfunctions.
(c) Infantile multisystemic form with encephalopathy usually associated with nephropathy and affectation of other organs.
(d) Isolated myopathy, characterized by muscle weakness, myoglobinuria, exercise intolerance, and elevated creatine kinase (CK).
(e) Steroid-resistant nephrotic syndrome.

Nevertheless, this classification is not updated because the phenotypic spectrum associated with CoQ deficiency is so heterogeneous that not all patients' syndromes can be classified within that subdivision. Moreover, mutations in the same gene may cause markedly different phenotypes. In parallel, some of the symptoms identified in patients with CoQ deficiency are similar to those found in other respiratory chain disorders (encephalomyopathy, ataxia, lactic acidosis, sensorineural deafness, retinitis pigmentosa, hypertrophic cardiomyopathy), while others are specific to CoQ deficiency, such as steroid-resistant nephrotic syndrome (SRNS) (191, 194).

Traditionally, CoQ deficiency was diagnosed based on biochemical assays. Later on, homozygous mapping analysis in consanguineous families or genetic linkage emerged as diagnostic tools. Today, the screening and diagnosis of CoQ deficiencies has been improved thanks to Next Generation Sequencing (NGS), greatly increasing the number of genetically diagnosed patients in the last ten years (194). Currently, mutations or deletions in 10 genes involved in the CoQ biosynthetic pathway have been reported in humans: *PSSS1* (195), *PDSS2* (196), *COQ2* (195, 197, 198), *COQ4* (199), *COQ5* (200), *COQ6* (201), *COQ7* (202, 203), *COQ8A* (or *ADCK3*) (204, 205), *COQ8B* (or *ADCK4*) (206, 207), and *COQ9* (208, 209). The age of onset may generally range from birth to early childhood (*PDSS1, PDSS2, COQ2, COQ4, COQ5, COQ6, COQ7* and *COQ9*), or from childhood to adolescence (*COQ8A* and *COQ8B*), but there are also some adult-onset cases (*COQ2, COQ8A* and *COQ8B*) (190) (Fig. 14).

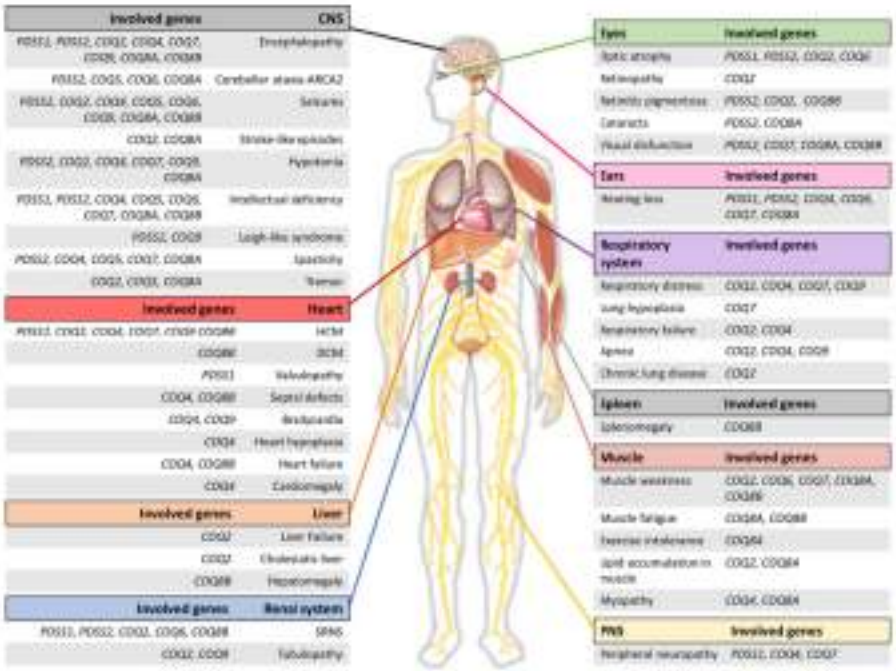

Figure 14. Organs and systems involved in CoQ primary deficiencies.
Organs and systems affected in individuals with primary CoQ deficiency, associating specific clinical manifestations with the genes involved in each one (190)**.**

1.2.1.1.2. Secondary Coenzyme Q Deficiency

Secondary CoQ deficiencies are more common than primary deficiencies, probably because of the diversity of biological functions and metabolic pathways in which CoQ is involved in mitochondrial and non-mitochondrial membranes. Secondary CoQ deficiency has been identified in patients with mutations in the aprataxin gene (*APTX*) characterized by ataxia and oculomotor (210-212); with mutations in the electron-transferring-flavoprotein dehydrogenase gene (*ETFDH*), showing isolated myopathy (213); and with mutations in the *BRAF* gene, developing a cardiofaciocutaneous (CFC) syndrome (214). Moreover,

CoQ deficiency has been reported in association with pathogenic mtDNA depletion, deletions, or point mutations (193, 215, 216). However, CoQ deficiency is not a constant clinical feature in these patients, as there are patients with *ETFDH* or *APTX* mutations and normal CoQ content in muscle or fibroblasts (191). The exact mechanisms by which these genetic defects cause CoQ deficiency are still unknown. Several hypotheses have been proposed: (a) an increased rate of CoQ degradation due to oxidative damage caused by a non-functional respiratory chain; (b) a decrease in CoQ through the interference with the signalling pathways involved in the process of biosynthesis; (c) the reduction in the stability of the CoQ biosynthetic complex or (d) a general deterioration of mitochondrial function (190, 193, 217).

In addition, secondary CoQ deficiency has been linked to a decrease in the levels of proteins of the Complex Q in various mouse models of mitochondrial diseases (185), as well as in the muscle and adipose tissue of patients and a mouse model with insulin resistance (187). Furthermore, CoQ seems to be reduced in the process of aging (96) and secondary CoQ deficiency may be a side effect of hypercholesterolaemia treatment with statins, since both cholesterol and CoQ share part of their biosynthetic pathways (218, 219). Other examples of secondary CoQ deficiency include multiple acyl-CoA dehydrogenase deficiency or methylmalonic aciduria (215). Recently, mutations in PARL, a protease located in the inner mitochondrial membrane with relevant but unclear physiological roles, have been also associated to secondary CoQ deficiency (220)

Some of the symptoms of secondary CoQ deficiencies are highly dependent on the original pathology. Myopathies presented as muscular weakness, hypotonia, exercise intolerance or myoglobinuria are commonly reported as muscular manifestations in diseases associated with secondary CoQ deficiencies. Neurological decline and ataxia are also often reported. It is possible that the primary disease symptoms are potentiated by the lack of CoQ, highlighting the importance of an early diagnosis also in these cases (190, 217).

1.2.1.1.3. Pathogenesis of Coenzyme Q Deficiency

The pathological mechanisms of CoQ deficiency are poorly understood. The identification of common pathogenic pathways for all patients is complex due to the heterogeneity in clinical presentation, age of onset and severity of the disease. In general, the pathogenesis of CoQ deficiency is connected to a bioenergetics defect but also to other physiological functions of CoQ that are not directly related to the OXPHOS system (191, 194). To clarify the pathophysiological consequences of CoQ deficiency, several *in vitro* and *in vivo* studies have been developed in the last two decades.

1.2.1.1.3.1. Pathogenesis of Coenzyme Q Deficiency: *in vitro* studies

The first experimental studies with fibroblasts from patients with CoQ deficiency were focused in the role of CoQ in mitochondrial bioenergetics and its antioxidant properties. In this context, in 2001, the analysis in the CoQ deficient fibroblast from two brothers showed mild

defects in mitochondrial respiration but no increase in superoxide anion production, lipid peroxidation, or apoptosis (221). Afterwards, it was demonstrated in fibroblasts with mutation in *COQ2* that the disruption in the CoQ levels was linked to an enzymatic defect in the CoQ-dependent complexes and reduced cell growth (197). *De novo* pyrimidine synthesis was also affected in fibroblast with *COQ2* mutation and the supplementation with CoQ_{10} normalized the cell growth after 24h (222). In parallel, fibroblasts with already described mutations in *COQ2* (197, 198), *PDSS2 (196)* and *COQ9* (208) were analyzed *in vitro*. Mutants in *PDSS2* and *COQ9* had residual CoQ levels of 10-15% and an important decrease in ATP synthesis but no oxidative stress signals o disruption in the antioxidant system. On the other hand, mutants in *COQ2* with residual CoQ levels of 30-50%, had a partial decrease in ATP synthesis but a great increase in ROS production, lipid peroxidation and cell death (223, 224). The strong relation between the CoQ levels, the bioenergetics defect and the oxidative stress has been confirmed later in other mutant in *COQ2* (225) with the use of 4-HB analogs (226, 227). In fact, in a neuronal cell model of CoQ deficiency by treatment of neuronal SH-SY5Y cell line with para-aminobenzoic acid (PABA), the reduction of neuronal CoQ levels induced a progressive decrease in mitochondrial respiratory chain activity and in ATP synthesis with an increased in mitochondrial oxidative stress (227). Moreover, it was confirmed in fibroblast the presence of the mitochondrial transition pore and its participation in the regulation of apoptosis (225).

1.2.1.1.3.2. Pathogenesis of Coenzyme Q Deficiency: *in vivo* studies

1.2.1.1.3.2.1. Invertebrate Models of CoQ Deficiency

Taking advantage of the fact that invertebrate models are easily generated and characterized, CoQ deficient worms (*Caenorhabditis Elegans*) and flies (*Drosophila Melanogaster*) have been produced.

Mutants in the *Drosophila qless* (*cg31005*) gene, an orthologue of the human *PDSS1*, and in the *sbo* (*cg9613* or *coq2*) gene, homolog of the human *COQ2,* have been generated. *Pdss1* mutant flies had an upregulation of markers of mitochondrial stress and caspase-dependent apoptosis in neurons. *Coq2* mutant flies developed a small larvae phenotype and more susceptibility to bacterial and fungal infections (228, 229). Interestingly, flies that are heterozygous for *sbo* show reduced CoQ production and a controversial extended lifespan (230). Additionally, other *Drosophila* model with mutation in *coq2* was generated in order to model human *COQ2* nephropathy. The disruption in c*oq2* is linked to an increases in ROS production that is reversed with glutathione and vanillic acid, an 4-HB analog (231). Moreover, RNAi against each one of the CoQ biosynthetic genes was used in *Drosophila* inducing a decrease in CoQ levels. The percentage of decrease depends on the affected gene and the intensity of the gene silencing. RNAi against the gene *cg10585* (human *PDSS2*) showed the hardest phenotype with flies arresting their development cycle after egg hatching. Gene interference of *qless* (*cg31005*)*, coq2, coq3, coq5, coq7, coq8, coq9*, or *coq10* produced lethality at larvae or pupae development stages. When

the silencing gene was *coq6*, flies managed to achieve the adult fly stage but suffered from severe CoQ deficiency. Demethoxyubiquinone (DMQ) was detected when *coq3, coq6, coq7*, and *coq9* were silenced, supporting the idea of a multi-enzymatic complex for CoQ biosynthesis (232, 233).

C. elegans mutants in the *clk-1* gene, homologous of the *COQ7* gene in humans, showed an increase in lifespan but with abnormalities in embryogenesis and larvae development. *Clk-1* mutant had a decrease in the CoQ levels and an accumulation of the intermediate DMQ, the substrate of COQ7, thus confirming the catalytic reaction of this enzyme. In *Clk-1* mutants was also described a profound defect in complex I+III activity associated to the accumulation of DMQ. This fact could explain the extension in lifespan because a disruption in the electron flow in the respiratory chain decreases the ROS production. Other hypothesis for the longevity of this model is that either the small amount of CoQ synthesized by *clk-1* mutant and/or the CoQ coming from the diet would stabilize complex III and increase the lifespan (234-237). Additional C. *elegans* mutant strains were generated. Knockouts mutations in the genes *coq-1*, *coq-2, coq-3* and *coq-8* produced larval development arrest highlighting the importance of CoQ in the early stages of development. *Coq-1* and *coq-2* knockouts mimicked the encephalomyopathic syndrome of CoQ deficiency with muscular atrophy and paralysis of the posterior half of the larval body (238, 239). Other *coq-1, coq2* and *coq-3* knockouts models developed symptoms consistent with cerebellar CoQ deficiency like progressive degeneration of GABA neurons with loss of motor coordination (240).

1.2.1.1.3.2.2. Vertebrate Models of CoQ Deficiency

Vertebrate models mimic, better than invertebrate models, the complexity of human cells. Specially, mammalian models of CoQ deficiency are useful tools to study the heterogeneity of these syndromes as it can simulate the cellular functions of CoQ and the tissue specificity that may exist in humans.

The generation of zebrafish models has emerged as a new opportunity to generate animal models with sophisticated mutagenesis and screening strategies on a large scale, and with a cost that is not possible in other vertebrate systems. In this context, a zebrafish model with mutation in the *ubiad1* gene, also known as barolo (*bar*), has been described as a model of CoQ deficiency. In zebrafish, Ubiad1 is involved in the CoQ biosynthetic pathway in the Golgi membrane. As a consequence, the *bar* mutants showed a decrease in the CoQ content in the cytosol with an important accumulation of ROS, leading to specific cardiovascular oxidative damage. At the same time, a knockdown of *Coq2* zebrafish model was associated with a mild increase in oxidative stress but without vascular or survival damage. Comparing both zebrafish models, the authors suggested that the Coq2-mediated CoQ production is mainly for mitochondrial respiratory chain function and energy production; whereas Ubiad1-mediated CoQ production is important for membrane redox signaling and protection from lipid peroxidation (241). Moreover, morpholino oligonucleotide (MO) knockdown of *Coq6* (201) and *Coq8b* (207) generated two new zebrafish models with CoQ deficiency. The first one produced apoptosis in the

embryos. The second one developed nephrotic phenotype with periorbital and total body edema.

The first mouse model with CoQ deficiency was published in 2001. Since then, mouse models with mutations in *Pdss2*, *Coq3*, *Coq6*, *Coq7*, *Coq8a*, *Coq8b* and *Coq9* have been generated in order to clarify the pathogenesis of CoQ deficiency.

A spontaneous mutation in *Pdss2* produced a mouse model (*Pdss2*$^{kd/kd}$) that developed a typical nephrotic syndrome that induced the death of the mice in 5 to 7 months (242). *Pdss2*$^{kd/kd}$ mice manifested widespread CoQ deficiency and abnormalities in the mitochondrial respiratory chain. However, other parameters such as ROS production, oxidative stress, mtDNA depletion, and citrate synthase activity, an index of mitochondrial mass, appeared only in affected organs (243). *Pdss2*$^{kd/kd}$ also showed a disruption in the sulphide oxidation pathway due to the decrease in the SQOR levels and low levels of glutathione, thus contributing to oxidative damage (159). Additionally, a tissue-specific conditional *Pdss2* knockout (KO) mouse was generated. The deletion of *Pdss2* was targeted to renal glomerular podocytes (*Podocin/cre,Pdss2*$^{loxP/loxP}$), renal tubular epithelium and hepatocytes (*PEPCK/cre,Pdss2*$^{loxP/loxP}$), monocytes (*LysM/cre,Pdss2*$^{loxP/loxP}$) and hepatocytes (*Alb/cre,Pdss2*$^{loxP/loxP}$). Interestingly, the kidney disease phenotype appeared only in *Podocin/cre,Pdss2*$^{loxP/loxP}$ KO mice, suggesting that the renal glomerular podocytes are particularly sensitive to Pdss2 dysfunction (244). Moreover, two cerebellar *Pdss2* conditional KO mouse models have been generated: the *Pax2/cre,Pdss2*$^{f/-}$ and the *Pcp2/cre,Pdss2*$^{f/-}$ mice. The first one mimicked the cerebellum atrophy

commonly observed in CoQ-deficient infants while in the second, the mutation was developed only in cerebellum Purkinje cells and suffered from an ataxic phenotype at old age (245, 246). Other podocyte-specific conditional knockout mouse models with nephrotic syndrome were created by mutations in *Coq6,* the *Coq6*^{podKO} mice, and *Coq8b*, the *Adck4*$^{\Delta Podocyte}$ mice.

On the other hand, constitutive homozygous knockout models for *Pdss2*, *Coq3* and *Coq7* were embryonically lethal, supporting the hypothesis that CoQ is essential for mouse embryonic development (244, 247-249). Consistent again with a dysfunctional COQ7 protein, the *Coq7*$^{-/-}$ embryos showed reduced CoQ levels and accumulation of DMQ (248, 249). In contrast, the homozygous knockout model for *Coq8a* resulted in a mild phenotype and tissue-specific CoQ deficiency. *Coq8a*$^{-/-}$ mice also showed a disruption in the complex Q, indicating the participation of Coq8a in the complex stability (250). Unlike *Coq7*$^{-/-}$ model, the heterozygous *Coq7*$^{+/-}$ mice is viable and without apparent phenotype. In fact, the CoQ levels are similar to the control mice. Nevertheless, *Coq7*$^{+/-}$ mice had a special distribution of the CoQ content in the cell: CoQ levels are low in the inner mitochondrial membrane but higher in the outer mitochondrial membrane. Consequently, young *Coq7*$^{+/-}$ mutants showed defects in mitochondrial bioenergetics as there was reported a reduction in the mitochondrial oxygen consumption, the electron transport and the mitochondrial ATP synthesis in this model. Importantly, CoQ supplementation normalized the CoQ levels in the mitochondrial membranes and rescued the bioenergetics dysfunction (247). Interestingly, an increase in lifespan was reported in *Coq7*$^{+/-}$ mice, similar as the one described in *C. elegans clk-1* mutants. The

improvement in lifespan has been associated to the induction of a mitohormesis protective physiological response (230). This could be supported by the slower ROS accumulation in *Coq7*$^{+/-}$ mitochondria due to the early hepatic mitochondrial dysfunction (251). An improvement in the immune system and in the resistance to neurological damage in the mutant mice have been also suggested as an explanation (252, 253).

At present, two models of CoQ deficiency due to mutations in the *Coq9* gene have been generated: the *Coq9*^{Q95X} knockout model and the *Coq9*^{R239X} knock-in model. In contrast with the embryonic lethality described in *Pdss2, Coq3*, and *Coq7* KO mice, *Coq9*^{Q95X} mouse was viable and showed moderate CoQ deficiency. This mutation in the *Coq9* gene produced a premature stop codon in amino acid 95, inducing a complete absence of COQ9 protein. The total absence of COQ9 does not induce a severe destabilization of the Complex Q and, as a result, the *Coq9*^{Q95X} mice developed a mild myopathy with exercise intolerance in females. Mitochondrial dysfunction was also reported with a reduction in the activity of complex I+III and mitochondrial respiration in skeletal muscle. *Coq9*^{Q95X} had a decrease in Coq7 levels demonstrating the interaction between Coq7 and Coq9 in CoQ biosynthesis (121). Curiously, *Coq9*^{Q95X} showed an increase in lifespan together with a decrease in body weight. Unlike *Coq7*$^{+/-}$ mice, a hepatic mitochondrial dysfunction as a cause of the increased lifespan has been rejected, because *Coq9*^{Q95X} mice had normal hepatic levels of CoQ. The mechanisms underlying this increased lifespan in *Coq9*^{Q95X} mice are still unknown (254). To understand the heterogeneity of CoQ deficiency, other mouse model with mutation in the Coq9 gene was generated in our group: the *Coq9*^{R239X}. This model presents the mutation homologue to

the one identified in a patient with CoQ_{10} deficiency (113, 208). The R239X mutation truncate the 75 terminal amino acids of COQ9 protein generating a mutated mRNA that is not fully degraded. Therefore, some residual levels of the truncated protein can be detected in the *Coq9*^{R239X} (121). *Coq9*^{R239X} mice suffered from a severe CoQ deficiency associated with fatal encephalomyopathy. The truncated version of COQ9 protein in *Coq9*^{R239X} mice destabilizes the Complex Q and produces a decreased in the COQ7 protein levels and, as a consequence, a widespread CoQ deficiency and accumulation of DMQ. Therefore, the stability of the complex Q clearly influences the CoQ biosynthesis rate and, consequently, the degree of the severity of CoQ deficiency and the development of tissue-specific phenotypes. The deficit in CoQ is linked to a decrease in mitochondrial respiration, particularly in the brain and kidneys, and to an increase in oxidative stress. These effects lead to neuronal death and demyelination with spongiosis and astrogliosis in the brain of *Coq9*^{R239X} mice, leading to a premature death (113). Importantly, the disruption of the mitochondrial sulphide oxidation pathway has emerged as one of the pathomechanisms associated to CoQ deficiency in both *Coq9*^{Q95X} and the *Coq9*^{R239X} models, similarly to *Pdss2*$^{kd/kd}$. In particular, CoQ deficiency severely reduces the SQOR protein levels leading to a dysfunction of H_2S oxidation, an accumulation of H_2S and a depletion of the glutathione system (158). Moreover, as previously mentioned, a proteomics analysis in the *Coq9*^{R239X} mice revealed that, at least in kidney, the levels of ETFDH, CHDH, DHODH, PRODH and PRODH2 show an increase (120), probably due to a compensatory mechanism. Nevertheless, it has not been yet evaluated the functional consequences of the changes of these CoQ-linked proteins in CoQ deficiency.

1.2.1.1.4. Treatment of Coenzyme Q Deficiency

Exogenous supplementation with high doses of CoQ_{10} is the classical therapeutic option for CoQ deficiency. However, CoQ_{10} has very low absorption and bioavailability, which limits its therapeutic potential, especially in cases of neurological syndrome (Table 1) (192). As many different aspects may influence the variability of the clinical response to CoQ_{10} supplementation, it is especially important to continue looking for new therapeutic alternatives.

Syndrome (No. of Patients)	CoQ10 Doses Duration	Response to Therapy
Encephalomyopathy (4)	150 mg/d; 3-8 mo	Improvement of muscle symptoms in 4/4 and encephalopathy in 1 patient
Isolated myopathy (8)	150-500 mg/d; 4-12 mo	Improvement in 6 patients
Isolated nephropathy (4)	30 mg/kg/d-300 mg/d; 2-50 mo	Reduced proteinuria in 3 patients; hearing improvement in 1/2 patients; no follow-up data in 1 patient
Infantile multisystemic disease (4)	30 mg/kg/d-300 mg/d; 5-36 mo	Improvement of myopathic symptoms and stabilization of encephalopathy in 1 patient; neurological, but not renal
Cerebellar ataxia (54)	5 mg/kg/d-3000 mg/d; 1 mo-12 y	Improvement of muscle symptoms in 13/20 patients; seizures in 3/14 patients; ataxia in 25/54 patients

Table 1. Clinical response to CoQ_{10} supplementation in mayor forms of CoQ Deficiency (192).

1.2.1.1.4.1 Treatment of Coenzyme Q Deficiency: CoQ_{10} Supplementation in Patients

The supplementation with high doses of CoQ_{10} has been effective for treating some cases of both primary and secondary CoQ deficiencies (255). In particular, high doses of CoQ_{10} has been published to be able to stop the progression of the disease in a multisystemic form with encephalopathy (256, 257), in six patients with isolated myopathy (213, 258) as well as in some patients with mutations in *COQ2* (259), *COQ4* (260) and *COQ7* (202). Moreover, CoQ_{10} supplementation was effective

in patients with mutation in the *ETFDH* gene only after the co-administration with riboflavin (213).

On the other hand, as previously mentioned, CoQ_{10} supplementation seams less effective in patients with neurological symptoms or multi-organ involvement. In a patient with an ataxic syndrome due to mutations in *COQ8A*,the therapy has no effect (205) o just a mild effect (204). Similar results were obtained in a patient with Leigh syndrome and nephropathy with mutation in *PDSS2* (196) and others with mutation in *COQ2* (261) and *COQ9* (208). In these cases, the disease was diagnosed in childhood and the treatment was quickly established, but this could not avoid the early death of the patients. Lastly, the alternative supplementation with idebenone, a short chain CoQ analog, was also tested in patients with primary CoQ deficiency but it was ineffective (202, 222, 256, 262).

Recently, a systematic review demonstrated the limited efficacy of CoQ_{10} supplementation. Of 89 patients with CoQ deficiency studied, only 24 reported improvements after the treatment. Moreover, in five cases, there was a deterioration in the patient's condition. The analysis indicate that most patients with CoQ deficiency treated with CoQ_{10} showed little or no response and, in the case of positive reports, the overall clinical benefit was only very limited (263). The failure of CoQ_{10} supplementation therapy in some cases of CoQ deficiency is not well understood. First, it can be related with the age of diagnosis. Generally, it is crucial to start the supplementation as soon as possible to promote the therapeutic response and to limit irreversible damage in critical tissues. Secondly, it is important to consider the dose of CoQ_{10}, ranging

from 5 mg/kg/day to 30–50 mg/kg/day in adults and children with CoQ deficiency (194, 259). Doses as high as 3000 mg/day have been also used in shorter clinical trials. However, 1200 mg/day has been established as the highest safe dose (194, 264). Furthermore, CoQ_{10} has high molecular weight and low aqueous solubility which complicates the absorption and bioavailability orally. This limitation is critic in patients with neurological syndromes where CoQ_{10} has also to cross the blood-brain barrier (192). As the reduced form of CoQ_{10}, ubiquinol-10, is more soluble, new pharmaceutic formulations have been developed in order to stabilize the CoQ_{10} molecule in this form. Nevertheless, the evidence is still limited and it is difficult to adjust the equivalent dose for ubiquinol (199, 265).

1.2.1.1.4.2 Treatment of Coenzyme Q Deficiency: Experimental Studies

CoQ_{10} supplementation has been tested *in vitro* in human skin fibroblast from patients with CoQ deficiency. A dose of 100 µM of CoQ_{10} for 72h induced a mild increase in complex II+III activity in CoQ deficient fibroblasts (225). A lower dose of 5 µM normalized the bioenergetics function in fibroblast with mutation in *PDSS2* (196), *COQ2* (197) and *COQ9* (208) when the treatment lasted one week. No effect in mitochondrial bioenergetics was achieved when the treatment was applied for 24h or with other CoQ short-tail analogs, like idebenone or CoQ_2 (262). These results suggested that high doses of CoQ_{10} should be administrated although it would produce a late clinical response as a consequence of the prolonged pharmacokinetics of CoQ (129, 259).

Moreover, it also discarded the use of short chain CoQ analogs, highlighting the important of the decaprenyl tail length.

The exogenous supplementation with CoQ_{10} has also been tested *in vivo*. For *Drosophila qless* and *sbo* mutants, oral supplementation with CoQ_{10} recued the phenotype in both cases (228, 229). Separately, *C. elegans clk-1* mutants were fed with genetically engineered bacteria that produced different isoforms of CoQ. CoQ_{10} was the CoQ isoform with higher antioxidant properties because rescued the phenotype by lowering oxidative stress, while the other isoforms had no effect (266, 267). Additionally, the phenotype of *C. elegans coq-1, coq-2* and *coq-3* mutants did not improve with the supplementation with CoQ_{10}. However, *coq-3* mutant phenotype was rescued by an extra-chromosomal array containing the own *C. elegans coq-3* gene (240, 268). On the other hand, the *Pdss2*$^{kd/kd}$ mice were treated with hydrosoluble CoQ_{10} at a dose of 200-400 mg/kg body weight/day in the water. No improvement in CoQ levels was detected but the severity of the nephrotic syndrome was reduced. *Pdss2*$^{kd/kd}$ mice were also treated with probucol. The treatment with probucol increased CoQ levels in kidney and liver and rescued the phenotype of the mutant mice more effectively than the CoQ_{10} therapy (269-271). Rapamycin was also tested in the *Pdss2*$^{kd/kd}$ model and managed to improve the renal pathology in a similar way as the supplementation with CoQ. Recently, a treatment with GDC-0879, a Braf/Mapk-targeting compound, has been published. However, it showed a mild therapeutic effect in *Pdss2*$^{kd/kd}$ mice (272, 273).

In the recent years, our group has analyzed the therapeutic effect of oral supplementation with ubiquinone-10 and ubiquinol-10 in the *Coq9*^{R239X} mouse model at a dose of 240 mg/kg/day for two months. The oxidized form of CoQ_{10} had limited efficacy while the reduced form provided better therapeutic results. Ubiquinol-10 therapy increased the CoQ levels and improved the CoQ-dependent respiratory chain activities in a better way than ubiquinone-10. Although there was an increased in the survival of the mutant mice, still 50% of the *Coq9*^{R239X} mice treated with ubiquinol-10 died before six month of age and the CoQ levels never reached control values. Nevertheless, supplementation with ubiquinol-10 during 2 months increased the SQOR levels in muscle while in kidneys, a trend toward increase was observed (274). Later on, it has been tested the therapeutic benefits of rapamycin administration in *Coq9*^{R239X} mice. However, neither a low nor a high dose of rapamycin were able to reduce the mitochondrial dysfunction (275).

Despite the advances in the last decades, there are still many open issues concerning CoQ_{10} deficiency and its therapy. New efforts should be done to develop alternative and effective strategies for the treatment of CoQ deficiency. On this point, novel therapeutic approaches based on the stimulation of the endogenous CoQ biosynthesis in patients and cells as emerged as a new field of research.

1.2.1.1.4.3 Treatment of Coenzyme Q Deficiency: 4-HB Analogs Therapy

The molecular understanding of the CoQ biosynthetic pathway allowed the design of experiments to bypass deficient biosynthetic steps

with analogs of 4-hydroxybenzoic acid (4-HB). 4-HB is the natural precursor of the CoQ benzoquinone ring and, after seven reactions of decarboxylation, hydroxylation and methylation, the fully substituted CoQ benzoquinone ring is produced. In fact, the supplementation with 4-HB in *COQ2* mutant cells normalized the CoQ protein levels and increased the synthesis of CoQ (276). Theoretically, the presence of a dysfunctional protein at any point in the CoQ biosynthetic pathway could be bypass by a 4-HB analog molecule that provide the defective chemical group (Fig. 15). Thus, the endogenous coenzyme Q biosynthesis would be reactivated (95).

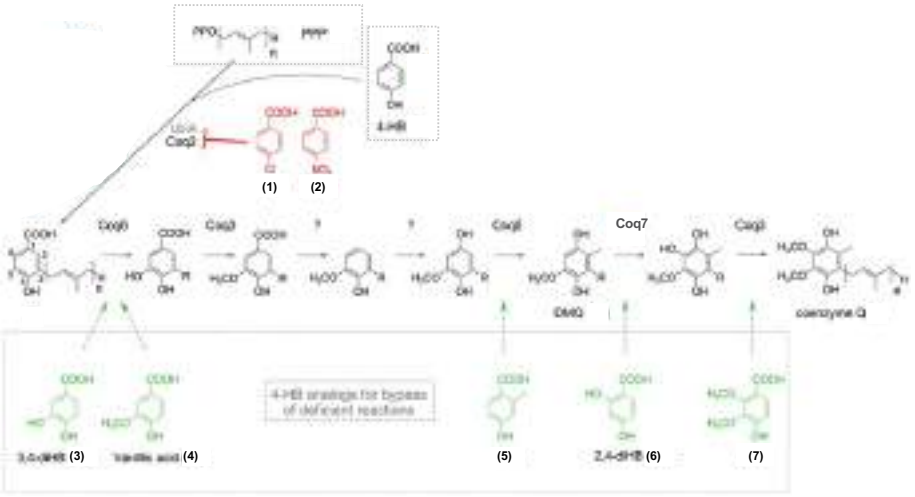

Figure 15. 4-HB analogs in the CoQ biosynthetic pathway.
4-HB analogs (in green) have potential (5, 7) or proven (3, 4, 6) capacities to bypass the biosynthetic steps indicated by the dashed arrows. 4-Chlorobenzoic acid (1) and 4-nitrobenzoic acid (2) (red) are inhibitors of Coq2/UbiA. Adapted from (95).

With this objective, 4-HB analogs have been rationally tested in different models of CoQ deficiency (277). Specifically, 2,4-dihydroxybenzoic acid (2,4-diHB), also named β-resorcylic acid (β-RA), has been used to bypass defects in *COQ7*. COQ7 protein catalyzes the

hydroxylation of the CoQ benzoquinone ring. β-RA has this hydroxyl group and, therefore, could bypass a defect in COQ7. Consistent with this, β-RA supplementation increased the levels of CoQ in *COQ7* null yeast and human skin fibroblasts with mutations in *COQ7* (202, 276, 278). Since an accumulation of DMQ is observed in *COQ7* defects, β-RA treatment also decreased DMQ levels, supporting this bypass mechanism (276). β-RA has also demonstrated therapeutic outcomes in defects in *COQ9*, based on the close connection between COQ9 and COQ7 previously mention. In *COQ9* mutant cells, β-RA supplementation increased CoQ levels and decreased DMQ levels (121, 276). *In vivo*, oral β-RA supplementation strongly rescued the phenotype of *Coq7* conditional knockout (*aogCoq7*) and $Coq9^{R239X}$ mice (279, 280). Remarkably, the maximal survival of $Coq9^{R239X}$ mice treated with β-RA reached a maximum of 25 months of age while, with the treatment of ubiquinol-10, the survival of the mutant mice was limited to 17 months of age. β-RA supplementation also reduced the spongiosis and reactive astrogliosis in $Coq9^{R239X}$ mice, improving the histopathological signs of the encephalopathy. However, the treatment did not rescued the SQOR levels and decreased the DMQ/CoQ ratio in peripheral tissues but not in the brain (279), suggesting that β-RA may act through additional therapeutic mechanisms. The possibility that β-RA could act through CoQ-independent therapeutic mechanisms was also checked in $Coq6^{podKO}$ and $Adck4^{\Delta Podocyte}$ mice models. The nephrotic syndrome was rescued after the treatment with β-RA. Nevertheless, CoQ levels after the treatment were not reported, so the therapeutic mechanism is still unknown but must not be related to a bypass effect (281, 282). In parallel, other 4-HB analogs, such as 3,4-hydroxybenzoic acid (3,4-diHB) and vanillic acid (VA), were able to bypass defects in COQ6 null yeasts and

human cells (106, 283, 284). Surprisingly, VA strongly upregulated COQ4 and stimulated CoQ biosynthesis in cells with a mutation in *COQ9*, leading to an increase in cell viability (276). However, VA has not been tested *in vivo* in a mammalian model of CoQ deficiency.

2. Hypothesis and Objectives

CoQ is a lipophilic molecule, composed by a benzoquinone ring and a polyprenoid tail, mainly synthesized in mitochondria. In mammals, the biosynthetic machinery is present in all tissues and is organized in the Complex Q. A reduction in the levels of CoQ manifests heterogeneous clinical symptoms, a fact that is not well understood.

The best-known CoQ function is the electron transfer in the mitochondrial respiratory chain, so it essential for the ATP synthesis. In this context, electrons are mainly transferred from complex I and complex II to CoQ. However, other mitochondrial enzymes, integrated in the Q-junction, can also reduce the CoQ. Specifically, the Q-junction directly connects the CoQ with ETF, ETFDH, DHODH, G3PDH, CHDH, PRODH, PRODH2 and SQOR enzymes. Thus, CoQ metabolism is linked to fatty acids β-oxidation, *de novo* pyrimidine synthesis, glycolysis, glycine, proline, arginine and H_2S metabolism. In fact, the levels of SQOR are profoundly deceased in CoQ deficiency. However, the importance of most of the proteins of the Q-junction in the pathogenesis and treatment of CoQ deficiency has not been properly evaluated.

The conventional treatment for CoQ deficiency is the exogenous supplementation of high doses of CoQ_{10}. However, this treatment has limited efficiency, especially in patients with neurological symptoms. The failure of CoQ_{10} therapy could be explained by the low absorption and bioavailability of exogenous CoQ_{10}, limiting the dose that access to the affected tissues. Moreover, CoQ_{10} supplementation does not reduce

the accumulation of intermediate metabolites or improve the endogenous biosynthesis of CoQ, although it can partially rescue the levels of SQOR. To overcome the disadvantages of the classical therapy, new therapeutic strategies based on the use of 4-HB analogs has been developed. In this line, mutations in *COQ7* and *COQ9* have been successfully treated *in vitro* and *in vivo* with β-RA. Specifically, the success of β-RA therapy in the $Coq9^{R239X}$ mouse model was explained by the better bioavailability of this compound, the modulation of Complex Q and the subsequent decrease of DMQ_9 levels, and the increase of mitochondrial bioenergetics in peripheral tissues but not in the brain, suggesting that additional therapeutic mechanisms might be involved in β-RA therapy. Moreover, other 4-HB analog, VA, stimulated CoQ biosynthesis in cells with mutation in *COQ9*. However, 4-HB analogs seem to have limitations in rescuing SQOR levels.

On the light of all the scientific background summarized above, this thesis is based upon the following hypotheses:

1. VA has better therapeutic potential than CoQ_{10} supplementation in CoQ deficiency because:
    1.1. VA is a water-soluble compound with low molecular weight and, therefore, higher absorption and bioavailability that CoQ_{10}.
    1.2. VA can stabilize the Complex Q and decrease the accumulation of toxic intermediates, e.g., DMQ.
    1.3. VA can stimulate CoQ endogenous biosynthesis, increasing the levels of both CoQ_9 and CoQ_{10} in mitochondria.

2. Both VA and β-RA have additional therapeutic mechanisms related with the CoQ-linked proteins in the Q-junction and can counteract the disruption produced in these pathways in CoQ deficiency.

3. The efficacy of CoQ_{10} supplementation in the treatment of mitochondrial disorders, as CoQ deficiency or CI deficiency, is connected with the direct stimulation of SQOR and the subsequent modulation of one carbon metabolism, since abnormalities in these pathways have been described in mitochondrial diseases.

4. Simultaneous administration of CoQ_{10} and VA may have synergic therapeutic effects in CoQ deficiency.

Based on these hypotheses, the following objectives are proposed:

1. To test *in vitro* and *in vivo* the therapeutic potential of VA in the treatment of primary CoQ deficiency due to mutations in *Coq9*.

2. To look for common therapeutic mechanisms of VA and β-RA in the treatment of $Coq9^{R239X}$ mice.

3. To analyze *in vitro* and *in vivo* the metabolic changes in sulfide metabolism and associated pathways induced by CoQ_{10} supplementation in CoQ deficiency and CI deficiency.

4. To study *in vitro* the metabolic modulation of the co-treatment of VA and CoQ_{10} in CoQ deficiency.

3. Materials and Methods

3.1. Animals and treatments

Coq9$^{+/+}$ (wild-type) and *Coq9*^{R239X} mice were used in the study, both of which harbour a C57BL/6J genetic background. The *Coq9*^{R239X} mouse model (MGI: 5473628) was previously generated and characterized (113, 121, 279). All animal manipulations were performed according to a protocol approved by the Institutional Animal Care and Use Committee of the University of Granada (procedures numbers 18/02/2019/016 18 February and 16/09/2019/153 16 September 2019) and were in accordance with the European Convention for the Protection of Vertebrate Animals used for Experimental and Other Scientific Purposes (CETS #123) and the Spanish law (R.D. 53/2013). Mice were housed in the Animal Facility of the University of Granada under an SPF zone with lights on at 7:00 AM and off at 7:00 PM. Mice had unlimited access to water and rodent chow (SAFE® 150, which provides 21%, 12.6% and 66.4% energy from proteins, lipids and nitrogen-free extracts, respectively). Unless stated otherwise, the analytical experiments were completed in animals at 3 months of age.

Vanillic acid (VA) and β-resorcylic acid (β-RA) (Merck Life Science S.L.U, Madrid, Spain) were given to the mice in the chow at a concentration of 1 % (w/w). β-RA at 1 % was previously reported as therapeutically successful in *Coq9*^{R239X} mice (279). A control group with vehicle at the same dose was studied. Mice began receiving the assigned treatments at 1 month of age (except in the experiment represented in Fig. 16B, in which the animals started the treatments at 3 months of age)

and the analyses were performed at the age indicated for each case. Animals were randomly assigned to experimental groups. Data were randomly collected and processed. The body weights were recorded once a month. The motor coordination was assessed at different months of age using the rotarod test by recording the length of time that mice could remain on the rod ("latency to fall"), rotating at a rate of 4 rpm, accelerating to 40 rpm in 300 s.

Control C57Bl6 mice were treated with ubiquinol-10 ($Q_{10}H_2$), which has better bioavailability *in vivo*, in the drinking water at a dose of 240 mg/kg bw/day (274). Ubiquinol-10 was provided by Kaneka (Japan) in a water-soluble formulation that contains gamma cyclodextrin. A control group with vehicle at the same dose was studied. The treatment started at 1 month of age, and the mice were euthanized for the experimental assays at 2 months of age. Livers were extracted and frozen at 80ºC until assayed for CoQ_{10} or protein quantification. *Ndufs4*$^{+/+}$ and *Ndufs4*$^{-/-}$ mice (MGI: 3793713), a model of Leigh syndrome due to Complex I deficiency (285) were euthanized at 4-5 weeks of age. Brains were extracted and frozen at -80ºC until assayed for CoQ_{10} or protein quantification. To quantify SQOR in the brain, mitochondria were freshly isolated, as previously described (158).

3.2. Cell culture and pharmacological treatments

Mouse embryonic fibroblasts (MEFs) from *Coq9*$^{+/+}$ and *Coq9*^{R239X} mice were grown in high glucose DMEM-GlutaMAX medium supplemented with 10% FBS, 1% MEM non-essential amino acids and 1% antibiotics/antimycotic in a humidified atmosphere of 5% CO_2 at 37

ºC. MEFs were treated with different concentrations of vanillic acid (1 mM, 500 µM, 250 µM, 50 µM, 5 µM and 0.5 µM) during 7 days. Vanillic acid was dissolved in 4% DMSO, giving a final concentration of DMSO in cell culture of 0.04%. After treatment, cells were collected and analyzed. A control group with vehicle at the same dose was studied.

Skin fibroblasts were provided by Holger Prokisch from the University of Munhen. Control and mutant skin fibroblasts were obtained from patients with mutations in different subunits of the mitochondrial Complex I or CoQ biosynthetic genes (see table 2). Fibroblasts were cultured at 37°C and 5% CO_2 in high glucose DMEM-GlutaMAX medium supplemented 1% MEM non-essential amino acids, and 1% antibiotics/antimycotic. Fibroblasts were treated with 100 µM CoQ_{10}, a dose commonly used in cell culture studies (225, 286), during 7 days. A pilot study with 20 µM CoQ_{10} for 7 days was also performed. CoQ_{10} was provided by Tishcon (USA) in a water-soluble formulation that contains gamma cyclodextrin. A control group with vehicle at the same dose was studied. CoQ_{10} or vehicle were dissolved in FBS prior to addition to culture medium (10% FBS). Sulfur aminoacids restriction was carried out by incubating for up to 24 h in DMEM lacking Met and Cys (Gibco) with 10% dialyzed FBS.

3.3. Histology and immunohistochemistry

After cervical dislocation, brains were isolated and embedded in paraffin. Sagittal sections (4 um) were mounted on glass slides for hematoxylin-eosin staining (287), Masson's trichrome and immunohistochemistry studies. Three consecutive sections

corresponding to the figure 104 of the mouse brain atlas (288) were selected for analysis by an examiner blinded to the different experimental groups. To identify neurons (NeuN, 1:300, Merck Milipore), astrocytes (GFAP, 1:500 Sigma Aldrich) and microglial activation (Iba1, 1:500, Wako), immunohistochemistry was performed. Briefly, after deparaffination, sections were boiled using 0.1 M sodium citrate buffer at pH 6, heating at 90ºC in a water bath for 40 min. After numerous washes in phosphate-buffered saline (PBS, 0.1M, 0.02% Triton-X100), sections were incubated with the primary antibody at 4ºC overnight. Then, secondary antibodies conjugated with AlexaFluor 488 or 594 were used at 37 ºC during 2h. Finally, the slides were mounted with ProLongTM Gold Andifade Mountant with DAPI (Invitrogen). Visualization and photography of the samples was carried out with an epifluorescence microscope (Nikon Ni-U). By using the ImageJ software (NH, Bethesda, USA), number of cells, morphology and fluorescence intensity were analyzed in cortex, brainstem and cerebellum.

3.4. Liquid chromatography – mass spectrometry (LC-MS) – based metabolomics

For metabolites extraction, 10 µl of serum was diluted in 1 ml lysis buffer composed of methanol/acetonitrile/H_2O (2:2:1) and shook for 10 min at 4ºC before centrifugation 15 min at full speed and 4ºC. For brain and kidney samples, 35-50 mg of tissue was ground in a mortar under liquid nitrogen, and metabolites were extracted by adding 500 µl lysis buffer and shaking for 20 min before centrifugation. The supernatants were collected for LC-MS analysis. The LC-MS analysis procedure and parameters were used as described before (289). LC-MS analysis was

performed on an Exactive mass spectrometer (Thermo Scientific) coupled with a Dionex Ultimate 3000 autosampler and pump (Thermo Scientific). The MS operated in polarity-switching mode with spray voltages of 4.5 kV and -3.5 kV. Metabolites were separated using a Sequant ZIC-pHILIC column (2.1 x 150 mm, 5 µm, guard column 2.1 x 20 mm, 5 µm; Merck) with elution buffers acetonitrile and eluent A (20 mM $(NH_4)_2CO_3$, 0.1% NH_4OH in ULC/MS grade water (Biosolve)). The flow rate was set at 150 µl/min and the gradient ran from 20% A to 60% A in 20 min, followed by a wash at 80% and re-equilibration at 20% A. Metabolites were identified and quantified using TraceFinder software (Thermo Scientific). Metabolites were identified based on exact mass within 5 ppm and further validated by concordance with retention times of standards. The peak areas of the identified metabolites were in their respective linear range of detection. Peak intensities were additionally normalized based on the total peak intensity of the total metabolites in order to correct for technical variations during mass spectrometry analysis.

3.5. Transcriptome analysis by RNA-Seq

The RNeasy Lipid Tissue Mini Kit (Qiagen) was used to extract total RNAs from the brainstem and kidneys of five animals in each experimental group. The RNAs were precipitated and their quality and quantity assessed using an Agilent Bioanalyzer 2100 and an RNA 6000 chip (Agilent Technologies). The cDNA libraries were then constructed using the TruSeq RNA Sample Prep Kit v2 (Illumina, Inc.) and their quality checked using an Agilent Bioanalyzer 2100 and a DNA 1000 chip (Agilent Technologies). The libraries were Paired End sequenced in

a HiSeq 4000 system (Illumina, Inc.) at Macrogen Inc. We aimed for 4–5 Giga Bases outcome per sample. The quality of the resulting sequencing reads was assessed using FastQC. The GRCm38.p5 fasta and gtf files of the reference mouse genome were downloaded from the Ensembl database and indexed using the bwtsw option of BWA (290). BWA, combined with *xa2multi.pl* and SAMtools (291), was also used for aligning the sequencing reads against the reference genome, and HTSeq was used for counting the number of reads aligned to each genomic locus (292). The alignments and counting were carried out in our local server following the protocols as described (293).

After elimination of the genomic loci that aligned to < 5 reads in < 5 samples and normalization of the read counts by library size, the differential gene expression was detected (279), using the Generalized Linear Model (glmLRT option) statistic in EdgeR. We used a 0.05 P-level threshold after False Discovery Rate correction for type I error. The heatmap figure was made using the heatmap function in R (https://www.r-project.org/). Annotation of the differentially expressed genes was obtained from the Mouse Genome Informatics (http://www.informatics.jax.org/).

The transcripts that filled the inclusion criteria were then subjected to gene classification, using a databank based on hand-curated literature mining for specific protein–protein interactions and regulatory networks (Ingenuity Pathway Analysis (IPA); Ingenuity Systems, Redwood City, CA, USA). The general canonical pathways, biological functions and diseases implicated for the significantly changed transcripts by Ingenuity Pathway Analysis were evaluated and P-values <0.01 were considered

significant. Furthermore, specific functional networks based on published knowledge on protein–protein interactions and regulatory networks were constructed using Ingenuity Pathway Analysis (294).

3.6. Mitochondrial proteomics analysis

Both *Coq9*$^{+/+}$ mice and *Coq9*$^{+/+}$ mice under 1% of VA and β-RA supplementation were sacrificed, and the brain and kidneys were removed and washed in saline buffer. The tissues were chopped with scissors in 3 ml HEENK (10 mM HEPES, 1 mM EDTA, 1 mM EGTA, 10 mM NaCl, 150 mM KCl, pH 7.1, 300 mOsm/l) containing 1 mM phenylmethanesulfonyl fluoride (from 0.1 M stock in isopropanol) and 1x protease inhibitor cocktail (Pierce). The tissues were homogenized with a 3 ml dounce homogenizer (5 passes of a tight-fitting Teflon piston). Each homogenate obtained was rapidly subjected to standard differential centrifugation methods until the mitochondrial pellet was obtained as previously described (295). Briefly, the homogenate was centrifuged at 600 g for 5 min at 4 °C (twice), and the resulting supernatant was centrifuged at 9,000 g for 5 min at 4 °C. The final pellet, corresponding to a crude mitochondrial fraction, was resuspended in 500 µl of HEENK medium without PMSF or protease inhibitor (295). Protein concentration was determined (using Bradford dye (BIO-RAD) and a Shimadzu spectrophotometer, resulting in approximately 3 mg protein for renal mitochondria and 1.5 mg for cerebral mitochondria. To verify the content of the mitochondrial fraction, Complex IV activity was determined by optical absorption of the difference spectrum at 550 nm, as previously described (158).

The purified mitochondria were spun down to remove the previous buffer, and lysis buffer (1% sodium deoxycholate SDC in 100 mM tris at pH 8.5) was added to the pellets. Samples were boiled for 5 minutes at 99ºC to denature all the proteins and then sonicated by microtip probe sonication (Hielscher UP100H Lab Homogenizer) for 2 min with pulses of 1s on and 1s off at 80% amplitude. Protein concentration was estimated by BCA assay and 200 µg were taken of each sample. 10 mM tris (2-carboxyethyl) phosphine and 40 mM chloroacetamide (final concentration) at 56 ºC were added to each of these 200 µg samples for 10 minutes to reduce and alkylate disulfide bridges. After this step, samples were digested with LysC (Wako) in an enzyme/protein ratio of 1:100 (w/w) for 1 h, followed by a trypsin digest (Promega) 1:50 (w/w) overnight. Protease activity was quenched with trifluoroacetic acid (TFA) to a final pH of ~2. Samples were then centrifuged at 5,000g for 10 minutes to eliminate the insoluble SDC, and loaded on an OASIS HLB (Waters) 96-well plate. Samples were washed with 0.1% TFA, eluted with a 50/50 ACN and 0.1% TFA, dried by SpeedVac (Eppendorf, Germany), and resuspended in 2% formic acid prior to MS analysis. 5 µg were taken from each sample and pooled in order to be used for quality control for MS (1 QC was analyzed every 12 samples) and to be fractionated at high-pH for the Match between runs.

Plasma was extracted in EDTA tubes and the most abundant proteins were removed using the Multiple Affinity Removal Spin Cartridge Mouse 3 (Agilent, 5188-5289). The cells were lysed by the addition of 5 µl of lysis buffer (1% SDC, 10 mM TCEP, 100 mM TRIS, 40 mM chloroacetamide at pH 8.5) for up to 20 µg of protein. Samples were boiled for 5 minutes at 95ºC to denature all the proteins and then

sonicated for 15 min with pulses of 30s on and 30s off (Bioruptor, model ACD-200, Diagenode). The pelleted cell debris was discarded after centrifugation at full speed for 10 min and the supernatant was digested overnight at 37ºC with LysC (Wako) in an enzyme/protein ratio of 1:75 (w/w) and with trypsin (Sigma) at 1:50 (w/w). Protease activity was quenched with formic acid (FA) to a final concentration of 2% FA. Samples were then centrifuged at 20,000g for 20 minutes to eliminate the insoluble SDC, and loaded on an OASIS HLB (Waters) 96-well plate. Samples were washed with 0.1% FA, eluted with a 50/50 ACN and 0.1% FA, dried by SpeedVac (Eppendorf, Germany), and resuspended in 2% formic acid prior to MS analysis.

All samples with the QC and 7 high-pH fractions were acquired using an UHPLC 1290 system (Agilent Technologies; Santa Clara, USA) coupled on-line to an Q Exactive HF mass spectrometer (Thermo Scientific; Bremen, Germany). Peptides were first trapped (Dr. Maisch Reprosil C18, 3 µm, 2 cm × 100 µm) prior to separation on an analytical column (Agilent Poroshell EC-C18, 2.7 µm, 50 cm × 75 µm). Trapping was performed for 5 min in solvent A (0.1% v/v formic acid in water), and the gradient was as follows: 13% – 44% solvent B (0.1% v/v formic acid in 80% v/v ACN) over 95 min, 44– 100% B over 2 min, then the column was cleaned for 4 min and equilibrated for 10 min (flow: 200 nL/min). The mass spectrometer was operated in a data-dependent mode. Full-scan MS spectra from m/z 375-1600 Th were acquired in the Orbitrap at a resolution of 60,000 after accumulation to a target value of 3E6 with a maximum injection time of 20 ms. The 15 most abundant ions were fragmented with a dynamic exclusion of 24 sec. HCD fragmentation spectra (MS/MS) were acquired in the Orbitrap at a

resolution of 30,000 after accumulation to a target value of 1E5 with an isolation window of 1.4 Th and maximum injection time 50 ms.

All raw files were analyzed by MaxQuant v1.6.10 software (296) using the integrated Andromeda Search engine and searched against the mouse UniProt Reference Proteome (November 2019 release with 55412 protein sequences) with common contaminants. Trypsin was specified as the enzyme, allowing up to two missed cleavages. Carbamidomethylation of cysteine was specified as fixed modification and protein N-terminal acetylation, oxidation of methionine, and deamidation of asparagine were considered variable modifications. We used all the default settings and activated "Match between runs" (time window of 0.7 min and alignment time window of 20 min) and LFQ with standard parameters. The files generated by MaxQuant were opened in Perseus for the preliminary data analysis: the LFQ data were first log2 transformed, then identifications present in at least N (3/5) biological replicates were kept for further analysis; missing values were then imputed using the standard settings of Perseus. Ingenuity Pathway Analysis (IPA) analysis was used to identify changes in metabolic canonical pathways and their z-score predictions (294).

3.7. Sample preparation and western blot analysis in tissues and cells

For western blot analyses, a glass-Teflon homogenizer was used to homogenize mouse kidneys, liver and brain samples at 1100 rpm in T-PER® buffer (Thermo Scientific) with protease and phosphatase inhibitor cocktail (Pierce). Homogenates were sonicated and centrifuged

at 1000g for 5 min at 4 ºC, and the resultant supernatants were used for western blot analyses. For western blot analyses in cells, the pellets containing the cells were re-suspended in RIPA buffer with protease inhibitor cocktail. About 40 μg of protein from the sample extracts were electrophoresed in 12% Mini-PROTEAN TGX precast gels (Bio-Rad) using the electrophoresis system mini-PROTEAN Tetra Cell (Bio-Rad). Proteins were transferred onto PVDF 0.45-μm membranes using a Trans-blot Cell (Bio-Rad) and probed with target antibodies. Protein–antibody interactions were detected using peroxidase-conjugated horse anti-mouse, anti-rabbit, or anti-goat IgG antibodies and Amersham ECLTM Prime Western Blotting Detection Reagent (GE Healthcare, Buckinghamshire, UK). Band quantification was carried out using an Image Station 2000R (Kodak, Spain) and a Kodak 1D 3.6 software. Protein band intensity was normalized to VDAC1 for mitochondrial proteins and to β-actin for cytosolic proteins. The data were expressed in terms of percent relative to wild-type mice or control cells.

The following primary antibodies were used: anti-COQ2 (Origene, TA341982), anti-COQ4 (Proteintech, 16654-1-AP), anti-COQ5 (Proteintech, 17453-AP), anti-COQ7 (Proteintech, 15083-1-AP), anti-PRODH (Cell Signaling, #22980), anti-OPA1 (Cell Signaling, #27733), anti-CRYAB (Cell Signaling, #15808), anti-DMGDH (Cell Signaling, #24813), anti-SERPINA1 (Cell Signaling, #16382), anti-SERPINA3 (Cell Signaling, #12192), anti-SQRDL (Proteintech, 17256-1-AP), anti-CBS (Proteintech, 14787-1-AP), anti-CSE (Proteintech, 12217-1-AP), anti-TST (Proteintech, 16311-1-AP), anti-ETHE1 (Sigma, HPA029029), anti-SUOX (Proteintech, 15075-1-AP), anti-3-MPST (Sigma, HPA001240), anti-PSAT1 (Proteintech, 10501-1-AP), anti-

EIF2AK2 (Proteintech, 18244-1-AP), anti-VDAC1 (Abcam, ab14734) and anti-ACTIN (Invitrogen, #MA5-15739-HRP).

3.8. Gene expression analyses

Total cellular RNA from tissue and cells was extracted following the TRI Reagent Solution protocol from Applied Biosystems and electrophoresed in agarose 1.5% to check RNA integrity. Total RNA was quantified by optical density at 260/280 nm and was used to generate cDNA with High-Capacity cDNA Reverse Transcription Kit (Applied Biosystems). Amplification was performed with quantitative real-time PCR, by standard curve method, with specific Taqman probes (from Applied Biosystems) for the targeted gene mouse *Coq2* (Mm01203260_m1), *Coq4* (Mm00618552_m1), *Coq5* (Mm00518239_m1), *Coq7* (Mm00501588_m1), *Ccl2* (Mm00441242_m1) and *Cxcl10* (Mm00445235_m1) and the mouse *Hprt* probe as a standard loading control (Mm01545399_m1); and with specific Taqman probes for the gene human *SQOR* (Hs01126963_m1), *CBS* (Hs01598251_m1), *CSE* (Hs00542284_m1), *TST* (Hs00361812_m1), *SUOX* (Hs00166578_m1), *PSAT1* (Hs00795278_mH), *MTHFD2L* (Hs01017321_m1), *CMPK2* (Hs01013364_m1), *EIF2AK2* (Hs00169345_m) and the human *GADPH* probe as a standard loading control (Hs99999905_m1),

3.9. Quantification of CoQ and DMQ levels in tissues and cells

CoQ_9 and CoQ_{10} from tissues were extracted by mixing tissue extracts with 1-propanol. After 2 min vortex, the solution was centrifuged at 13,000 rpm for 5 min. For cells, the pellet was re-suspended in water and transfer to a tube containing 1 ml of 0.1 M SDS, 1 ml of EtOH and 2 ml of hexane. After 2 min vortex, the solution was centrifuged at 3,500 rpm for 5 min. The upper phase was transfer to a new vial and the lower phase was vortex for 1 min after adding 2.5 ml of hexane. The solution was centrifuged at 3,500 rpm for 5 min one more time. The resulting upper phase was transfer to the previous vial and the hexane was evaporated. Finally, the lipid extract was re-suspended in 1-propanol.

The resultant supernatant was injected in a HPLC system (Gilson, WI, USA) and the lipid components were separated by reverse phase Symmetry C18 3.5 µm, 4.6 x 150 mm column (Waters, Spain), using a mobile phase consisting of methanol, ethanol, 2-propanol, acetic acid (500:500:15:15) and 50 mM sodium acetate at a flow rate of 0.9 ml/min. The electrochemical detector consisted of an ESA Coulochem III with the following setting: guard cell (upstream of the injector) at +900 mV, conditioning cell at -600 mV (downstream of the column), followed by the analytical cell at +350 mV. Since DMQ is not commercially available, its identification is based in the mass of the molecule and its retention time, as previously shown (113). Then, a standard curve of CoQ_9 and CoQ_{10} was used for a quantitative estimation. The results were expressed in ng CoQ/mg protein.

3.10. CoQ-dependent respiratory chain activities

Coenzyme Q-dependent respiratory chain activities were measured in tissue samples of brain, kidneys and liver. Tissue samples were homogenized in CPT medium (0.05 M Tris-HCl, 0.15 M KCl, pH 7.5) at 1,100 rpm in a glass–Teflon homogenizer. Homogenates were sonicated and centrifuged at 600 g for 20 min at 4 °C, and the supernatants obtained were used to measure CoQ-dependent respiratory chain activities (CI + III and CII + III) as previously described (274). Complex I + III activity was measured at 30 °C in the presence of 0.5 mM potassium cyanide, 0.2 mM NADH and 0.1 mM cytochrome c, as the rotenone-sensitive reduction of cytochrome c at 550 nm. The results were expressed in nmol reduced cyt c/min/mg prot. Complex II + III activity was measured at 30 °C in the presence of 0.5 mM KCN, 0.3 mM succinate and 0.01 mM rotenone. The reaction was initiated by addition of 0.1 mM cytochrome c and decrease in absorbance was monitored at 550 nm. The results were expressed in nmol reduced cyt c/min/mg prot and nmol reduced cyt c/min/citrate synthase activity. The citrate synthase activity was measured, with the previously obtained supernatants, at 30ºC in the presence of 0.3 mM acetyl-CoA and 0.1 mM DTNB (5,5-dithio-bis-(2-nitrobenzoic acid)). The reaction was initiated by the addition of 0.5 mM oxalacetate and the absorbance was monitored at 412 nm.

3.11. Mitochondrial respiration

To isolate fresh mitochondria, mice were sacrificed and the organs were extracted rapidly on ice. Brain was homogenated (1:10, w/v) in a

respiration buffer C (0.32 M sucrose, 1 mM EDTA-K^+, 10 mM Tris-HCl, pH 7.4) at 500 rpm at 4ºC in glass-teflon homogenizer. The homogenate was centrifuged at 13,000g for 3 min at 4ºC. The supernatant (s1) was kept on ice and the pellet was re-suspender in 5 ml of buffer A and centrifuged at 13,000 g for 3 min at 4ºC. The subsequent supernatant (s2) was combined with s1 and centrifuged at 21,200 g for 10 min at 4ºC. Mitochondrial pellet of this step was re-suspended on 0.85 ml extraction buffer A containing 15% Percoll, poured into ultracentrifuge tubes containing a Percoll gradient formed by 1 ml 40% Percoll and 1 ml 23% Percoll in buffer A, and centrifuged at 63,000g for 30min at 4ºC. Pure mitochondria, corresponding to the fraction between 23% and 40% Percoll, were collected, washed twice with 1 ml of buffer A at 10,300g for 10 min at 4ºC. Mitochondrial pellets were suspended in MAS 1X (120 mM sucrose, 220 mM mannitol, 10 mM KH_2PO_4, 5 mM $MgCl_2$, 2 mM HEPES, 1 mM EGTA) medium. Kidney homogenated (1:10, m/v) in a respiration buffer A (250 mM sucrose, 0.5 mM Na_2EDTA, 10 mM Tris and 1% free fatty acid albumin) at 800 rpm in a glass-teflon homogenizer. Then, homogenate was centrifuged at 500g for 7 min at 4ºC and the supernatant was centrifuged at 7,800g for 10min at 4ºC. The pellet was then resuspended in respiration buffer B (250 mM sucrose, 0.5 mM Na_2EDTA and 10 mM Tris) and an aliquot was used for protein determination. The remaining sample was then centrifuged at 6,000g for 10 min at 4ºC. The pellet was resuspended in buffer A and centrifuged again at 6,000g for 10 min at 4ºC. the final crude mitochondrial pellet was re-suspended in MAS 1X medium.

Mitochondrial respiration was measured using an XFe24 Extracellular Flux Analyzer (Seahorse Bioscience) (45, 279, 297).

Mitochondria were first diluted in cold MAS 1X for plating (3.5 µg/ in brain; 2 µg/well in kidney). Next, 50 µl of mitochondrial suspension was delivered to each well (except for background correction wells) while the plate was on ice. The plate was then centrifuged at 2,000g for 10 min at 4°C. After centrifugation, 450 µl of MAS 1X + substrate (10 mM succinate, 2 mM malate, 2 mM glutamate and 10 mM pyruvate) was added to each well. Respiration by the mitochondria was sequentially measured in a coupled state with the substrate present (basal respiration or State 2) followed by State 3o (phosphorylating respiration, in the presence of ADP and substrates). State 4 (non-phosphorylating or resting respiration) was measured after addition of oligomycin when all ADP was consumed, and then maximal uncoupler- stimulated respiration was measured by FCCP (State 3u). Injections were as follows: port A, 50 µl of 40 mM ADP (4 mM final); port B, 55 µl of 30 µg/ml oligomycin (3 µg/ml final); port C, 60 µl of 40 µM FCCP (4 µM final); and port D, 65 µl of 40 µM antimycin A (4 µM final). All data were expressed in pmol/min/mg protein.

3.12. Quantification of VA levels in mice tissues

Tissues from mice were homogenized in water. The homogenate samples were then treated with a solution of methanol/water (80:20, v/v), shook for 1 minute, sonicated for 15 minutes and then centrifuged at 5,000g for 25 minutes at 4ºC (298).

The supernatants were analyzed using a Thermo Scientific™ UltiMate™ 3000 UHPLC system (Waltham, Massachusetts, United States), consisting of an UltiMate™ 3000 UHPLC RS binary pump and

an UltiMate™ 3000 UHPLC sample manager coupled to a Thermo Scientific™ Q Exactive™ Focus Hybrid Quadrupole-Orbitrap™ detector of mass spectrometer (MS/MS) with an electrospray ionization in negative mode (Waltham, Massachusetts, United States). The analytical separation column was a Hypersil GOLD™ C18, 3 μm, 4.6 × 150 mm column (Thermo Scientific™) and the flow rate was 0.6 ml/min. The mobile phase consisted of two solutions: eluent A (H_2O + 0.1% Formic acid, MS grade, Thermo Scientific™) and eluent B (acetonitrile + 0.1% Formic acid, MS grade, Thermo Scientific™). Samples were eluted over 30 min with a gradient as follow: 0 min, 95% eluent A; 0-25 min, 70% eluent A; 25-25.1 min, 95 % eluent A; 25.1-30 min, 95% eluent A. Capillary and auxiliary gas temperatures were set at 275 and 450 °C, respectively. Sheath gas flow rate used was at 55 arbitrary units, the auxiliary gas flow rate used was at 15 arbitrary units, and sweep gas flow was used at 3 arbitrary units. Mass spectrometry analyses were carried out in full scan mode between 110 and 190 uma. To quantify the levels of VA, we used a standard curve with the compound at a concentration of 100 ng/ml, 10 ng/ml and 1 ng/ml.

3.13. Serine and glycine quantification.

Serine and glycine were quantified as described (Nemkov et al., 2015). Cell pellets were stored at -80°C and extracted immediately before analysis in ice-cold lysis/extraction buffer (methanol: acetonitrile: water 5:3:2 v/v). Samples were concentrated in a speedvac system and the resulting dry residues were resuspended in water. Standards of serine and glycine were dissolved in water at a concentration of 10, 100, 10000 ng/ml. Samples were separated through a 5 min isocratic elution on a

Kinetex XB-C18 column (150 × 2.1 mm i.d., 1.7 μm particle size – Phenomenex, Torrance, CA, USA) at 250 μl/min (mobile phase: 5% acetonitrile, 95% 18 mΩ H_2O, 0.1% formic acid; column temperature: 25°C). The UHPLC system was coupled online with a Q Exactive Focus mass spectrometer (Thermo, San Jose, CA, USA), scanning in Full MS mode (2 μscans) at 70,000 resolution from 60-200 m/z. Calibration was performed before each analysis using a positive calibration mix (Piercenet – Thermo Fisher, Rockford, IL, USA). Data were analyzed using Tracefinder 4.1 software (Thermo, San Jose, CA, USA). Analyte retention times were confirmed by comparison with external standard retention times.

3.14. Evaluation of supercomplex formation by BNGE

Blue native gel electrophoresis (BNGE) was performed on crude mitochondrial fractions from mice kidneys or human fibroblasts. Mitochondrial isolation from kidneys was performed as previously described (299). One aliquot of the crude mitochondrial fraction was used for protein determination. The remaining samples were then centrifuged at 13,000g for 3 min at 4 °C. The mitochondrial pellets were suspended in an appropriate volume of medium C (1 M aminocaproic acid, 50 mM Bis-Tris-HCl [pH 7.0]) to create a protein concentration of 10 mg/ml, and the membrane proteins were solubilized in digitonin (4 g/g) and incubated for 10 min in ice. After centrifugation for 30 min at 13,000g (4 °C), the supernatants were collected and 3 μl of 5% Brilliant Blue G dye, prepared in 1 M aminocaproic acid, was added.

Approximately, 2 x10^6 cells were used for mitochondrial isolation in human skin fibroblasts. Cell pellets were resuspended in phosphate buffered saline (PBS), then digitonin was added at a concentration of 8 mg/ml and the mixture incubated for 10 min in ice for solubilizing cell membranes. The samples were centrifuged for 5 min at 10,000g (4 ºC) and resuspended in PBS, then centrifuged for a second time at the same conditions. The pellets were resuspended in mitochondrial cell buffer (1.5 M aminocaproic acid, 50 mM Bis-Tris-HCl [pH 7.0]). Then, the mitochondrial membrane proteins were solubilized with digitonin at a final concentration of 1% and incubated for 5 min in ice. Samples were centrifuged for 30 min at 18,000g (4ºC). The supernatants were combined with 5% Brilliant Blue G dye, prepared in 1 M aminocaproic acid.

Mitochondrial proteins were then loaded and run on a 4-16% gradient native gel (Thermo Scientific, BN1002BOX) as previously described (72). After electrophoresis, the complexes were electroblotted onto PVDF membranes and sequentially tested with specific antibodies against CI, anti-NDUFA9 (Abcam, ab14713), CIII, anti-ubiquinol-cytochrome c reductase core protein I (Abcam, ab110252), anti-SQRDL (Proteintech, 17256-1-AP), anti-Vdac1 (Abcam, ab14734) and anti-rabbit (Thermofisher, 31460).

3.15. Lentiviral vectors constructs, vector production and cell transduction

The CSQORWP LV plasmid was constructed by standard cloning techniques using PstI/BamHI restriction enzymes to replace the eGFP in

the CEWP backbone by the SQOR cDNA (obtained by gene synthesis from Genscript).

Vector production was performed by fast growing 293T cells plated on amine-coated petri dishes (Sarsted,Newton, NC) in order to achieve 80-90% confluence for transfection. 293T cells were cotransfected with the vector (CSQORWP), the packaging (pCMVΔR8.91) and the envelope (pMD2.G) plasmids using LipoD293 (SignaGen, Gainthersburg, MD, USA). Viral supernatants were collected 48h after transfection and the particles were frozen or concentrated by ultrafiltration at 2000 g and 4°C, using 100 Kd centrifugal filter devices (Amicon Ultra-15, Millipore, Billerica, MA). LV particles were used to transduce skin fibroblasts by adding different volumes to the cell cultures in order to achieve the desired multiplicities of infection (MOI). The medium was changed after 5 hours of incubation.

3.16. Statistical analysis

The number of animals in each group were calculated in order to detect gross ~60% changes in the biomarker measurements (based upon alpha=0.05 and power of beta=0.8). We used the application available at http://www.biomath.info/power/index.htm. Animals were genotyped and randomly assigned to experimental groups in separate cages by the technician of the animal facility. Most statistical analyses were performed using the Prism 9 scientific software. Data are expressed as the mean ± SD of five to ten experiments per group. A one-way ANOVA with a Tukey's post hoc test was used to compare the differences between the three experimental groups. Studies with two experimental groups were evaluated using unpaired Student's t-test. A P value of <

0.05 was considered to be statistically significant. Survival curve was analyzed by log-rank (Mantel-Cox) and the Gehan-Breslow-Wilcoxon tests. The statistical tests used for the transcriptomics and proteomics analyses are described in their respective sections.

3.17. Data Availability

The mass spectrometry proteomics data were deposited to the ProteomeXchange (http://www.proteomexchange.org/) on December 11th, 2021. Consortium via the PRIDE partner repository with the dataset identifier PXD030303.

RNA-Seq data were generated as described above. The files have been uploaded to the repository Gene Expression Omnibus. The accession numbers are PRJNA796310 and PRJNA636102. All data can be found at https://www.ncbi.nlm.nih.gov/geo/query/acc.cgi?acc=PRJNA796310 and https://www.ncbi.nlm.nih.gov/bioproject/PRJNA636102/.

4. Results

The results in this thesis have been published in the following international articles:

Publication 1:

"The Q-junction and the inflammatory response are critical pathological and therapeutic factors in CoQ deficiency". Redox Biology, 2022. DOI: 10.1016/j.redox.2022.102403

Pilar González-García, María Elena Díaz-Casado, Agustín Hidalgo-Gutiérrez, Laura Jiménez-Sánchez, Mohammed Bakkali, Eliana Barriocanal-Casado, Germaine Escames, Riccardo Zenezini Chiozzi, Franziska Völlmy, Esther A.Zaal, Celia R.Berkers Albert J.R.Heck and Luis C.López

Publication 2:

"Coenzyme Q_{10} modulates sulfide metabolism and links the mitochondrial respiratory chain to pathways associated to one carbon metabolism". Human Molecular Genetics, 2020. DOI: 10.1093/hmg/ddaa214

Pilar González-García, Agustín Hidalgo-Gutiérrez, Cristina Mascaraque, Eliana Barriocanal-Casado, Mohammed Bakkali, Marcello Ziosi, Ussipbek Botagoz Abdihankyzy, Sabina Sánchez-Hernández, Germaine Escames, Holger Prokisch, Francisco Martín, Catarina M. Quinzii and Luis C.López

4. Results

4.1. *4-HB Analogs Therapy in CoQ Deficiency*

4.1.1 Vanillic acid supplementation rescues the phenotype of *Coq9^{R239X}* mice and induces a remarkable improvement in the histopathological signs of encephalopathy

We have previously characterized *Coq9^{R239X}* mice as a model of fatal mitochondrial encephalopathy with widespread CoQ deficiency and accumulation of DMQ. The deficit in CoQ induces a brain-specific impairment of mitochondrial bioenergetics performance which lead to neuronal death and demyelinization with severe vacuolization and astrogliosis in the brain of *Coq9^{R239X}* mice that consequently die between 3 and 7 months of age (113). Oral supplementation with β-RA at a concentration of 1% or 0.33% (w/w) increase the survival of *Coq9^{R239X}* mice to a maximum lifespan of 25 or 34 months, respectively (279, 287). Similarly, here, we show that oral supplementation with VA, starting at 1 month of age, results in a remarkable increase in the survival of the mutant mice, with a maximum lifespan of 30 months and a median survival of 22 months, which was comparable to the survival of wild-type mice (Fig. 16A). Additionally, *Coq9^{R239X}* mice treated with VA starting at 3 months of age exceed the lifespan of the mutant mice without treatment and remained alive until at least 15 months of age (Fig. 16B). Therefore, VA shows therapeutic benefits when the treatment starts at different stages of disease progression. The survival of the wild-type mice was not significantly modified by supplementation with VA (Fig. 16A).

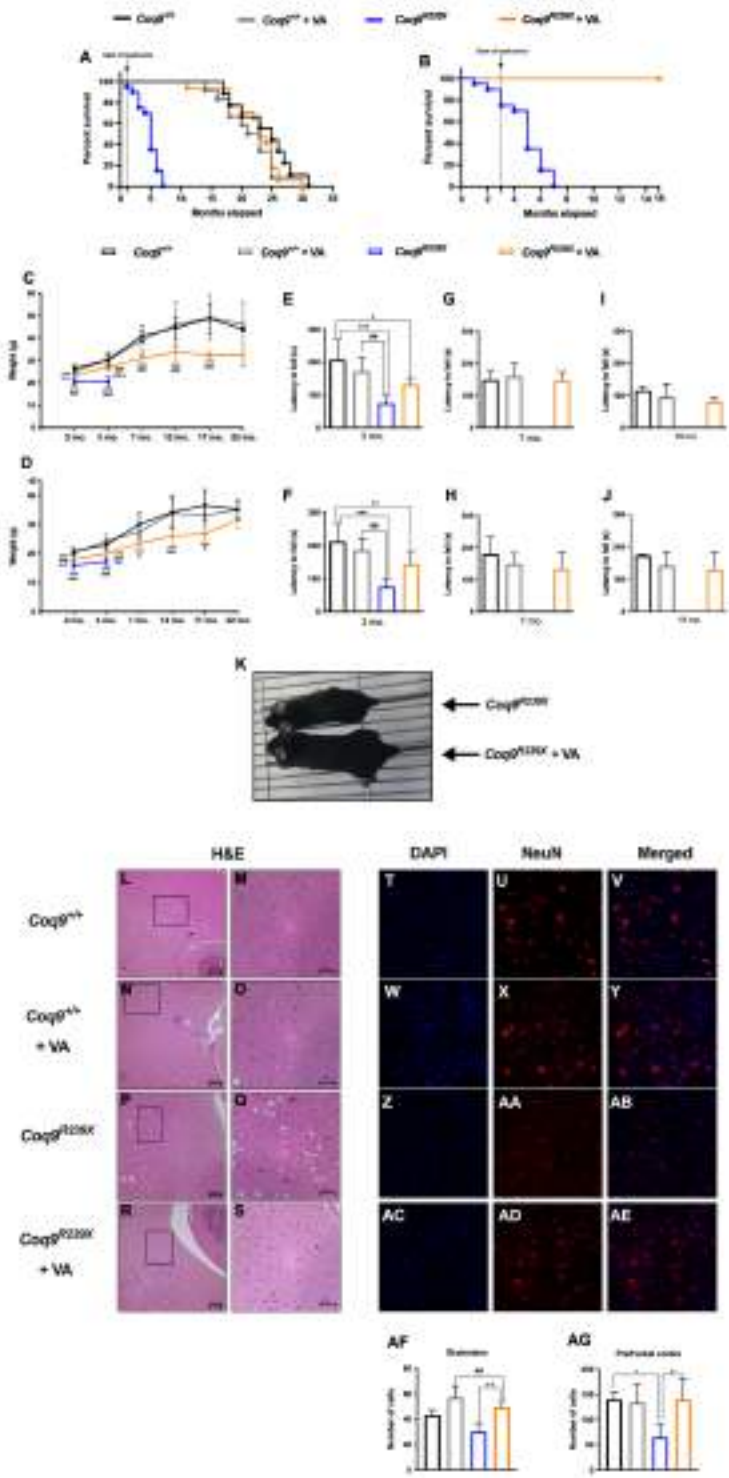

Figure 16. Survival, phenotypic characterization and pathological features of the brain of *Coq9*^{R239X} mice after VA treatment.

(A) Survival curve of *Coq9*$^{+/+}$ mice, *Coq9*$^{+/+}$ mice under 1% VA supplementation, *Coq9*^{R239X} mice and *Coq9*^{R239X} mice under 1% VA supplementation. The treatments started at 1 month of age [Log-rank (Mantel-Cox) test or Gehan-Breslow-Wilcoxon test]. *Coq9*$^{+/+}$, n = 10; *Coq9*$^{+/+}$ after VA treatment, n = 15; *Coq9*^{R239X}, n = 20; *Coq9*^{R239X} after VA treatment, n = 17.

(B) Survival curve of *Coq9*^{R239X} mice and *Coq9*^{R239X} mice after 1% VA treatment started at 3 months of age. Coq9R239X, n = 20; Coq9R239X after VA treatment, n = 7.

(C) Body weight of male *Coq9*$^{+/+}$ mice, *Coq9*$^{+/+}$ mice under 1% VA supplementation, *Coq9*^{R239X} mice and *Coq9*^{R239X} mice after 1% VA supplementation. *Coq9*$^{+/+}$, n = 17; *Coq9*$^{+/+}$ after VA treatment, n = 19; *Coq9*^{R239X}, n = 18; *Coq9*^{R239X} after VA treatment, n = 22.

(D) Body weight of female *Coq9*$^{+/+}$ mice, *Coq9*$^{+/+}$ mice under 1% VA supplementation, *Coq9*^{R239X} mice and *Coq9*^{R239X} mice after 1% VA supplementation. *Coq9*$^{+/+}$, n = 20; *Coq9*$^{+/+}$ after VA treatment, n = 15; *Coq9*^{R239X}, n = 12; *Coq9*^{R239X} after VA treatment, n = 20.

(E, G and I) Rotarod test of male *Coq9*$^{+/+}$ mice, *Coq9*$^{+/+}$ mice under 1% VA supplementation, *Coq9*^{R239X} mice and *Coq9*^{R239X} mice under 1% VA supplementation at 3 months of age (E), 7 months of age (G) and 18 months of age (I). n = 9–16 for each group.

(F, H and J) Rotarod test of female *Coq9*$^{+/+}$ mice, *Coq9*$^{+/+}$ mice under 1% VA supplementation, *Coq9*^{R239X} mice and *Coq9*^{R239X} mice under 1% VA supplementation at 3 months of age (H), 7 months of age (I) and 18 months of age (J). n = 9–16 for each group.

(K) Comparative image of a *Coq9*^{R239X} mouse and a *Coq9*^{R239X} mouse after 1% VA treatment at 3 months of age.

(L–S) H&E stain in the brainstem of *Coq9*$^{+/+}$ mice (L and M), *Coq9*$^{+/+}$ mice under 1% VA supplementation (N and O), Coq9R239X *Coq9*^{R239X} mice (P and Q) and *Coq9*^{R239X} mice under 1% VA supplementation (R and S) at 3 months of age.

(T-AE) NeuN stain in the brainstem of *Coq9*$^{+/+}$ mice (T, U and V), *Coq9*$^{+/+}$ mice under 1% VA supplementation (W, X and Y), *Coq9*^{R239X} mice (Z, AA and AB) and *Coq9*^{R239X} mice under 1% VA supplementation (AC, AD and AE) at 3 months of age.

(AF and AG) Number of neurons in brainstem (AF) and prefrontal cortex (AG) of *Coq9*$^{+/+}$ mice, *Coq9*$^{+/+}$ mice under 1% VA supplementation, *Coq9*^{R239X} mice and *Coq9*^{R239X} mice under 1% VA supplementation at 3 months of age.

Data are expressed as mean ± SD. *P < 0.05, **P < 0.01, ***P < 0.001, differences versus *Coq9*$^{+/+}$; #P < 0.05, ##P < 0.01, ###P < 0.001, differences versus *Coq9*$^{+/+}$ after VA treatment; +P < 0.05, ++P < 0.01, +++P < 0.001, versus *Coq9*^{R239X}; (one-way ANOVA with a Tukey's post hoc test; n = 5–22 for each group).

The survival increase induced by VA in *Coq9*^{R239X} mice was accompanied by a phenotypic rescue. The body weight of *Coq9*^{R239X} mice treated with VA significantly increase compared with that of *Coq9*^{R239X} mice, in both males (Fig. 16C) and females (Fig. 16D). In contrast to β-RA (287), VA does not alter the body weight of wild-type mice (Fig. 16C and D). Treatment with VA also improves the motor coordination in *Coq9*^{R239X} mice. The latency to fall decreases in *Coq9*^{R239X} mice compared to wild-type mice at 3 months of age, and supplementation with VA produces a slight increase in this parameter in the mutant, while no differences are detectable in wild-type mice (Fig. 16E and F). Subsequent rotarod assays at 7 and 18 months of age show that the improvement in the motor phenotype of the treated *Coq9*^{R239X} mice persisted over time (Fig. 16G–J). The phenotypic rescue is easily identifiable by an overall improvement in the health status of the treated *Coq9*^{R239X} (Fig. 16K).

Spongiform degeneration is absent in *Coq9*$^{+/+}$ mice before (Fig. 16L and M) and after VA supplementation (Fig. 16N and O) but is a histopathological feature of the encephalopathy in *Coq9*^{R239X} mice (Fig. 16P and Q) (113). This spongiosis clearly diminishes in the brainstem (Fig. 16R and S) and diencephalon (Fig 172 A-H) of the mutant mice treated with VA. Additionally, as well as no changes are detected in the *Coq9*$^{+/+}$ with and without the treatment (Fig. 16T–Y and AF), a significant decrease in neurons, marked as NeuN-positive cells, is

detected in the brainstem of *Coq9*^{R239X} mice (Fig. 16Z-AB and AF) compared to wild-type mice. VA supplementation normalizes the presence of NeuN-positive cells in the affected areas (Fig 16AC-AF). Similar results are achieved for the number of NeuN-positive cells in the prefrontal cortex (Fig. 16AG; Fig 17 I-T). In contrast, the kidneys, liver and spleen of untreated and treated *Coq9*^{R239X} mice and wild-type mice show similar structures, with no differences between the experimental groups (Fig. 17). In wild-type mice, treatment with VA does not induce morphological alterations in the kidneys, liver, or spleen (Fig. 17).

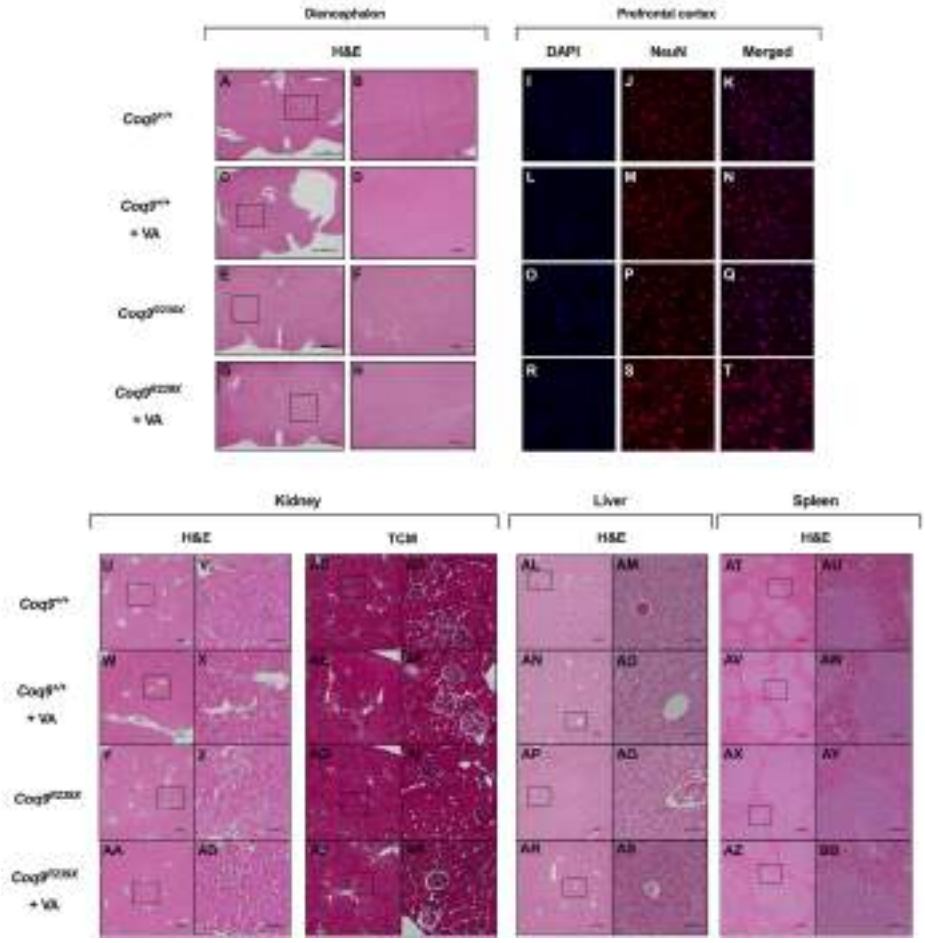

Figure 17. Morphological and histological features of the brain, liver, kidney and spleen of *Coq9*^{R239X} mice under 1% of VA treatment.

(A-H) H&E stain in the diencephalon of *Coq9*$^{+/+}$ mice (A and B), *Coq9*$^{+/+}$ mice under 1% VA supplementation (C and D), *Coq9*^{R239X} mice (E and F) and *Coq9*^{R239X} mice under 1% VA supplementation (G and H) at 3 months of age.
(I-T) NeuN stain in the prefrontal cortex of *Coq9*$^{+/+}$ mice (I, J and K), *Coq9*$^{+/+}$ mice under 1% VA supplementation (L, M and N), *Coq9*^{R239X} mice (O, P and Q) and *Coq9*^{R239X} mice under 1% VA supplementation (R, S and T) at 3 months of age.
(U-AB; AL-BB) H&E stain in the kidney, liver and spleen of *Coq9*$^{+/+}$ mice (U, V; AL, AM; AT, AU) *Coq9*$^{+/+}$ mice under 1% VA supplementation (W, X; AN, AO; AV, AW), *Coq9*^{R239X} mice (Y, Z; AP, AQ; AX, AY) and *Coq9*^{R239X} mice under 1% VA supplementation (AA, AB; AR, AS; AZ, BB) at 3 months of age.
(AC-AK) Masson's trichrome stain in the kidney of *Coq9*$^{+/+}$ mice (AC and AD), *Coq9*$^{+/+}$ mice under 1% VA supplementation (AE and AF), *Coq9*^{R239X} mice (AG and AI) and *Coq9*^{R239X} mice under 1% VA supplementation (AJ and AK) at 3 months of age.

4.1.2. VA induces tissue-specific modulation of CoQ metabolism

Since VA is an analog of the natural precursor of the CoQ biosynthetic pathway, we investigated whether the rescue of the phenotype observed after VA treatment was due to the modulation of CoQ biosynthesis. To that end, we measured the levels of CoQ_9, DMQ_9 (major forms of CoQ and DMQ in rodents) and DMQ_9/CoQ_9 ratio, as molecular responsible of the progression of the clinical symptoms in some cases of CoQ deficiency (279, 287), in mouse embryonic fibroblasts (MEFs) and in the most relevant tissues of *Coq9*^{R239X} mice. MEFs and tissues from *Coq9*^{R239X} mice show severe deficiency of CoQ_9, accumulation of DMQ_9 and an increased DMQ_9/CoQ_9 ratio (113, 279) (Fig. 18). Treatment with VA increases levels of CoQ_9, decreases levels of DMQ_9 and decreases DMQ_9/CoQ_9 ratio in a dose-dependent manner (Fig. 18A, B and 2C). In vivo, supplementation with VA does not modify the CoQ_9 levels (Fig. 18D), the DMQ_9 levels (Fig. 18E) or the

DMQ_9/CoQ_9 ratio (Fig. 18F) in the brain. However, VA treatment produces a slight increase in CoQ_9 levels and significantly decreases the DMQ_9 levels and the DMQ_9/CoQ_9 ratio in the kidneys (Fig. 18G–I) and the liver (Fig. 18J-L). A slight increase in CoQ_9 levels is also detected in skeletal muscle (Fig. 18M) of the mutant mice after VA treatment but not in DMQ_9 levels or the DMQ_9/CoQ_9 ratio (Fig. 18N and O). No changes are detected in the heart after the treatment (Fig. 18P–R) (Fig. 19). These results are similar to those previously obtained with β-RA, although they were less pronounced (279). In wild-type animals, VA induces a slight decrease in CoQ_9 levels (Fig. 18D, G, J, M and P).

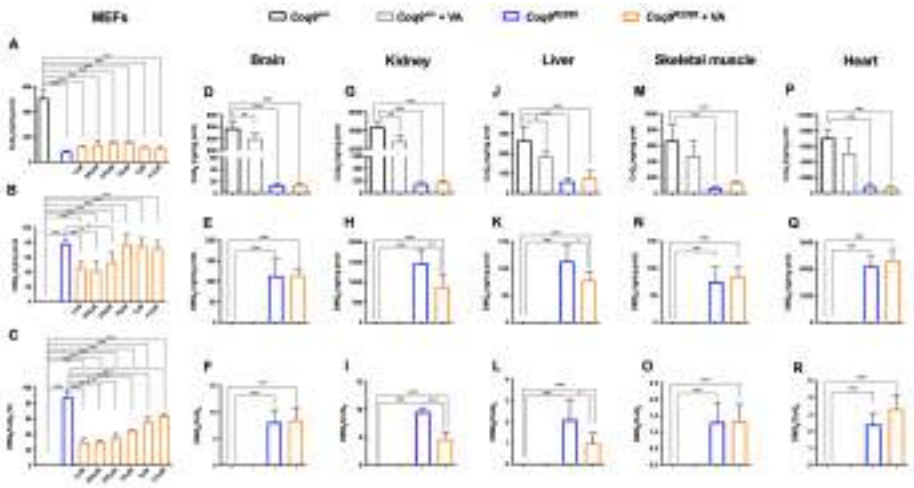

Figure 18. Levels of CoQ_9, DMQ_9 and DMQ_9/CoQ_9 ratio in *Coq9*^{R239X} mice MEFs and tissues after VA treatment.

(A, B and C) Levels of CoQ_9 (A), DMQ_9 (B) and DMQ_9/CoQ_9 ratio (C) in MEFs from *Coq9*$^{+/+}$ and *Coq9*^{R239X} mice after the supplementation with VA at 1 mM, 500 µM, 250 µM, 50 µM, 5 µM and 0,5 µM.

(D-R) Levels of CoQ_9 (D, G, J, M and P), DMQ_9 (E, H, K, N and Q) and DMQ_9/CoQ_9 ratio (F, I, L, O and R) in brain (D, E and F), kidney (G, H and I), liver (J, K and L), skeletal muscle (M, N and O) and heart (P, Q and R) of *Coq9*$^{+/+}$ mice, *Coq9*$^{+/+}$ mice after 1% VA treatment, *Coq9*^{R239X} mice and *Coq9*^{R239X} mice after 1% VA treatment.

Data are expressed as mean ± SD. *P < 0.05, **P < 0.01, ***P < 0.001, differences versus *Coq9*$^{+/+}$; +P < 0.05, ++P < 0.01, +++P < 0.001, versus *Coq9*^{R239X}; (one-way ANOVA with a Tukey's post hoc test; n = 5 for each group).

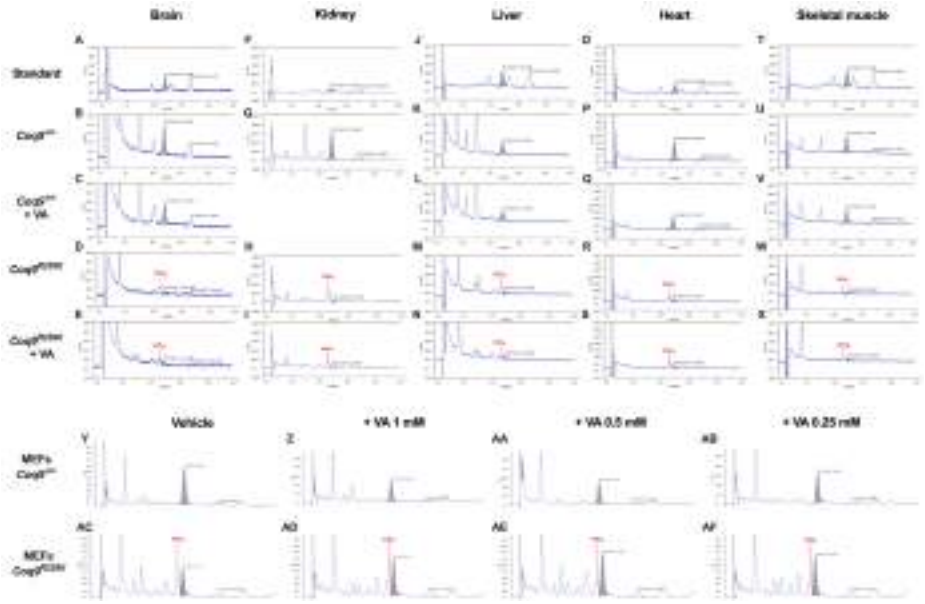

Figure 19. Representative chromatographs of CoQ_9 and DMQ_9 in MEFs and mice tissues after VA treatment.

(A, F, J, O and T) Chromatographs from CoQ standard.

(B-E) Chromatographs from brain samples of *Coq9*$^{+/+}$ mice (B), *Coq9*$^{+/+}$ mice under 1% VA supplementation (C), *Coq9*^{R239X} mice (D) and *Coq9*^{R239X} mice under 1% VA supplementation (E) at 3 months of age.

(G, H and I) Chromatographs from kidney samples of *Coq9*$^{+/+}$ mice (G), *Coq9*^{R239X} mice (H) and *Coq9*^{R239X} mice under 1% VA supplementation (I) at 3 months of age.

(K-N) Chromatographs from liver samples of *Coq9*$^{+/+}$ mice (K), *Coq9*$^{+/+}$ mice under 1% VA supplementation (L), *Coq9*^{R239X} mice (M) and *Coq9*^{R239X} mice under 1% VA supplementation (N) at 3 months of age.

(P-S) Chromatographs from heart samples of *Coq9*$^{+/+}$ mice (P), *Coq9*$^{+/+}$ mice under 1% VA supplementation (Q), *Coq9*^{R239X} mice (R) and *Coq9*^{R239X} mice under 1% VA supplementation (S) at 3 months of age.

(U-X) Chromatographs from skeletal muscle samples of *Coq9*$^{+/+}$ mice (U), *Coq9*$^{+/+}$ mice under 1% VA supplementation (V), *Coq9*^{R239X} mice (W) and *Coq9*^{R239X} mice under 1% VA supplementation (X) at 3 months of age.
(Y-AB) Chromatographs from *Coq9*$^{+/+}$ MEFs treated 7 days with vehicle (Y), VA 1mM (Z), VA 0.5 mM (AA), VA 0.25 mM (AB).
(AC-AF) Chromatographs from *Coq9*^{R239X} MEFs treated 7 days with vehicle (AC), VA 1mM (AD), VA 0.5 mM (AE), VA 0.25 mM (AF).

To determine whether the tissue-specific differences in the response of the CoQ biosynthetic pathway to VA supplementation could be due to the bioavailability of this compound, we analyzed the levels of VA in the brain (Fig. 20A), kidneys (Fig. 20B) and liver (Fig. 20C) of *Coq9*^{R239X} mice after oral supplementation with VA. The brain shows the lowest values of VA, although those are in the same range than those in the liver. Thus, the bioavailability of VA is not the only reason for the tissue-specific differences in CoQ biosynthesis, although that requires further investigation.

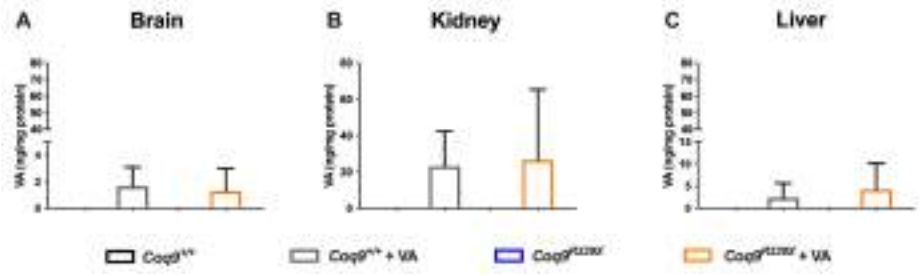

Figure 20. Levels of VA in mouse tissues after de oral supplementation of VA.
(A, B and C) Levels of VA in brain (A), kidney (B) and liver (C) of *Coq9*$^{+/+}$ mice, *Coq9*$^{+/+}$ mice under 1% VA supplementation, *Coq9*^{R239X} mice and *Coq9*^{R239X} mice under 1% VA supplementation at 3 months of age.
Data are expressed as mean ± SD (one-way ANOVA with a Tukey's post hoc test; n = 5 for each group).

To determine whether VA interferes with the Complex Q, we analyzed the levels of the protein components of Complex Q. MEFs from *Coq9*^{R239X} mice show normal levels of COQ2 and COQ5 but decrease levels of COQ4 and COQ7 (Fig. 21A–D). Supplementation with VA at a concentration of 1 mM increase the levels of COQ4 (Fig. 21B), COQ5 (Fig. 21C) and COQ7 (Fig. 21D). These increases in protein levels are not due to increases in the mRNA levels (Fig. 21E–H). *In vivo*, the levels of COQ2, COQ4, COQ5 and COQ7 are decreased in the brain (Fig. 21I and J, K and L) and, to a greater extent, except for COQ2, in the kidneys (Fig. 21M − P) and liver (Fig. 21Q–T) of *Coq9*^{R239X} mice compared to the same tissues in *Coq9*$^{+/+}$ mice. Treatment with VA increases the levels of COQ4 and COQ5 in the kidneys (Fig. 21N and O) and to a smaller extent in the liver (Fig. 21R and S). However, the corresponding mRNA levels are not altered (Fig. 21U–Z), only increased for *Coq5* in the kidneys (Fig. 3X) and *Coq4* in the liver (Fig. 21Y) in the treated *Coq9*^{R239X} mice. In contrast, the levels of COQ2, COQ4, COQ5 and COQ7 in the brain are not altered after the treatment (Fig. 21I-L). This is consistent with the data previously reported for treatment with β-RA in the same animal model (279), although VA has a more intense effect on the upregulation of COQ4. In samples from *Coq9*$^{+/+}$ mice, supplementation with VA also produces changes in the levels of CoQ biosynthetic proteins. In *Coq9*$^{+/+}$ MEFs, VA decreases the levels of COQ2 (Fig. 21A) but increases the levels of COQ5 (Fig. 21C) and COQ7 (Fig. 21D). *In vivo*, the levels of COQ4 and COQ5 are significantly increased in the brain (Fig. 3J and K), kidneys (Fig. 21N and O) and liver (Fig. 21R and S) in *Coq9*$^{+/+}$ mice treated with VA. The levels of COQ7 are also increased in the liver in the treated *Coq9*$^{+/+}$ mice (Fig. 21T). Together, these results indicate that VA increases the levels of COQ4

and COQ5 in both *Coq9*$^{+/+}$ and *Coq9*^{R239X} mice, probably via a compensatory mechanism caused by competition, with higher km, with 4-hydroxibezoic acid (4-HB), the natural substrate for COQ2 (85).

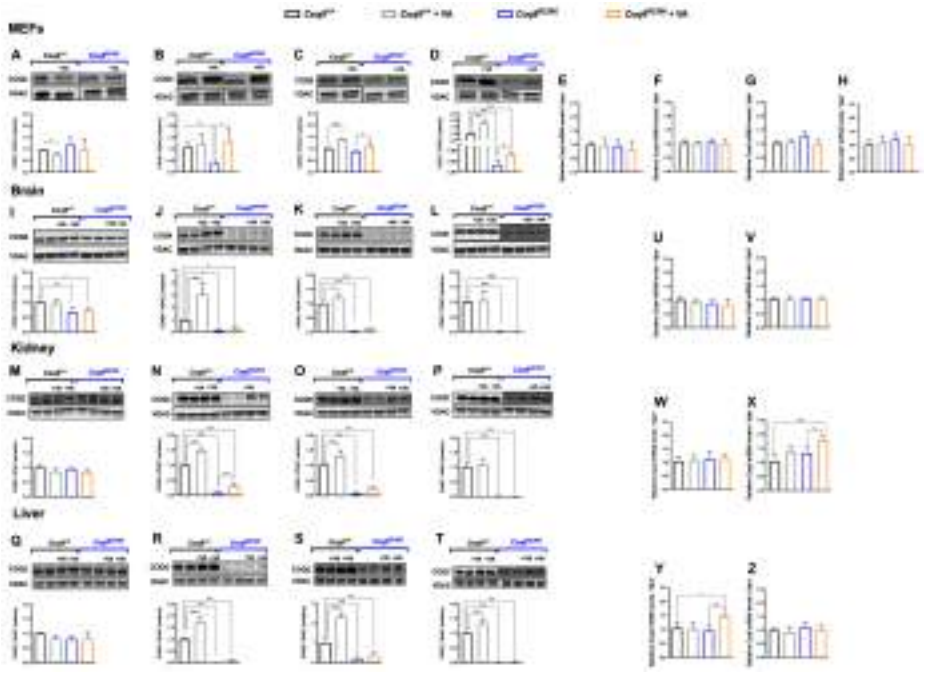

Figure. 21. Effect of VA treatment on the levels of CoQ biosynthetic proteins and mRNA levels in the MEFs and tissues of *Coq9*^{R239X} mice.

(A-D) Representative images of Western blots of the CoQ biosynthetic proteins COQ2 (A), COQ4 (B), COQ5 (C) and COQ7 (D), and the quantitation of the protein bands in MEFs from *Coq9*$^{+/+}$ and *Coq9*^{R239X} mice after supplementation with VA at 1 mM

(E-H) Relative mRNA levels for the genes Coq2 (E), Coq4 (F), Coq5 (G) and Coq7 (H) in MEFs from *Coq9*$^{+/+}$ and *Coq9*^{R239X} mice after supplementation with VA at 1 mM

(I-L) Representative images of Western blots of the CoQ biosynthetic proteins COQ2 (I), COQ4 (J), COQ5 (K) and COQ7 (L), and the quantitation of the protein bands in the brain of *Coq9*$^{+/+}$ mice, *Coq9*$^{+/+}$ mice after 1% VA treatment, *Coq9*^{R239X} mice and *Coq9*^{R239X} mice after 1% VA treatment.

(M-P) Representative images of Western blots of the CoQ biosynthetic proteins COQ2 (M), COQ4 (N), COQ5 (O) and COQ7 (P), and the quantitation of the protein bands in

the kidney of *Coq9*$^{+/+}$ mice, *Coq9*$^{+/+}$ mice after 1% VA treatment, *Coq9*^{R239X} mice and *Coq9*^{R239X} mice after 1% VA treatment.
(Q-T) Representative images of Western blots of the CoQ biosynthetic proteins COQ2 (Q), COQ4 (R), COQ5 (S) and COQ7 (T), and the quantitation of the protein bands in the liver of *Coq9*$^{+/+}$ mice, *Coq9*$^{+/+}$ mice after 1% VA treatment, *Coq9*^{R239X} mice and *Coq9*^{R239X} mice after 1% VA treatment.
(U and V) Relative mRNA levels of the genes *Coq4* (U) and *Coq5* (V) in brain from *Coq9*$^{+/+}$ and *Coq9*^{R239X} mice after the supplementation with VA at 1 mM
(W and X) Relative mRNA levels of the genes *Coq4* (W) and *Coq5* (X) in the kidneys from *Coq9*$^{+/+}$ and *Coq9*^{R239X} mice after the supplementation with VA at 1 mM
(Y and Z) Relative mRNA levels of the genes *Coq4* (Y) and *Coq5* (Z) in the liver from *Coq9*$^{+/+}$ and *Coq9*^{R239X} mice after the supplementation with VA at 1 mM.
Data are expressed as mean ± SD. *P < 0.05, **P < 0.01, ***P < 0.001, differences versus *Coq9*$^{+/+}$; +P < 0.05, ++P < 0.01, +++P < 0.001, versus *Coq9*^{R239X}; (one-way ANOVA with a Tukey's post hoc test; n = 3 for each group for cell samples, n = 5 for each group for tissue samples).

4.1.3. VA induces a DMQ/CoQ ratio-dependent increase in mitochondrial bioenergetics

Due to the role of CoQ in mitochondrial function and due to the fact that VA partially modulates CoQ biosynthesis, we evaluated the effect of the treatment on mitochondrial bioenergetics. In the brain, kidneys and liver of *Coq9*^{R239X} mice, the activities of CoQ-dependent mitochondrial complexes I+III (CI+III) and CII+III (Fig. 22A-O) and the mitochondrial oxygen consumption rate (OCR) (Fig. 22P–Q) are significantly decreased compared to the values in wild-type animals. Treatment with VA does not improve any of these parameters in the brain of the treated mutant mice (Fig. 22A–E and P). In the kidneys, however, VA treatment normalizes the CI+III activity (Fig. 22F and I) and induces a significant increase in OCR (Fig. 22Q). Furthermore, VA treatment

partially normalizes CII+III activity (Fig. 22L) in the liver. Overall, these results demonstrate that the tissue-specific responses of CoQ metabolism to VA determine the extent of improvement in mitochondrial bioenergetics, a fact that was also previously observed with β-RA therapy (279).

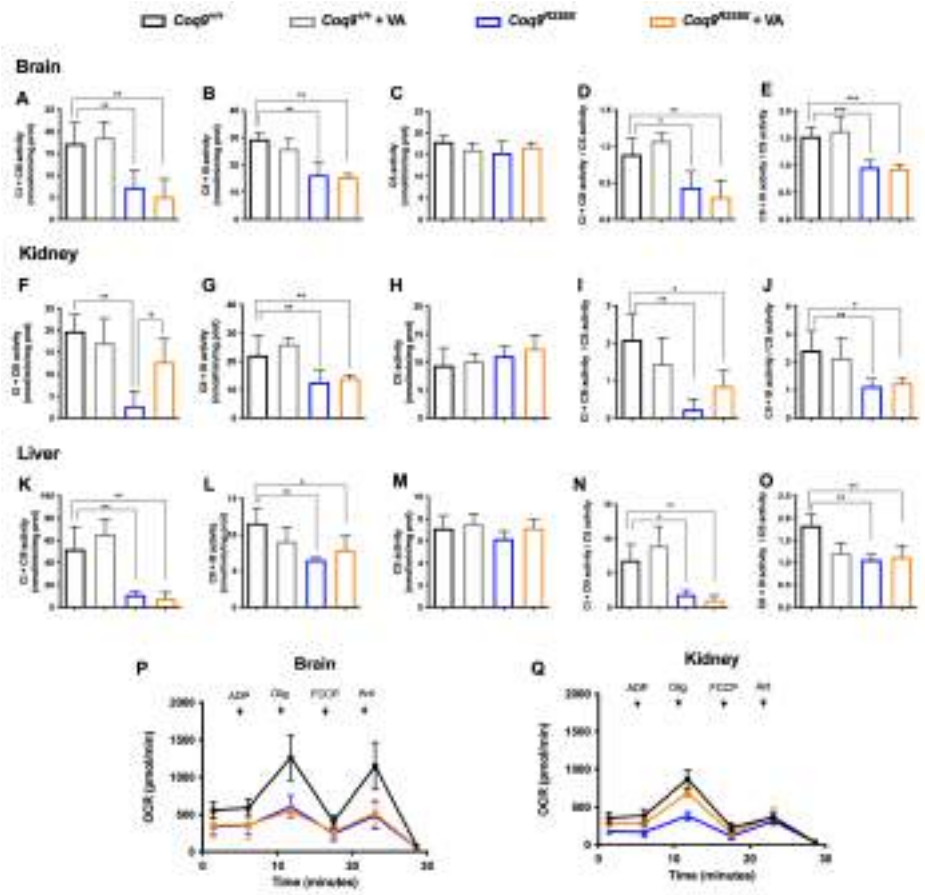

Figure 22. Tissue mitochondrial function after VA treatment in *Coq9*^{R239X} mice.

(A, F and K) CoQ-dependent Complex I+III activities in the brain (A), kidneys (F) and liver (K) of *Coq9*$^{+/+}$ mice, *Coq9*$^{+/+}$ mice after 1% VA treatment, *Coq9*^{R239X} mice and *Coq9*^{R239X} mice after 1% VA treatment.

(B, G and L) CoQ-dependent Complex II+III activities in the brain (B), kidneys (G) and liver (L) of *Coq9*$^{+/+}$ mice, *Coq9*$^{+/+}$ mice after 1% VA treatment, *Coq9*^{R239X} mice and *Coq9*^{R239X} mice after 1% VA treatment.

(C, H and M) Citrate synthase activity of the brain (C), kidneys (H) and liver (M) in *Coq9*$^{+/+}$ mice, *Coq9*$^{+/+}$ mice after 1% VA treatment, *Coq9*^{R239X} mice and *Coq9*^{R239X} mice after 1% VA treatment.
(D, I and N) CoQ-dependent Complex I+III activities normalized by citrate synthase activity in the brain (D), kidneys (I) and liver (N) of *Coq9*$^{+/+}$ mice, *Coq9*$^{+/+}$ mice after 1% VA treatment, *Coq9*^{R239X} mice and *Coq9*^{R239X} mice after 1% VA treatment.
(E, J and O) CoQ-dependent Complex II+III activities normalized by citrate synthase activity in the brain (E), kidney (J) and liver (O) of *Coq9*$^{+/+}$ mice, *Coq9*$^{+/+}$ mice after 1% VA treatment, *Coq9*^{R239X} mice and *Coq9*^{R239X} mice after 1% VA treatment.
(P and Q) Mitochondrial oxygen consumption rate (represented as State 3°, in the presence of ADP and substrates) in the brain (P) and kidneys (Q) of *Coq9*$^{+/+}$ mice, *Coq9*^{R239X} mice and *Coq9*^{R239X} mice after 1% VA treatment. The data represent three technical replicates and the figures are representative of three biological replicates. *Coq9*$^{+/+}$ mice, *Coq9*^{R239X} mice and *Coq9*^{R239X} mice after 1% VA treatment were included in all graphs. ADP = adenosine diphosphate; Olig = oligomycin; FCCP = carbonyl cyanide-p-trifluoromethoxyphenylhydrazone; Ant = antimycin A.
Data are expressed as mean ± SD. *P < 0.05, **P < 0.01, ***P < 0.001, differences versus *Coq9*$^{+/+}$; +P < 0.05, ++P < 0.01, +++P < 0.001, versus *Coq9*^{R239X}; (one-way ANOVA with a Tukey's post hoc test; n = 5 for each group).

4.1.4. 4-HB analogs induce anti-neuroinflammatory effects

Keeping in mind the previously described results, as well as the similarity between them and the results previously reported in *Coq9*^{R239X} mice treated with β-RA (279, 287), we decided to analyze the transcriptomic profiles of *Coq9*^{R239X} mice treated with either VA or β-RA to find potential common therapeutic mechanisms. We thus carried out an RNA-Seq experiment on the mouse brainstem, since we did not find cerebral changes neither in CoQ metabolism or mitochondrial bioenergetics, even though the encephalopathic phenotype was rescued with both treatments. For this analysis, we divided the mice into four

experimental groups: *Coq9*$^{+/+}$, *Coq9*^{R239X}, *Coq9*^{R239X} treated with 1% β-RA and *Coq9*^{R239X} treated with 1% VA. The analysis reveals upregulation of canonical pathways related to the inflammatory signaling pathway in *Coq9*^{R239X} mice compared to *Coq9*$^{+/+}$ mice (Fig. 23A). In particular, the genes *Ccl2* and *Cxcl10*, which encode the proinflammatory cytokines CXCL10 and CCL2, respectively, are highly expressed in the mutant mice compared to the *Coq9*$^{+/+}$ mice (Fig. 23B). This was confirmed by quantifying the gene expression of *Ccl2* and *Cxcl10* by quantitative real-time PCR (Figs. 24A–B) and determining CCL2 and CXC10 levels with a ProcartaPlex Inmunoassay (Fig. 23C and D). Remarkably, treatment with either VA or β-RA normalizes the levels of the altered genes (Fig. 23A and B; Fig. 24A–B), as well as the levels of the cytokines (Fig. 23C and D). Other neuroinflammatory genes are also upregulated in the brainstem of *Coq9*^{R239X} mice (Fig. 23A and B) and repressed under both treatments (Fig. 23A and B). Moreover, the proinflammatory cytokine IL-1β shows a trend toward decreased levels (Fig. 23E and F), while the anti-inflammatory cytokines IL-6 and IL-10 show a trend toward increased levels (Fig. 23G and H) under both treatments.

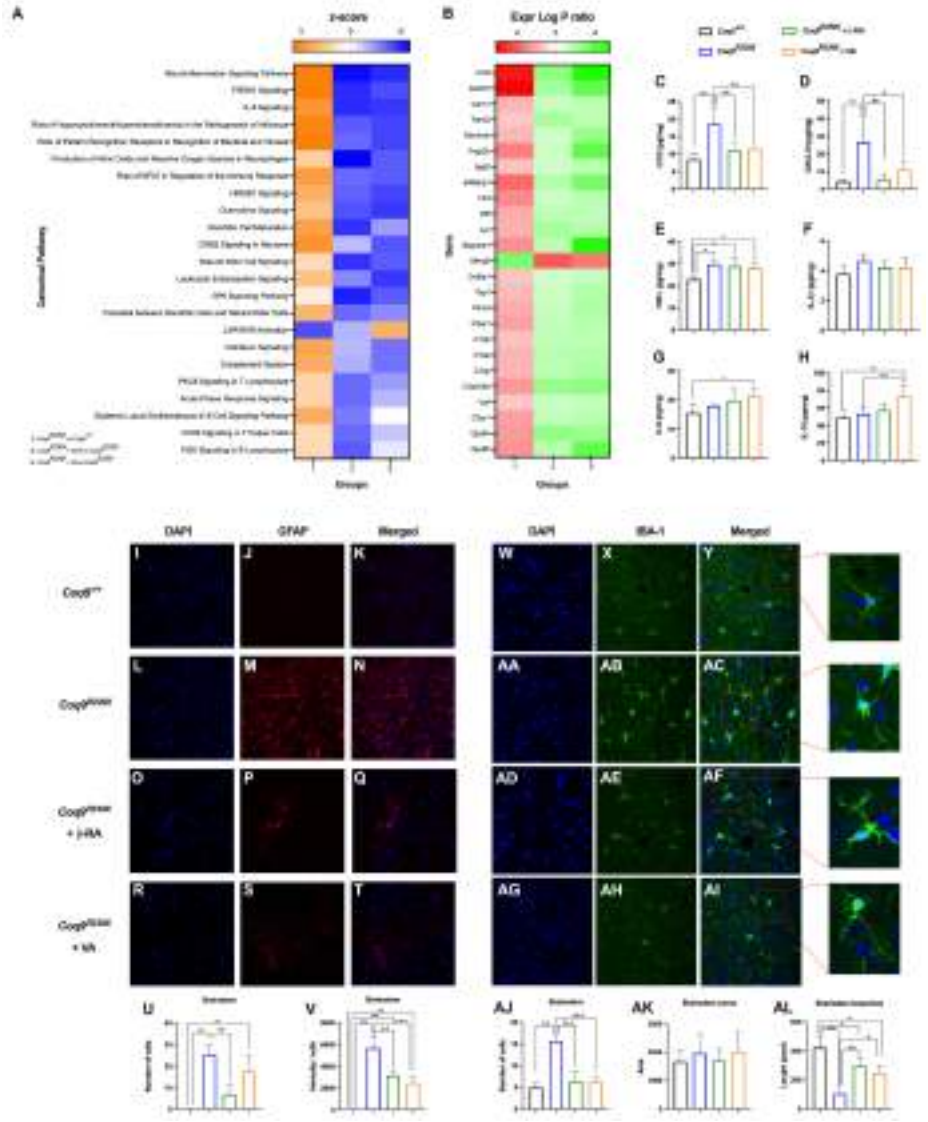

Figure 23. Gene expression profile and characterization of the neuroinflammatory status after treatment of *Coq9*^{R239X} mice with 4-HB analogs.

(A) Representative heatmap of the canonical pathways altered by the mutation and normalized by either β-RA or VA treatments in the brainstem of *Coq9*$^{+/+}$ mice, *Coq9*^{R239X} mice, *Coq9*^{R239X} mice after 1% β-RA treatment and *Coq9*^{R239X} mice after 1% VA treatment at 3 months of age.

(B) Representative heatmap of the expression level of the genes altered by the mutation and normalized by either β-RA or VA treatments in the brainstem of *Coq9*$^{+/+}$ mice,

Coq9^{R239X} mice, *Coq9*^{R239X} mice after 1% β-RA treatment and *Coq9*^{R239X} mice after 1% VA treatment at 3 months of age.

(C–H) Levels of the cytokines CCl2 (C), CXCL10 (D), TNFα (E), IL-1β (F), IL-6 (G) and IL-10 (H) in the brainstem of *Coq9*$^{+/+}$ mice, *Coq9*^{R239X} mice, *Coq9*^{R239X} mice after 1% β-RA treatment and *Coq9*^{R239X} mice after 1% VA treatment at 3 months of age.

(I–T) GFAP stain in the brainstem of *Coq9*$^{+/+}$ mice (I, J and K), *Coq9*^{R239X} mice (L, M and N), *Coq9*^{R239X} mice under 1% β-RA supplementation (O, P and Q) and *Coq9*^{R239X} mice under 1% VA supplementation (R, S and T) at 3 months of age.

(U and V) Quantification of GFAP expression by number of cells (U) and intensity/cells (V) in the brainstem of *Coq9*$^{+/+}$ mice, *Coq9*^{R239X} mice, *Coq9*^{R239X} mice under 1% β-RA supplementation and *Coq9*^{R239X} mice under 1% VA supplementation at 3 months of age.

(W-AI) IBA-1 stain in the brainstem of *Coq9*$^{+/+}$ mice (W, X and Y), *Coq9*^{R239X} mice (AA, AB and AC), *Coq9*^{R239X} mice under 1% β-RA supplementation (AD, AE and AF) and *Coq9*^{R239X} mice under 1% VA supplementation (AG, AH and AI) at 3 months of age.

(AJ, AK and AL) Quantification of IBA-1 expression by number of cells (AJ) and phenotype analysis of soma area (AK) and branches length (AL) in the brainstem of *Coq9*$^{+/+}$ mice, *Coq9*^{R239X} mice, *Coq9*^{R239X} mice under 1% β-RA supplementation and *Coq9*^{R239X} mice under 1% VA supplementation at 3 months of age.

Data are expressed as mean ± SD. *P < 0.05, **P < 0.01, ***P < 0.001, differences versus *Coq9*$^{+/+}$; +P < 0.05, ++P < 0.01, +++P < 0.001, versus *Coq9*^{R239X}; (one-way ANOVA with a Tukey's post hoc test; n = 5 for each group).

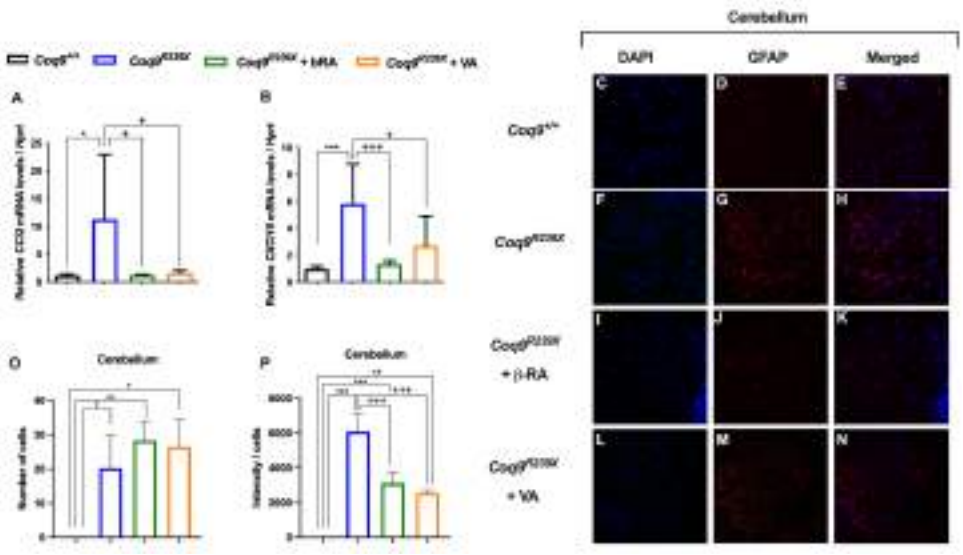

Figure 24. Validation of CCl2 and CXCl10 in brainstem and GFAP stain in the cerebellum of the mutant mice after b-RA and VA treatment.

(A and B) Relative mRNA levels of *CCl2* (A) and *CXCL10* (B) in the brain of *Coq9*$^{+/+}$, *Coq9*^{R239X} mice, *Coq9*^{R239X} mice under 1% β-RA and *Coq9*^{R239X} mice under 1% VA supplementation at 3 months of age.

(C-N) GFAP stain in the cerebellum of *Coq9*$^{+/+}$mice (C, D and E), *Coq9*^{R239X} mice (F, G and H), *Coq9*^{R239X} mice under 1% β-RA supplementation (I, J and K) and *Coq9*^{R239X} mice under 1% VA supplementation (L, M and N) at 3 months of age.

(O and P) Quantification of GFAP expression by number of cells (O) and intensity/cells (P) in the cerebellum of *Coq9*$^{+/+}$mice, *Coq9*^{R239X} mice, *Coq9*^{R239X} mice under 1% β-RA supplementation and *Coq9*^{R239X} mice under 1% VA supplementation at 3 months of age. Data are expressed as mean ± SD. *P < 0.05, **P < 0.01, ***P < 0.001, differences versus *Coq9*$^{+/+}$; +P < 0.05, ++P < 0.01, +++P < 0.001, versus *Coq9*^{R239X}; (one-way ANOVA with a Tukey's post hoc test; n = 5 for each group).

Neuroinflammation in neurodegenerative diseases is typically mediated by gliosis. Accordingly, compared to *Coq9*$^{+/+}$ mice (Fig. 23I, J and K; Fig S6C, D and E), the brainstem (Fig. 23L, M, and N) and cerebellum (Fig 24F, G and H) of *Coq9*^{R239X} mice showed features of

reactive astrogliosis (113). Both the β-RA and VA treatments significantly diminish the number and intensity of reactive astrocytes, marked as GFAP-positive cells, in the brainstem (Fig. 23O–V) and cerebellum (Fig. 24I-P). Additionally, proliferation of microglia, marked as IBA-1-positive cells, compared to the wild-type mice (Fig. 23W, X and Y), is apparent in the brainstem of the mutant mice (Fig. 23AA, AB, AC and AJ). Moreover, the microglia in the brainstem of *Coq9*^{R239X} mice shows a reactive morphology, with hypertrophy, thickened soma, and short branches, which are the typical features of a proinflammatory state (Fig. 23AA, AB, AC, AK and AL). Supplementation with either β-RA or VA reduces the number and reactivity of microglia (Fig. 23AD-AL), thus promoting an anti-inflammatory phenotype (Fig. 23AK and AL). The individual effects of β-RA and VA on microglia distribution and reactivity are also observed in the prefrontal cortex and cerebellum (Fig. 25).

Together, these results reveal the antineuroinflammatory effects of both 4-HB analogs as a key therapeutic approach for rescuing the encephalopathic phenotype associated with CoQ deficiency.

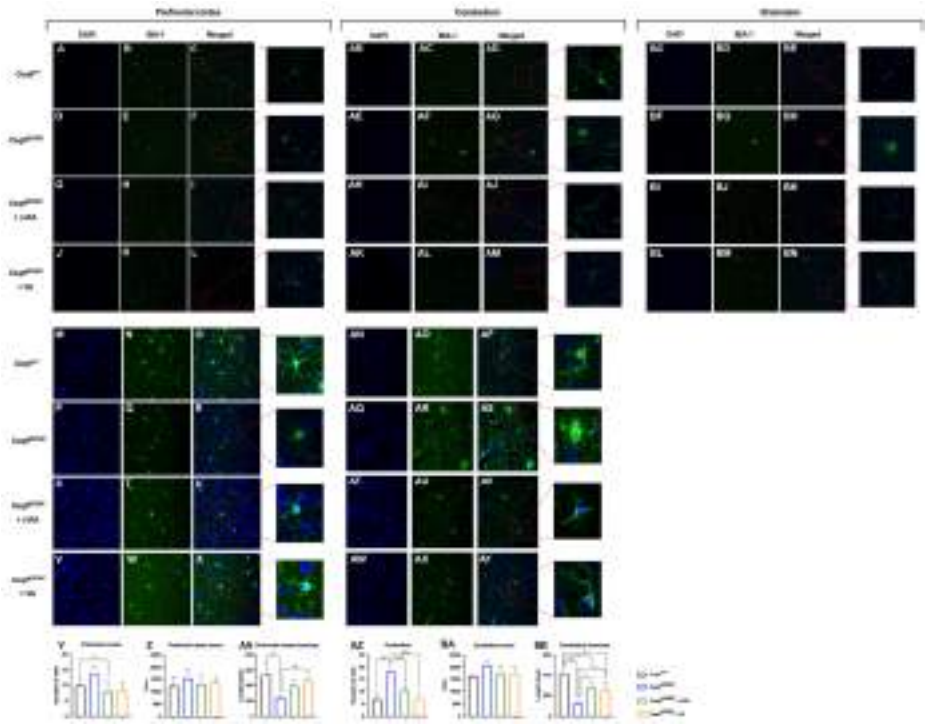

Figure 25. IBA-1 stain in the brain of the mutant mice after b-RA and VA treatment.

(A-X) IBA-1 stain in the prefrontal cortex of *Coq9*$^{+/+}$ mice, *Coq9*^{R239X} mice, *Coq9*^{R239X} mice under 1% β-RA supplementation and *Coq9*^{R239X} mice under 1% VA supplementation at 3 months of age under confocal microscope (A-L) and fluorescence microscope (M-X).

(Y, Z and AA) Quantification of IBA-1 expression by number of cells (Y) and phenotype analysis of soma area (Z) and branches length (AA) in the prefrontal cortex of *Coq9*$^{+/+}$ mice, *Coq9*^{R239X} mice, *Coq9*^{R239X} mice under 1% β-RA supplementation and *Coq9*^{R239X} mice under 1% VA supplementation at 3 months of age.

(AB-AY) IBA-1 stain in the cerebellum of *Coq9*$^{+/+}$ mice, *Coq9*^{R239X} mice, *Coq9*^{R239X} mice under 1% β-RA supplementation and *Coq9*^{R239X} mice under 1% VA supplementation at 3 months of age under confocal microscope (AB-AM) and fluorescence microscope (ANAY).

(AZ, BA and BB) Quantification of IBA-1 expression by number of cells (AZ) and phenotype analysis of soma area (BA) and branches length (BB) in the cerebellum of *Coq9*$^{+/+}$ mice, *Coq9*^{R239X} mice, *Coq9*^{R239X} mice under 1% β-RA supplementation and *Coq9*^{R239X} mice under 1% VA supplementation at 3 months of age.

(BC-BN) IBA-1 stain in the brainstem of *Coq9*$^{+/+}$ mice, *Coq9*^{R239X} mice, *Coq9*^{R239X} mice under 1% β-RA supplementation and *Coq9*^{R239X} mice under 1% VA supplementation at 3 months of age under confocal microscope.
Data are expressed as mean ± SD. *P < 0.05, **P < 0.01, ***P < 0.001, differences versus *Coq9*$^{+/+}$; +P < 0.05, ++P < 0.01, +++P < 0.001, versus *Coq9*^{R239X}; (one-way ANOVA with a Tukey's post hoc test; n = 5 for each group).

4.1.5. 4-HB analogs modify the levels of secreted proteins in the plasma

Since the observed antineuroinflammatory effects could be mediated by an indirect mechanism through potential endocrine factors, we analyzed the plasma proteome in the same groups. The analyses identify proteins whose levels are significantly altered in *Coq9*^{R239X} mice compared to wild-type mice, and normalize by both treatments. Specifically, 5 proteins (Fig. 26A) met that criterion, i.e.: SERPINA3, pregnancy zone protein (PZP), mannose-binding lectin-associated serine protease-1 (MASP1), collagen α-1 chain (COL1A1) and anaphylatoxin-like domain-containing protein (AI182371). Specifically, SERPINA3, MASP1, COL1A1 and AI182371 are downregulated in the mutant mice, and PZP is upregulated. Treatment with either β-RA or VA upregulates SERPINA3, MASP1, COL1A1 and AI182371 and downregulates PZP (Fig. 26B). Interestingly, some of these proteins have been related to immune functions, e.g., SERPINA 3 (300), MASP1 (301) and AI182371 (GO annotation), or to pathophysiological conditions of the CNS, e.g., SERPINA 3 (302) and PZP (303, 304). The levels of the other 11 proteins are also modified after β-RA and VA treatment compared to vehicle treatment, although they are not altered in *Coq9*^{R239X} mice compared to wild-type mice (Fig. 26A).

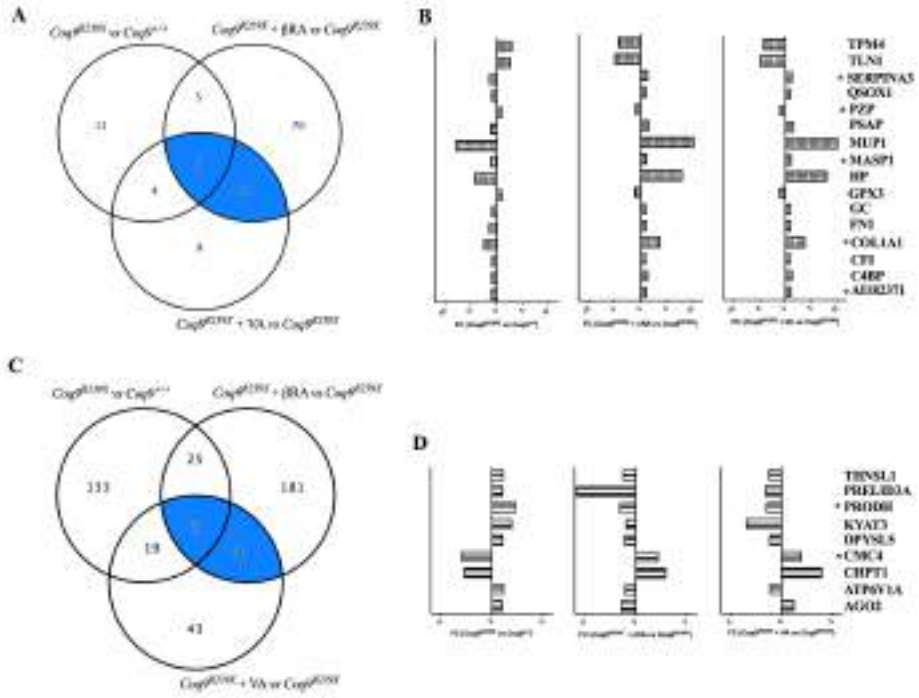

Figure 26. Mitochondrial proteome modulation after 4-HB analogs treatment in the plasma and brain of *Coq9*^{R239X} mice.

(A) Global differences in the protein levels between experimental groups in plasma. In blue are marked the 5 proteins altered by the mutation and by β-RA and VA treatments and the 11 proteins modified by β-RA and VA treatments.

(B) Fold change of the proteins modified by the mutation and normalized by β-RA and VA treatments in the plasma. *p < 0.05. *Coq9*$^{+/+}$, n = 7; *Coq9*^{R239X}, n = 7; *Coq9*^{R239X} after β-RA treatment, n = 7; *Coq9*^{R239X} after VA treatment, n = 7.

(C) Global differences in the protein levels between experimental groups in brain. In blue are marked the 2 proteins altered by the mutation and by β-RA and VA treatments and the 9 proteins modified by β-RA and VA treatments.

(D) Fold change of the proteins modified by the mutation and normalized by b-RA and VA treatments in the brain mitochondrial proteome. *p < 0.05. Mitochondrial proteomics was performed in isolated mitochondria. *Coq9*$^{+/+}$, n = 5; *Coq9*^{R239X}, n = 5; *Coq9*^{R239X} after β-RA treatment, n = 6; *Coq9*^{R239X} after VA treatment, n = 5.

4.1.6. 4-HB analogs normalize the mitochondrial proteome in the context of CoQ deficiency

Tissues from *Coq9*^{R239X} mice show an altered mitochondrial proteome (120). Thus, to further evaluate the common therapeutic mechanism of 4-HB analogs, we performed quantitative proteomics analysis of mitochondrial fractions from the brain and kidneys of mice in the same experimental groups and with the previously described criteria. In the brain, proline dehydrogenase (PRODH) and Cx9C motif-containing protein 4 (CMC4) levels are significantly altered in *Coq9*^{R239X} mice compared to wild-type mice, and these changes are normalized by both treatments. PRODH, a CoQ-dependent enzyme involved in proline metabolism and the urea cycle, is upregulated in *Coq9*^{R239X} mice compared to wild-type mice, while CMC4, a protein with nonessential role in cytochrome c oxidase subassembly (305), is downregulated in the mutant mice. Treatment with either β-RA or VA reverses this pattern, as it induced a downregulation of PRODH and an upregulation of CMC4 (Figs. 26C and D; Fig. 27A). Moreover, nine additional proteins are also modified after β-RA and VA treatments compared to vehicle treatment, although they are not altered in *Coq9*^{R239X} mice compared to wild-type mice (Fig. 26C).

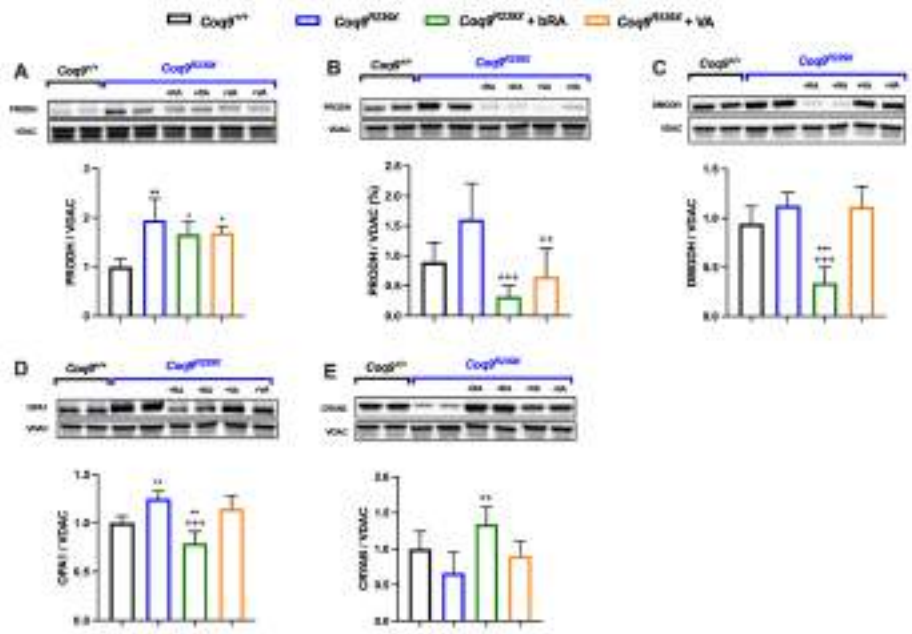

Figure 27. Validation of some key proteins identified in the proteomics analyses.
(A) Western blot of PRODH in brain homogenates of *Coq9*$^{+/+}$, *Coq9*^{R239X} mice, *Coq9*^{R239X} mice under 1% β-RA and *Coq9*^{R239X} mice under 1% VA supplementation at 3 months of age.
(B-E) Western blot of PRODH (B), DMGDH (C), OPA1 (D) and CRYAB (E) in kidney homogenates of *Coq9*$^{+/+}$, *Coq9*^{R239X} mice, *Coq9*^{R239X} mice under 1% β-RA and *Coq9*^{R239X} mice under 1% VA supplementation at 3 months of age.
Data are expressed as mean ± SD. *P < 0.05, **P < 0.01, ***P < 0.001, differences versus *Coq9*$^{+/+}$; +P < 0.05, ++P < 0.01, +++P < 0.001, versus *Coq9*^{R239X}; (one-way ANOVA with a Tukey's post hoc test; n = 5 for each group).

In the kidneys, 74 mitochondrial proteins meet the previously described criteria, and 60 additional proteins are also modified with either β-RA or VA treatments compared to vehicle treatment, although they are not altered in *Coq9*^{R239X} mice compared to wild-type (Fig. 28A). All of these proteins were grouped in the MitoPathways (306) (Fig. 28B–H). Interestingly, the CoQ-dependent enzymes electron transfer

flavoprotein dehydrogenase (ETFDH), proline dehydrogenase 2 (PRODH2), PRODH, dihydroorotate dehydrogenase (DHODH) and choline dehydrogenase (CHDH) are upregulated in *Coq9*^{R239X} mice compared to *Coq9*$^{+/+}$ mice (Fig. 28B and I), probably as a response to low levels of CoQ. These proteins are part of the Q-junction (Fig. 6I) and they are directly or indirectly involved in fatty acid oxidation, branched-chain amino acid metabolism, lysine and glycine metabolism, choline and betaine metabolism, proline metabolism, glyoxylate and pyruvate metabolism, nucleotide metabolism, folate and 1-C metabolism, the urea and tricarboxylic acid (TCA) cycles, as well as the transsulfuration pathway and the methionine cycle (Fig. 28I) (124, 306, 307). Most likely due to this alteration in the Q-junction and its linked pathways, upregulation of proteins involved in beta-oxidation (Fig. 28C), folate and glycine metabolism (Fig. 28D), nucleotide metabolism (Fig. 28E), the TCA cycle (Fig. 28F), the carnitine pathway (Fig. 28G) and the OxPhos system (Fig. 28H) is also detected in the mutant mice. Importantly, treatment with either β-RA or VA induces the downregulation of these proteins (Fig. 28B–H). The results for PRODH, DMGDH, OPA1 and CRYAB were validated by western blotting of tissue homogenates (Figs. 27B–E). Similar changes are observed for proteins related to protein synthesis, mitochondrial protein import, carriers, mitochondrial fusion, chaperones, and others (Fig. 29). Therefore, treatment with β-RA or VA partially normalizes the mitochondrial proteome disruption caused by dysfunctional Q-junction.

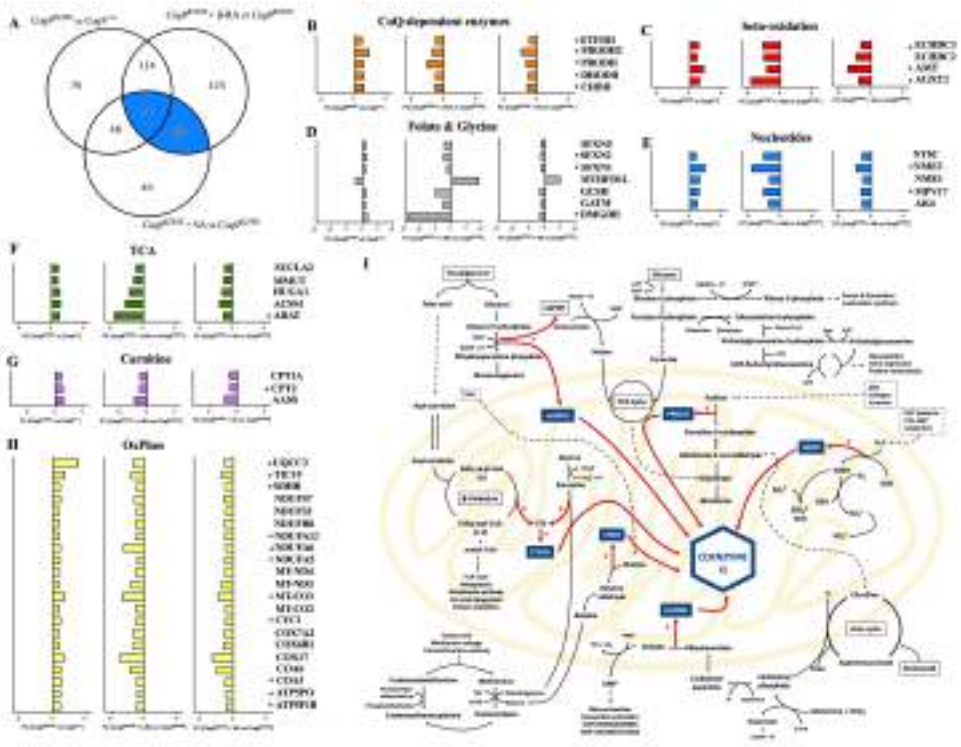

Figure 28. Mitochondrial proteome after 4-HB analogs treatment in the kidneys of *Coq9*^{R239X} mice.

(A) Global differences in protein levels between experimental groups. The blue segment represents the 74 proteins altered by the mutation and by β-RA and VA treatments, and the 60 proteins modified by β-RA and VA treatments.

(B–H) Fold change of the level of the proteins modified by the mutation and normalized by either β-RA or VA treatments in the renal mitochondrial proteome in the kidney of *Coq9*$^{+/+}$ mice, *Coq9*^{R239X} mice, *Coq9*^{R239X} mice after 1% β-RA treatment and *Coq9*^{R239X} mice after 1% VA treatment at 3 months of age. Proteins are classified according to their functions in CoQ-dependent enzyme (B), beta-oxidation (C), folate and glycine (D), nucleotides (E), citric acid cycle (TCA) (F), carnitine (G) and OxPhos system (H). *$p < 0.05$. Mitochondrial proteomics was performed in isolated mitochondria. *Coq9*$^{+/+}$, n = 5; *Coq9*^{R239X}, n = 5; *Coq9*^{R239X} after β-RA treatment, n = 6; *Coq9*^{R239X} after VA treatment, n = 5.

(I) Schematic representation of the Q-junction and its connection with the cell metabolism.

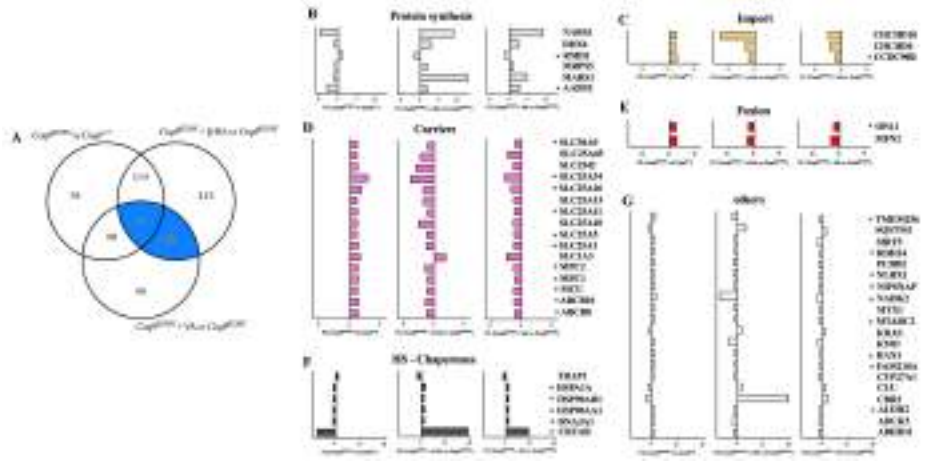

Figure 29. Additional proteomics analysis in the kidneys of *Coq9*^{R239X} mice after 4-HB analogs treatment.

(A) Global differences in the protein levels between experimental groups. In blue are marked the 74 proteins altered by the mutation and by β-RA and VA treatments and the 60 proteins modified by β-RA and VA treatments.

(B-H) Fold change of the proteins modified by the mutation and normalized by β-RA and VA treatments in the renal mitochondrial proteome in the kidney of *Coq9*$^{+/+}$ mice, *Coq9*^{R239X} mice, *Coq9*^{R239X} mice after 1% β-RA treatment and *Coq9*^{R239X} mice after 1% VA treatment at 3 months of age. Proteins are classified according to its function in protein synthesis (B), import (C), carriers (D), fusion (E), chaperones (F) and others (G).

*p < 0.05. Mitochondrial proteomics was performed in isolated mitochondria. *Coq9*$^{+/+}$, n = 5; *Coq9*^{R239X}, n = 5; *Coq9*^{R239X} after β-RA treatment, n = 6; *Coq9*^{R239X} after VA treatment, n = 5.

4.1.7. β-RA and VA restore the CoQ-dependent metabolism in the context of CoQ deficiency

The changes in the mitochondrial proteome must lead to adaptations in mitochondrial metabolism. Thus, we explored the metabolic changes induced by β-RA and VA in the same experimental groups previously

subjected to transcriptomics and proteomics analyses, following the same analytical criteria (Fig. 30A-M and Fig. 31A–F). Metabolites were also sorted based on their VIP score values (Fig. 30, Fig. 31A) and grouped in metabolic pathways based on an enrichment analysis (Fig. 32). In the brain (Fig. 30D), kidneys (Fig. 30J) and plasma (Fig. 31D), decreased levels of both N-Ac-glucosamine and N-Ac-glucosamine-6P levels are detected in the *Coq9*^{R239X} mice, compared to those in the wild-type mice. Both metabolites are involved in the hexosamine biosynthetic pathway, a branch of glycolysis that can be adapted to changes in the TCA cycle (308) (Fig. 28I). This pathway is involved in O-linked-N-acetylglucosaminylation (O-GlcNAcylation) (Fig. 28I), which is crucial for neuronal survival and is affected by aging and in neurodegenerative diseases (309-319). Either β-RA or VA supplementation increases the levels of both metabolites in the mutant mice (Fig. 30, Fig. 31D), most likely due to overcompensation to normalize the TCA cycle.

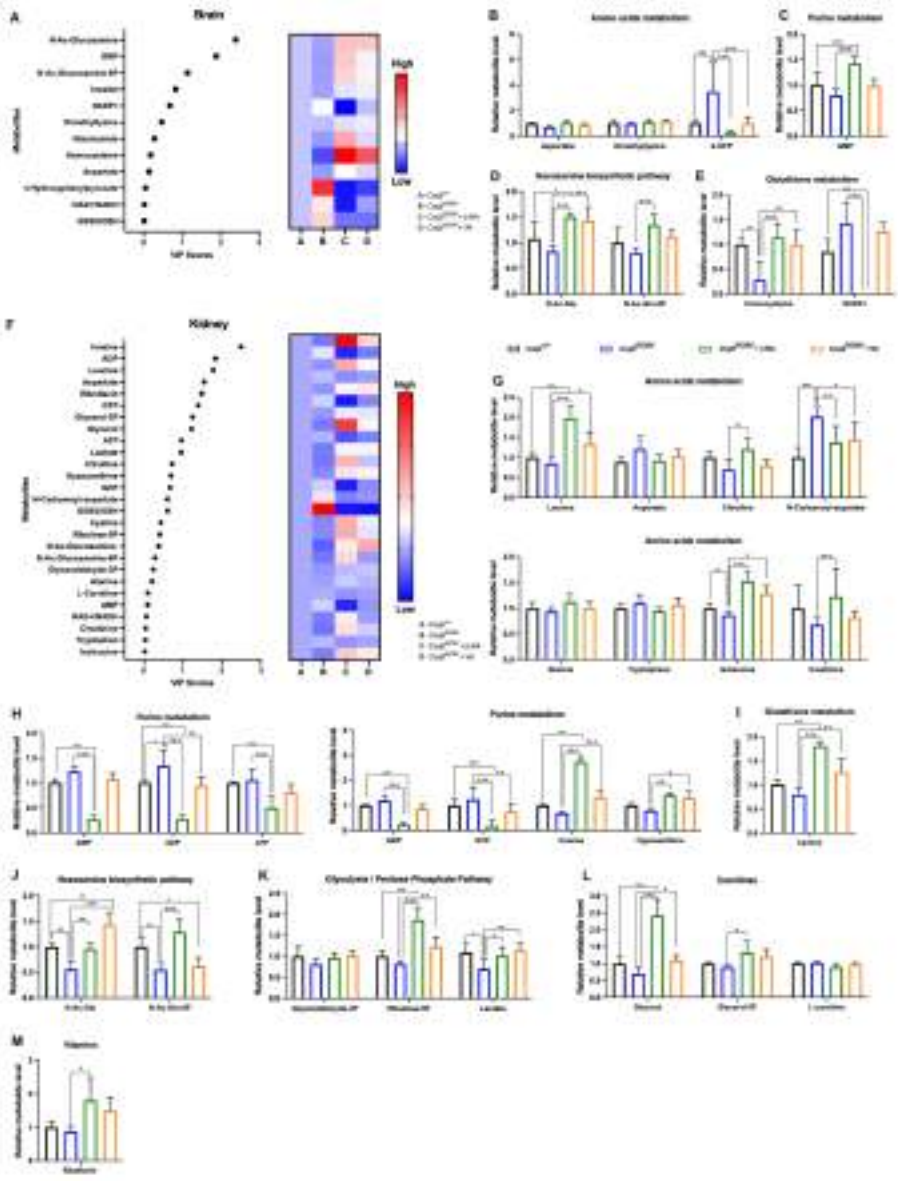

Figure 30. Effect of the treatment with 4-HB analogs in the cerebral and renal metabolism of *Coq9*^{R239X} mice.

(A) Variable importance in projection (VIP) scores plots for the metabolites modified by the mutation and normalized by β-RA and VA treatments in the brain. The right heatmap indicates the metabolite levels for each experimental group.

(B-E) Key metabolites related to amino acid metabolism (B), purine metabolism (C), hexosamines biosynthetic pathway (D) and glutathione metabolism (E) detected in the

brain of *Coq9*$^{+/+}$ mice, *Coq9*^{R239X} mice, *Coq9*^{R239X} mice after 1% β-RA treatment and *Coq9*^{R239X} mice after 1% VA treatment at 3 months of age.

(F) Variable importance in projection (VIP) scores plots for the metabolites modified by the mutation and normalized by β-RA and VA treatments in the kidneys. The right heatmap indicates the metabolite levels for each experimental group.

(G-M) Key metabolites related to amino acids metabolism (G), purine metabolism (H), glutathione metabolism (I), hexosamines biosynthetic pathway (J), glycolysis/pentose phosphate pathway (K), carnitines (L) and vitamins (M) detected in the kidneys of *Coq9*$^{+/+}$ mice, *Coq9*^{R239X} mice, *Coq9*^{R239X} mice after 1% β-RA treatment and *Coq9*^{R239X} mice after 1% VA treatment at 3 months of age.

Data are expressed as average peak area ±SD compared to wild-type. *P < 0.05, **P < 0.01, ***P < 0.001, differences versus *Coq9*$^{+/+}$; +P < 0.05, ++P < 0.01, +++P < 0.001, versus *Coq9*^{R239X}; (one-way ANOVA with a Tukey's post hoc test; n = 5 for each group).

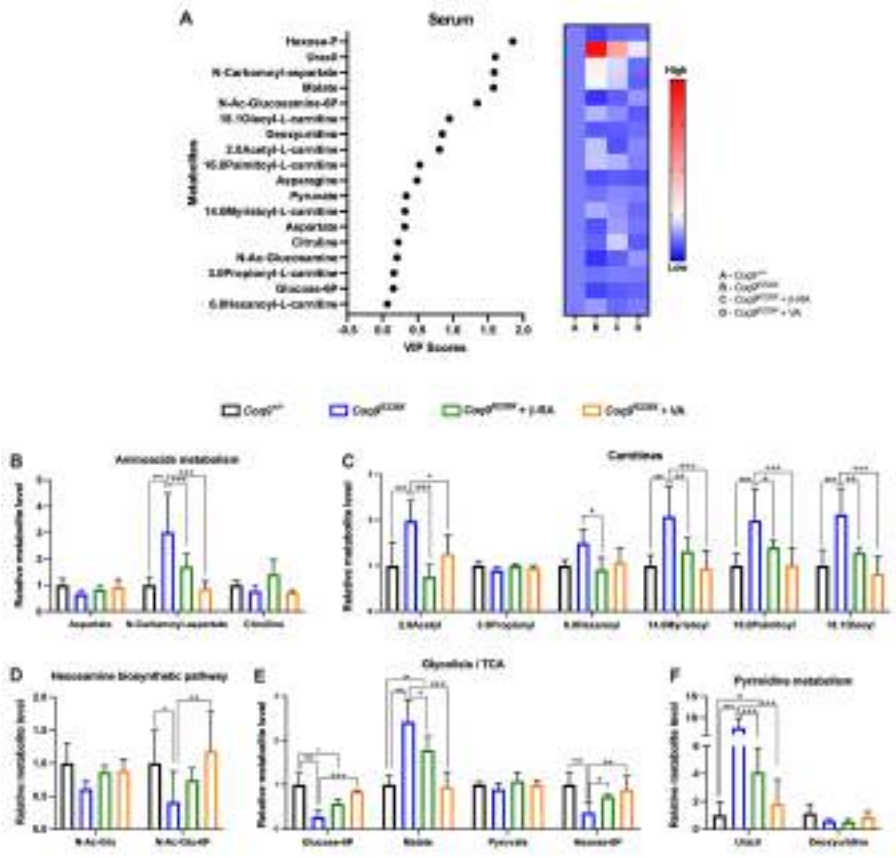

Figure 31. Effect of the treatment with 4-HB analogs on serum metabolites in *Coq9*^{R239X} mice.

(A) Variable importance in projection (VIP) scores plots for the metabolites modified by the mutation and normalized by β-RA and VA treatments in the brain. The right heatmap indicates the metabolite levels for each experimental group.

(B–F) Key metabolites related to amino acid metabolism (B), carnitines (C), hexosamines biosynthetic pathway (D), glycolysis/TCA (E) and pyrimidine metabolism (F) detected in the serum of *Coq9*$^{+/+}$ mice, *Coq9*^{R239X} mice, *Coq9*^{R239X} mice after 1% β-RA treatment and *Coq9*^{R239X} mice after 1% VA treatment at 3 months of age.

Data are expressed as average peak area ±SD compared to wild-type. *P < 0.05, **P < 0.01, ***P < 0.001, differences versus *Coq9*$^{+/+}$; +P < 0.05, ++P < 0.01, +++P < 0.001, versus *Coq9*^{R239X}; (one-way ANOVA with a Tukey's post hoc test; n = 5 for each group).

It is also interesting that 4-hydroxyphenylpyruvate (4-HPP) is accumulated in the brains of the mutant mice (Fig. 30B). This metabolite is an intermediate in the synthesis of the CoQ benzoquinone ring (Fig. 8), and therefore, a feedback mechanism induced by the defect in CoQ biosynthesis in *Coq9*^{R239X} mice could be the origin of this abnormality. Consistent with that possibility, either β-RA or VA restores 4-HPP levels (Fig. 30D), indicating that both compounds are used in the CoQ biosynthetic pathway.

In the kidneys, inosine and hypoxanthine levels are moderately decreased in the mutant mice compared to the wild-type mice, and the treatments with 4-HB analogs significantly increase the levels of both metabolites in *Coq9*^{R239X} mice (Fig. 30H). Additionally, some of the identified metabolites are related to the metabolic pathways linked to the enzymes of the Q-junction. For instance, 1) the catabolic pathway for the essential amino acids leucine and isoleucine is linked to ETFDH activity. Both leucine and isoleucine show a trend toward decreased levels in *Coq9*^{R239X} mice compared to *Coq9*$^{+/+}$ mice and a significant increase after either β-RA or VA supplementation (Fig. 30G). 2) Aspartate degradation is related to the urea cycle and to the activity of the CoQ-dependent enzymes PRODH and DHODH, while N-carbamoyl-aspartate is mainly connected to DHODH activity (Fig. 28I). The levels of aspartate and N-carbamoyl-aspartate increase in the mutant mice and to decrease after the treatments (Fig. 30G). 3) Glycerol-3P and glycerol are metabolites of the glycerol phosphate shuttle linked to GPDH activity (Fig. 28I). Both metabolites show a trend toward decrease levels in the mutant mice, and both treatments lead to an increase in their levels (Fig. 30L).

In the serum, five carnitines are highly increased in the serum of *Coq9*^{R239X} mice, i.e., 2.0 acetyl-l-carnitine, 6.0 hexanoyl-l-carnitine, 14.0 myristoyl-l-carnitine, 16.0 palmitoyl-l-carnitine and the 18.1 oleoyl-l-carnitine (Fig. 31C). Treatment with the 4-HB analogs significantly decreases the levels of these carnitine metabolites. However, the levels of 3.0 propionyl-l-carnitine are similar in the four experimental groups (Fig. 31C). These changes may be related to the levels and activity of the CoQ-dependent enzyme ETFDH, which participates in β-oxidation (Fig. 28I). In fact, an accumulation of carnitines in plasma has also been described in other models of CoQ deficiency (270, 320). The levels of N-carbamoyl-aspartate significantly increase in *Coq9*^{R239X} mice compared to wild-type mice, and supplementation with either β-RA or VA normalizes these levels (Fig. 31B), similar to the results in the kidneys. The N-carbamoyl-aspartate is related to the CoQ-dependent enzyme DHODH and to the ribonucleotide metabolism (Fig. 28I). As a possible consequence, the uracil levels are significantly increased, while the deoxyuridine levels were decreased in the mutant mice (Fig. 31F). Supplementation with 4-HB analogs induces normalization of the levels of these metabolites. Since the metabolism of glucosamines is linked to the pentose phosphate pathway (PPP), changes in the glucosamine pathway could explain the modifications observed in the levels of hexose-P and glucose-6P (Fig. 31E). Hexose-P and glucose-6P levels significantly decrease in *Coq9*^{R239X} mice compared to the wild-type mice, and the β-RA and VA treatments normalize these levels. Together, the metabolic profiles reveal a metabolic adaptation in response to the disruption in the Q-junction and a powerful metabolic correction effect

of the 4-HB analogs, even though the levels of CoQ and DMQ were not completely normalized.

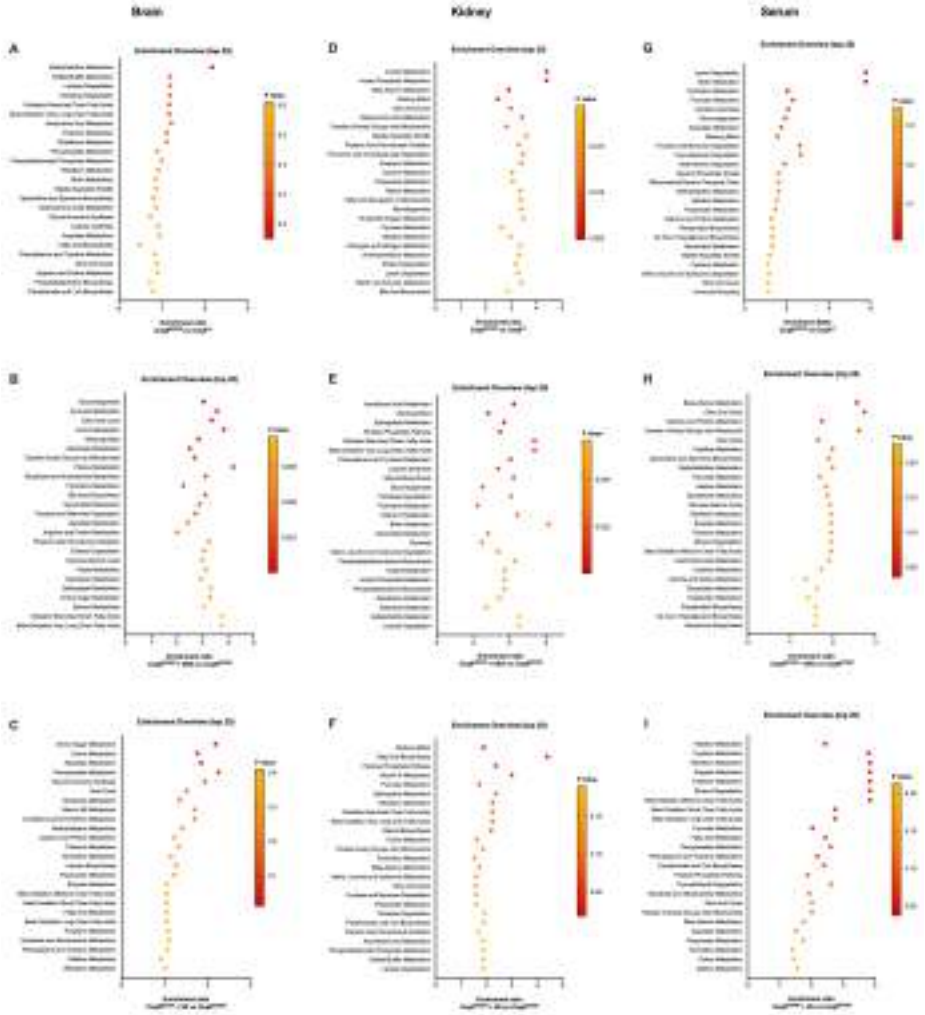

Figure 32. Metabolomics enrichment analysis in the mutant mice.

(A-C) Enrichment analysis of brain samples in the comparison *Coq9*^{R239X} vs *Coq9*$^{+/+}$ (A), *Coq9*^{R239X} + β-RA vs *Coq9*^{R239X} (B) and *Coq9*^{R239X} + VA vs *Coq9*^{R239X} (C).

(D-F) Enrichment analysis of kidney samples in the comparison *Coq9*^{R239X} vs *Coq9*$^{+/+}$ (D), *Coq9*^{R239X} + β-RA vs *Coq9*^{R239X} (E) and *Coq9*^{R239X} + VA vs *Coq9*^{R239X} (F).

(G-I) Enrichment analysis of serum samples in the comparison *Coq9*^{R239X} vs *Coq9*$^{+/+}$ (G), *Coq9*^{R239X} + β-RA vs *Coq9*^{R239X} (H) and *Coq9*^{R239X} + VA vs *Coq9*^{R239X} (I).

Coq9$^{+/+}$, n = 5; *Coq9*^{R239X}, n = 5; *Coq9*^{R239X} after β-RA treatment, n = 5; *Coq9*^{R239X} after VA treatment, n = 5.

4.2. *Therapeutic Mechanisms Associated to Coenzyme Q_{10} Supplementation in Mitochondrial Diseases.*

4.2.1. CoQ_{10} supplementation modifies sulfide metabolism and the pathways associated to one carbon metabolism

We first analyzed the effect of CoQ_{10} supplementation in the transcriptomic profiles of skin fibroblasts from a control subject and a patient with Complex I deficiency due to a mutation in the *NDUFS1* gene (Table 2). Both control and *NDUFS1* mutant cells have similar levels of CoQ_{10} and supplementation with 100 μM CoQ_{10} significantly increases the cellular content of CoQ_{10} (Table 3), although the majority of these CoQ_{10} molecules would be located in the cell membrane and a low proportion would enter into the mitochondria (262, 321). The increase of the cell content of CoQ_{10} modifies a variety of canonical pathways involved in cell metabolism, being the number of the altered pathways higher in the treated mutant cells than in the control treated cells (Fig. 33A and B).

Defect	Gene	Mutations	Residual C-I activity
Complex I Deficiency	*ND3*	10158T>C, p.Ser34Pro	52%
	ND6	14459G>A, p.Ala72Val	57%
	NDUFB3	c.64T>C, p.Trp22Arg c.208G>T, p.Gly70X	17%
	NDUFB9	c.191T>C homo, p.L64P	18%
	NDUFS1	c.683T>C, p.V228A c.755A>G, p.D252G	37%
	NDUFS3	c.595C>T homo, p.R199W	40%
	NDUFS8	c.187G>C homo, p.Glu63Gln	54%
			Residual CoQ_{10} levels
CoQ_{10} Deficiency	*PDSS2*	c.[964C>T];[1145C>T]	15%
	COQ4	c.[155T>C];[518_520delCCA]	27%

Table 2. Human skin fibroblasts with CI or CoQ_{10} deficiency used in this study. Reference in (196, 322-325).

Gene	Regular Medium (A) CoQ_{10} (ng/mg prot)	Regular Medium + 100 uM CoQ_{10} (B) CoQ_{10} (ng/mg prot)	(B/A) CoQ_{10} Increase Fold
Controls	83.2 ± 13.3	715335 ± 304041 +++	8597
ND3	86.4 ± 2.1	446180 ± 166429 +++	5164
ND6	82.4 ± 30.1	450973 ± 50294 +++	4881
NDUFB3	88 ± 22.8	3260636 ± 1498894 +++	37074
NDUFB9	84.6 ± 7.5	195247 ± 31905 +++	2308
NDUFS1	75 ± 8.6	265735 ± 144425 +++	3543
NDUFS3	93 ± 9.2	446627 ± 169118 +++	4802
NDUFS8	87.4 ± 9.3	591155 ± 415712 +++	6768
PDSS2	18.8 ± 11.2 ***	2046794 ± 9957 +++	108872
COQ4	27.4 ± 13.4 ***	472774 ± 166429 +++	17255

Table 3. Levels of CoQ_{10} in untreated and CoQ_{10}-supplemented cells.

Data are expressed as mean ± SD. ***P < 0.001, differences versus controls; +++ P < 0.001, differences versus untreated cells (A).

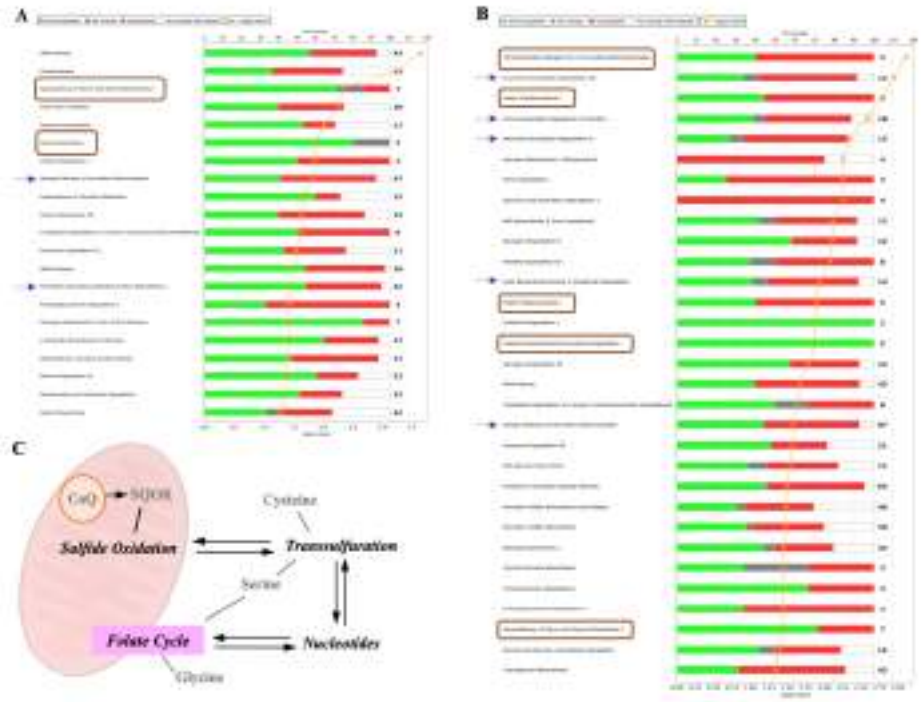

Figure 33. CoQ_{10} supplementation induces changes in pathways that are direct or indirectly related to sulfide metabolism.

(A and B) Results of the pathway analysis showing the canonical pathways most enriched in the differentially expressed gene list of the CoQ_{10} treated cells dataset. The pathways related to sulfide metabolism are indicated by a brown square or a purple arrow. (A) Analysis of the control cells. (B) Analysis of the *NDUFS1* mutant cells.

(C) Pathways related to sulfide metabolism. SQOR, the first enzyme in the mitochondrial hydrogen sulfide oxidation pathway, is the target of CoQ_{10}.

About 20–35% of the canonical pathways that CoQ_{10} modifies are related to sulfide metabolism or to pathways associated to one carbon metabolism. Specifically, CoQ_{10} supplementation in control cells affects the pathways of serine and glycine biosynthesis, the salvage pathway of pyrimidine biosynthesis and the pyrimidine deoxyribonucleotides *de novo* biosynthesis (Fig. 33A). CoQ_{10} supplementation in the *NDUFS1* mutant cells modifies the tetrahydrofolate salvage from 5,10-methenyltetrahydrefolate, folate transformation I, folate polyglutamylation, cysteine biosynthesis/homocysteine degradation, the pathway of serine and glycine biosynthesis, the guanosine nucleotides degradation III, the purine nucleotides degradation II, the adenosine nucleotides degradation II, the urate biosynthesis/inosine 5′-phosphate degradation and the salvage pathways of pyrimidine ribonucleotides (Fig. 33B). Importantly, all these pathways are interconnected in the cell's metabolism (Fig. 33C).

Further analysis of the indicated pathways shows that, in the sulfide metabolism, CoQ_{10} supplementation up-regulates *SQOR* (sulfide oxidation pathway) and down-regulates *CSE* and *CBS* (transsulfuration pathway), in both control and mutant cells (Fig. 34A and B). In the serine biosynthesis, five key genes (*PHGDH, PSAT1, PSDH, PSAT1P3* and *PSAT1P4*), are under-expressed after CoQ_{10} supplementation in both control and mutant cells (Fig. 34C and D). An unbalance in the genes that encode mitochondrial proteins is observed in the folate cycle, in form of a decrease in the expression of *SHMT2* and *MTHFD2* and an increase in the expression of *MTHFD2L* after CoQ_{10} supplementation in

both control and mutant cells (Fig. 34E and F). Additionally, in the nucleotides' metabolism, *PRKCH, MAP2K8, MAP2K6, DMPK, AK4* and *IMPDH2* are under-expressed, while *EIF2AK2, CMPK2, APOBEC3G, APOBEC3F, APOBEC3B, AK5* and *XDH* are over-expressed after CoQ_{10} supplementation in both control and mutant cells (Fig. 34G and H). The direction of the fold change for some of these genes after CoQ_{10} supplementation, e.g. *SQOR, CSE, PSAT1P4, PHGDH, MTHFD1, PRKCH, EIF2AK2, DMK, CMPK2, APOBEC3G, APOBEC3F, APOBEC3B* or *AK4*, is the opposite to the fold change direction in the mutant cells compared with control cells (Fig. 35). To check whether those changes in genes expression result in a metabolic adaptation, we also quantified the levels of serine and glycine, two metabolites involved in one carbon metabolism that are altered under mitochondrial dysfunction. Serine/glycine ratio slightly decreases in fibroblasts with *NDUFS1* mutation, compared with control fibroblasts. Interestingly, serine/glycine ratio increases in control and mutant cells (Fig. 34I). Therefore, these data indicate that CoQ_{10} supplementation modifies sulfide metabolism and associated pathways, being all on them related to mitochondrial metabolism (Fig. 36).

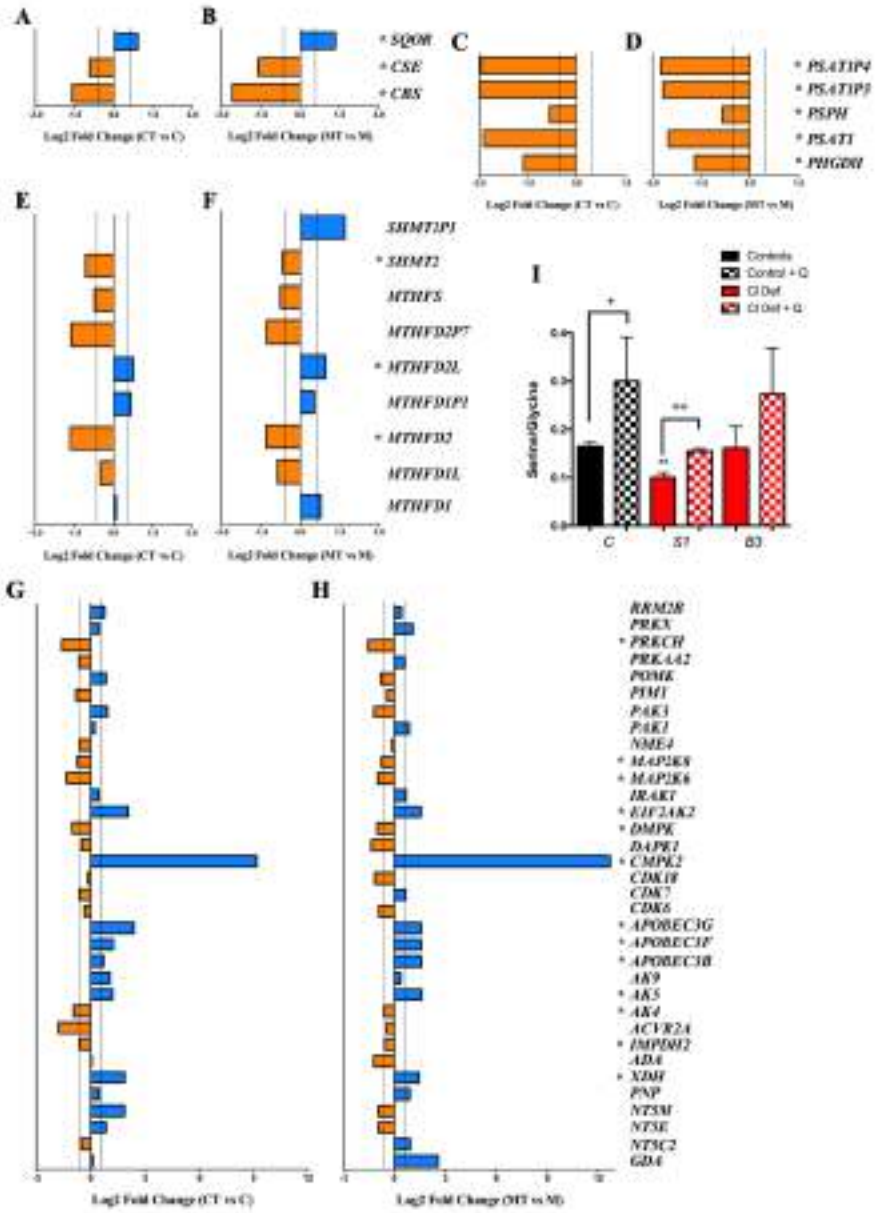

Figure 34. Changes in gene expression of pathways related to sulfide metabolism in response to CoQ_{10} supplementation.

(A and B) Changes in the expression of genes related to cysteine biosynthesis and sulfide metabolism in control (A) and mutant (B) cells after CoQ_{10} supplementation.

(C and D) Changes in the expression of genes related to serine/glycine biosynthesis in control (C) and mutant (D) cells after CoQ_{10} supplementation.

(E and F) Changes in the expression of genes related to the folate cycle in control (E) and mutant (F) cells after CoQ_{10} supplementation.

(G and H) Changes in the expression of genes related to nucleotides metabolism in control (G) and mutant (H) cells after CoQ_{10} supplementation.

Bars in blue indicate genes overexpressed; bars in orange indicates genes underexpressed. Dotted lines indicate the threshold considered for overexpression (log2 FC = 0.585) or underexpression (log2 FC = −0.585). Asterisks indicates the genes that exceed the fold change threshold and have P-values less than 0.05 in the comparison of treated and untreated cells in both control and mutant cells. C, control; CT, control treated with CoQ_{10}; M, *NDUFS1* mutant; MT, *NDUFS1* mutant treated with CoQ_{10}.

(I) Serine/Glycine ratio in control (black bars) and patients' cells (red bars) with mutations in *NDUFS1* and *NDUFB3*, and their response to CoQ_{10} supplementation (checkered bars).

Data are expressed as mean ± SD. **P < 0.01; differences versus control. +P < 0.05; ++P < 0.01; control versus control + CoQ_{10} or Complex I deficiency versus Complex I deficiency + CoQ_{10} (t-test; n = 3 for each group; n = 3 for each group).

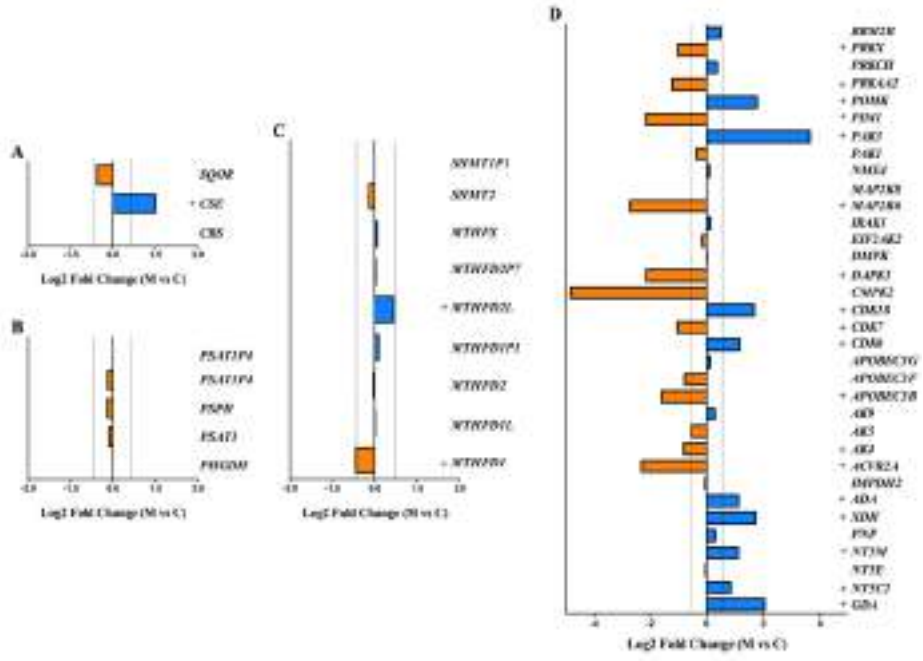

Figure 35. Changes in gene expression in the pathways related to sulfide metabolism in *NDUFS1* mutant cells.

(A) Changes in the expression of genes related to sulfide metabolism.

(B) Changes in the expression of genes related to cysteine biosynthesis.

(C) Changes in the expression of genes related to the folate cycle.

(D) Changes in the expression of genes related to nucleotides.

Bars in blue indicates genes overexpressed; bars in orange indicates genes underexpressed. Botted lines indicate the limit chosen for overexpression (log2 FC = 0.585) or underexpression (log2 FC = -0.585). Asterisks indicates the genes that exceed the chosen fold change limit and have p-values less than 0.05 in the comparison of treated and untreated cells in both control and mutant cells.

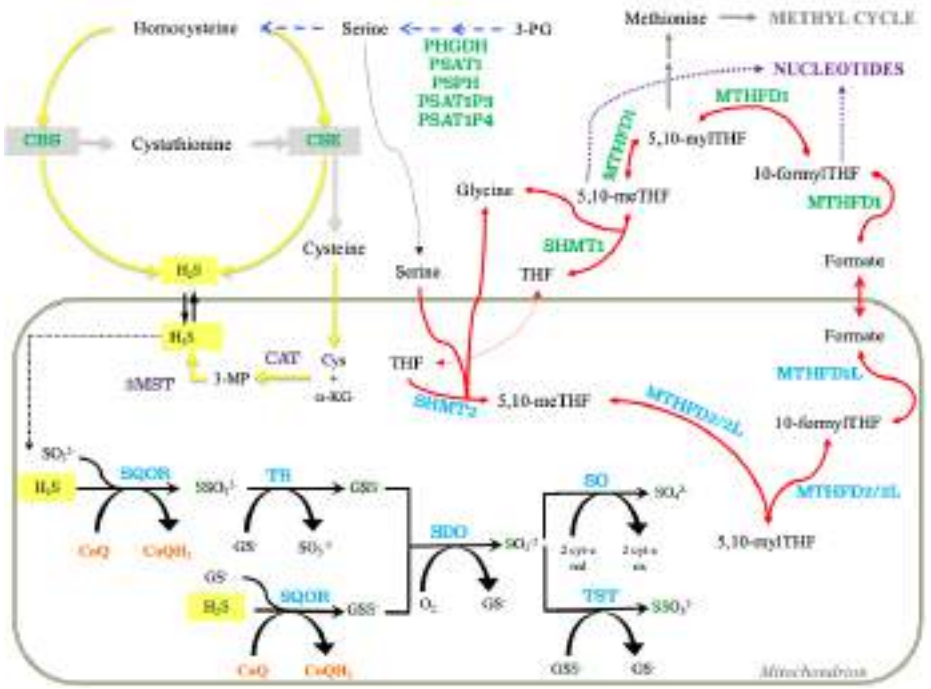

Figure 36. Relation between pathways, with some key genes indicated.

Sulfide oxidation pathway (black arrows); transsulfuration pathway (grey arrows); sulfide synthesis (yellow arrows); folate cycle (red arrows); serine biosynthesis (blue arrows); nucleotides metabolism (purple arrows).

4.2.2. CoQ_{10} supplementation modifies sulfide metabolism gene expression in cells with mutations in different Complex I or CoQ-biosynthetic genes

Among all changes described above, the upregulation of *SQOR* is likely the primary effect of CoQ_{10} since that enzyme requires CoQ_{10} for its normal activity and CoQ_{10} deficiency causes a reduction in the levels of SQOR (157, 158). Furthermore, SQOR needs the supply of hydrogen sulfide produced by cystathionine β-synthase (CBS) and cystathionine γ-lyase (CSE) in the transsulfuration pathway (Fig. 36). Thus, we extended the study by quantifying of the gene expression of enzymes of the hydrogen sulfide oxidation pathway, i.e. SQOR, thiosulfate sulfurtransferase (TST) and sulfite oxidase (SUOX), and the transsulfuration/hydrogen sulfide production pathways, i.e. CBS, CSE and 3-mercaptopyruvate sulfurtransferase (3MST), in additional cells that carry mutations in different Complex I subunits or CoQ-biosynthetic genes (Table 2).

Those cells have different residual levels of CI activity (Table 2), and we observed that the abnormalities in the levels of *SQOR* and *CSE* detected in the *NDUFS1* mutant cells are not a common pattern in all Complex I deficiency cells. Specifically, *SQOR* mRNA levels are 10–20% significantly reduced in *NDUFS1, NUUFS3* and *NDUFS8* mutant cells compared with controls cells (Fig. 37A). *TST* mRNA levels are significantly increased in *NDUFS3, NUUFS8, ND3, COQ4* and *PDSS2* mutant cells compared with control cells (Fig. 37B). The levels of *SOUX* and *CBS* mRNA are similar in mutant and control cells (Fig. 37C and D). *CSE* mRNA levels are significantly increased in *ND6, COQ4* and *PDSS2*

mutant cells compared with control cells (Fig. 37E). *3MST* mRNA levels are only significantly increased in *COQ4* mutant cells compared with control cells (Fig. 37B). Therefore, the changes on *SQOR* and *CSE* detected in the RNAseq analysis in the *NDUFS1* cells are not a common pattern in all Complex I deficiency cells.

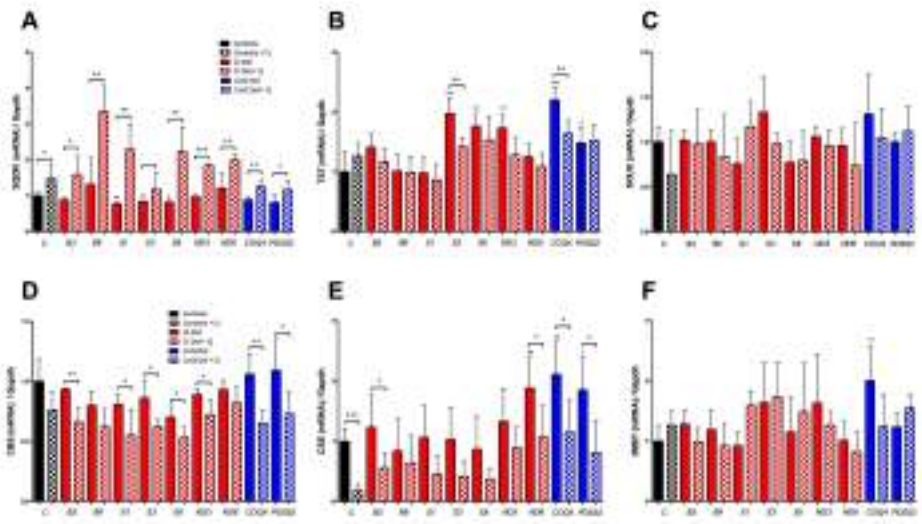

Figure 37. CoQ_{10} supplementation modifies the expression of key genes in the mitochondrial hydrogen sulfide oxidation pathway and the transsulfuration pathway.

(A–C) Expression levels of genes involved in the mitochondrial hydrogen sulfide oxidation pathway.

(D–F) Expression levels of genes involved in the transsulfuration pathway.

Black bars indicate control cells; red bars indicate cells with mutation in Complex I genes; blue bars indicate cells with mutations in CoQ_{10} biosynthetic genes. Solid bars indicate untreated cells; checkered bars indicate CoQ_{10}-treated cells.

Data are expressed as mean ± SD. *P < 0.05; **P < 0.01; ***P < 0.001; differences versus Control. +P < 0.05; ++P < 0.01; +++P < 0.001; control versus control + CoQ_{10} or Complex I deficiency versus Complex I deficiency + CoQ_{10} or CoQ_{10} deficiency versus CoQ_{10} deficiency + CoQ_{10} (t-test; n = 3 for each group; n = 3 for each group). C, control; B3, *NDUFB3* mutant; B9, *NDUFB9* mutant; S1, *NDUFS1* mutant; S3, *NDUFS3* mutant; S8, *NDUFS8* mutant; ND3, *ND3* mutant; ND6, *ND6* mutant; COQ4,

COQ4 mutant; PDSS2, *PDSS2* mutant; CI Def, cells with Complex I deficiency; CoQ Def, cells with CoQ_{10} deficiency; Q, CoQ_{10}.

CoQ_{10} supplementation significantly increases the cellular content of CoQ_{10} in all cell lines (Table 3). That increase in the cell content of CoQ_{10} induces a consistent increase of *SQOR* mRNA levels and decrease of *CBS* and *CSE* mRNA levels in all cells (Fig. 37A, D and E), although no generalized changes are detected on *TST, SOUX* or *3MST* mRNA levels (Fig. 37B, C and F). Specifically, the increase of *SQOR* mRNA levels is statistically significant in controls cells and *NDUFB3, NDUFB9, NDUFS1, NDUFS8, ND3, ND6, COQ4* and *PDSS2* mutant cells (Fig. 37A); the decrease of *CBS* mRNA levels is statistically significant in *NDUFB3, NDUFS1, NDUFS3, NDUFS8, ND3, COQ4* and *PDSS2* mutant cells (Fig. 37D); and the decrease of *CSE* mRNA levels is statistically significant in control cells and *NDUFB3, ND3, ND6, COQ4* and *PDSS2* mutant cells (Fig. 37E). Also, a significant decrease in *TST* mRNA levels is detected only in *NDUFS3* and *COQ4* mutant cells after CoQ_{10} supplementation (Fig. 37B). Therefore, we found a remarkable inverse correlation between the mRNA levels of *SQOR* and the mRNA levels of *CBS* and *CSE* after CoQ_{10} supplementation.

4.2.3. The modification of the expression of the sulfide oxidation genes after CoQ_{10} supplementation correlates with the changes in the levels of the sulfide oxidation proteins, and is independent of sulfur aminoacids availability

We assessed whether CoQ_{10} supplementation modified sulfide enzymes protein levels, as a result of the change in their gene expression. Moreover, since it has been reported that sulfide metabolism can be

adapted to dietary restriction in sulfur aminoacids (SAAR) (326, 327), we also evaluated whether the availability of sulfur aminoacids affects sulfide metabolism in CI and CoQ_{10} deficiency. Before CoQ_{10} supplementation, the levels of SQOR were significantly lower in two (out of three) of the cells with the lowest CI activity (*NDUFB3* and *NDUFS1*) and in the CoQ_{10} deficiency cells, compared with controls, although the levels of SQOR were normal in the cells with 40–60% of residual CI activity, as well as in one (out of three) of the mutant cells with the lowest CI activity (*NDUFB9*) (Fig. 38A and B; Fig. 39A and B). The levels of TST and SUOX were similar in mutant and control cells, except for the increased levels of TST in *NDUFS3* and *COQ4* mutant cells (Fig. 38A, C and D; Fig. 39A, C and D). All these changes were similar in the cells cultured under SAAR (Fig. 38 and 39; quantitative data not shown). Therefore, there was a general correlation between mRNA and protein levels in the mutant cells, with some exceptions. Interestingly, the levels of SQOR are consistently increased in all cell types after CoQ_{10} supplementation compared with the untreated cells, being the differences statistically significant in controls, *NDUFB3, NDUFS1, NDUFS8, ND3, COQ4* and *PDSS2* mutant cells (Fig. 38A and B; Fig. 39A and B). Moreover, the levels of SQOR were rescued in *NDUFB3, NDUFS1, COQ4* and *PDSS2* mutant cells after CoQ_{10} supplementation (Fig. 38A and B; Fig. 39A and B). On the contrary, the levels of TST and SUOX did not change after CoQ_{10} supplementation, except for a partial decrease of TST levels in *ND6* mutant cells after CoQ_{10} supplementation (Fig. 38A, C and D; Fig. 39A, C and D). All these changes were similar in the cells cultured under SAAR (Fig. 38 and 39; quantitative data not shown). Therefore, SQOR is the most affected enzyme in the H_2S oxidation pathway under CI

deficiency or low/high levels of CoQ_{10}, and those changes are not affected by SAAR.

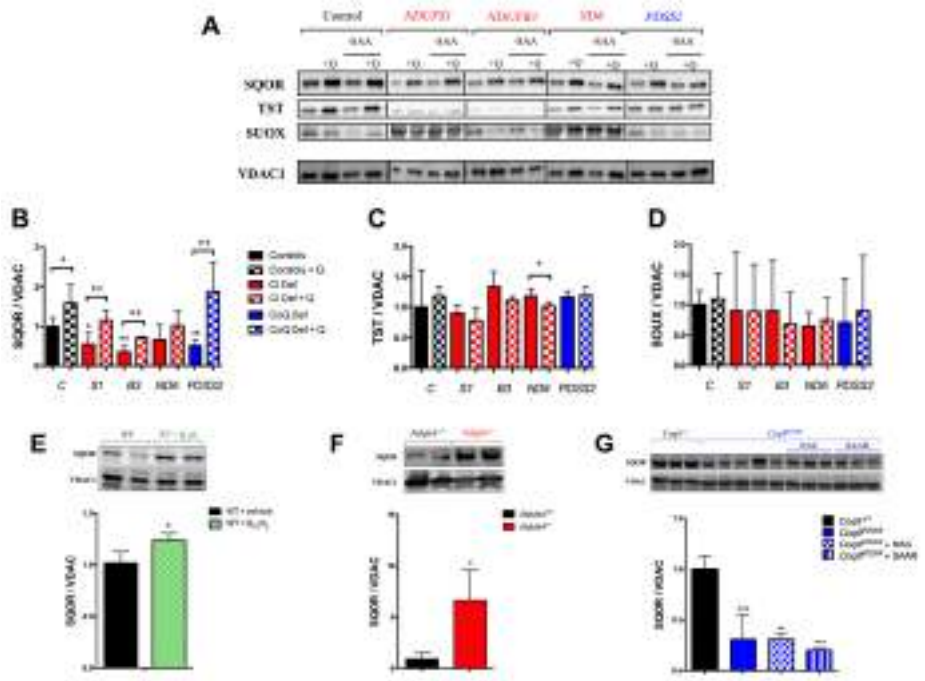

Figure 38. The levels of SQOR are modified under mitochondrial dysfunction or CoQ_{10} supplementation, independently of sulfur amino acids availability.

(A–D) Levels of the proteins of the mitochondrial hydrogen sulfide oxidation pathway in human skin fibroblasts from control and patients with mutations in Complex I subunits or CoQ_{10} biosynthetic genes.

Data are expressed as mean ± SD. *P < 0.05; **P < 0.01; ***P < 0.001; differences versus Control. +P < 0.05; ++P < 0.01; +++P < 0.001; Control versus Control + CoQ_{10} or Complex I deficiency versus Complex I deficiency + CoQ10 or CoQ_{10} deficiency versus CoQ_{10} deficiency + CoQ_{10} (t-test; n = 3 for each group; n = 3 for each group). C, control; S1, *NDUFS1* mutant; B3, *NDUFB3* mutant; S3, *NDUFS3* mutant; ND6, *ND6* mutant; PDSS2, *PDSS2* mutant; CI Def, cells with Complex I deficiency; CoQ Def, cells with CoQ_{10} deficiency; Q, CoQ_{10}; -SAA, medium without sulfur aminoacids. The blot image (A) has been made from three different membranes, as follow: blot 1, control and *PDSS2*; blot 2, *NDUFS1* and *ND6*; blot 3, *NDUFB3*.

(E) Levels of SQOR in the liver of C57bl6j mice supplemented with ubiquinol-10 for 1 month. Data are expressed as mean ± SD. *P < 0.05; **P < 0.01; ***P < 0.001; WT versus WT + $CoQ_{10}H_2$ (t-test; n = 4 for each group).

(F) Levels of SQOR in the brain of *Ndufs4*$^{-/-}$ mice. Data are expressed as mean ± SD. *P < 0.05; **P < 0.01; ***P < 0.001; *Ndufs4*$^{+/+}$ versus *Ndufs4*$^{-/-}$ (t-test; n = 5 for each group).

(G) Levels of SQOR in the kidneys of *Coq9*^{R239X} with vehicle, NAC or under SAAR. Data are expressed as mean ± SD. *P < 0.05; **P < 0.01; ***P < 0.001; differences versus *Coq9*$^{+/+}$ (t-test; n = 3 for each group; n = 3–5 for each group).

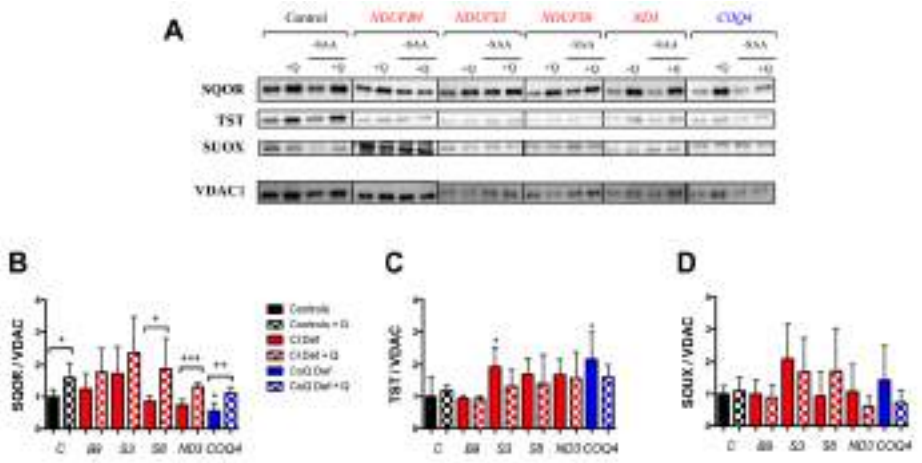

Figure 39. The levels of SQOR are modified under mitochondrial dysfunction or CoQ_{10} supplementation, independently of sulfur amino acids availability.

(A, B, C, D) Levels of the proteins of the mitochondrial hydrogen sulfide oxidation pathway in human skin fibroblasts from control and patients with mutations in Complex I subunits or CoQ_{10} biosynthetic genes.

Data are expressed as mean ± SD. *P < 0.05; **P < 0.01; ***P < 0.001; differences versus Control. +P < 0.05; ++P < 0.01; +++P < 0.001; Control versus Control + CoQ_{10} or Complex I deficiency versus Complex I deficiency + CoQ_{10} or CoQ_{10} deficiency versus CoQ_{10} deficiency + CoQ_{10} (t-test; n = 3 for each group); n = 3 for each group). C = control; B9 = *NDUFB9* mutant; S1 = *NDUFS1* mutant; S3 = *NDUFS3* mutant; S8 = *NDUFS8* mutant; ND3 = *ND3* mutant; COQ4 = *COQ4* mutant; CI Def = cells with Complex I deficiency; CoQ Def = cells with CoQ_{10} deficiency; Q = CoQ_{10}; -SAA = medium without sulfur aminoacids. The blot image (A) has been made from three

different membranes, as follow: blot 1, control; blot 2, *NDUFB9*; blot 3, *NDUFS3*, *ND3* and *COQ4*; blot 4, *NDUFS8*.

To assess whether the effects of CoQ_{10} supplementation, CI deficiency or different availability of sulfur aminoacids on SQOR levels observed *in vitro* also occur *in vivo*, we measured SQOR levels in three different systems: (1) in the liver of C57BL/6 J mice after $CoQ_{10}H_2$ supplementation, because the liver is the tissue that accumulates more CoQ_{10} when it is orally administrated (270, 274); (2) in the brain of *Ndufs4*$^{-/-}$ mice, the symptomatic tissue in this model of Leigh Syndrome due to CI deficiency (285) and (3) in the kidney of *Coq9*^{R239X} mice under supplementation with N-acetylcysteine (NAC), a sulfur-containing aminoacid, or a diet with restriction in sulfur aminoacids (SAAR), since the kidney has a very active sulfide metabolism and it has reduced levels of SQOR in this model of CoQ deficiency (158, 328). The levels of total CoQ ($CoQ_9 + CoQ_{10}$) increase in the liver of C57BL/6J mice after 1 month of water-soluble $CoQ_{10}H_2$ supplementation (Table 4). Consistent with this result, also the levels of SQOR increase in the liver of the same treated mice, compared with the untreated mice (Fig. 38E). The brain of *Ndufs4*$^{-/-}$ mice shows normal levels of CoQ_9, as compared with those in *Ndufs4*$^{+/+}$ mice (Table 4). However, the SQOR levels are significantly increased in mitochondria from the brain of *Ndufs4*$^{-/-}$ mice, compared with *Ndufs4*$^{+/+}$ mice (Fig. 38F). The levels of CoQ_9 and SQOR are significantly lower in the kidneys of *Coq9*^{R239X} mice than in the kidneys of *Coq9*$^{+/+}$, and they are not rescued by NAC or SAAR supplementation (Table 4 and Fig. 38G). These results indicate that CoQ_{10} is one of the factors that may regulate the levels of SQOR in vivo, independently of the sulfur-aminoacids availability. Moreover, SQOR is up-regulated,

probably as a compensatory response, in the brain of the mouse model of Leigh Syndrome due to severe CI deficiency.

Model	Tissue	No treatment Total CoQ (ng/mg prot)	Treatment with oral Q_0H_2 Total CoQ (ng/mg prot)	
C57Bl6J	Liver	352.9 ± 13.3	1885.7 ± 412.6 +++	
		CoQs (ng/mg prot)		
Ndufs4+/+	Brain	315.3 ± 50.3		
Ndufs4-/-	Brain	365.7 ± 77.8		
		Vehicle CoQs (ng/mg prot)	Treatment with NAC CoQs (ng/mg prot)	Under SAAR CoQs (ng/mg prot)
Coq9+/+	Kidney	1042.3 ± 222.4		
Coq9R239X	Kidney	19.2 ± 2.1 ***	16.2 ± 2.1 ***	21.9 ± 4.1 ***

Table 4. Levels of CoQ in tissues of the mouse models used in this study

Data are expressed as mean ± SD. ***P < 0.001, differences versus wild-type; +++ P < 0.001, differences versus untreated animals.

4.2.4. The abnormalities of SQOR levels in mitochondrial dysfunction are independent of mitochondrial supercomplexes formation

Since we have not identified a robust correlation between the SQOR levels and the residual CI activity, and because SQOR could interact with the mitochondrial supercomplexes though one of its components, i.e. CoQ, we evaluated the mitochondrial supercomplexes in control and mutant cells and mice. In the *in vitro* experiments, we used *NDUFS8*, *NDUFS1* and *NDUFB3* mutant cells, which have 54, 37 and 17% of residual CI activity, respectively, and a decrease in SQOR levels in the two latter cases. A decrease in the CI bound to supercomplexes is observed in the three mutant cells compared with control cells (Fig. 40A–C), while free CI is almost undetectable (Fig. 40A and D). Moreover, a decrease in the CIII bounds to supercomplexes and an increase of the free CIII are observed in the three mutant cells compared with control

cells (Fig. 40E–H). Therefore, we did not observe a correlation between the disruption of the mitochondrial supercomplexes and the decrease in SQOR levels.

To test whether SQOR could be detected in association with some mitochondrial complex/supercomplex, we performed BNGE-Page with mitochondria from kidneys of wild-type, *Ndufs4*$^{-/-}$ and *Coq9*^{R239X} mice and incubated the membranes with an anti-SQOR antibody. The pattern of bands is similar to those obtained for CIII (Fig. 40I). However, if we incubate the membrane with the anti-rabbit secondary antibody a similar pattern of bands is obtained (Fig. 40J), and this mainly corresponds to CIII (Fig. 40K), indicating some kind of cross-reaction between anti-rabbit antibody and some subunit of the CIII. Thus, we are not able to detect SQOR associated to any mitochondrial complex/supercomplex. Those results correlate with the data obtained by Van Strien and colleagues in a proteomic analysis in blue native gels run with samples of skin fibroblasts from control subjects (329). The representation of those data shows that the major proportion of SQOR is not bound to respiratory complexes or supercomplexes (Fig. 40L–N).

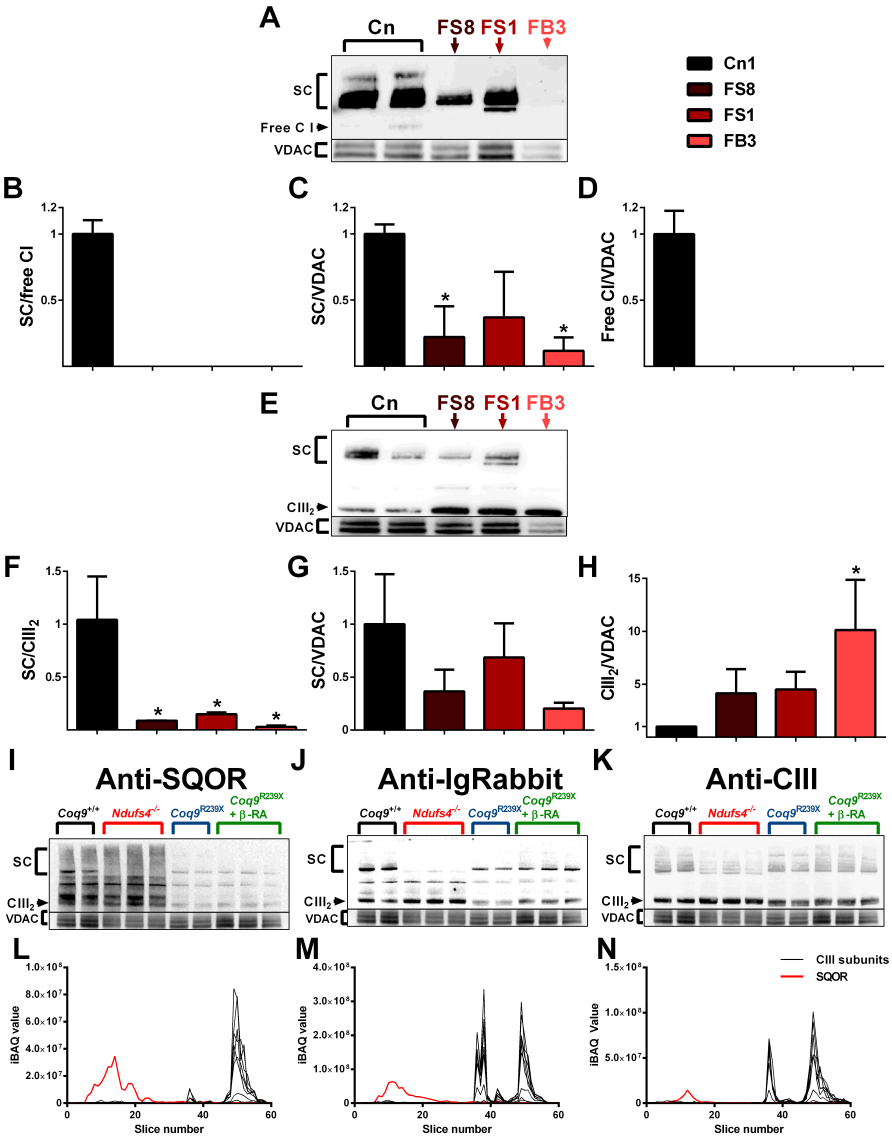

Figure 40. The changes of SQOR levels under mitochondrial dysfunction do not depend of mitochondrial supercomplexes formation.

(A-D) Blue-native gel electrophoresis (BNGE) followed by C-I immunoblotting analysis of mitochondrial supercomplexes in Control and CI deficiency skin fibroblasts. AntiVDAC was used as loading control.

(E-H) Blue-native gel electrophoresis (BNGE) followed by C-III immunoblotting analysis of mitochondrial supercomplexes in Control and CI deficiency skin fibroblasts. Anti-VDAC was used as loading control.

(I-K) Blue-native gel electrophoresis (BNGE) followed by SQOR, Ig rabbit or CIII immunoblotting to check the presence of SQOR in mitochondrial supercomplexes in mitochondria isolated from kidneys of mouse models with CI or CoQ deficiency. Test made in 6 different membranes using different conditions.
(L-N) Migration pattern of Complex III subunits and SQOR proteins from human skin fibroblasts of three different controls. Data extracted from (329).
Data are expressed as mean SD. *P < 0.05; **P < 0.01; ***P < 0.001; Control cells versus deficiency skin fibroblasts. (t-test; n = 3 for each group); n = 3 for each group).

4.2.5. CoQ_{10} supplementation downregulates the transsulfuration pathway, independently of sulfur aminoacids availability

To evaluate whether the transsulfuration pathway may adapt to the changes of SQOR levels, we quantified the levels of CBS, CSE and 3MST *in vitro* in the same experimental groups used to study the H_2S oxidation pathway. The levels of CBS are significantly increased in *NDUFS3*, *COQ4* and *PDSS2* mutant cells (Fig. 41A and B; Fig. 42A and B). The levels of CSE are increased in *NDUFS1*, *NDUFS3*, *ND3* and *COQ4* mutant cells (Fig. 41A and C; Fig. 42A and B). The levels of 3MST do not change in any mutant cells compared with control cells. Therefore, CBS and CSE are increased in certain cases of CI or CoQ deficiency.

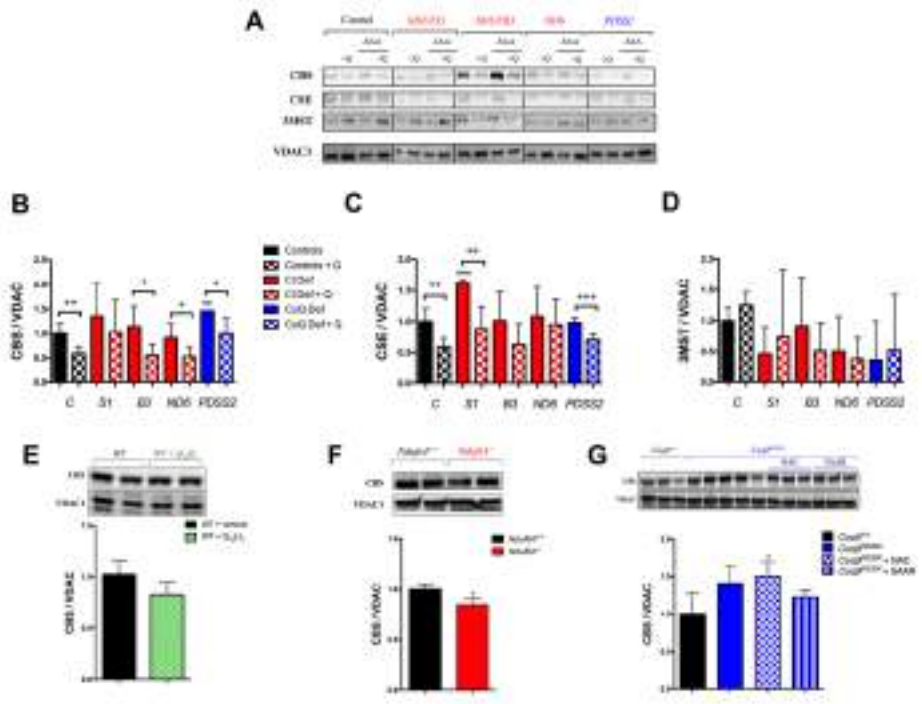

Figure 41. CoQ_{10} regulates the enzymes of transsulfuration pathway independently of sulfur amino acids availability.

(A–D) Levels of the proteins of the transsulfuration pathway in human skin fibroblasts from control and patients with mutations in Complex I subunits or CoQ_{10} biosynthetic genes.

Data are expressed as mean ± SD. *P < 0.05; **P < 0.01; ***P < 0.001; differences versus Control. +P < 0.05; ++P < 0.01; +++P < 0.001; Control versus Control + CoQ_{10} or Complex I deficiency versus Complex I deficiency + CoQ_{10} or CoQ_{10} deficiency versus CoQ_{10} deficiency + CoQ_{10} (t-test; n = 3 for each group; n = 3 for each group). C, control; S1, *NDUFS1* mutant; B3, *NDUFB3* mutant; S3, *NDUFS3* mutant; ND6, *ND6* mutant; PDSS2, *PDSS2* mutant; CI Def, cells with Complex I deficiency; CoQ Def, cells with CoQ_{10} deficiency; Q, CoQ_{10}; -SAA, medium without sulfur aminoacids. The blot image (A) has been made from three different membranes, as follow: blot 1, control and *PDSS2*; blot 2, *NDUFS1* and *ND6*; blot 3, *NDUFB3*.

(E) Levels of CBS in the liver of C57bl6j mice supplemented with ubiquinol-10 for 1 month. Data are expressed as mean ± SD. *P < 0.05; **P < 0.01; ***P < 0.001; WT versus WT + $CoQ_{10}H_2$ (t-test; n = 4 for each group).

(F) Levels of CBS in the brain of *Ndufs4*$^{-/-}$ mice. Data are expressed as mean ± SD. *P < 0.05; **P < 0.01; ***P < 0.001; *Ndufs4*$^{+/+}$ versus *Ndufs4*$^{-/-}$ (t-test; n = 5 for each group).

(G) Levels of SQOR in the kidneys of *Coq9*^{R239X} with vehicle, NAC or under SAAR. Data are expressed as mean ± SD. *P < 0.05; **P < 0.01; ***P < 0.001; differences versus *Coq9*$^{+/+}$ (t-test; n = 3 for each group; n = 3–5 for each group).

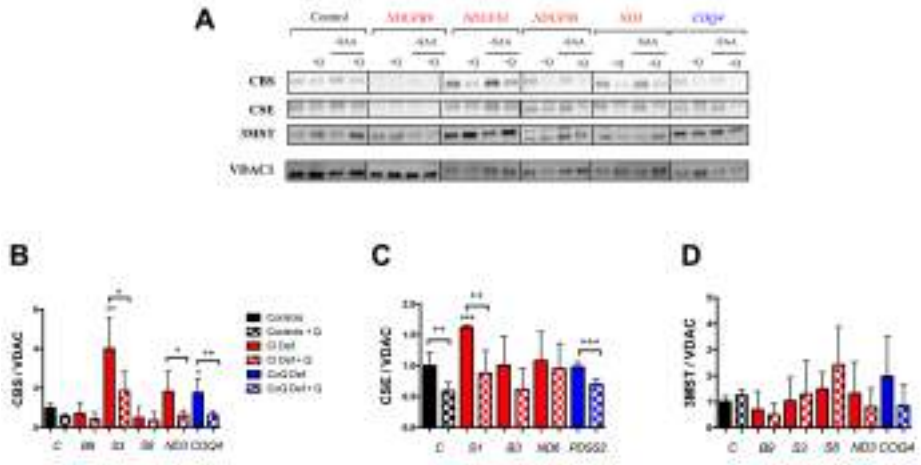

Figure 42. CoQ_{10} regulates the enzymes of transsulfuration pathway independently of sulfur amino acids availability.

(A, B, C, D) Levels of the proteins of the transsulfuration pathway in human skin fibroblasts from control and patients with mutations in Complex I subunits or CoQ_{10} biosynthetic genes.

Data are expressed as mean ± SD. *P < 0.05; **P < 0.01; ***P < 0.001; differences versus Control. +P < 0.05; ++P < 0.01; +++P < 0.001; Control versus Control + CoQ_{10} or Complex I deficiency versus Complex I deficiency + CoQ_{10} or CoQ_{10} deficiency versus CoQ_{10} deficiency + CoQ_{10} (t-test; n = 3 for each group). C = control; B9 = *NDUFB9* mutant; S1 = *NDUFS1* mutant; S3 = *NDUFS3* mutant; S8 = *NDUFS8* mutant; ND3 = *ND3* mutant; COQ4 = *COQ4* mutant; CI Def = cells with Complex I deficiency; CoQ Def = cells with CoQ_{10} deficiency; Q = CoQ_{10}; -SAA = medium without sulfur aminoacids. The blot image (A) has been made from three different membranes, as follow: blot 1, control; blot 2, *NDUFB9*; blot 3, *NDUFS3*, *ND3* and *COQ4*; blot 4, *NDUFS8*.

After supplementation with CoQ_{10}, the levels of CBS and CSE consistently decrease in all cell lines, compared with untreated cells (Fig. 41A–C; Fig. 42A–C), although the decrease is statistically significantly only in controls and *NDUFB3*, *NDUFS3*, *ND3*, *ND6*, *COQ4* and *PDSS2* mutant cells for CBS (Fig. 41B and Fig. 42B); and controls and *NDUFB9*, *NDUFS1* and *PDSS2* mutant cells for CSE (Fig. 41C and Fig. 42C). On the contrary, the levels of 3MST are not modified after CoQ_{10} supplementation (Fig. 41A and D; Fig. 42A and D). All these changes are similar in the cells cultured under SAAR (Fig. 41A and Fig. 42A; quantitative data not shown). Therefore, there is also an indirect correlation between the protein levels of SQOR and the protein levels of CBS and CSE after CoQ_{10} supplementation. The effect of CoQ_{10} over SQOR and CBS is also confirmed with a lower concentration of CoQ_{10} (Fig. 43).

In vivo, the levels of CBS are slightly decreased in the liver of C57BL/6 J mice treated with $CoQ_{10}H_2$ and in the brain of *Ndufs4*$^{-/-}$ mice, compared with the respective control animals (Fig. 41E and F). In the kidneys of *Coq9*^{R239X} mice, the levels of CBS slightly increased compared with *Coq9*$^{+/+}$ mice and this change was maintained under supplementation with NAC or SAAR (Fig. 41G). Therefore, the inverse correlation between SQOR and CBS also occurs *in vivo*.

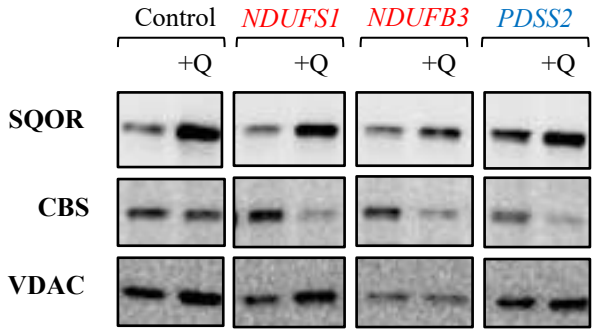

Figure 43. The levels of SQOR and CBS in control and mutant cells after supplementation with 20 µM CoQ_{10}.

C = control; S1 = *NDUFS1* mutant; B3 = *NDUFB3* mutant; PDSS2 = *PDSS2* mutant; Q = CoQ_{10}.

4.2.6. CoQ_{10} indirectly regulates the transsulfuration pathway through SQOR and/or other transcriptional regulatory pathways, and independently of oxidative stress

To assess whether CoQ_{10} regulates the enzymes of the transsulfuration pathway directly or through the modulation of SQOR, we overexpressed SQOR in control cells and *NDUFB3* and *NDUFS1* mutant, and measured mRNA and protein levels of SQOR, CBS and CSE. The transduction with SQOR-LV produces significant increases of *SQOR* mRNA and protein levels in control and mutant cell, compared with the matched non-transduced cells (Fig. 44A, D and E). In parallel, the mRNA and protein levels of CBS and CSE are significantly decreased in the cells transduced with the SQOR-LV, compared with the matched non-transduced cells (Fig. 44B, C, D, F and G), suggesting that the effect of CoQ_{10} over CBS and CSE is an indirect action through the modulation of SQOR levels. We also assessed the effects of SQOR overexpression on serine biosynthesis, folate cycle and nucleotides

metabolism, and observed that SQOR overexpression reproduces the gene expression profile changes caused by CoQ_{10} supplementation (Fig. 44H–K). Specifically, the expression of *PSAT1* slightly decreases in both control and *NDUFS1* SQOR-transduced cells (Fig. 44H); and the expression of *MTHFFD2*, *CMPK2* and *EIF2AK2* significantly increases in both control and *NDUFS1* SQOR-transduced cells (Fig. 44I–K).

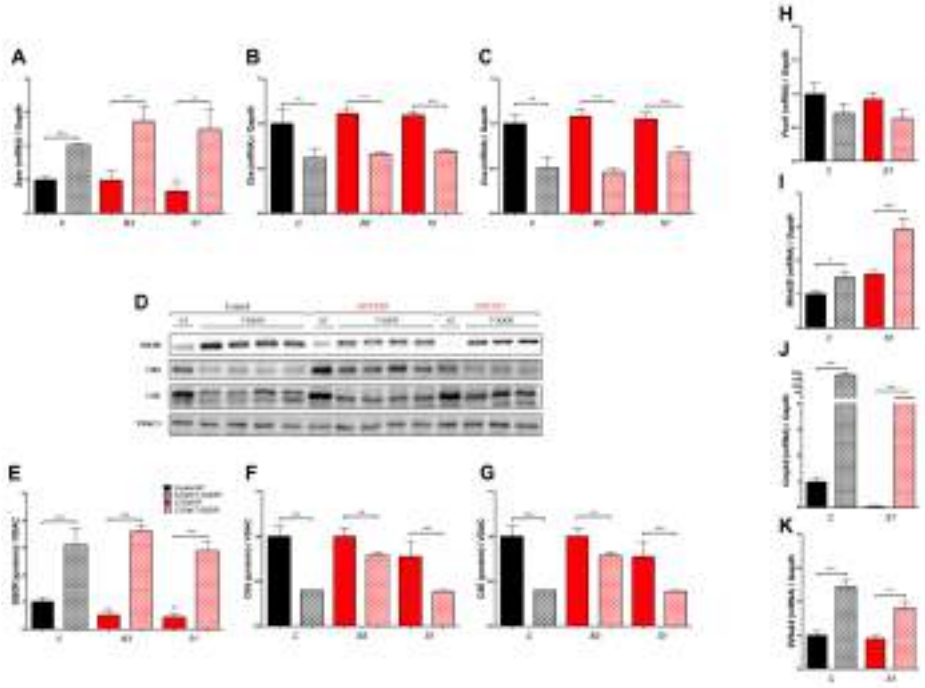

Figure 44. CoQ_{10} indirectly regulates the transsulfuration pathway through SQOR.

(A–C) Effect of genetic overexpression of SQOR in the expression levels of the genes *SQOR*, *CBS* and *CSE*.

(D–G) Effect of genetic overexpression of SQOR in the levels of the proteins *SQOR*, *CBS* and *CSE*.

(H–K) Effect of genetic overexpression of SQOR in the expression levels of the genes *PSAT1*, *MTHFD2L*, *CMPK2* and *EIF2AK2*. C, control; B3, *NDUFB3* mutant; S1, *NDUFS1* mutant; NT, non-transduced; T-SQOR, lentiviral vector containing SQOR cDNA.

Data are expressed as mean ± SD. *P < 0.05; **P < 0.01; ***P < 0.001; differences versus Control NT. +P < 0.05; ++P < 0.01; +++P < 0.001; Control NT versus Control T-SQOR or Complex I deficiency NT versus Complex I deficiency T-SQOR or CoQ_{10} deficiency NT versus CoQ_{10} deficiency T-SQOR (t-test; n = 3 for each group; n = 3–4 for each group).

Nevertheless, we also investigated whether the effects of CoQ_{10} on the changes of the expression of the identified genes could be attributed to a direct interaction of CoQ_{10} with pathways involved in transcriptional regulation or cell signaling. Transcriptomics analysis reveals that CoQ_{10} partially modifies the STAT3 (Fig. 45A, B, E, F) and the HIF1α signaling (Fig. 45A, C, E, G) pathways in both control (Fig. 45A–C) and *NDUFS1* mutant (Fig. 45E–G) cells. Moreover, the sumoylation pathway is altered in control cells treated with CoQ_{10} (Fig. 45A and D), and the NRF2 response in the *NDUFS1* mutant cells treated with CoQ_{10} (Fig. 45A and D). Therefore, we cannot exclude that CoQ_{10} supplementation effects on the transsulfuration pathway are partially mediated by its effects on other transcriptional regulators.

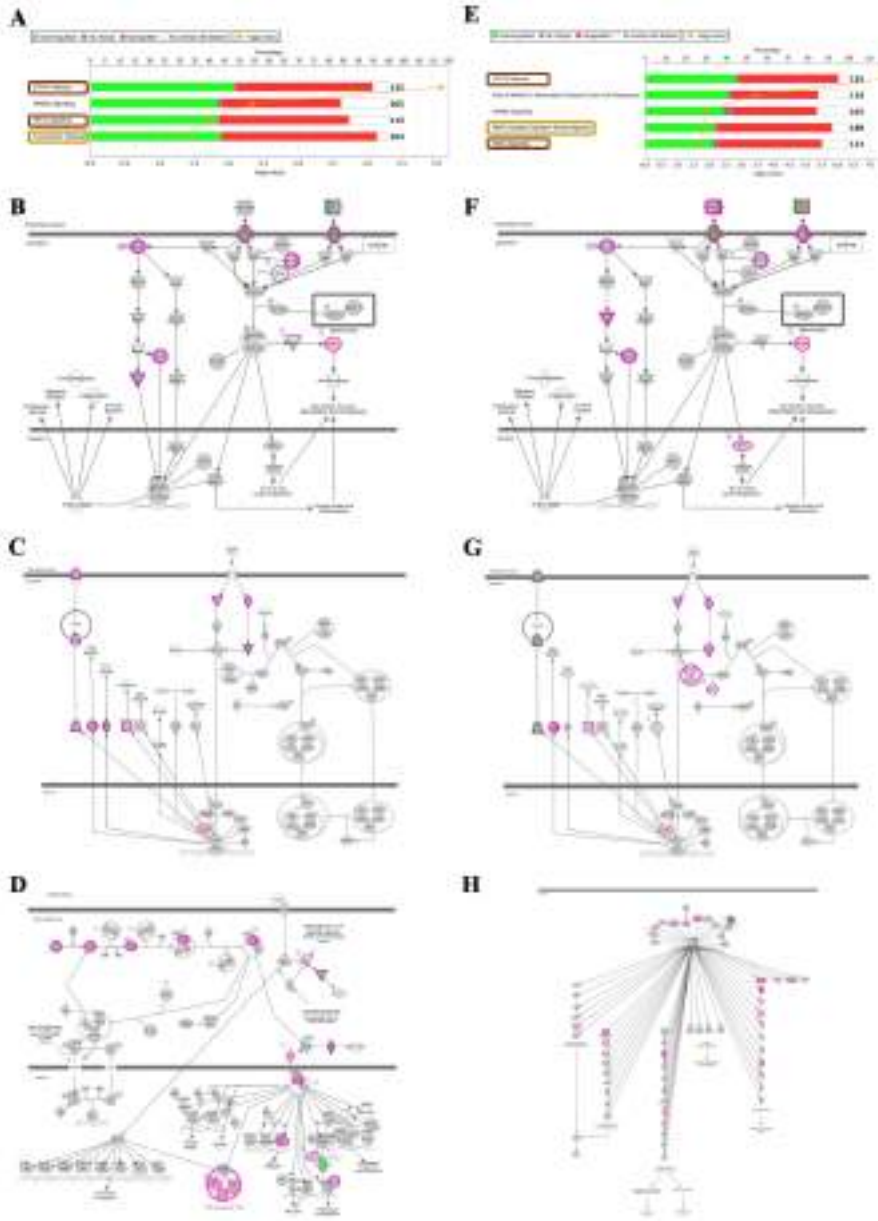

Figure 45. Transcriptional regulation and cell signaling pathways altered by CoQ_{10} supplementation.

(A) Canonical pathways most enriched in the differentially expressed gene list, related to transcriptional regulation and cells signaling, of the CoQ10 treated control cells dataset.

(B) STAT3 pathway in control cells.

(C) HIG1a signaling pathway in control cells.

(D) Sumoylation pathway in control cells.

(E) Canonical pathways most enriched in the differentially expressed gene list, related to transcriptional regulation and cells signaling, of the CoQ_{10} treated *NDUFS1* cells dataset.

(F) STAT3 pathway in *NDUFS1* mutant cells.

(G) HIG1a signaling pathway in *NDUFS1* mutant cells.

(H) NRF2 pathway in *NDUFS1* cells.

The shape with green filling means that the gene is downregulated; the shape with pink filling means that the gene is upregulated.

To know whether the mechanism of action of CoQ_{10} over sulfide metabolism may be mediated by oxidative stress, we also tested the effects of other antioxidants, i.e. idebenone (262), NAC or melatonin (aMT) (330), in the levels of SQOR. Idebenone induces a profound cell death at the same dose than CoQ_{10}, as reported in other studies (331). The treatments with NAC or melatonin do not modify the levels of SQOR in control cells and mutated in *NDUFS1*, *NDUFB3* and *PDSS2* (Fig. 46), suggesting that oxidative stress is not involve in the regulation of SQOR *in vitro*.

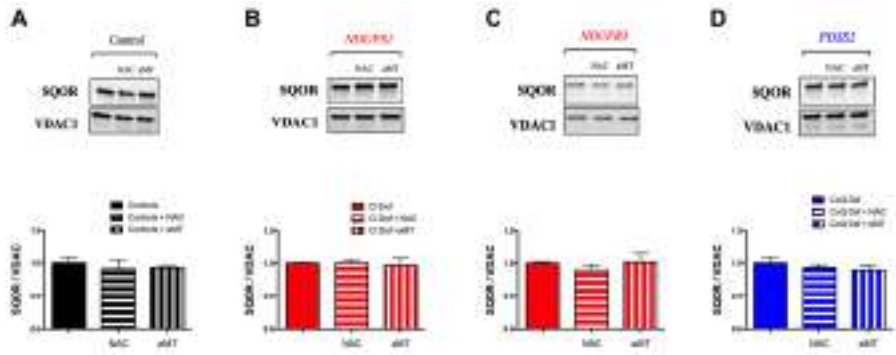

Figure 46. Levels of SQOR after the treatment with the antioxidants NAC or aMT.

(A) Levels of SQOR in control cells

(B) Levels of SQOR in *NDUFS1* mutant cells

(C) Levels of SQOR in *NDUB3* mutant cells

(D) Levels of SQOR in *PDSS2* mutant cells

4.3. *Co-Administration of Vanillic Acid and Coenzyme Q_{10} in CoQ Deficiency.*

4.3.1. Both VA treatment and VA and CoQ_{10} co-treatment reduce the DMQ/CoQ ratio *in vitro* through different mechanisms

First, we analyzed the effect of VA and CoQ_{10} supplementation in CoQ metabolism in skin fibroblast from a control and two patients with CoQ deficiency due to different mutations in the *COQ7* gene. Patient 1 (P1) has a frameshift deletion (c.161_161delG, p.Val55fs) in exon 2 and a missense mutation (c.319C>T, p.Arg107Trp) in the exon 3. Patient 2 (P2) has two variants in compound heterozygosis in the *COQ7* gene: c.3G>T, p.(Met1?)/c.205G>A, p.(Gly69Arg) and one variant in heterozygosis in gene *SLC2A1* (c.1403G>A, p.(Arg468Gln). *COQ7* mutant cells have low levels of CoQ_{10} compared to controls and supplementation with 20µM CoQ_{10} significantly increases the cellular content of CoQ_{10} in both control and mutant cells (Fig. 47A). However, as previously mentioned, the majority of these CoQ_{10} molecules would be located in the cell membrane and a low proportion would enter into the mitochondria. VA supplementation with 1mM slightly increases the CoQ_{10} levels in *COQ7* mutant cells, especially in P2 (Fig. 47A). Co-administration of VA at 1mM and CoQ_{10} at 20µM significantly increases the cellular content of CoQ_{10} in control and *COQ7* mutants at levels similar to the ones achieved with the single administration of CoQ_{10} (Fig. 47A).

In parallel, an accumulation of DMQ_{10} was detected in *COQ7* mutant cells (Fig. 47B). Surprisingly, the supplementation with 20µM

CoQ_{10} significantly increases the cellular content of DMQ_{10} in both control and mutant cells (Fig. 47B). However, this DMQ_{10} seems to be present in the stock used to prepare the CoQ_{10} at 20µM. In the chromatograph of a single injection of the stock of CoQ_{10} at 20µM, a peak with the same size and retention time of the one of DMQ_{10} in the *COQ7* cells is detected (Fig. 48). Thus, the DMQ_{10} levels measured after the supplementation with CoQ_{10} are due to a contamination from the CoQ_{10} stock and not to an endogenous production by the cells. In contrast, supplementation with 1mM VA slightly decreases DMQ_{10} levels in *COQ7* mutant cells (Fig. 47B). Moreover, CoQ_{10} and VA co-treatment significantly increases the cellular content of DMQ_{10} in control and mutant cells, presumably due to the presence of DMQ_{10} in the CoQ_{10} stock. Nevertheless, the levels were not as high as the ones achieved with the single administration of CoQ_{10}, most likely due to the effects of VA in reducing the endogenous levels of DMQ_{10} (Fig. 47B). Consequently, the DMQ_{10}/CoQ_{10} ratio is reduced in all treatments, being the lowest values after the CoQ_{10} and VA co-treatment (Fig. 47C).

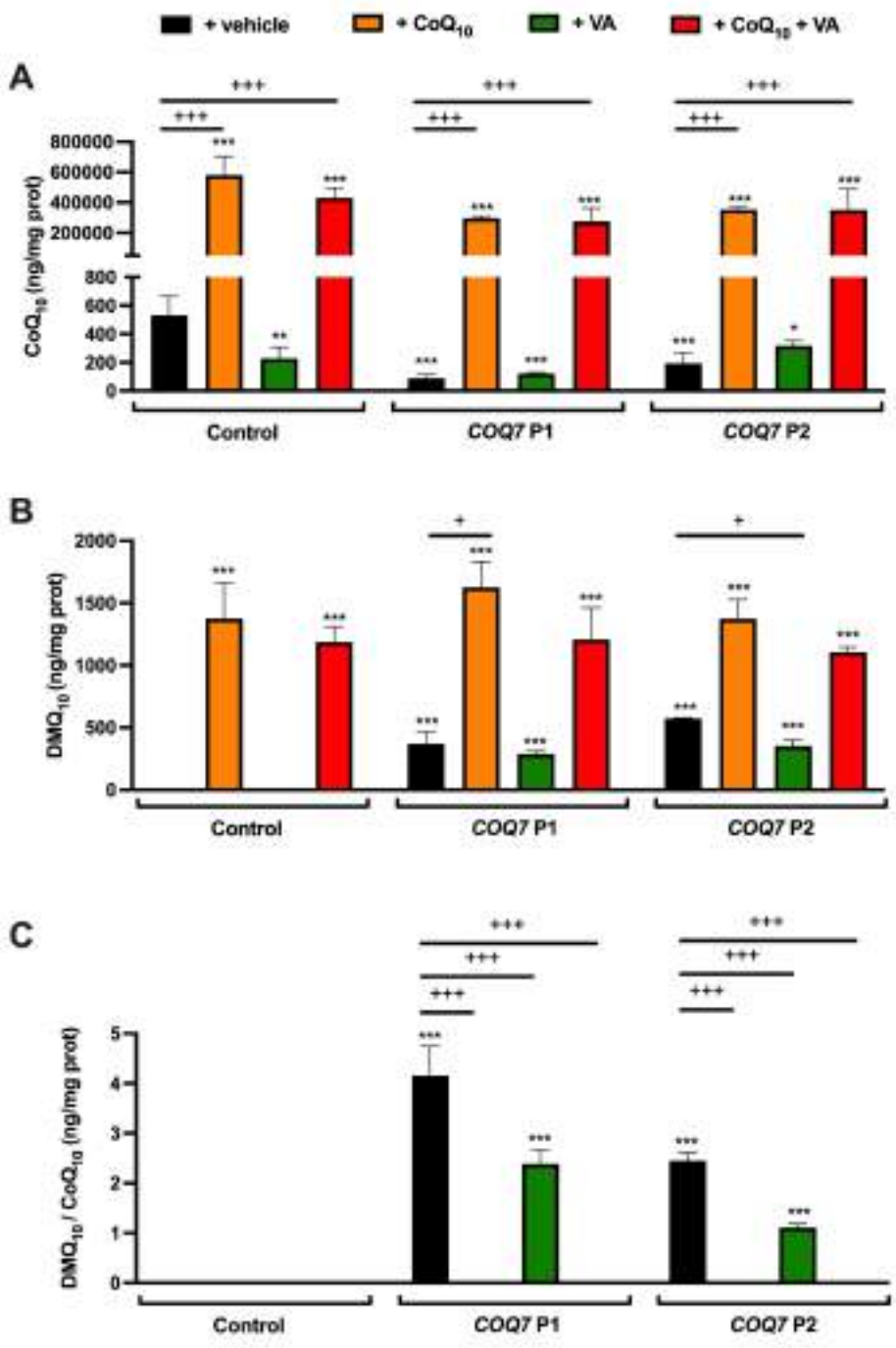

Figure 47. CoQ_{10}, DMQ_{10} and DMQ_{10}/CoQ_{10} levels in human skin fibroblast after the co-administration of VA and CoQ_{10} *in vitro*.

(A, B and C) Levels of CoQ_{10} (A), DMQ_{10} (B) and DMQ_{10}/CoQ_{10} ratio (C) in human skin fibroblast from controls and patients with mutation in *COQ7* (P1 and P2) after the

supplementation with CoQ_{10} at 20 µM, VA at 1 mM and the simultaneous administration of both.

Data are expressed as mean ± SD. *P < 0.05, **P < 0.01, ***P < 0.001, differences versus control; +P < 0.05, ++P < 0.01, +++P < 0.001, versus *COQ7* mutant; (one-way ANOVA with a Tukey's post hoc test; n = 3 for each group).

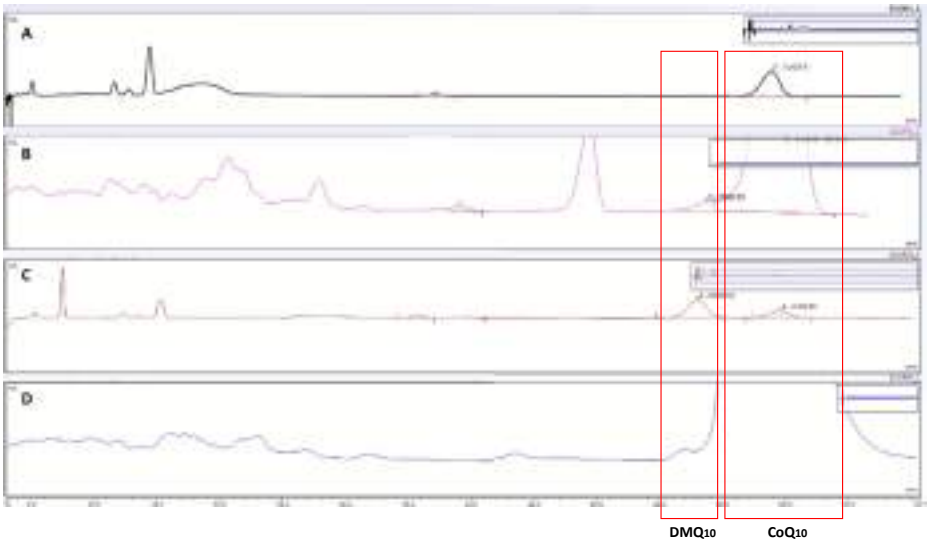

Figure 48. Representative chromatographs of CoQ_{10} and DMQ_{10} levels in human skin fibroblast after the co-administration of VA and CoQ_{10} *in vitro.*

(A) Chromatograph of control cells treated with vehicle.

(B) Chromatograph of control cells treated with CoQ_{10} at 20µM.

(C) Chromatograph of *COQ7* mutant cells treated with vehicle.

(D) Chromatograph of a single injection of the stock of CoQ_{10} at 20µM.

4.3.2. VA and CoQ_{10} co-treatment modifies 1-carbon metabolism gene expression in cells with CoQ deficiency

Before, it was demonstrated that CoQ_{10} supplementation induces an adaptation of metabolic pathways closely connected to sulfide metabolism, such as serine biosynthesis, folate cycle and nucleotides metabolism, all together involved in 1-carbon (1C) metabolism. This

could explain the therapeutic effect of CoQ_{10} therapy in those mitochondrial diseases in which these pathways are altered. In this context, we have assessed whether the co-supplementation of CoQ_{10} and VA induces similar effects than CoQ_{10} supplementation in gene expression and protein levels of components involved in 1C metabolism in control and CoQ deficient cells. The mRNA levels of *PSAT1* gene, involved in serine biosynthesis, are increased in *COQ7* mutant cells compared to the control, being statistically significant for P1 cells (Fig. 49A). The supplementation with 20μM CoQ_{10} significantly decreases *PSAT1* mRNA levels in *COQ7* P1 cells while an increase is detected in *COQ7* P2 cells. Moreover, 1mM VA supplementation increases *PSAT1* mRNA levels in controls and *COQ7* mutant cells. CoQ_{10} and VA co-treatment decreases *PSAT1* mRNA levels in all cell lines, being statistically significant for *COQ7* P1. In the case of *COQ7* mutant cells, the co-supplementation of CoQ_{10} and VA normalizes the *PSAT1* mRNA levels with values similar to the ones detected in the control cells (Fig. 49A). On the other hand, the expression of *MTHFD2L* gene, involved in the folate cycle, does not show any difference between control and *COQ7* mutants, both in basal conditions and in response to the treatments (Fig. 49B). However, a tendency to increase the mRNA levels of *MTHFD2L* is detected in *COQ7* P1 cells compared to the control. Additionally, CoQ_{10} or VA supplementation induce a tendency to decrease the expression of *MTHFD2L* in *COQ7* P1 cells, but not the co-administration of both compounds (Fig. 49B). Finally, the modulation of nucleotides' metabolism was checked by the determination of the mRNA levels of *CMPK2* and *EIF2AK2*. *CMPK2* expression is downregulated in *COQ7* mutant cells compared to controls and the decrease is even higher after the supplementation with VA, although

those changes are not statistically significant (Fig. 49C). On the contrary, the administration of CoQ_{10} induces a tendency to increase the mRNA levels of *CMPK2* in control and *COQ7* mutants (Fig. 49C). Moreover, co-administration of CoQ_{10} and VA highly upregulates the expression of *CMPK2* (Fig. 49C). *EIF2AK2* expression is not modified in CoQ deficient cells compared to controls (Fig. 49D). Supplementation with VA does not induce any change in the mRNA levels of *EIF2AK2* in control cells but a slightly tendency to decrease *EIF2AK2* expression is observed in *COQ7* mutants (Fig. 49D). However, the exogenous administration of CoQ_{10} shows a tendency to increase the *EIF2AK2* expression in all cell lines and this increase is even higher with the co-administration of CoQ_{10} and VA (Fig. 49D). Thus, CoQ_{10} and/or VA supplementation seems to modulate nucleotides' metabolism in the same way in control and CoQ deficient cells, at least regarding in the gene expression of *CMPK2* and *EIF2AK2.*

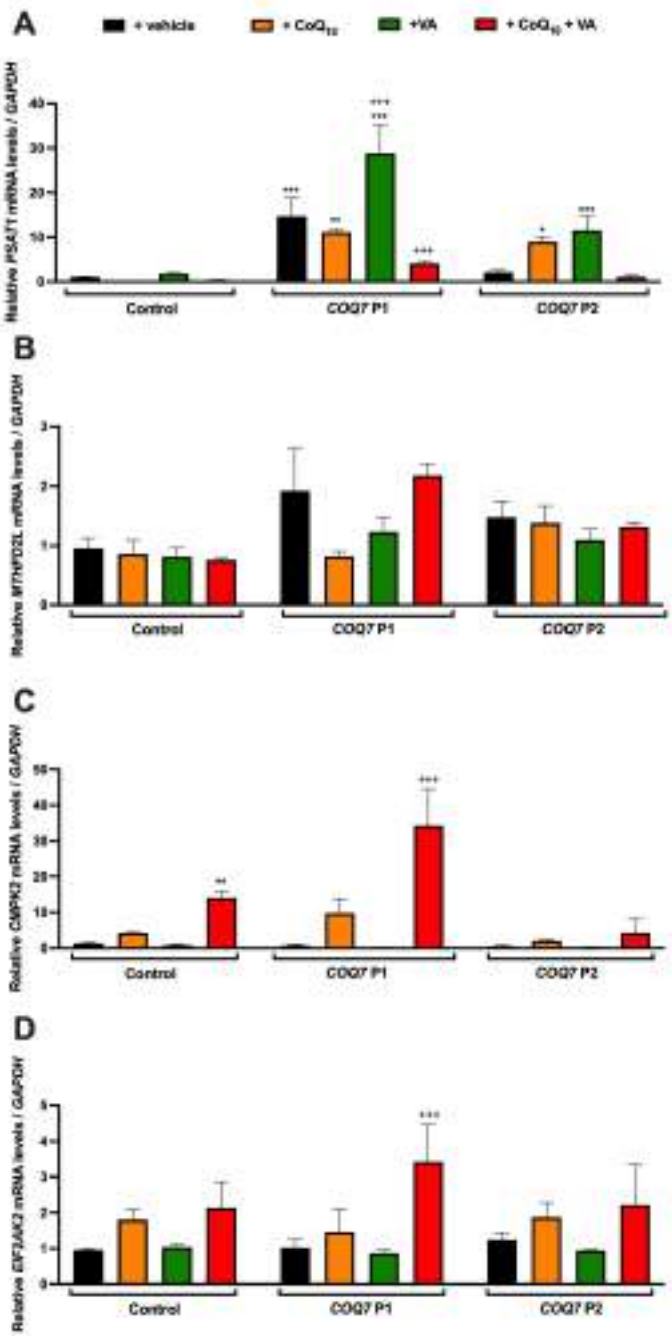

Figure 49. CoQ_{10} and VA supplementation modifies the expression of key genes involved in 1C-metabolism.

(A) Expression levels of *PSAT1,* involved in serine biosynthesis, in human skin fibroblast from controls and patients with mutation in *COQ7* (P1 and P2) after the supplementation with CoQ_{10} at 20 μM, VA at 1 mM and the simultaneous administration of both.
(B) Expression levels of *MTHFD2L,* involved in the folate cycle, in human skin fibroblast from controls and patients with mutation in *COQ7* (P1 and P2) after the supplementation with CoQ_{10} at 20 μM, VA at 1 mM and the simultaneous administration of both.
(C, D) Expression levels of *CMPK2* (C) and *EIF2AK2* (D), involved in nucleotides' metabolism, in human skin fibroblast from controls and patients with mutation in *COQ7* (P1 and P2) after the supplementation with CoQ_{10} at 20 μM, VA at 1 mM and the simultaneous administration of both.
Data are expressed as mean ± SD. *P < 0.05, **P < 0.01, ***P < 0.001, differences versus control; +P < 0.05, ++P < 0.01, +++P < 0.001, versus *COQ7* mutant; (one-way ANOVA with a Tukey's post hoc test; n = 3 for each group).

4.3.3. The modification of the expression of 1-C metabolism genes after CoQ_{10} and VA co-treatment correlates with the changes in the protein levels

Following the quantification of mRNA levels, we assessed if the changes detected in the gene expression of 1-C metabolism genes after CoQ_{10} and VA co-supplementation were followed by alterations in the protein levels. Based on the previous gene expression studies, we decided to analyze the protein levels of PSAT1 and EIF2AK2 in control and *COQ7* mutant cells treated with vehicle, CoQ_{10} and/or VA. COQ7 protein levels was also checked, as it is the affected protein in the mutant cells. Changes in PSAT1 protein levels correlates with gene expression data. PSAT1 protein levels are increased in *COQ7* mutant cells compared to the controls, being statistically significant for both P1 and P2 cells (Fig. 50A, B, E, F, I and J). The supplementation with 20μM

CoQ_{10} significantly decreases PSAT1 protein levels in *COQ7* P1 cells, while an increase in detected in *COQ7* P2 cells. Moreover, 1mM VA supplementation increases PSAT1 protein levels in controls and *COQ7* P2 mutant. CoQ_{10} and VA co-treatment decreases PSAT1 protein levels in controls and COQ7 P1 cells (Fig. 50A, B, E, F, I and J). Thus, a tendency to normalize PSAT1 protein levels is only detected in *COQ7* P1 cells after the treatment with CoQ_{10} and the co-treatment with VA. In contrast with the gene expression data, EIF2AK2 protein levels decrease in *COQ7* mutants compared to the controls (Fig. 50A, C, E, G, I and K). In control cells, CoQ_{10} and/or VA supplementation significantly decreases EIF2AK2 protein levels (Fig. 50A and C). In *COQ7* mutant cells, CoQ_{10} supplementation does not produce any effect in the modulation of EIF2AK2 protein levels. VA supplementation only decreases EIF2AK2 protein in *COQ7* P1 cells. In parallel with gene expression analysis, EIF2AK2 protein levels are highly increased in the mutant cells after the co-administration of CoQ_{10} and VA, normalizing EIF2AK2 protein levels (Fig. 50E, G, I and K). As expected, no residual levels of COQ7 protein are detected in *COQ7* mutants and none of the treatments induce any change (Fig. 50E, H, I and L). An upregulation of COQ7 protein is detected in control cells after VA administration as well as in co-administration with CoQ_{10} (Fig. 50A and D), suggesting the presence of a close connection between VA and COQ7 in the CoQ biosynthetic pathway.

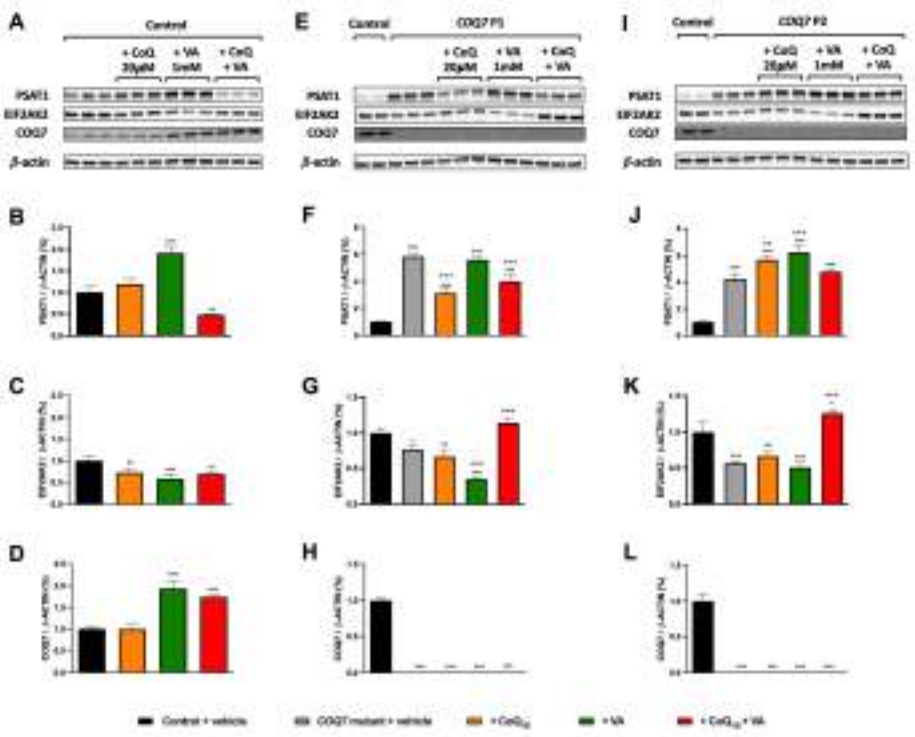

Figure 50. Protein levels of PSAT1, EIF2AK2 and COQ7 in CoQ deficiency and after CoQ_{10} and /or VA supplementation *in vitro*.

(A) Representative images of Western blots of PSAT1, EIF2AK2 and COQ7 proteins in human skin fibroblast from a control patient after the supplementation with CoQ_{10} at 20 µM, VA at 1 mM and the simultaneous administration of both.

(B-D) Quantification of the protein bands of PSAT1 (B), EIF2AK2 (C) and COQ7 (D) in human skin fibroblast from a control patient after the supplementation with CoQ_{10} at 20 µM, VA at 1 mM and the simultaneous administration of both.

(E and I) Representative images of Western blots of PSAT1, EIF2AK2 and COQ7 proteins in human skin fibroblast from patient 1 (P1) (E) and patient 2 (P2) (I) with mutation in *COQ7* after the supplementation with CoQ_{10} at 20 µM, VA at 1 mM and the simultaneous administration of both.

(F-H) Quantification of the protein bands of PSAT1 (F), EIF2AK2 (G) and COQ7 (H) in human skin fibroblast from a from patient 1 (P1) with mutation in *COQ7* after the supplementation with CoQ_{10} at 20 µM, VA at 1 mM and the simultaneous administration of both.

(J-L) Quantification of the protein bands of PSAT1 (J), EIF2AK2 (K) and COQ7 (L) in human skin fibroblast from a from patient 2 (P2) with mutation in *COQ7* after the supplementation with CoQ_{10} at 20 μM, VA at 1 mM and the simultaneous administration of both.

Data are expressed as mean ± SD. *P < 0.05, **P < 0.01, ***P < 0.001, differences versus control; +P < 0.05, ++P < 0.01, +++P < 0.001, versus *COQ7* mutant; (one-way ANOVA with a Tukey's post hoc test; n = 3 for each group).

5. Discussion

5.1. *The Q-Junction and the Inflammatory Response are Critical Pathological and Therapeutic Factors in CoQ Deficiency*

The metabolic consequences of low CoQ levels have not been clearly elucidated in the context of the multiple metabolic pathways linked to the Q-junction. Nevertheless, 4-HB analogs induce powerful therapeutic effects in different animal models of CoQ deficiency (279-282, 287), although the precise mechanisms are not completely understood. Here, we answer these central scientific questions by demonstrating that low levels of CoQ induce an adaptation of the mitochondrial proteome, most likely due to the disruption of the Q-junction as a primary event. Additionally, CoQ deficiency, together with the accumulation of DMQ, induces reactive astrogliosis and microgliosis, promoting neuroinflammation and spongiform degeneration. Importantly, oral treatment with 4-HB analogs induces partial normalization of the DMQ/CoQ ratio, particularly in peripheral tissues, leading to profound normalization of the mitochondrial proteome and metabolism. Furthermore, 4-HB analogs reduce gliosis and neuroinflammation, with subsequent rescue of the encephalopathic phenotype in *Coq9*^{R239X} mice.

Different pathophysiological mechanisms have been previously identified as explanations for the clinical heterogeneity of CoQ deficiency. Mainly, a decline in ATP synthesis (113, 222-224), increased oxidative stress (223, 224, 243, 332), the disruption of the sulfide

metabolism (157, 158), and a defect in the de novo biosynthesis of pyrimidines (222) were previously described as consequences of CoQ deficiency. Using a more integrative approach, our study reveals that the disruption of the Q-junction is the origin of a metabolic disarrangement caused by CoQ deficiency. Interestingly, proteins of the Q-junction respond differently to CoQ deficiency and to the treatments with 4-HB analogs, e.g., 1) the levels of SQOR are decreased under CoQ deficiency and 4-HB analogs do not significantly reverse that change; 2) the levels of GPDH remain stable both under CoQ deficiency and after treatment with 4-HB analogs; and 3) the levels of PRODH, ETFDH, DHODH and CHDH are increased in the context of CoQ deficiency and normalized by treatment with 4-HB analogs. A similar specific response to CoQ deficiency has been recently shown in the *mon* zebrafish model, which exhibits CoQ deficiency and a preferential use of the CoQ pool by the DHODH during erythropoiesis (333). Our study also shows tissue-specific differences in the Q-junction, which may contribute to the phenotype development and therapeutic success. Another remarkable finding of this work is the identification of neuroinflammation as a key feature and therapeutic target of the encephalopathic phenotype associated with CoQ deficiency. Neuroinflammation has been identified as a key pathologic mechanism in other mouse models of mitochondrial disease and neurodegeneration (334, 335). Neuroinflammatory mediators can be released by both reactive astrocytes and microglia (336), particularly in the brainstem, diencephalon, and cerebellum, resembling the pathological features of Leigh syndrome (337, 338).

Therapeutically, previous studies have shown that β-RA rescues the phenotype of different models of CoQ deficiency (279-282, 287). In this

study, we show that another 4-HB analog, VA, is also able to rescue the encephalopathic phenotype of *Coq9*^{R239X} mice. Importantly, we reveal common therapeutic mechanisms of both phenolic acids, mainly related to their specific effects on CoQ metabolism and the functioning of the Q-junction and the ability to reduce reactive gliosis, neuroinflammation and spongiosis. The effects on the Q-junction and related pathways are more intense in the kidneys than in the brain, suggesting that this particular effect could be mainly linked to the reduction in the DMQ/CoQ ratio. Thus, the accumulation of DMQ and the decrease in CoQ levels alter not only the function of CI+III (339) but also the activities of other dehydrogenases of the Q-junction. Accordingly, in the opposite context of supraphysiological levels of CoQ_{10}, SQOR is upregulated, leading to a decrease in the levels of enzymes of the transsulfuration pathway and a subsequent adaptation of the serine biosynthesis and folate cycle (340). The second therapeutic mechanism described here, the anti-inflammatory effects, could be directly or indirectly mediated by phenolic compounds and remains to be elucidated. Thus, some complementary hypotheses could explain the therapeutic effects of 4-HB analogs in the brain of *Coq9*^{R239X} mice. First, 4-HB analogs may have CoQ-independent functions with therapeutic potential for mitochondrial encephalopathies; second, 4-HB analogs may have effects in some specific cell types of the brain, a fact that may be masked in the analyses in the whole brain; and third, since 4-HB analogs may have some limitations to cross the blood brain barrier due to the binding to serum albumin (341, 342), the observed effects may be due to tissue–brain crosstalk after the reduction of DMQ_9/CoQ_9 ratio in peripheral tissues and the subsequent improvement of the mitochondrial bioenergetics, thus leading to the reduction of gliosis, spongiosis, and

neuroinflammation. In this context, a few plasma proteins with potential involvement in neuroinflammation have been identified. Additionally, these anti-inflammatory effects could explain the therapeutic benefits of β-RA in the *Coq6*^{podKO} and *Adck4*$^{\Delta Podocyte}$ mouse models, since an immune response has been described as part of the nephrotic phenotype associated with CoQ deficiency (343, 344).

In addition to the common response to both β-RA and VA, the omics and molecular analyses also revealed some differences between the two treatments. For example, VA strongly upregulates COQ4 (276) and COQ5, while β-RA minimally affects the levels of these proteins (279). Thus, the different effects of the two compounds on the DMQ/CoQ ratio could be explained by different mechanisms of action in the Complex Q, although this has not been yet investigated. Moreover, we generally observed more intense effects of β-RA in the DMQ/CoQ ratio and in the omics data than those of VA. Such differences might be important for potential translation into the clinic and for dose adjustment. Additionally, it is remarkable that only β-RA is able to decrease the white adipose tissue content in wild-type mice (287).

From the translational perspective, the omics data from the serum are also important, since they could potentially be useful biomarkers to follow the progression of the disease and the response to treatment. In particular, we found different types of potential biomarkers. 1) An increase in acylcarnitines was observed, which has also been reported in the *Pdss2* and *Adck2* mouse models (157, 320), most likely as a result of the impairment of fatty acid oxidation due to the dysfunctional Q-junction (ETFDH and GPDH, in particular). 2) A decrease in N-Ac-Glu

and N-Ac-Glu-6P levels in the serum, brain and kidneys was observed. These two metabolites work in the hexosamine biosynthetic pathway and are involved in O-linked glycosylation, which has been associated with the regulation of mitochondrial function (345), and is related to neuroinflammation and myelinization (346, 347). 3) A decrease in the levels of SERPINA3, MASP1, COL1A1 and AI182371 and an increase in PZP was observed. Importantly, all these changes were normalized by treatment with either β-RA or VA. Nevertheless, the use of these potential biomarkers requires further validation in animal models, as well as in the clinic.

Taken together, this preclinical study provides plausible mechanistic explanations and a better understanding of the phenotypic heterogeneity of CoQ deficiency syndrome, the molecular and metabolic consequences of CoQ deficiency and the integrative response to the treatment with 4-HB analogs. These data are mechanistically relevant beyond primary CoQ deficiency, since other diseases with secondary CoQ deficiency, e.g., mitochondrial diseases (185, 216, 348), metabolic syndrome (187) or neurodegenerative diseases (349, 350), may share common pathologic mechanisms and respond to treatments with 4-HB analogs. Furthermore, our data are relevant for the potential translation of these therapeutic options into the clinic.

5.2. *Sulfide Metabolism and Pathways Associated to One Carbon Metabolism are modulated by Coenzyme Q_{10} Therapy in Mitochondrial Diseases*

Mitochondrial dysfunction causes heterogeneous clinical presentations, due to the variable involvement of multiple metabolic pathways related to the mitochondrial metabolism, e.g. one carbon metabolism or fatty acids oxidation (180-182, 185). Therefore, finding therapeutic approaches for those dysfunctions is challenging. Oral CoQ_{10} supplementation is a common recommended therapeutic approach in patients with mitochondrial disorders and other diseases with secondary mitochondrial involvement. However, its rationale use is not well understood, particularly in patient with normal CoQ_{10} levels. Here, we show that supraphysiological levels of CoQ_{10} induce the overexpression of SQOR, the first enzyme of the mitochondrial hydrogen sulfide oxidation pathway (sulfide catabolization), leading to downregulation of CBS and CSE. These two latter enzymes belong to the transsulfuration pathway (sulfide biosynthesis), which is metabolically connected to serine biosynthesis, the folate cycle and the nucleotides metabolism (180, 351). Thus, supraphysiological levels of CoQ_{10} result in a modulation of these pathways, restoring the function that is altered by mitochondrial dysfunction (180-182, 185).

We previously reported that CoQ deficiency causes a severe reduction in the levels of SQOR, leading to a disruption of the sulfide metabolism and a decrease in the glutathione levels (157, 158). In the current study, we show that CoQ deficiency also affects the transsulfuration pathway, independently of the availability of sulfur

aminoacids. Additionally, we show that specific molecular defects in Complex I subunits cause disruption of the sulfide metabolism. However, those alterations do not correlate with the residual Complex I activity and are not due to an interaction of the SQOR with the mitochondrial supercomplexes. These findings suggest that the variable response of the sulfide metabolism to complex I deficiency could influence the heterogenous disease phenotype (352), in part because of the effects of that response on the metabolism of glutathione, which requires the balanced metabolism of cysteine and glycine (351, 353).

Importantly, supplementation with CoQ_{10} in both controls and Complex I deficiency cells causes a consistent upregulation of SQOR and downregulation of the transsulfuration pathway, independently of the availability of sulfur aminoacids. This modulation of the sulfide metabolism causes a therapeutic adaptation of metabolic pathways that are closely connected to the transsulfuration pathway, i.e. the serine biosynthesis, the folate cycle and the nucleotides metabolism. These metabolic pathways are unbalanced in a variety of models of mitochondrial diseases (180-182, 185), probably due to the activation of serine catabolism (354). Specifically, *CBS*, *CSE*, *PSAT1*, *SHMT2* and *PHGDH* are upregulated after 24 h of pharmacological inhibition of Complex I in cell culture (183); *Mthfd2* is induced in the skeletal muscle, heart and brown adipose tissue of the Deletor mice, resulting in a remodeling of the one carbon metabolism (180, 182, 355); *Mthfd2* and *Shmt2* are induced in the heart of five different mouse models of mitochondrial diseases due to disruption of key genes that regulate mtDNA gene expression, mtDNA replication or translation (185); *CBS*, *CSE*, *PHGDH*, *PSPH* and *PSAT1* are induced after pharmacologically

induced mtDNA depletion in vitro, leading to an increase in serine biosynthesis and transsulfuration (181); or *MTHFD1L*, *MTHFD2*, *PSAT1*, *PHGDH* and *SHMT2* are upregulated in the muscle of patients with mitochondrial myopathy due to mtDNA single or multiple deletion(s) (182). Importantly, our *in vitro* analyses show that supraphysiological levels of CoQ_{10} can rescue all these abnormalities, inducing the downregulation of *CBS*, *CSE*, *PHGDH*, *PSPH*, *PSAT1*, *MTHFD1L* and *MTHFD2*, among others, in both control and Complex I deficiency cells. Furthermore, the serine/glycine ratio, which is decreased in mouse models of secondary CoQ deficiency (185), increases after CoQ_{10} supplementation, most likely due to a compensation in the biosynthesis and use of serine, together with a decrease of glycine production in the folate cycle. These changes in the transsulfuration, serine biosynthesis and folate cycle correlate with the increase in SQOR and an alteration in the nucleotide metabolism. However, these effects are not likely due to an stimulation of the OXPHOS system, where CoQ plays a central role in the Q junction (356), since CoQ_{10} is able to stimulate the mitochondrial complexes activities in cells with CoQ_{10} deficiency but its effect in cells with normal levels of CoQ_{10} is limited (225). Therefore, high doses of CoQ_{10} supplementation may provide therapeutic benefits in patients with mitochondrial disorders and alterations in sulfide metabolism, serine biosynthesis, folate cycle or nucleotide metabolism. Moreover, the effect of CoQ_{10} on the upregulation of SQOR and downregulation of CBS and CSE could reduce the clinical consequences of the accumulation of hydrogen sulfide and reduction in glutathione levels in patients with ethylmalonic encephalopathy due to mutations in *ETHE1* (353, 357) or in patients with Leigh Syndrome due to mutations in *SQOR* (358).

Furthermore, the effects of CoQ_{10} in sulfide metabolism could benefit patients with colon cancer, thyroid carcinomas or Chron's disease, since the increase of transsulfuration pathway has been identified as a key pathogenic mechanism in both cases (165, 359, 360). However, an important limitation of the exogenous CoQ_{10} supplementation is the low absorption and bioavailability of this molecule. CoQ_{10}, orally or intraperitoneally administrated, mainly localizes in the spleen and the liver, with a low proportion localized in the heart, muscle and kidneys, and a very low proportion in the brain (274, 321). Therefore, effective strategies to increase the bioavailability of CoQ_{10} are necessary to enhance its therapeutic potential.

The current study also contributes to elucidate the mechanisms of how CoQ_{10} is able to induces metabolic changes at the transcriptional level. Our data demonstrate that the overexpression of SQOR alone, could lead to the downregulation of the transsulfuration pathway and to the adaptation of the other metabolic pathways. Most likely, all these changes are mediated by the detection of the levels of the SQOR products, i.e. thiosulfate ($SSO3^{2-}$) or GSH persulfide (GSS^-), as it happens with the CstR in bacteria (361). However, homologous sensors/regulators have not been identified in mammals yet (362). Nevertheless, the supplementation with thiosulfate in HUVEC cells induces a decrease in CSE levels (363). Additionally, the results of our transcriptome analysis suggest that some other mechanisms could mediate the adaptative response to the supraphysiological levels of CoQ_{10}: (1) repression of STAT3 pathway (364), and the subsequent reduction of the binding of STAT3 into the CSE promoter, which reduces CSE expression (365); (2) activation of the Sumoylation that could

downregulate CBS (366, 367) and/or (3) alteration of HIF1α signaling that could downregulate CBS (161).

Although further studies are needed to elucidate the detailed mechanisms of the transcriptional regulation mediated by CoQ_{10}, we demonstrate that supraphysiological levels of CoQ_{10} induce SQOR and downregulates the transsulfuration pathway, leading to a downregulation of serine biosynthesis and an adaptation of the linked pathways of folate cycle and nucleotides metabolism. All these metabolic changes could be mediated by the CoQ_{10}–SQOR interaction, and they could explain the therapeutic benefits of CoQ_{10} supplementation in some patients with mitochondrial disorders. They, therefore, are very likely relevant for the treatment of mitochondrial dysfunction in other common diseases.

5.3. *Coenzyme Q_{10} and Vanillic Acid Co-Supplementation is a Valid Alternative Therapy in CoQ Deficiency*

The conventional treatment in primary CoQ deficiency is the supplementation with high doses of CoQ_{10}. However, previous studies have demonstrated the limited effects of CoQ_{10} therapy in a high percentage of patients due to different factors: 1) the low absorption and bioavailability of the exogenous CoQ_{10}, together with its low capacity to cross the blood-brain barrier; 2) the lack of effect over the accumulation of intermediate metabolites in the synthesis of CoQ (some of these metabolites, such as DMQ, may contribute to the disease phenotype by inhibiting the transfer of electrons in the mitochondrial electron transport chain); and 3) the lack of effect over the complex Q and the endogenous

biosynthesis of CoQ. Nevertheless, here, we have demonstrated that CoQ_{10} supplementation have complementary therapeutic mechanisms related to the regulation of sulfide metabolism and, as a consequence, serine biosynthesis, the folate cycle and the nucleotides metabolism. These pathways have been described as altered in mitochondrial dysfunction (180-182, 185), so supraphysiological levels of CoQ_{10} may result in therapeutic benefits. On the other hand, our results have demonstrated that VA supplementation modulates the endogenous CoQ metabolism and, consequently, the Q-junction, leading to better therapeutic outcomes than CoQ_{10} in *Coq9*^{R239X} mice. However, VA supplementation, similar to β-RA (279), does not rescue the disruption in sulfide metabolism in *Coq9*^{R239X} mice. Importantly, the co-administration of CoQ_{10} and VA *in vitro* leads to synergic effects. First, CoQ_{10} and VA co-treatment highly increases the CoQ_{10} cellular content and reduces the accumulation of DMQ_{10}. Importantly, the increase in the CoQ_{10} levels is, at least in part, related to the endogenous stimulation of CoQ biosynthesis due to the participation of VA in the CoQ biosynthetic pathway. Furthermore, the disruption produced by CoQ deficiency in the *PSAT1* gene from serine biosynthesis, is normalized by the co-supplementation of CoQ_{10} and VA, while the administration of these compounds separately is unable to restore the normal levels of *PSAT1* expression. Additionally, CoQ_{10} and VA co-treatment also normalizes *CMPK2* mRNA levels and highly increases the expression of *EIF2AK2*, suggesting the participation of the co-treatment in the regulation of enzymes involved in the nucleotides' metabolism. The changes in gene expression correlate with those of protein levels analyzed after the treatments, except for *MTHFD2L*.

In summary, our *in vitro* analysis reveals that CoQ_{10} and VA co-treatment could be a better therapeutic strategy compared to isolated CoQ_{10} or VA therapies. However, the co-treatment may share the limitation of the low absorption and bioavailability of CoQ_{10}. Therefore, some of the effects observed *in vitro* may only be observed in some particular tissues *in vivo*, such as liver, muscle and heart (274). Therefore, a detailed evaluation of the CoQ_{10}-VA co-treatment *in vivo* is needed to test its potential for possible translation into the clinic.

6. Conclusions

The most relevant conclusions drawn from the studies presented as part of this thesis can be summarized as follows:

1. CoQ deficiency induces an adaptation in the mitochondrial proteome and metabolism due to the disruption of the Q-junction, together with the accumulation of DMQ, promoting microgliosis, astrogliosis, neuroinflammation and spongiform degeneration in *Coq9*^{R239X} mice.

2. 4-HB analogs therapy, with β-RA or VA, partially decreases the DMQ/CoQ ratio in peripheral tissues, normalizes the mitochondrial proteome and metabolism, and reduces the microgliosis, astrogliosis, neuroinflammation and spongiosis, with the subsequent rescue of the encephalopathic phenotype in *Coq9*^{R239X} mice.

3. β-RA and VA also normalize the serum levels of acylcarnitines and some other metabolites and proteins that have the potential to be used as biomarkers to follow the progression of the disease and the response to treatments in CoQ deficiency.

4. Supplementation with CoQ_{10} in CoQ or Complex I deficiency induces the overexpression of SQOR, a component of the Q-junction and the first enzyme of the mitochondrial hydrogen sulfide oxidation pathway, leading to a downregulation of CBS

and CSE, enzymes from the transsulfuration pathway. These changes are independent of sulfur aminoacids availability.

5. The modulation of sulfide metabolism induced by CoQ_{10} causes the adaptation of metabolic pathways closely connected to the transsulfuration pathway and unbalanced in a variety of models of mitochondrial diseases, such as the serine biosynthesis, the folate cycle and the nucleotides metabolism.

6. CoQ_{10} and VA co-supplementation *in vitro* leads to synergic effects in regulating pathways altered in CoQ deficiency.

7. Conclusiones

Las conclusiones más relevantes extraídas de los estudios presentados como parte de esta tesis se pueden resumir de la siguiente manera:

1. La deficiencia en CoQ produce una adaptación en el proteoma y el metabolismo mitocondrial debido a la disrupción de la confluencia Q, junto con la acumulación de DMQ, dando lugar a microgliosis, astrogliosis, neuroinflamación y degeneración espongiforme en los ratones *Coq9*^{R239X}.

2. La terapia con análogos del 4-HB, β-RA o VA, disminuye parcialmente el cociente DMQ/CoQ en tejidos periféricos, normaliza el proteoma y el metabolismo mitocondrial, y reduce la microgliosis, astrogliosis, neuroinflamación y espongiosis, con el consiguiente rescate del fenotipo encefalopático en ratones *Coq9*^{R239X}.

3. β-RA y VA también normalizan los niveles séricos de acilcarnitinas y otros metabolitos y proteínas que podrían usarse potencialmente como biomarcadores para seguir la progresión de la enfermedad y la respuesta a los tratamientos en casos de deficiencia en CoQ.

4. El suplemento con CoQ_{10} en la deficiencia en CoQ o Complejo I induce la sobreexpresión de SQOR, uno de los componentes de la confluencia Q y la primera enzima de la ruta de oxidación mitocondrial del sulfuro de hidrógeno. Esto da lugar a una menor

expresión de CBS y CSE, enzimas de la ruta de transulfuración. Estos cambios son independientes de la disponibilidad de aminoácidos azufrados.

5. La modulación del metabolismo del sulfuro inducida por la CoQ_{10} provoca la adaptación de rutas metabólicas estrechamente conectadas a la ruta de transulfuración y alteradas en varios modelos de enfermedade mitocondrial, como la biosíntesis de serina, el ciclo del folato y el metabolismo de nucleótidos.

6. La co-suplementación *in vitro* de CoQ_{10} y VA produce efectos sinérgicos en las vías de alteradas en la deficiencia en CoQ.

8. Bibliography

1. Rappocciolo E, Stiban J. Prokaryotic and Mitochondrial Lipids: A Survey of Evolutionary Origins. Adv Exp Med Biol. 2019;1159:5-31.
2. Baum DA, Baum B. An inside-out origin for the eukaryotic cell. BMC Biol. 2014;12:76.
3. Rich PR, Marechal A. The mitochondrial respiratory chain. Essays Biochem. 2010;47:1-23.
4. Duchen MR. Mitochondria in health and disease: perspectives on a new mitochondrial biology. Mol Aspects Med. 2004;25(4):365-451.
5. Cogliati S, Enriquez JA, Scorrano L. Mitochondrial Cristae: Where Beauty Meets Functionality. Trends Biochem Sci. 2016;41(3):261-73.
6. Nunnari J, Suomalainen A. Mitochondria: in sickness and in health. Cell. 2012;148(6):1145-59.
7. Lopez-Garcia P, Eme L, Moreira D. Symbiosis in eukaryotic evolution. J Theor Biol. 2017;434:20-33.
8. Keeling PJ. The impact of history on our perception of evolutionary events: endosymbiosis and the origin of eukaryotic complexity. Cold Spring Harb Perspect Biol. 2014;6(2).
9. Martin WF, Garg S, Zimorski V. Endosymbiotic theories for eukaryote origin. Philos Trans R Soc Lond B Biol Sci. 2015;370(1678):20140330.
10. Lopez-Garcia P, Moreira D. Open Questions on the Origin of Eukaryotes. Trends Ecol Evol. 2015;30(11):697-708.
11. Mentel M, Martin W. Energy metabolism among eukaryotic anaerobes in light of Proterozoic ocean chemistry. Philos Trans R Soc Lond B Biol Sci. 2008;363(1504):2717-29.
12. Lane N, Martin W. The energetics of genome complexity. Nature. 2010;467(7318):929-34.
13. Poole AM, Gribaldo S. Eukaryotic origins: How and when was the mitochondrion acquired? Cold Spring Harb Perspect Biol. 2014;6(12):a015990.
14. Embley TM, Martin W. Eukaryotic evolution, changes and challenges. Nature. 2006;440(7084):623-30.
15. Martin WF, Neukirchen S, Zimorski V, Gould SB, Sousa FL. Energy for two: New archaeal lineages and the origin of mitochondria. Bioessays. 2016;38(9):850-6.
16. Pittis AA, Gabaldon T. Late acquisition of mitochondria by a host with chimaeric prokaryotic ancestry. Nature. 2016;531(7592):101-4.

17. Zachar I, Szathmary E. Breath-giving cooperation: critical review of origin of mitochondria hypotheses : Major unanswered questions point to the importance of early ecology. Biol Direct. 2017;12(1):19.
18. Martin W, Kowallik K. Annotated English translation of Mereschkowsky's 1905 paper ‘Über Natur und Ursprung der Chromatophoren imPflanzenreiche’. European Journal of Phycology. 1999;34(3):287-95.
19. Portier P. Les symbiotes: Masson; 1918.
20. Wallin IE. Symbionticism and the Origin of Species: Рипол Классик; 1927.
21. Brown JA, Sammy MJ, Ballinger SW. An evolutionary, or "Mitocentric" perspective on cellular function and disease. Redox Biol. 2020;36:101568.
22. Sagan L. On the origin of mitosing cells. J Theor Biol. 1967;14(3):255-74.
23. Margulis L. Archaeal-eubacterial mergers in the origin of Eukarya: phylogenetic classification of life. Proc Natl Acad Sci U S A. 1996;93(3):1071-6.
24. Lake JA. Lynn Margulis (1938-2011). Nature. 2011;480(7378):458.
25. Schwartz RM, Dayhoff MO. Origins of Prokaryotes, Eukaryotes, Mitochondria, and Chloroplasts. Science. 1978;199(4327):395-403.
26. Dyall SD, Brown MT, Johnson PJ. Ancient invasions: from endosymbionts to organelles. Science. 2004;304(5668):253-7.
27. Gray MW, Burger G, Lang BF. Mitochondrial evolution. Science. 1999;283(5407):1476-81.
28. Nisbet EG, Sleep NH. The habitat and nature of early life. Nature. 2001;409(6823):1083-91.
29. Martin W, Hoffmeister M, Rotte C, Henze K. An overview of endosymbiotic models for the origins of eukaryotes, their ATP-producing organelles (mitochondria and hydrogenosomes), and their heterotrophic lifestyle. Biol Chem. 2001;382(11):1521-39.
30. Margulis L, Dolan MF, Whiteside JH. “Imperfections and oddities” in the origin of the nucleus. Paleobiology. 2005;31(sp5):175-91, 17.
31. Moreira D, Lopez-Garcia P. Symbiosis between methanogenic archaea and delta-proteobacteria as the origin of eukaryotes: the syntrophic hypothesis. J Mol Evol. 1998;47(5):517-30.
32. Cavalier-Smith T. The phagotrophic origin of eukaryotes and phylogenetic classification of Protozoa. Int J Syst Evol Microbiol. 2002;52(Pt 2):297-354.

33. Cavalier-Smith T. Only six kingdoms of life. Proc Biol Sci. 2004;271(1545):1251-62.
34. Martin W, Muller M. The hydrogen hypothesis for the first eukaryote. Nature. 1998;392(6671):37-41.
35. Vellai T, Takacs K, Vida G. A new aspect to the origin and evolution of eukaryotes. J Mol Evol. 1998;46(5):499-507.
36. Leblanc C, Richard O, Kloareg B, Viehmann S, Zetsche K, Boyen C. Origin and evolution of mitochondria: what have we learnt from red algae? Curr Genet. 1997;31(3):193-207.
37. Roger AJ, Munoz-Gomez SA, Kamikawa R. The Origin and Diversification of Mitochondria. Curr Biol. 2017;27(21):R1177-R92.
38. Muller M, Mentel M, van Hellemond JJ, Henze K, Woehle C, Gould SB, et al. Biochemistry and evolution of anaerobic energy metabolism in eukaryotes. Microbiol Mol Biol Rev. 2012;76(2):444-95.
39. Scheffler IE. Mitochondria: John Wiley & Sons; 2011.
40. Kuhlbrandt W. Structure and function of mitochondrial membrane protein complexes. BMC Biol. 2015;13:89.
41. Fontanesi F. Mitochondria: Structure and Role in Respiration. eLS. p. 1-13.
42. Bayrhuber M, Meins T, Habeck M, Becker S, Giller K, Villinger S, et al. Structure of the human voltage-dependent anion channel. Proc Natl Acad Sci U S A. 2008;105(40):15370-5.
43. Colombini M, Blachly-Dyson E, Forte M. VDAC, a channel in the outer mitochondrial membrane. Ion Channels. 1996;4:169-202.
44. Pfanner N, Wiedemann N. Mitochondrial protein import: two membranes, three translocases. Curr Opin Cell Biol. 2002;14(4):400-11.
45. Hengartner MO. The biochemistry of apoptosis. Nature. 2000;407(6805):770-6.
46. Pfanner N, Meijer M. The Tom and Tim machine. Current biology : CB. 1997;7(2):R100-3.
47. Herrmann JM, Neupert W. Protein insertion into the inner membrane of mitochondria. IUBMB life. 2003;55(4-5):219-25.
48. Wollweber F, von der Malsburg K, van der Laan M. Mitochondrial contact site and cristae organizing system: A central player in membrane shaping and crosstalk. Biochimica et biophysica acta Molecular cell research. 2017;1864(9):1481-9.
49. Herrmann JM, Riemer J. The intermembrane space of mitochondria. Antioxidants & redox signaling. 2010;13(9):1341-58.
50. Pagliarini DJ, Calvo SE, Chang B, Sheth SA, Vafai SB, Ong S-E, et al. A mitochondrial protein compendium elucidates complex I disease biology. Cell. 2008;134(1):112-23.

51. Calvo SE, Mootha VK. The mitochondrial proteome and human disease. Annual review of genomics and human genetics. 2010;11:25.
52. Gorman GS, Chinnery PF, DiMauro S, Hirano M, Koga Y, McFarland R, et al. Mitochondrial diseases. Nature Reviews Disease Primers. 2016;2(1):16080.
53. Pfanner N, Warscheid B, Wiedemann N. Mitochondrial proteins: from biogenesis to functional networks. Nature reviews Molecular cell biology. 2019;20(5):267-84.
54. Dröse S, Brandt U, Wittig I. Mitochondrial respiratory chain complexes as sources and targets of thiol-based redox-regulation. Biochimica et Biophysica Acta (BBA) - Proteins and Proteomics. 2014;1844(8):1344-54.
55. Spinelli JB, Haigis MC. The multifaceted contributions of mitochondria to cellular metabolism. Nature cell biology. 2018;20(7):745-54.
56. Nunnari J, Suomalainen A. Mitochondria: In Sickness and in Health. Cell. 2012;148(6):1145-59.
57. Viscomi C, Bottani E, Zeviani M. Emerging concepts in the therapy of mitochondrial disease. Biochimica et Biophysica Acta (BBA) - Bioenergetics. 2015;1847(6):544-57.
58. Cox M, Lehninger A, Nelson D. Principios de bioquímica. São Paulo. 2006.
59. Gonzalez-Garcia P, Barriocanal-Casado E, Diaz-Casado ME, Lopez-Herrador S, Hidalgo-Gutierrez A, Lopez LC. Animal Models of Coenzyme Q Deficiency: Mechanistic and Translational Learnings. Antioxidants (Basel). 2021;10(11).
60. Kumar S, Saxena J, Srivastava VK, Kaushik S, Singh H, Abo-EL-Sooud K, et al. The Interplay of Oxidative Stress and ROS Scavenging: Antioxidants as a Therapeutic Potential in Sepsis. Vaccines. 2022;10(10):1575.
61. Ziad M, Zaher MAJ, Saleh AA. Nonenzymatic Exogenous and Endogenous Antioxidants. In: Kusal D, Swastika D, Mallanagouda Shivanagouda B, Varaprasad B, Tata SS, editors. Free Radical Medicine and Biology. Rijeka: IntechOpen; 2019. p. Ch. 6.
62. Schulz JB, Lindenau J, Seyfried J, Dichgans J. Glutathione, oxidative stress and neurodegeneration. European journal of biochemistry. 2000;267(16):4904-11.
63. Ibrahim W, Lee US, Yeh CC, Szabo J, Bruckner G, Chow CK. Oxidative stress and antioxidant status in mouse liver: effects of dietary lipid, vitamin E and iron. The Journal of nutrition. 1997;127(7):1401-6.
64. Javadov S, Jang S, Chapa-Dubocq XR, Khuchua Z, Camara AKS. Mitochondrial respiratory supercomplexes in mammalian cells:

structural versus functional role. Journal of Molecular Medicine. 2021;99(1):57-73.
65. Chance B, Williams GR. A Method for the Localization of Sites for Oxidative Phosphorylation. Nature. 1955;176(4475):250-4.
66. Chance B, Estabrook RW, Lee CP. Electron Transport in the Oxysome. Science. 1963;140(3565):379-80.
67. Hatefi Y, Haavik AG, Griffiths DE. Studies on the electron transfer system. XL. Preparation and properties of mitochondrial DPNH-coenzyme Q reductase. The Journal of biological chemistry. 1962;237:1676-80.
68. Hackenbrock CR, Chazotte B, Gupte SS. The random collision model and a critical assessment of diffusion and collision in mitochondrial electron transport. J Bioenerg Biomembr. 1986;18(5):331-68.
69. Schägger H, Pfeiffer K. Supercomplexes in the respiratory chains of yeast and mammalian mitochondria. The EMBO journal. 2000;19(8):1777-83.
70. Schäfer E, Dencher NA, Vonck J, Parcej DN. Three-dimensional structure of the respiratory chain supercomplex I1III2IV1 from bovine heart mitochondria. Biochemistry. 2007;46(44):12579-85.
71. Schägger H, Pfeiffer K. The ratio of oxidative phosphorylation complexes I-V in bovine heart mitochondria and the composition of respiratory chain supercomplexes. The Journal of biological chemistry. 2001;276(41):37861-7.
72. Acín-Pérez R, Fernández-Silva P, Peleato ML, Pérez-Martos A, Enriquez JA. Respiratory active mitochondrial supercomplexes. Mol Cell. 2008;32(4):529-39.
73. Sousa PMF, Silva STN, Hood BL, Charro N, Carita JN, Vaz F, et al. Supramolecular organizations in the aerobic respiratory chain of Escherichia coli. Biochimie. 2011;93(3):418-25.
74. Hochman JH, Schindler M, Lee JG, Ferguson-Miller S. Lateral mobility of cytochrome c on intact mitochondrial membranes as determined by fluorescence redistribution after photobleaching. Proceedings of the National Academy of Sciences. 1982;79(22):6866-70.
75. Schägger H. Respiratory chain supercomplexes. IUBMB life. 2001;52(3-5):119-28.
76. Lobo-Jarne T, Ugalde C. Respiratory chain supercomplexes: Structures, function and biogenesis. Seminars in Cell & Developmental Biology. 2018;76:179-90.
77. Crane FL. Discovery of ubiquinone (coenzyme Q) and an overview of function. Mitochondrion. 2007;7 Suppl:S2-7.

78. Festenstein GN, Heaton FW, Lowe JS, Morton RA. A constituent of the unsaponifiable portion of animal tissue lipids (lambda max. 272 m mu). Biochem J. 1955;59(4):558-66.
79. Crane FL, Hatefi Y, Lester RL, Widmer C. Isolation of a quinone from beef heart mitochondria. Biochim Biophys Acta. 1957;25(1):220-1.
80. Turunen M, Olsson J, Dallner G. Metabolism and function of coenzyme Q. Biochim Biophys Acta. 2004;1660(1-2):171-99.
81. Wolf DE, Hoffman CH, Trenner NR, Arison BH, Shunk CH, Linn BO, et al. Coenzyme Q. I. Structure studies on the coenzyme Q group. Journal of the American Chemical Society. 1958;80:4752-.
82. Alcázar-Fabra M, Navas P, Brea-Calvo G. Coenzyme Q biosynthesis and its role in the respiratory chain structure. Biochimica et Biophysica Acta (BBA) - Bioenergetics. 2016;1857(8):1073-8.
83. Stefely JA, Pagliarini DJ. Biochemistry of Mitochondrial Coenzyme Q Biosynthesis. Trends Biochem Sci. 2017;42(10):824-43.
84. Kawamukai M. Biosynthesis and bioproduction of coenzyme Q10 by yeasts and other organisms. Biotechnol Appl Biochem. 2009;53(Pt 4):217-26.
85. Fernández-Del-Río L, Clarke CF. Coenzyme Q Biosynthesis: An Update on the Origins of the Benzenoid Ring and Discovery of New Ring Precursors. Metabolites. 2021;11(6).
86. Teclebrhan H, Jakobsson-Borin A, Brunk U, Dallner G. Relationship between the endoplasmic reticulum-Golgi membrane system and ubiquinone biosynthesis. Biochimica et Biophysica Acta (BBA) - Lipids and Lipid Metabolism. 1995;1256(2):157-65.
87. Mugoni V, Medana C, Santoro MM. 13C-isotope-based protocol for prenyl lipid metabolic analysis in zebrafish embryos. Nature Protocols. 2013;8(12):2337-47.
88. Eisenberg-Bord M, Tsui HS, Antunes D, Fernandez-Del-Rio L, Bradley MC, Dunn CD, et al. The Endoplasmic Reticulum-Mitochondria Encounter Structure Complex Coordinates Coenzyme Q Biosynthesis. Contact (Thousand Oaks). 2019;2:2515256418825409.
89. Wang Y, Hekimi S. The Complexity of Making Ubiquinone. Trends Endocrinol Metab. 2019;30(12):929-43.
90. Wang Y, Hekimi S. Understanding Ubiquinone. Trends in Cell Biology. 2016;26(5):367-78.
91. González-Mariscal I, García-Testón E, Padilla S, Martín-Montalvo A, Pomares Viciana T, Vazquez-Fonseca L, et al. The regulation of coenzyme q biosynthesis in eukaryotic cells: all that yeast can tell us. Mol Syndromol. 2014;5(3-4):107-18.

92. Lapointe CP, Stefely JA, Jochem A, Hutchins PD, Wilson GM, Kwiecien NW, et al. Multi-omics Reveal Specific Targets of the RNA-Binding Protein Puf3p and Its Orchestration of Mitochondrial Biogenesis. Cell Systems. 2018;6(1):125-35.e6.
93. Niemi NM, Wilson GM, Overmyer KA, Vögtle FN, Myketin L, Lohman DC, et al. Pptc7 is an essential phosphatase for promoting mammalian mitochondrial metabolism and biogenesis. Nature Communications. 2019;10(1):3197.
94. Martín-Montalvo A, González-Mariscal I, Pomares-Viciana T, Padilla-López S, Ballesteros M, Vazquez-Fonseca L, et al. The phosphatase Ptc7 induces coenzyme Q biosynthesis by activating the hydroxylase Coq7 in yeast. The Journal of biological chemistry. 2013;288(39):28126-37.
95. Pierrel F. Impact of Chemical Analogs of 4-Hydroxybenzoic Acid on Coenzyme Q Biosynthesis: From Inhibition to Bypass of Coenzyme Q Deficiency. Front Physiol. 2017;8:436.
96. Díaz-Casado ME, Quiles JL, Barriocanal-Casado E, González-García P, Battino M, López LC, et al. The Paradox of Coenzyme Q10 in Aging. Nutrients. 2019;11(9):2221.
97. Morgan PN, Gibson MI, Gibson F. Conversion of Shikimic Acid to Aromatic Compounds. Nature. 1962;194(4835):1239-41.
98. Lawrence J, Cox GB, Gibson F. Biosynthesis of Ubiquinone in Escherichia coli K-12: Biochemical and Genetic Characterization of a Mutant Unable to Convert Chorismate into 4-Hydroxybenzoate. Journal of Bacteriology. 1974;118(1):41-5.
99. Cox GB, Gibson F. Biosynthesis of vitamin K and ubiquinone relation to the shikimic acid pathway in Escherichia coli. Biochimica et Biophysica Acta (BBA) - General Subjects. 1964;93(1):204-6.
100. Marbois B, Xie LX, Choi S, Hirano K, Hyman K, Clarke CF. para-Aminobenzoic Acid Is a Precursor in Coenzyme Q6 Biosynthesis in Saccharomyces cerevisiae*. Journal of Biological Chemistry. 2010;285(36):27827-38.
101. Pierrel F, Hamelin O, Douki T, Kieffer-Jaquinod S, Mühlenhoff U, Ozeir M, et al. Involvement of Mitochondrial Ferredoxin and Para-Aminobenzoic Acid in Yeast Coenzyme Q Biosynthesis. Chemistry & biology. 2010;17(5):449-59.
102. Banh RS, Kim ES, Spillier Q, Biancur DE, Yamamoto K, Sohn ASW, et al. The polar oxy-metabolome reveals the 4-hydroxymandelate CoQ10 synthesis pathway. Nature. 2021;597(7876):420-5.
103. Lombard J, Moreira D. Origins and early evolution of the mevalonate pathway of isoprenoid biosynthesis in the three domains of life. Mol Biol Evol. 2011;28(1):87-99.

104. Awad AM, Bradley MC, Fernández-Del-Río L, Nag A, Tsui HS, Clarke CF. Coenzyme Q(10) deficiencies: pathways in yeast and humans. Essays Biochem. 2018;62(3):361-76.
105. Desbats MA, Morbidoni V, Silic-Benussi M, Doimo M, Ciminale V, Cassina M, et al. The COQ2 genotype predicts the severity of coenzyme Q10 deficiency. Human Molecular Genetics. 2016;25(19):4256-65.
106. Ozeir M, Mühlenhoff U, Webert H, Lill R, Fontecave M, Pierrel F. Coenzyme Q biosynthesis: Coq6 is required for the C5-hydroxylation reaction and substrate analogs rescue Coq6 deficiency. Chemistry & biology. 2011;18(9):1134-42.
107. Jonassen T, Clarke CF. Isolation and functional expression of human COQ3, a gene encoding a methyltransferase required for ubiquinone biosynthesis. J Biol Chem. 2000;275(17):12381-7.
108. Nguyen TP, Casarin A, Desbats MA, Doimo M, Trevisson E, Santos-Ocaña C, et al. Molecular characterization of the human COQ5 C-methyltransferase in coenzyme Q10 biosynthesis. Biochim Biophys Acta. 2014;1841(11):1628-38.
109. Marbois BN, Clarke CF. The COQ7 gene encodes a protein in saccharomyces cerevisiae necessary for ubiquinone biosynthesis. J Biol Chem. 1996;271(6):2995-3004.
110. Reidenbach AG, Kemmerer ZA, Aydin D, Jochem A, McDevitt MT, Hutchins PD, et al. Conserved Lipid and Small-Molecule Modulation of COQ8 Reveals Regulation of the Ancient Kinase-like UbiB Family. Cell chemical biology. 2018;25(2):154-65.e11.
111. Lohman DC, Aydin D, Von Bank HC, Smith RW, Linke V, Weisenhorn E, et al. An Isoprene Lipid-Binding Protein Promotes Eukaryotic Coenzyme Q Biosynthesis. Mol Cell. 2019;73(4):763-74.e10.
112. He CH, Black DS, Nguyen TP, Wang C, Srinivasan C, Clarke CF. Yeast Coq9 controls deamination of coenzyme Q intermediates that derive from para-aminobenzoic acid. Biochim Biophys Acta. 2015;1851(9):1227-39.
113. García-Corzo L, Luna-Sánchez M, Doerrier C, García JA, Guarás A, Acín-Pérez R, et al. Dysfunctional Coq9 protein causes predominant encephalomyopathy associated with CoQ deficiency. Hum Mol Genet. 2013;22(6):1233-48.
114. Tsui HS, Pham NVB, Amer BR, Bradley MC, Gosschalk JE, Gallagher-Jones M, et al. Human COQ10A and COQ10B are distinct lipid-binding START domain proteins required for coenzyme Q function. J Lipid Res. 2019;60(7):1293-310.

115. Marbois B, Gin P, Gulmezian M, Clarke CF. The yeast Coq4 polypeptide organizes a mitochondrial protein complex essential for coenzyme Q biosynthesis. Biochim Biophys Acta. 2009;1791(1):69-75.
116. Floyd BJ, Wilkerson EM, Veling MT, Minogue CE, Xia C, Beebe ET, et al. Mitochondrial Protein Interaction Mapping Identifies Regulators of Respiratory Chain Function. Mol Cell. 2016;63(4):621-32.
117. Xie LX, Hsieh EJ, Watanabe S, Allan CM, Chen JY, Tran UC, et al. Expression of the human atypical kinase ADCK3 rescues coenzyme Q biosynthesis and phosphorylation of Coq polypeptides in yeast coq8 mutants. Biochimica et Biophysica Acta (BBA) - Molecular and Cell Biology of Lipids. 2011;1811(5):348-60.
118. Stefely Jonathan A, Licitra F, Laredj L, Reidenbach Andrew G, Kemmerer Zachary A, Grangeray A, et al. Cerebellar Ataxia and Coenzyme Q Deficiency through Loss of Unorthodox Kinase Activity. Molecular Cell. 2016;63(4):608-20.
119. Hsieh EJ, Gin P, Gulmezian M, Tran UC, Saiki R, Marbois BN, et al. Saccharomyces cerevisiae Coq9 polypeptide is a subunit of the mitochondrial coenzyme Q biosynthetic complex. Archives of Biochemistry and Biophysics. 2007;463(1):19-26.
120. Lohman DC, Forouhar F, Beebe ET, Stefely MS, Minogue CE, Ulbrich A, et al. Mitochondrial COQ9 is a lipid-binding protein that associates with COQ7 to enable coenzyme Q biosynthesis. Proc Natl Acad Sci U S A. 2014;111(44):E4697-705.
121. Luna-Sánchez M, Díaz-Casado E, Barca E, Tejada M, Montilla-García Á, Cobos EJ, et al. The clinical heterogeneity of coenzyme Q10 deficiency results from genotypic differences in the Coq9 gene. EMBO Mol Med. 2015;7(5):670-87.
122. Allan CM, Hill S, Morvaridi S, Saiki R, Johnson JS, Liau WS, et al. A conserved START domain coenzyme Q-binding polypeptide is required for efficient Q biosynthesis, respiratory electron transport, and antioxidant function in Saccharomyces cerevisiae. Biochim Biophys Acta. 2013;1831(4):776-91.
123. Cirilli I, Damiani E, Dludla PV, Hargreaves I, Marcheggiani F, Millichap LE, et al. Role of Coenzyme Q10 in Health and Disease: An Update on the Last 10 Years (2010–2020). Antioxidants. 2021;10(8):1325.
124. Hidalgo-Gutiérrez A, González-García P, Díaz-Casado ME, Barriocanal-Casado E, López-Herrador S, Quinzii CM, et al. Metabolic Targets of Coenzyme Q10 in Mitochondria. Antioxidants. 2021;10(4):520.
125. Lenaz G, Genova ML. Kinetics of integrated electron transfer in the mitochondrial respiratory chain: random collisions vs. solid state

electron channeling. American journal of physiology Cell physiology. 2007;292(4):C1221-39.
126. Lapuente-Brun E, Moreno-Loshuertos R, Acín-Pérez R, Latorre-Pellicer A, Colás C, Balsa E, et al. Supercomplex Assembly Determines Electron Flux in the Mitochondrial Electron Transport Chain. Science. 2013;340(6140):1567-70.
127. Guarás A, Perales-Clemente E, Calvo E, Acín-Pérez R, Loureiro-Lopez M, Pujol C, et al. The CoQH2/CoQ Ratio Serves as a Sensor of Respiratory Chain Efficiency. Cell Rep. 2016;15(1):197-209.
128. Scialò F, Fernández-Ayala DJ, Sanz A. Role of Mitochondrial Reverse Electron Transport in ROS Signaling: Potential Roles in Health and Disease. Front Physiol. 2017;8:428.
129. Bentinger M, Brismar K, Dallner G. The antioxidant role of coenzyme Q. Mitochondrion. 2007;7 Suppl:S41-50.
130. Ayala A, Muñoz MF, Argüelles S. Lipid peroxidation: production, metabolism, and signaling mechanisms of malondialdehyde and 4-hydroxy-2-nonenal. Oxidative medicine and cellular longevity. 2014;2014:360438.
131. James AM, Smith RA, Murphy MP. Antioxidant and prooxidant properties of mitochondrial Coenzyme Q. Arch Biochem Biophys. 2004;423(1):47-56.
132. Stadtman ER, Levine RL. Protein oxidation. Annals of the New York Academy of Sciences. 2000;899:191-208.
133. Forsmark-Andrée P, Persson B, Radi R, Dallner G, Ernster L. Oxidative Modification of Nicotinamide Nucleotide Transhydrogenase in Submitochondrial Particles: Effect of Endogenous Ubiquinol. Archives of Biochemistry and Biophysics. 1996;336(1):113-20.
134. Ernster L, Dallner G. Biochemical, physiological and medical aspects of ubiquinone function. Biochimica et Biophysica Acta (BBA) - Molecular Basis of Disease. 1995;1271(1):195-204.
135. Klingenberg M, Huang SG. Structure and function of the uncoupling protein from brown adipose tissue. Biochim Biophys Acta. 1999;1415(2):271-96.
136. Echtay KS, Winkler E, Frischmuth K, Klingenberg M. Uncoupling proteins 2 and 3 are highly active H(+) transporters and highly nucleotide sensitive when activated by coenzyme Q (ubiquinone). Proc Natl Acad Sci U S A. 2001;98(4):1416-21.
137. Echtay KS, Roussel D, St-Pierre J, Jekabsons MB, Cadenas S, Stuart JA, et al. Superoxide activates mitochondrial uncoupling proteins. Nature. 2002;415(6867):96-9.

138. Echtay KS, Winkler E, Klingenberg M. Coenzyme Q is an obligatory cofactor for uncoupling protein function. Nature. 2000;408(6812):609-13.
139. Jaburek M, Garlid KD. Reconstitution of recombinant uncoupling proteins: UCP1, -2, and -3 have similar affinities for ATP and are unaffected by coenzyme Q10. The Journal of biological chemistry. 2003;278(28):25825-31.
140. Esteves TC, Echtay KS, Jonassen T, Clarke CF, Brand MD. Ubiquinone is not required for proton conductance by uncoupling protein 1 in yeast mitochondria. Biochem J. 2004;379(Pt 2):309-15.
141. Bernardi P. Mitochondrial transport of cations: channels, exchangers, and permeability transition. Physiological reviews. 1999;79(4):1127-55.
142. Bernardi P, Scorrano L, Colonna R, Petronilli V, Di Lisa F. Mitochondria and cell death. Mechanistic aspects and methodological issues. European journal of biochemistry. 1999;264(3):687-701.
143. Fontaine E, Ichas F, Bernardi P. A ubiquinone-binding site regulates the mitochondrial permeability transition pore. J Biol Chem. 1998;273(40):25734-40.
144. Walter L, Miyoshi H, Leverve X, Bernard P, Fontaine E. Regulation of the mitochondrial permeability transition pore by ubiquinone analogs. A progress report. Free Radic Res. 2002;36(4):405-12.
145. Papucci L, Schiavone N, Witort E, Donnini M, Lapucci A, Tempestini A, et al. Coenzyme q10 prevents apoptosis by inhibiting mitochondrial depolarization independently of its free radical scavenging property. J Biol Chem. 2003;278(30):28220-8.
146. Dixon SJ, Lemberg KM, Lamprecht MR, Skouta R, Zaitsev EM, Gleason CE, et al. Ferroptosis: an iron-dependent form of nonapoptotic cell death. Cell. 2012;149(5):1060-72.
147. Ingold I, Berndt C, Schmitt S, Doll S, Poschmann G, Buday K, et al. Selenium utilization by GPX4 is required to prevent hydroperoxide-induced ferroptosis. Cell. 2018;172(3):409-22. e21.
148. Doll S, Freitas FP, Shah R, Aldrovandi M, da Silva MC, Ingold I, et al. FSP1 is a glutathione-independent ferroptosis suppressor. Nature. 2019;575(7784):693-8.
149. Bersuker K, Hendricks JM, Li Z, Magtanong L, Ford B, Tang PH, et al. The CoQ oxidoreductase FSP1 acts parallel to GPX4 to inhibit ferroptosis. Nature. 2019;575(7784):688-92.
150. Gnaiger E, editor Mitochondrial pathways and respiratory control: An Introduction to OXPHOS Analysis. 5th ed2020.

151. Watmough NJ, Frerman FE. The electron transfer flavoprotein: Ubiquinone oxidoreductases. Biochimica et Biophysica Acta (BBA) - Bioenergetics. 2010;1797(12):1910-6.
152. Evans DR, Guy HI. Mammalian pyrimidine biosynthesis: fresh insights into an ancient pathway. J Biol Chem. 2004;279(32):33035-8.
153. Quinlan CL, Perevoschikova IV, Goncalves RLS, Hey-Mogensen M, Brand MD. Chapter Twelve - The Determination and Analysis of Site-Specific Rates of Mitochondrial Reactive Oxygen Species Production. In: Cadenas E, Packer L, editors. Methods in Enzymology. 526: Academic Press; 2013. p. 189-217.
154. Salvi F, Gadda G. Human choline dehydrogenase: medical promises and biochemical challenges. Arch Biochem Biophys. 2013;537(2):243-52.
155. Moxley MA, Tanner JJ, Becker DF. Steady-state kinetic mechanism of the proline:ubiquinone oxidoreductase activity of proline utilization A (PutA) from Escherichia coli. Archives of Biochemistry and Biophysics. 2011;516(2):113-20.
156. Kabil O, Vitvitsky V, Banerjee R. Sulfur as a signaling nutrient through hydrogen sulfide. Annu Rev Nutr. 2014;34:171-205.
157. Ziosi M, Di Meo I, Kleiner G, Gao XH, Barca E, Sanchez-Quintero MJ, et al. Coenzyme Q deficiency causes impairment of the sulfide oxidation pathway. EMBO Mol Med. 2017;9(1):96-111.
158. Luna-Sánchez M, Hidalgo-Gutiérrez A, Hildebrandt TM, Chaves-Serrano J, Barriocanal-Casado E, Santos-Fandila Á, et al. CoQ deficiency causes disruption of mitochondrial sulfide oxidation, a new pathomechanism associated with this syndrome. EMBO Mol Med. 2017;9(1):78-95.
159. Quinzii CM, Luna-Sanchez M, Ziosi M, Hidalgo-Gutierrez A, Kleiner G, Lopez LC. The Role of Sulfide Oxidation Impairment in the Pathogenesis of Primary CoQ Deficiency. Front Physiol. 2017;8:525.
160. Módis K, Coletta C, Erdélyi K, Papapetropoulos A, Szabo C. Intramitochondrial hydrogen sulfide production by 3-mercaptopyruvate sulfurtransferase maintains mitochondrial electron flow and supports cellular bioenergetics. FASEB journal : official publication of the Federation of American Societies for Experimental Biology. 2013;27(2):601-11.
161. Paul BD, Snyder SH. Gasotransmitter hydrogen sulfide signaling in neuronal health and disease. Biochem Pharmacol. 2018;149:101-9.
162. Libiad M, Yadav PK, Vitvitsky V, Martinov M, Banerjee R. Organization of the human mitochondrial hydrogen sulfide oxidation pathway. The Journal of biological chemistry. 2014;289(45):30901-10.

163. Hildebrandt TM, Grieshaber MK. Three enzymatic activities catalyze the oxidation of sulfide to thiosulfate in mammalian and invertebrate mitochondria. The FEBS journal. 2008;275(13):3352-61.
164. Szabo C, Ransy C, Módis K, Andriamihaja M, Murghes B, Coletta C, et al. Regulation of mitochondrial bioenergetic function by hydrogen sulfide. Part I. Biochemical and physiological mechanisms. British journal of pharmacology. 2014;171(8):2099-122.
165. Mottawea W, Chiang CK, Mühlbauer M, Starr AE, Butcher J, Abujamel T, et al. Altered intestinal microbiota-host mitochondria crosstalk in new onset Crohn's disease. Nat Commun. 2016;7:13419.
166. Pfeffer G, Horvath R, Klopstock T, Mootha VK, Suomalainen A, Koene S, et al. New treatments for mitochondrial disease-no time to drop our standards. Nat Rev Neurol. 2013;9(8):474-81.
167. Wang W, Karamanlidis G, Tian R. Novel targets for mitochondrial medicine. Sci Transl Med. 2016;8(326):326rv3.
168. Angelis A, Tordrup D, Kanavos P. Socio-economic burden of rare diseases: A systematic review of cost of illness evidence. Health policy (Amsterdam, Netherlands). 2015;119(7):964-79.
169. Nguengang Wakap S, Lambert DM, Olry A, Rodwell C, Gueydan C, Lanneau V, et al. Estimating cumulative point prevalence of rare diseases: analysis of the Orphanet database. European journal of human genetics : EJHG. 2020;28(2):165-73.
170. Pfeffer G, Majamaa K, Turnbull DM, Thorburn D, Chinnery PF. Treatment for mitochondrial disorders. The Cochrane database of systematic reviews. 2012;2012(4):Cd004426.
171. Craven L, Alston CL, Taylor RW, Turnbull DM. Recent Advances in Mitochondrial Disease. Annu Rev Genomics Hum Genet. 2017;18:257-75.
172. DiMauro S, Schon EA, Carelli V, Hirano M. The clinical maze of mitochondrial neurology. Nat Rev Neurol. 2013;9(8):429-44.
173. Goto Y, Nonaka I, Horai S. A mutation in the tRNA(Leu)(UUR) gene associated with the MELAS subgroup of mitochondrial encephalomyopathies. Nature. 1990;348(6302):651-3.
174. Shoffner JM, Lott MT, Lezza AMS, Seibel P, Ballinger SW, Wallace DC. Myoclonic epilepsy and ragged-red fiber disease (MERRF) is associated with a mitochondrial DNA tRNALys mutation. Cell. 1990;61(6):931-7.
175. Holt IJ, Harding AE, Petty RK, Morgan-Hughes JA. A new mitochondrial disease associated with mitochondrial DNA heteroplasmy. American journal of human genetics. 1990;46(3):428-33.

176. Wallace DC, Singh G, Lott MT, Hodge JA, Schurr TG, Lezza AMS, et al. Mitochondrial DNA Mutation Associated with Leber's Hereditary Optic Neuropathy. Science. 1988;242(4884):1427-30.
177. Moraes CT, DiMauro S, Zeviani M, Lombes A, Shanske S, Miranda AF, et al. Mitochondrial DNA Deletions in Progressive External Ophthalmoplegia and Kearns-Sayre Syndrome. New England Journal of Medicine. 1989;320(20):1293-9.
178. Rotig A, Colonna M, Bonnefont JP, Blanche S, Fischer A, Saudubray JM, et al. MITOCHONDRIAL DNA DELETION IN PEARSON'S MARROW/PANCREAS SYNDROME. The Lancet. 1989;333(8643):902-3.
179. Koopman WJH, Willems PHGM, Smeitink JAM. Monogenic Mitochondrial Disorders. New England Journal of Medicine. 2012;366(12):1132-41.
180. Nikkanen J, Forsstrom S, Euro L, Paetau I, Kohnz RA, Wang L, et al. Mitochondrial DNA Replication Defects Disturb Cellular dNTP Pools and Remodel One-Carbon Metabolism. Cell Metab. 2016;23(4):635-48.
181. Bao XR, Ong S-E, Goldberger O, Peng J, Sharma R, Thompson DA, et al. Mitochondrial dysfunction remodels one-carbon metabolism in human cells. eLife. 2016;5:e10575.
182. Forsström S, Jackson CB, Carroll CJ, Kuronen M, Pirinen E, Pradhan S, et al. Fibroblast Growth Factor 21 Drives Dynamics of Local and Systemic Stress Responses in Mitochondrial Myopathy with mtDNA Deletions. Cell Metabolism. 2019;30(6):1040-54.e7.
183. Krug AK, Gutbier S, Zhao L, Pöltl D, Kullmann C, Ivanova V, et al. Transcriptional and metabolic adaptation of human neurons to the mitochondrial toxicant MPP(+). Cell death & disease. 2014;5(5):e1222.
184. Hargreaves IP. Coenzyme Q10 as a therapy for mitochondrial disease. Int J Biochem Cell Biol. 2014;49:105-11.
185. Kühl I, Miranda M, Atanassov I, Kuznetsova I, Hinze Y, Mourier A, et al. Transcriptomic and proteomic landscape of mitochondrial dysfunction reveals secondary coenzyme Q deficiency in mammals. eLife. 2017;6:e30952.
186. Yubero D, Montero R, Martín MA, Montoya J, Ribes A, Grazina M, et al. Secondary coenzyme Q10 deficiencies in oxidative phosphorylation (OXPHOS) and non-OXPHOS disorders. Mitochondrion. 2016;30:51-8.
187. Fazakerley DJ, Chaudhuri R, Yang P, Maghzal GJ, Thomas KC, Krycer JR, et al. Mitochondrial CoQ deficiency is a common driver of mitochondrial oxidants and insulin resistance. Elife. 2018;7.

188. Ogasahara S, Engel AG, Frens D, Mack D. Muscle coenzyme Q deficiency in familial mitochondrial encephalomyopathy. Proc Natl Acad Sci U S A. 1989;86(7):2379-82.
189. Hughes BG, Harrison PM, Hekimi S. Estimating the occurrence of primary ubiquinone deficiency by analysis of large-scale sequencing data. Scientific Reports. 2017;7(1):17744.
190. Alcázar-Fabra M, Trevisson E, Brea-Calvo G. Clinical syndromes associated with Coenzyme Q(10) deficiency. Essays Biochem. 2018;62(3):377-98.
191. Doimo M, Desbats MA, Cerqua C, Cassina M, Trevisson E, Salviati L. Genetics of Coenzyme Q10 Deficiency. Molecular Syndromology. 2014;5(3-4):156-62.
192. Emmanuele V, Lopez LC, Berardo A, Naini A, Tadesse S, Wen B, et al. Heterogeneity of coenzyme Q10 deficiency: patient study and literature review. Arch Neurol. 2012;69(8):978-83.
193. Desbats MA, Lunardi G, Doimo M, Trevisson E, Salviati L. Genetic bases and clinical manifestations of coenzyme Q10 (CoQ 10) deficiency. J Inherit Metab Dis. 2015;38(1):145-56.
194. Alcázar-Fabra M, Rodríguez-Sánchez F, Trevisson E, Brea-Calvo G. Primary Coenzyme Q deficiencies: A literature review and online platform of clinical features to uncover genotype-phenotype correlations. Free Radical Biology and Medicine. 2021;167:141-80.
195. Mollet J, Giurgea I, Schlemmer D, Dallner G, Chretien D, Delahodde A, et al. Prenyldiphosphate synthase, subunit 1 (PDSS1) and OH-benzoate polyprenyltransferase (COQ2) mutations in ubiquinone deficiency and oxidative phosphorylation disorders. The Journal of clinical investigation. 2007;117(3):765-72.
196. Lopez LC, Schuelke M, Quinzii CM, Kanki T, Rodenburg RJ, Naini A, et al. Leigh syndrome with nephropathy and CoQ10 deficiency due to decaprenyl diphosphate synthase subunit 2 (PDSS2) mutations. Am J Hum Genet. 2006;79(6):1125-9.
197. Quinzii C, Naini A, Salviati L, Trevisson E, Navas P, Dimauro S, et al. A mutation in para-hydroxybenzoate-polyprenyl transferase (COQ2) causes primary coenzyme Q10 deficiency. Am J Hum Genet. 2006;78(2):345-9.
198. Diomedi-Camassei F, Di Giandomenico S, Santorelli FM, Caridi G, Piemonte F, Montini G, et al. COQ2 nephropathy: a newly described inherited mitochondriopathy with primary renal involvement. J Am Soc Nephrol. 2007;18(10):2773-80.
199. Salviati L, Trevisson E, Rodriguez Hernandez MA, Casarin A, Pertegato V, Doimo M, et al. Haploinsufficiency of COQ4 causes coenzyme Q10 deficiency. J Med Genet. 2012;49(3):187-91.

200. Malicdan MCV, Vilboux T, Ben-Zeev B, Guo J, Eliyahu A, Pode-Shakked B, et al. A novel inborn error of the coenzyme Q10 biosynthesis pathway: cerebellar ataxia and static encephalomyopathy due to COQ5 C-methyltransferase deficiency. Human mutation. 2018;39(1):69-79.
201. Heeringa SF, Chernin G, Chaki M, Zhou W, Sloan AJ, Ji Z, et al. COQ6 mutations in human patients produce nephrotic syndrome with sensorineural deafness. The Journal of clinical investigation. 2011;121(5):2013-24.
202. Freyer C, Stranneheim H, Naess K, Mourier A, Felser A, Maffezzini C, et al. Rescue of primary ubiquinone deficiency due to a novel COQ7 defect using 2,4-dihydroxybensoic acid. J Med Genet. 2015;52(11):779-83.
203. Wang Y, Smith C, Parboosingh JS, Khan A, Innes M, Hekimi S. Pathogenicity of two COQ7 mutations and responses to 2,4-dihydroxybenzoate bypass treatment. Journal of cellular and molecular medicine. 2017;21(10):2329-43.
204. Lagier-Tourenne C, Tazir M, Lopez LC, Quinzii CM, Assoum M, Drouot N, et al. ADCK3, an ancestral kinase, is mutated in a form of recessive ataxia associated with coenzyme Q10 deficiency. Am J Hum Genet. 2008;82(3):661-72.
205. Mollet J, Delahodde A, Serre V, Chretien D, Schlemmer D, Lombes A, et al. CABC1 gene mutations cause ubiquinone deficiency with cerebellar ataxia and seizures. Am J Hum Genet. 2008;82(3):623-30.
206. Feng C, Wang Q, Wang J, Liu F, Shen H, Fu H, et al. Coenzyme Q10 supplementation therapy for 2 children with proteinuria renal disease and ADCK4 mutation: Case reports and literature review. Medicine. 2017;96(47).
207. Ashraf S, Gee HY, Woerner S, Xie LX, Vega-Warner V, Lovric S, et al. ADCK4 mutations promote steroid-resistant nephrotic syndrome through CoQ10 biosynthesis disruption. The Journal of clinical investigation. 2013;123(12):5179-89.
208. Duncan AJ, Bitner-Glindzicz M, Meunier B, Costello H, Hargreaves IP, Lopez LC, et al. A nonsense mutation in COQ9 causes autosomal-recessive neonatal-onset primary coenzyme Q10 deficiency: a potentially treatable form of mitochondrial disease. Am J Hum Genet. 2009;84(5):558-66.
209. Danhauser K, Herebian D, Haack TB, Rodenburg RJ, Strom TM, Meitinger T, et al. Fatal neonatal encephalopathy and lactic acidosis caused by a homozygous loss-of-function variant in COQ9. European journal of human genetics : EJHG. 2016;24(3):450-4.

210. Musumeci O, Naini A, Slonim AE, Skavin N, Hadjigeorgiou GL, Krawiecki N, et al. Familial cerebellar ataxia with muscle coenzyme Q10 deficiency. Neurology. 2001;56(7):849-55.
211. Quinzii CM, Kattah AG, Naini A, Akman HO, Mootha VK, DiMauro S, et al. Coenzyme Q deficiency and cerebellar ataxia associated with an aprataxin mutation. Neurology. 2005;64(3):539-41.
212. Le Ber I, Dubourg O, Benoist JF, Jardel C, Mochel F, Koenig M, et al. Muscle coenzyme Q10 deficiencies in ataxia with oculomotor apraxia 1. Neurology. 2007;68(4):295-7.
213. Gempel K, Topaloglu H, Talim B, Schneiderat P, Schoser BG, Hans VH, et al. The myopathic form of coenzyme Q10 deficiency is caused by mutations in the electron-transferring-flavoprotein dehydrogenase (ETFDH) gene. Brain : a journal of neurology. 2007;130(Pt 8):2037-44.
214. Aeby A, Sznajer Y, Cavé H, Rebuffat E, Van Coster R, Rigal O, et al. Cardiofaciocutaneous (CFC) syndrome associated with muscular coenzyme Q10 deficiency. J Inherit Metab Dis. 2007;30(5):827.
215. Yubero D, Montero R, Martín MA, Montoya J, Ribes A, Grazina M, et al. Secondary coenzyme Q10 deficiencies in oxidative phosphorylation (OXPHOS) and non-OXPHOS disorders. Mitochondrion. 2016;30:51-8.
216. Montero R, Sánchez-Alcázar JA, Briones P, Navarro-Sastre A, Gallardo E, Bornstein B, et al. Coenzyme Q10 deficiency associated with a mitochondrial DNA depletion syndrome: A case report. Clinical Biochemistry. 2009;42(7):742-5.
217. Navas P, Cascajo MV, Alcázar-Fabra M, Hernández-Camacho JD, Sánchez-Cuesta A, Rodríguez ABC, et al. Secondary CoQ(10) deficiency, bioenergetics unbalance in disease and aging. Biofactors. 2021;47(4):551-69.
218. Marcoff L, Thompson PD. The Role of Coenzyme Q10 in Statin-Associated Myopathy: A Systematic Review. Journal of the American College of Cardiology. 2007;49(23):2231-7.
219. Uličná O, Vančová O, Waczulíková I, Božek P, Šikurová L, Bada V, et al. Liver mitochondrial respiratory function and coenzyme Q content in rats on a hypercholesterolemic diet treated with atorvastatin. Physiological research. 2012;61(2):185-93.
220. Spinazzi M, Radaelli E, Horré K, Arranz AM, Gounko NV, Agostinis P, et al. PARL deficiency in mouse causes Complex III defects, coenzyme Q depletion, and Leigh-like syndrome. Proc Natl Acad Sci U S A. 2019;116(1):277-86.

221. Geromel V, Kadhom N, Ceballos-Picot I, Chrétien D, Munnich A, Rötig A, et al. Human cultured skin fibroblasts survive profound inherited ubiquinone depletion. Free Radic Res. 2001;35(1):11-21.
222. López-Martín JM, Salviati L, Trevisson E, Montini G, DiMauro S, Quinzii C, et al. Missense mutation of the COQ2 gene causes defects of bioenergetics and de novo pyrimidine synthesis. Hum Mol Genet. 2007;16(9):1091-7.
223. Quinzii CM, López LC, Gilkerson RW, Dorado B, Coku J, Naini AB, et al. Reactive oxygen species, oxidative stress, and cell death correlate with level of CoQ10 deficiency. FASEB journal : official publication of the Federation of American Societies for Experimental Biology. 2010;24(10):3733-43.
224. Quinzii CM, López LC, Von-Moltke J, Naini A, Krishna S, Schuelke M, et al. Respiratory chain dysfunction and oxidative stress correlate with severity of primary CoQ10 deficiency. FASEB journal : official publication of the Federation of American Societies for Experimental Biology. 2008;22(6):1874-85.
225. Rodríguez-Hernández A, Cordero MD, Salviati L, Artuch R, Pineda M, Briones P, et al. Coenzyme Q deficiency triggers mitochondria degradation by mitophagy. Autophagy. 2009;5(1):19-32.
226. Quinzii CM, Tadesse S, Naini A, Hirano M. Effects of inhibiting CoQ10 biosynthesis with 4-nitrobenzoate in human fibroblasts. PLoS One. 2012;7(2):e30606.
227. Duberley KE, Abramov AY, Chalasani A, Heales SJ, Rahman S, Hargreaves IP. Human neuronal coenzyme Q10 deficiency results in global loss of mitochondrial respiratory chain activity, increased mitochondrial oxidative stress and reversal of ATP synthase activity: implications for pathogenesis and treatment. J Inherit Metab Dis. 2013;36(1):63-73.
228. Grant J, Saldanha JW, Gould AP. A Drosophila model for primary coenzyme Q deficiency and dietary rescue in the developing nervous system. Disease models & mechanisms. 2010;3(11-12):799-806.
229. Cheng W, Song C, Anjum K, Chen M, Li D, Zhou H, et al. Coenzyme Q plays opposing roles on bacteria/fungi and viruses in Drosophila innate immunity. International journal of immunogenetics. 2011;38(4):331-7.
230. Liu J, Wu Q, He D, Ma T, Du L, Dui W, et al. Drosophila sbo regulates lifespan through its function in the synthesis of coenzyme Q in vivo. Journal of Genetics and Genomics. 2011;38(6):225-34.
231. Hermle T, Braun DA, Helmstädter M, Huber TB, Hildebrandt F. Modeling monogenic human nephrotic syndrome in the Drosophila

garland cell nephrocyte. Journal of the American Society of Nephrology. 2017;28(5):1521-33.
232. Fernandez-Ayala D, Guerra I, Sanz A, Navas P, editors. coq7 (cg14437) interference courses a primary coenzyme Q deficiency in Drosophila. FEBS JOURNAL; 2012: WILEY-BLACKWELL 111 RIVER ST, HOBOKEN 07030-5774, NJ USA.
233. Guerra I, Fernández-Ayala DJ, Navas P. RNA interference (RNAi) of genes involved in Coenzyme Q biosynthesis in Drosophila melanogaster models Coenzyme Q deficiency in humans. 2012.
234. Kamath RS, Fraser AG, Dong Y, Poulin G, Durbin R, Gotta M, et al. Systematic functional analysis of the Caenorhabditis elegans genome using RNAi. Nature. 2003;421(6920):231-7.
235. Wong A, Boutis P, Hekimi S. Mutations in the clk-1 gene of Caenorhabditis elegans affect developmental and behavioral timing. Genetics. 1995;139(3):1247-59.
236. Cristina D, Cary M, Lunceford A, Clarke C, Kenyon C. A regulated response to impaired respiration slows behavioral rates and increases lifespan in Caenorhabditis elegans. PLoS genetics. 2009;5(4):e1000450.
237. Arroyo A, Santos-Ocaña C, Ruiz-Ferrer M, Padilla S, Gavilán Á, Rodríguez-Aguilera JC, et al. Coenzyme Q is irreplaceable by demethoxy-coenzyme Q in plasma membrane of Caenorhabditis elegans. FEBS letters. 2006;580(7):1740-6.
238. Gavilán Á, Asencio C, Cabello J, Rodríguez-Aguilera JC, Schnabel R, Navas P. C. elegans knockouts in ubiquinone biosynthesis genes result in different phenotypes during larval development. Biofactors. 2005;25(1-4):21-9.
239. Hihi AK, Gao Y, Hekimi S. Ubiquinone Is Necessary for Caenorhabditis elegansDevelopment at Mitochondrial and Non-mitochondrial Sites. Journal of Biological Chemistry. 2002;277(3):2202-6.
240. Earls LR, Hacker ML, Watson JD, Miller III DM. Coenzyme Q protects Caenorhabditis elegans GABA neurons from calcium-dependent degeneration. Proceedings of the National Academy of Sciences. 2010;107(32):14460-5.
241. Mugoni V, Postel R, Catanzaro V, De Luca E, Turco E, Digilio G, et al. Ubiad1 is an antioxidant enzyme that regulates eNOS activity by CoQ10 synthesis. Cell. 2013;152(3):504-18.
242. Lyon MF, Hulse E. An inherited kidney disease of mice resembling human nephronophthisis. Journal of Medical Genetics. 1971;8(1):41.

243. Quinzii CM, Garone C, Emmanuele V, Tadesse S, Krishna S, Dorado B, et al. Tissue-specific oxidative stress and loss of mitochondria in CoQ-deficient Pdss2 mutant mice. The FASEB Journal. 2013;27(2):612-21.
244. Peng M, Falk MJ, Haase VH, King R, Polyak E, Selak M, et al. Primary coenzyme Q deficiency in Pdss2 mutant mice causes isolated renal disease. PLoS genetics. 2008;4(4):e1000061.
245. Lu S, Lu L-Y, Liu M-F, Yuan Q-J, Sham M-H, Guan X-Y, et al. Cerebellar defects in Pdss2 conditional knockout mice during embryonic development and in adulthood. Neurobiology of disease. 2012;45(1):219-33.
246. Zhang XM, Ng AHL, Tanner JA, Wu WT, Copeland NG, Jenkins NA, et al. Highly restricted expression of Cre recombinase in cerebellar Purkinje cells. genesis. 2004;40(1):45-51.
247. Lapointe J, Wang Y, Bigras E, Hekimi S. The submitochondrial distribution of ubiquinone affects respiration in long-lived Mclk1+/− mice. Journal of Cell Biology. 2012;199(2):215-24.
248. Levavasseur F, Miyadera H, Sirois J, Tremblay ML, Kita K, Shoubridge E, et al. Ubiquinone is necessary for mouse embryonic development but is not essential for mitochondrial respiration. Journal of Biological Chemistry. 2001;276(49):46160-4.
249. Nakai D, Yuasa S, Takahashi M, Shimizu T, Asaumi S, Isono K, et al. Mouse homologue of coq7/clk-1, longevity gene in Caenorhabditis elegans, is essential for coenzyme Q synthesis, maintenance of mitochondrial integrity, and neurogenesis. Biochemical and biophysical research communications. 2001;289(2):463-71.
250. Stefely JA, Licitra F, Laredj L, Reidenbach AG, Kemmerer ZA, Grangeray A, et al. Cerebellar ataxia and coenzyme Q deficiency through loss of unorthodox kinase activity. Molecular cell. 2016;63(4):608-20.
251. Lapointe J, Stepanyan Z, Bigras E, Hekimi S. Reversal of the mitochondrial phenotype and slow development of oxidative biomarkers of aging in long-lived Mclk1+/− mice. Journal of biological chemistry. 2009;284(30):20364-74.
252. Zheng H, Lapointe J, Hekimi S. Lifelong protection from global cerebral ischemia and reperfusion in long-lived Mclk1+/− mutants. Experimental neurology. 2010;223(2):557-65.
253. Gu R, Zhang F, Chen G, Han C, Liu J, Ren Z, et al. Clk1 deficiency promotes neuroinflammation and subsequent dopaminergic cell death through regulation of microglial metabolic reprogramming. Brain, behavior, and immunity. 2017;60:206-19.
254. Rodríguez-Hidalgo M, Luna-Sánchez M, Hidalgo-Gutiérrez A, Barriocanal-Casado E, Mascaraque C, Acuña-Castroviejo D, et al.

Reduction in the levels of CoQ biosynthetic proteins is related to an increase in lifespan without evidence of hepatic mitohormesis. Scientific reports. 2018;8(1):1-10.
255. Potgieter M, Pretorius E, Pepper MS. Primary and secondary coenzyme Q10 deficiency: the role of therapeutic supplementation. Nutrition Reviews. 2013;71(3):180-8.
256. Rötig A, Appelkvist EL, Geromel V, Chretien D, Kadhom N, Edery P, et al. Quinone-responsive multiple respiratory-chain dysfunction due to widespread coenzyme Q10 deficiency. Lancet (London, England). 2000;356(9227):391-5.
257. Salviati L, Sacconi S, Murer L, Zacchello G, Franceschini L, Laverda AM, et al. Infantile encephalomyopathy and nephropathy with CoQ10 deficiency: a CoQ10-responsive condition. Neurology. 2005;65(4):606-8.
258. Di Giovanni S, Mirabella M, Spinazzola A, Crociani P, Silvestri G, Broccolini A, et al. Coenzyme Q10 reverses pathological phenotype and reduces apoptosis in familial CoQ10 deficiency. Neurology. 2001;57(3):515-8.
259. Montini G, Malaventura C, Salviati L. Early coenzyme Q10 supplementation in primary coenzyme Q10 deficiency. N Engl J Med. 2008;358(26):2849-50.
260. Caglayan AO, Gumus H, Sandford E, Kubisiak TL, Ma Q, Ozel AB, et al. COQ4 Mutation Leads to Childhood-Onset Ataxia Improved by CoQ10 Administration. Cerebellum (London, England). 2019;18(3):665-9.
261. Scalais E, Chafai R, Van Coster R, Bindl L, Nuttin C, Panagiotaraki C, et al. Early myoclonic epilepsy, hypertrophic cardiomyopathy and subsequently a nephrotic syndrome in a patient with CoQ10 deficiency caused by mutations in para-hydroxybenzoate-polyprenyl transferase (COQ2). European journal of paediatric neurology : EJPN : official journal of the European Paediatric Neurology Society. 2013;17(6):625-30.
262. López LC, Quinzii CM, Area E, Naini A, Rahman S, Schuelke M, et al. Treatment of CoQ(10) deficient fibroblasts with ubiquinone, CoQ analogs, and vitamin C: time- and compound-dependent effects. PLoS One. 2010;5(7):e11897.
263. Wang Y, Hekimi S. The efficacy of coenzyme Q(10) treatment in alleviating the symptoms of primary coenzyme Q(10) deficiency: A systematic review. Journal of cellular and molecular medicine. 2022;26(17):4635-44.

264. Hathcock JN, Shao A. Risk assessment for coenzyme Q10 (Ubiquinone). Regulatory Toxicology and Pharmacology. 2006;45(3):282-8.
265. Desbats MA, Vetro A, Limongelli I, Lunardi G, Casarin A, Doimo M, et al. Primary coenzyme Q10 deficiency presenting as fatal neonatal multiorgan failure. Eur J Hum Genet. 2015;23(9):1254-8.
266. Ishii N, Senoo-Matsuda N, Miyake K, Yasuda K, Ishii T, Hartman PS, et al. Coenzyme Q10 can prolong C. elegans lifespan by lowering oxidative stress. Mechanisms of ageing and development. 2004;125(1):41-6.
267. Yang Y-Y, Gangoiti JA, Sedensky MM, Morgan PG. The effect of different ubiquinones on lifespan in Caenorhabditis elegans. Mechanisms of ageing and development. 2009;130(6):370-6.
268. Gomez F, Saiki R, Chin R, Srinivasan C, Clarke CF. Restoring de novo coenzyme Q biosynthesis in Caenorhabditis elegans coq-3 mutants yields profound rescue compared to exogenous coenzyme Q supplementation. Gene. 2012;506(1):106-16.
269. Saiki R, Lunceford AL, Shi Y, Marbois B, King R, Pachuski J, et al. Coenzyme Q10 supplementation rescues renal disease in Pdss2 kd/kd mice with mutations in prenyl diphosphate synthase subunit 2. American Journal of Physiology-Renal Physiology. 2008;295(5):F1535-F44.
270. Kleiner G, Barca E, Ziosi M, Emmanuele V, Xu Y, Hidalgo-Gutierrez A, et al. CoQ10 supplementation rescues nephrotic syndrome through normalization of H2S oxidation pathway. Biochimica et Biophysica Acta (BBA)-Molecular Basis of Disease. 2018;1864(11):3708-22.
271. Falk MJ, Polyak E, Zhang Z, Peng M, King R, Maltzman JS, et al. Probucol ameliorates renal and metabolic sequelae of primary CoQ deficiency in Pdss2 mutant mice. EMBO molecular medicine. 2011;3(7):410-27.
272. Peng M, Ostrovsky J, Kwon YJ, Polyak E, Licata J, Tsukikawa M, et al. Inhibiting cytosolic translation and autophagy improves health in mitochondrial disease. Human molecular genetics. 2015;24(17):4829-47.
273. Sidhom E-H, Kim C, Kost-Alimova M, Ting MT, Keller K, Avila-Pacheco J, et al. Targeting a Braf/Mapk pathway rescues podocyte lipid peroxidation in CoQ-deficiency kidney disease. The Journal of clinical investigation. 2021;131(5).
274. García-Corzo L, Luna-Sánchez M, Doerrier C, Ortiz F, Escames G, Acuña-Castroviejo D, et al. Ubiquinol-10 ameliorates mitochondrial encephalopathy associated with CoQ deficiency. Biochimica et

Biophysica Acta (BBA)-Molecular Basis of Disease. 2014;1842(7):893-901.
275. Barriocanal-Casado E, Hidalgo-Gutiérrez A, Raimundo N, González-García P, Acuña-Castroviejo D, Escames G, et al. Rapamycin administration is not a valid therapeutic strategy for every case of mitochondrial disease. EBioMedicine. 2019;42:511-23.
276. Herebian D, Seibt A, Smits SHJ, Rodenburg RJ, Mayatepek E, Distelmaier F. 4-Hydroxybenzoic acid restores CoQ(10) biosynthesis in human COQ2 deficiency. Ann Clin Transl Neurol. 2017;4(12):902-8.
277. Pesini A, Hidalgo-Gutierrez A, Quinzii CM. Mechanisms and Therapeutic Effects of Benzoquinone Ring Analogs in Primary CoQ Deficiencies. Antioxidants. 2022;11(4):665.
278. Xie LX, Ozeir M, Tang JY, Chen JY, Jaquinod S-K, Fontecave M, et al. Overexpression of the Coq8 kinase in Saccharomyces cerevisiae coq null mutants allows for accumulation of diagnostic intermediates of the coenzyme Q6 biosynthetic pathway. Journal of Biological Chemistry. 2012;287(28):23571-81.
279. Hidalgo-Gutiérrez A, Barriocanal-Casado E, Bakkali M, Díaz-Casado ME, Sánchez-Maldonado L, Romero M, et al. β-RA reduces DMQ/CoQ ratio and rescues the encephalopathic phenotype in Coq9R239X mice. EMBO molecular medicine. 2019;11(1):e9466.
280. Wang Y, Oxer D, Hekimi S. Mitochondrial function and lifespan of mice with controlled ubiquinone biosynthesis. Nature communications. 2015;6(1):1-14.
281. Widmeier E, Airik M, Hugo H, Schapiro D, Wedel J, Ghosh CC, et al. Treatment with 2, 4-dihydroxybenzoic acid prevents FSGS progression and renal fibrosis in podocyte-specific Coq6 knockout mice. Journal of the American Society of Nephrology. 2019;30(3):393-405.
282. Widmeier E, Yu S, Nag A, Chung YW, Nakayama M, Fernández-del-Río L, et al. ADCK4 deficiency destabilizes the coenzyme Q complex, which is rescued by 2, 4-dihydroxybenzoic acid treatment. Journal of the American Society of Nephrology. 2020;31(6):1191-211.
283. Doimo M, Trevisson E, Airik R, Bergdoll M, Santos-Ocaña C, Hildebrandt F, et al. Effect of vanillic acid on COQ6 mutants identified in patients with coenzyme Q10 deficiency. Biochimica et Biophysica Acta (BBA)-Molecular Basis of Disease. 2014;1842(1):1-6.
284. Lopez MJA, Trevisson E, Canton M, Vazquez-Fonseca L, Morbidoni V, Baschiera E, et al. Research Article Vanillic Acid Restores Coenzyme Q Biosynthesis and ATP Production in Human Cells Lacking COQ6. 2019.

285. Quintana A, Kruse SE, Kapur RP, Sanz E, Palmiter RD. Complex I deficiency due to loss of Ndufs4 in the brain results in progressive encephalopathy resembling Leigh syndrome. Proc Natl Acad Sci U S A. 2010;107(24):10996-1001.
286. De la Mata M, Garrido-Maraver J, Cotán D, Cordero MD, Oropesa-Ávila M, Izquierdo LG, et al. Recovery of MERRF Fibroblasts and Cybrids Pathophysiology by Coenzyme Q10. Neurotherapeutics. 2012;9(2):446-63.
287. Hidalgo-Gutiérrez A, Barriocanal-Casado E, Díaz-Casado ME, González-García P, Zenezini Chiozzi R, Acuña-Castroviejo D, et al. β-RA Targets Mitochondrial Metabolism and Adipogenesis, Leading to Therapeutic Benefits against CoQ Deficiency and Age-Related Overweight. Biomedicines. 2021;9(10).
288. Gf P, Franklin K. The Mouse Brain In Stereotaxic Coordinates2003.
289. Zaal EA, Wu W, Jansen G, Zweegman S, Cloos J, Berkers CR. Bortezomib resistance in multiple myeloma is associated with increased serine synthesis. Cancer & metabolism. 2017;5:7.
290. Linden DR, Furne J, Stoltz GJ, Abdel-Rehim MS, Levitt MD, Szurszewski JH. Sulphide quinone reductase contributes to hydrogen sulphide metabolism in murine peripheral tissues but not in the CNS. British journal of pharmacology. 2012;165(7):2178-90.
291. Li H, Handsaker B, Wysoker A, Fennell T, Ruan J, Homer N, et al. The Sequence Alignment/Map format and SAMtools. Bioinformatics (Oxford, England). 2009;25(16):2078-9.
292. Mishanina TV, Libiad M, Banerjee R. Biogenesis of reactive sulfur species for signaling by hydrogen sulfide oxidation pathways. Nature Chemical Biology. 2015;11(7):457-64.
293. Bakkali M, Martin-Blazquez R. RNA-Seq reveals large quantitative differences between the transcriptomes of outbreak and non-outbreak locusts. Sci Rep. 2018;8(1):9207.
294. Raimundo N, Vanharanta S, Aaltonen LA, Hovatta I, Suomalainen A. Downregulation of SRF–FOS–JUNB pathway in fumarate hydratase deficiency and in uterine leiomyomas. Oncogene. 2009;28(9):1261-73.
295. Liu F, Lössl P, Rabbitts BM, Balaban RS, Heck AJR. The interactome of intact mitochondria by cross-linking mass spectrometry provides evidence for coexisting respiratory supercomplexes. Molecular & cellular proteomics : MCP. 2018;17(2):216-32.
296. Cox J, Mann M. MaxQuant enables high peptide identification rates, individualized p.p.b.-range mass accuracies and proteome-wide protein quantification. Nature Biotechnology. 2008;26(12):1367-72.

297. Rogers GW, Brand MD, Petrosyan S, Ashok D, Elorza AA, Ferrick DA, et al. High Throughput Microplate Respiratory Measurements Using Minimal Quantities Of Isolated Mitochondria. PLOS ONE. 2011;6(7):e21746.
298. Borges TH, Pereira JA, Cabrera-Vique C, Lara L, Oliveira AF, Seiquer I. Characterization of Arbequina virgin olive oils produced in different regions of Brazil and Spain: Physicochemical properties, oxidative stability and fatty acid profile. Food Chemistry. 2017;215:454-62.
299. Fernández-Vizarra E, López-Pérez MJ, Enriquez JA. Isolation of biogenetically competent mitochondria from mammalian tissues and cultured cells. Methods (San Diego, Calif). 2002;26(4):292-7.
300. Aslam MS, Yuan L. Serpina3n: potential drug and challenges, mini review. Journal of drug targeting. 2020;28(4):368-78.
301. Choudhary K, Patel PK, Are VN, Makde RD, Hajela K. Mannose-binding lectin-associated serine protease-1 cleaves plasminogen and plasma fibronectin: prefers plasminogen over known fibrinogen substrate. Blood Coagulation & Fibrinolysis. 2021;32(7):504-12.
302. Zamanian JL, Xu L, Foo LC, Nouri N, Zhou L, Giffard RG, et al. Genomic analysis of reactive astrogliosis. Journal of neuroscience. 2012;32(18):6391-410.
303. Nijholt DA, Ijsselstijn L, van der Weiden MM, Zheng P-P, Sillevis Smitt PA, Koudstaal PJ, et al. Pregnancy zone protein is increased in the Alzheimer's disease brain and associates with senile plaques. Journal of Alzheimer's Disease. 2015;46(1):227-38.
304. IJsselstijn L, Dekker LJ, Stingl C, van der Weiden MM, Hofman A, Kros JM, et al. Serum levels of pregnancy zone protein are elevated in presymptomatic Alzheimer's disease. Journal of proteome research. 2011;10(11):4902-10.
305. Gladyck S, Aras S, Hüttemann M, Grossman LI. Regulation of COX Assembly and Function by Twin CX9C Proteins—Implications for Human Disease. Cells. 2021;10(2):197.
306. Rath S, Sharma R, Gupta R, Ast T, Chan C, Durham TJ, et al. MitoCarta3. 0: an updated mitochondrial proteome now with sub-organelle localization and pathway annotations. Nucleic acids research. 2021;49(D1):D1541-D7.
307. Banerjee R, Purhonen J, Kallijärvi J. The mitochondrial coenzyme Q junction and complex III: Biochemistry and pathophysiology. The FEBS journal. 2021.
308. Li T, Zhang Z, Kolwicz Jr SC, Abell L, Roe ND, Kim M, et al. Defective branched-chain amino acid catabolism disrupts glucose

metabolism and sensitizes the heart to ischemia-reperfusion injury. Cell metabolism. 2017;25(2):374-85.
309. Lee BE, Suh P-G, Kim J-I. O-GlcNAcylation in health and neurodegenerative diseases. Experimental & Molecular Medicine. 2021;53(11):1674-82.
310. Wheatley EG, Albarran E, White III CW, Bieri G, Sanchez-Diaz C, Pratt K, et al. Neuronal O-GlcNAcylation improves cognitive function in the aged mouse brain. Current biology. 2019;29(20):3359-69. e4.
311. White III CW, Fan X, Maynard JC, Wheatley EG, Bieri G, Couthouis J, et al. Age-related loss of neural stem cell O-GlcNAc promotes a glial fate switch through STAT3 activation. Proceedings of the National Academy of Sciences. 2020;117(36):22214-24.
312. Wang Z, Li X, Spasojevic I, Lu L, Shen Y, Qu X, et al. Increasing O-GlcNAcylation is neuroprotective in young and aged brains after ischemic stroke. Experimental neurology. 2021;339:113646.
313. Liu F, Iqbal K, Grundke-Iqbal I, Hart GW, Gong C-X. O-GlcNAcylation regulates phosphorylation of tau: a mechanism involved in Alzheimer's disease. Proceedings of the National Academy of Sciences. 2004;101(29):10804-9.
314. Liu F, Shi J, Tanimukai H, Gu J, Gu J, Grundke-Iqbal I, et al. Reduced O-GlcNAcylation links lower brain glucose metabolism and tau pathology in Alzheimer's disease. Brain : a journal of neurology. 2009;132(7):1820-32.
315. Balana AT, Levine PM, Craven TW, Mukherjee S, Pedowitz NJ, Moon SP, et al. O-GlcNAc modification of small heat shock proteins enhances their anti-amyloid chaperone activity. Nature chemistry. 2021;13(5):441-50.
316. Kumar A, Singh PK, Parihar R, Dwivedi V, Lakhotia SC, Ganesh S. Decreased O-linked GlcNAcylation protects from cytotoxicity mediated by huntingtin exon1 protein fragment. Journal of Biological Chemistry. 2014;289(19):13543-53.
317. Grima JC, Daigle JG, Arbez N, Cunningham KC, Zhang K, Ochaba J, et al. Mutant huntingtin disrupts the nuclear pore complex. Neuron. 2017;94(1):93-107. e6.
318. Hsieh Y-L, Su F-Y, Tsai L-K, Huang C-C, Ko Y-L, Su L-W, et al. NPGPx-mediated adaptation to oxidative stress protects motor neurons from degeneration in aging by directly modulating O-GlcNAcase. Cell Reports. 2019;29(8):2134-43. e7.
319. Lüdemann N, Clement A, Hans VH, Leschik J, Behl C, Brandt R. O-glycosylation of the tail domain of neurofilament protein M in human neurons and in spinal cord tissue of a rat model of amyotrophic

lateral sclerosis (ALS). Journal of Biological Chemistry. 2005;280(36):31648-58.
320. Vázquez-Fonseca L, Schäefer J, Navas-Enamorado I, Santos-Ocaña C, Hernández-Camacho JD, Guerra I, et al. ADCK2 haploinsufficiency reduces mitochondrial lipid oxidation and causes myopathy associated with CoQ deficiency. Journal of clinical medicine. 2019;8(9):1374.
321. Bentinger M, Dallner G, Chojnacki T, Swiezewska E. Distribution and breakdown of labeled coenzyme Q10 in rat. Free Radic Biol Med. 2003;34(5):563-75.
322. Haack TB, Haberberger B, Frisch EM, Wieland T, Iuso A, Gorza M, et al. Molecular diagnosis in mitochondrial complex I deficiency using exome sequencing. J Med Genet. 2012;49(4):277-83.
323. Alston CL, Howard C, Oláhová M, Hardy SA, He L, Murray PG, et al. A recurrent mitochondrial p.Trp22Arg NDUFB3 variant causes a distinctive facial appearance, short stature and a mild biochemical and clinical phenotype. J Med Genet. 2016;53(9):634-41.
324. Haack TB, Madignier F, Herzer M, Lamantea E, Danhauser K, Invernizzi F, et al. Mutation screening of 75 candidate genes in 152 complex I deficiency cases identifies pathogenic variants in 16 genes including NDUFB9. J Med Genet. 2012;49(2):83-9.
325. Brea-Calvo G, Haack TB, Karall D, Ohtake A, Invernizzi F, Carrozzo R, et al. COQ4 mutations cause a broad spectrum of mitochondrial disorders associated with CoQ10 deficiency. Am J Hum Genet. 2015;96(2):309-17.
326. Kabil H, Kabil O, Banerjee R, Harshman LG, Pletcher SD. Increased transsulfuration mediates longevity and dietary restriction in Drosophila. Proceedings of the National Academy of Sciences. 2011;108(40):16831-6.
327. Hine C, Mitchell JR. Calorie restriction and methionine restriction in control of endogenous hydrogen sulfide production by the transsulfuration pathway. Experimental gerontology. 2015;68:26-32.
328. Siow YL. Metabolic imbalance of homocysteine and hydrogen sulfide in kidney disease. Current Medicinal Chemistry. 2018;25(3):367-77.
329. Van Strien J, Guerrero-Castillo S, Chatzispyrou IA, Houtkooper RH, Brandt U, Huynen MA. COmplexome Profiling ALignment (COPAL) reveals remodeling of mitochondrial protein complexes in Barth syndrome. Bioinformatics (Oxford, England). 2019;35(17):3083-91.

330. Acuna Castroviejo D, C Lopez L, Escames G, Lopez A, A Garcia J, J Reiter R. Melatonin-mitochondria interplay in health and disease. Current topics in medicinal chemistry. 2011;11(2):221-40.
331. Varricchio C, Beirne K, Heard C, Newland B, Rozanowska M, Brancale A, et al. The ying and yang of idebenone: not too little, not too much–cell death in NQO1 deficient cells and the mouse retina. Free Radical Biology and Medicine. 2020;152:551-60.
332. Duberley K, Heales S, Abramov A, Chalasani A, Land J, Rahman S, et al. Effect of Coenzyme Q10 supplementation on mitochondrial electron transport chain activity and mitochondrial oxidative stress in Coenzyme Q10 deficient human neuronal cells. The international journal of biochemistry & cell biology. 2014;50:60-3.
333. Rossmann MP, Hoi K, Chan V, Abraham BJ, Yang S, Mullahoo J, et al. Cell-specific transcriptional control of mitochondrial metabolism by TIF1γ drives erythropoiesis. Science. 2021;372(6543):716-21.
334. Van De Wal MA, Adjobo-Hermans MJ, Keijer J, Schirris TJ, Homberg JR, Wieckowski MR, et al. Ndufs4 knockout mouse models of Leigh syndrome: pathophysiology and intervention. Brain : a journal of neurology. 2022;145(1):45-63.
335. Filograna R, Lee S, Tiklova K, Jonsson V, Ringner M, Giavalisco P, et al. Mitochondrial dysfunction in adult midbrain dopamine neurons triggers an immune response at an early disease stage. Cell Reports. 2020.
336. Linnerbauer M, Wheeler MA, Quintana FJ. Astrocyte crosstalk in CNS inflammation. Neuron. 2020;108(4):608-22.
337. Lake NJ, Compton AG, Rahman S, Thorburn DR. Leigh syndrome: one disorder, more than 75 monogenic causes. Annals of neurology. 2016;79(2):190-203.
338. Chourasia N, Adejumo RB, Patel RP, Koenig MK. Involvement of cerebellum in Leigh syndrome: Case report and review of the literature. Pediatric neurology. 2017;74:97-9.
339. Yang Y-Y, Vasta V, Hahn S, Gangoiti JA, Opheim E, Sedensky MM, et al. The role of DMQ9 in the long-lived mutant clk-1. Mechanisms of ageing and development. 2011;132(6-7):331-9.
340. González-García P, Hidalgo-Gutiérrez A, Mascaraque C, Barriocanal-Casado E, Bakkali M, Ziosi M, et al. Coenzyme Q10 modulates sulfide metabolism and links the mitochondrial respiratory chain to pathways associated to one carbon metabolism. Human molecular genetics. 2020;29(19):3296-311.
341. Zhang Y, Wu S, Qin Y, Liu J, Liu J, Wang Q, et al. Interaction of phenolic acids and their derivatives with human serum albumin:

Structure–affinity relationships and effects on antioxidant activity. Food chemistry. 2018;240:1072-80.
342. Myint O, Wattanapongpitak S, Supawat B, Kothan S, Udomtanakunchai C, Tima S, et al. Protein binding of 4-hydroxybenzoic acid and 4-hydroxy-3-methoxybenzoic acid to human serum albumin and their anti-proliferation on doxorubicin-sensitive and doxorubicin-resistant leukemia cells. Toxicology Reports. 2021;8:1381-8.
343. Hancock WW, Tsai T-L, Madaio MP, Gasser DL. Cutting edge: Multiple autoimmune pathways in kd/kd mice. The Journal of Immunology. 2003;171(6):2778-81.
344. Hallman TM, Peng M, Meade R, Hancock WW, Madaio MP, Gasser DL. The mitochondrial and kidney disease phenotypes of kd/kd mice under germfree conditions. Journal of autoimmunity. 2006;26(1):1-6.
345. Tan EP, McGreal SR, Graw S, Tessman R, Koppel SJ, Dhakal P, et al. Sustained O-GlcNAcylation reprograms mitochondrial function to regulate energy metabolism. Journal of Biological Chemistry. 2017;292(36):14940-62.
346. Brandt AU, Sy M, Bellmann-Strobl J, Newton BL, Pawling J, Zimmermann HG, et al. Association of a marker of N-acetylglucosamine with progressive multiple sclerosis and neurodegeneration. JAMA neurology. 2021;78(7):842-52.
347. Sy M, Brandt AU, Lee S-U, Newton BL, Pawling J, Golzar A, et al. N-acetylglucosamine drives myelination by triggering oligodendrocyte precursor cell differentiation. Journal of Biological Chemistry. 2020;295(51):17413-24.
348. Montero R, Grazina M, López-Gallardo E, Montoya J, Briones P, Navarro-Sastre A, et al. Coenzyme Q10 deficiency in mitochondrial DNA depletion syndromes. Mitochondrion. 2013;13(4):337-41.
349. Collaboration M-SAR. Mutations in COQ2 in familial and sporadic multiple-system atrophy. New England Journal of Medicine. 2013;369(3):233-44.
350. Barca E, Kleiner G, Tang G, Ziosi M, Tadesse S, Masliah E, et al. Decreased coenzyme Q10 levels in multiple system atrophy cerebellum. Journal of Neuropathology & Experimental Neurology. 2016;75(7):663-72.
351. Ducker GS, Rabinowitz JD. One-carbon metabolism in health and disease. Cell metabolism. 2017;25(1):27-42.
352. Fassone E, Rahman S. Complex I deficiency: clinical features, biochemistry and molecular genetics. Journal of medical genetics. 2012;49(9):578-90.

353. Sahebekhtiari N, Fernandez-Guerra P, Nochi Z, Carlsen J, Bross P, Palmfeldt J. Deficiency of the mitochondrial sulfide regulator ETHE1 disturbs cell growth, glutathione level and causes proteome alterations outside mitochondria. Biochimica et Biophysica Acta (BBA)-Molecular Basis of Disease. 2019;1865(1):126-35.
354. Yang L, Canaveras JCG, Chen Z, Wang L, Liang L, Jang C, et al. Serine catabolism feeds NADH when respiration is impaired. Cell metabolism. 2020;31(4):809-21. e6.
355. Tyynismaa H, Carroll CJ, Raimundo N, Ahola-Erkkilä S, Wenz T, Ruhanen H, et al. Mitochondrial myopathy induces a starvation-like response. Human molecular genetics. 2010;19(20):3948-58.
356. Lemieux H, Blier PU, Gnaiger E. Remodeling pathway control of mitochondrial respiratory capacity by temperature in mouse heart: electron flow through the Q-junction in permeabilized fibers. Scientific reports. 2017;7(1):1-13.
357. Tiranti V, Viscomi C, Hildebrandt T, Di Meo I, Mineri R, Tiveron C, et al. Loss of ETHE1, a mitochondrial dioxygenase, causes fatal sulfide toxicity in ethylmalonic encephalopathy. Nature medicine. 2009;15(2):200-5.
358. Friederich MW, Elias AF, Kuster A, Laugwitz L, Larson AA, Landry AP, et al. Pathogenic variants in SQOR encoding sulfide: quinone oxidoreductase are a potentially treatable cause of Leigh disease. Journal of inherited metabolic disease. 2020;43(5):1024-36.
359. Phillips CNM, Zatarain JR, Nicholls ME, Porter C, Widen SG, Thanki K, et al. Upregulation of Cystathionine-β-Synthase in Colonic Epithelia Reprograms Metabolism and Promotes CarcinogenesisA Role for CBS in Colon Carcinogenesis. Cancer research. 2017;77(21):5741-54.
360. Turbat-Herrera EA, Kilpatrick MJ, Chen J, Meram AT, Cotelingam J, Ghali G, et al. Cystathione β-synthase is increased in thyroid malignancies. Anticancer research. 2018;38(11):6085-90.
361. Luebke JL, Shen J, Bruce KE, Kehl-Fie TE, Peng H, Skaar EP, et al. The CsoR-like sulfurtransferase repressor (CstR) is a persulfide sensor in S taphylococcus aureus. Molecular microbiology. 2014;94(6):1343-60.
362. Shimizu T, Masuda S. Persulphide-responsive transcriptional regulation and metabolism in bacteria. The Journal of Biochemistry. 2020;167(2):125-32.
363. Leskova A, Pardue S, Glawe JD, Kevil CG, Shen X. Role of thiosulfate in hydrogen sulfide-dependent redox signaling in endothelial cells. American Journal of Physiology-Heart and Circulatory Physiology. 2017;313(2):H256-H64.

364. Lee S-Y, Lee SH, Yang E-J, Kim J-K, Kim E-K, Jung K, et al. Coenzyme Q10 inhibits Th17 and STAT3 signaling pathways to ameliorate colitis in mice. Journal of medicinal food. 2017;20(9):821-9.
365. You J, Shi X, Liang H, Ye J, Wang L, Han H, et al. Cystathionine-γ-lyase promotes process of breast cancer in association with STAT3 signaling pathway. Oncotarget. 2017;8(39):65677.
366. Kabil O, Zhou Y, Banerjee R. Human cystathionine β-synthase is a target for sumoylation. Biochemistry. 2006;45(45):13528-36.
367. Agrawal N, Banerjee R. Human polycomb 2 protein is a SUMO E3 ligase and alleviates substrate-induced inhibition of cystathionine β-synthase sumoylation. PloS one. 2008;3(12):e4032.